ABSTRACT

GIBSON, NATALIE MARIE. Modified Nanodiamonds for Detoxification. (Under the direction of Dr. Tzy-Jiun Mark Luo).

Nanodiamonds (NDs) are an emerging class of biomaterials that are reaching world-wide attention due to their biocompatible, nontoxic properties and abundant surface chemistries that lend them to a wide range of biomedical applications. Furthermore, surface functional groups of NDs can easily be tailored to exhibit desirable chemical, physical and biological properties. Such characteristics naturally allow for NDs' surface to be considered as ideal carriers for various molecules and biomolecules intended for the delivery or removal of molecules *in vivo*.

NDs have already shown to have a high affinity for various biological molecules, including DNA and proteins. This dissertation, however, expands NDs' use to the adsorption of carcinogenic mycotoxins, aflatoxin B1 (AfB1) and ochratoxin A (OTA). It has been estimated that myocotoxins are found in approximately 25 % of the world's crops each year. Ingestion of mycotoxins contaminated crops has been linked to hepatocellular carcinoma, disease and death. Therefore, we aim to develop ND enterosorbents, for the binding and removal of mycotoxins within the gastrointestinal (GI) tract, thereby eliminating the effects of these toxins.

While NDs are readily available, raw, unmodified NDs, like those typically received from vendors, possess inhomogeneous aggregate sizes and surface characteristics. Our research first explored several ND modification techniques to enhance ND's adsorption of AfB1 and OTA. Modification methods assessed in this research include size reduction techniques, plasma treatments, silane surface coatings and homogenous surface group

termination, including carboxylation, hydrogenation and hydroxylation. The effectiveness of these NDs for mycotoxins removal was determined by calculations of maximum capacities and binding constants, as obtained through the Langmuir isotherm and related transform equations. Several of these treatments also showed heightening of the NDs' inherent zeta potentials (ZPs), which were essential for interacting with charged molecules, like OTA. Furthermore, the increased ZPs lead to improved colloidal stabilities over a wide range of pH, which is important for their interaction in the GI tract. While the dyes and OTA illustrated primarily electrostatic adsorption mechanisms, neutrally charged AfB1's adsorption was predominantly based upon the aggregate size of the ND substrate.

In addition to mycotoxins, fluorescent dyes, including propidium iodide, pyranine and 2,2'-azino-bis(3-ethylbenzthiazoline-6-sulphonic acid) (ABTS), were initially utilized during methodological development. Fluorescent dye investigations helped assesses the adsorption mechanisms of NDs and demonstrated the significance of electrostatic interactions. Beyond electrostatic adsorption mechanisms, surface functional groups were also responsible for the amount of dye adsorbed, as was also true in OTA adsorption. Therefore, surface characterization was carried out for several ND samples by FTIR, TOF-SIMS and TDMS analysis.

Final results of our studies show that our modified NDs perform better than yeast cells walls and other NDs but comparable to activated charcoal in the adsorption of AfB1, and outperform clay minerals in OTA studies. Moreover, it was demonstrated that adsorption can be maintained in a wide range of pH, thereby, increasing the possibility of NDs use in mycotoxins enterosorbent applications.

Modified Nanodiamonds for Detoxification

by
Natalie Marie Gibson

A dissertation submitted to the Graduate Faculty of
North Carolina State University
in partial fulfillment of the
requirements for the degree of
Doctor of Philosophy

Materials Science and Engineering

Raleigh, North Carolina

2010

APPROVED BY:

Dr. Tzy-Jiun Mark Luo Committee Chair	Dr. Donald W. Brenner Committee Co-Chair
Dr. Yaroslava Yingling	Dr. Gary Payne

Dr. Olga Shenderova

DEDICATION

To my loving family and Andy.

In memory of James Gibson.

BIOGRAPHY

Natalie Marie Gibson was born on June 20, 1984, in Torrance, California, to James and Penny Gibson. She moved to Pittsburgh, Pennsylvania, at an early age where she was fortunate enough to grow up surrounded by her grandparents and cousins. Growing up, Natalie attended North Allegheny School District, where she found that she enjoyed creative pursuits, such as the arts and dance. In 2000, she moved to Wake Forest, North Carolina, where she finished her last two years at Wakefield High School. Seeking new experiences, Natalie enrolled in many fashion-related clubs where she held several leadership roles. In this new environment, Natalie began to focus more seriously on her studies, though her primary focus was on fashion and designing exotic creations. In her Senior Year, she became President of Family, Career and Community Leaders of America (FCCLA). In this role, Natalie setup a visit to North Carolina State University's (NCSU) College of Textiles. This experience combined with her inherent interest in fashion, led to her enrollment at NCSU.

Though she had intentions of becoming a fashion designer, the textile program required completion of several science and math courses. These courses sparked her innate curiosity and creativity. Furthermore, these science based textile classes opened her eyes to new, exciting opportunities. Natalie quickly changed her major to Textile Technology with a focus on Biomedical Textiles where she graduated with a 3.94 GPA in May of 2006. In the fall, Natalie began the Material Science and Engineering program at NCSU with a hunger to

expand her knowledge of biomaterials. Her passion and drive comes from the desire to develop new materials and advance technology to help improve the human condition.

Natalie appreciated her atypical path to the doctoral program as her creative background has assisted her to think outside the box. Natalie also credits much of her inventiveness and determination to dance. Natalie, a classically trained dancer, has been dancing for 21 years and was fortunately able to continue her dance career under the NCSU Dance Program's Dance Visions and the Panoramic Dance Project during her undergraduate and graduate years. Natalie has worked with several nationally renowned choreographers who continue to inspire her creativity, expose her to new techniques and teach her to overcome challenges. In her free time, Natalie still dances with and occasionally instructs classes for the Dance Program. Aside from this, she loves spending time with her family and boyfriend, Andy, who she has been with since 2001.

ACKNOWLEDGMENTS

I would like to express my appreciation to all those that have contributed to my success in the doctoral program. First, I would like to sincerely thank my advisor, Dr. Tzy-Jiun Mark Luo for giving me this opportunity. His guidance and wisdom has helped advance my graduate career. I would also like to express my appreciation for the advice and support offered to me by my co-advisor, Dr. Donald W. Brenner. He and Professor Luo instilled confidence in me-- I shall never forget them.

I want to give special thanks to Dr. Olga Shenderova. She was such an important source of inspiration to me. She truly opened my eyes to the fascinating world of research, and taught me so many lessons both personally and professionally. I am forever indebted to her for her mentorship and friendship. I look forward to her many years of friendship and future collaborations. I would also like to express my gratitude to my committee members, Dr. Yaroslava Yingling and Dr. Gary Payne whose inquiries and suggestions during the preliminary examination have helped guide experiments throughout this past year. I am equally thankful to the International Technology Center (ITC), specifically Dr. Gary McGuire and Dr. Suzanne Hens. My residency at ITC for the first several years of my graduate career has led to many valuable discussions and perspectives. There are so many others that provided me help and support during my graduate years. Please know that I truly appreciate all that you have done for me during my graduate studies, and forgive me for not mentioning you by name.

I would like to pay my final acknowledgments to my family, especially my parents, grandparents and Andy. They provided love, encouragement and support, without which my doctoral studies would not have been possible. They helped make my dream a reality.

TABLE OF CONTENTS

LIST OF TABLES

LIST OF FIGURES

Chapter 1

Introduction

1.0 Introduction

Advances in research of nanomaterials coupled with an ever increasing knowledge of human biology are creating the advances in medicine at rates that few ever thought possible. Much of this success is due to nanobiotechnology, an emerging field, which relies on the discovery and synthesis of new biomaterials. Within this field, nanodiamonds are emerging as a newly explored biomaterial to overcome limitations present with traditional materials. Nanodiamonds (NDs), first identified in the 1960's in Soviet Russia [1], are now reaching world-wide attention as scientists are recognizing its unique properties based on its high biocompatibility and easily modified surfaces. Such characteristics are leading to exponential growth in ND adsorbent research, where various molecules and biomolecules are being targeted on the ND's surface for delivery or removal of molecules *in vivo*. The current dissertation specifically focuses on the development of ND enterosorbents for the removal and detoxification of ingested mycotoxins. In this chapter the fundamentals of NDs and ND research will be discussed (Section 1.1). Section 1.2 introduces mycotoxins with a focus on current mycotoxin enterosorbents and the limitations of these enterosorbents. To better understand adsorption mechanisms of ND materials several dyes, mentioned in Section 1.3, are utilized during methodological development.

1.1 Nanodiamonds

The family of nanocarbons is quite diverse including well-known materials such as carbon nanotubes, fullerenes, and nano-carbon black [1, 2] . NDs, also falling under the nanocarbon family, have traditionally remained less common in literature. However, as knowledge is gaining of ND materials, their use is rapidly expanding to include them in various research areas, including biology, materials science and chemical engineering disciplines. Many varieties of NDs exist, stemming from their three basic manufacturing steps: (1) synthesis, (2) post-synthesis processing, and (3) modification (Figure 1.1). In this work the research focus is on detonation nanodiamonds (DND), often called *ultradispersed diamond*, although NDs formed through high-pressure high-temperature (HPHT) [3] and chemical vapor deposition (CVD) [4] techniques, as well as naturally occurring diamondoids [5] also exist.

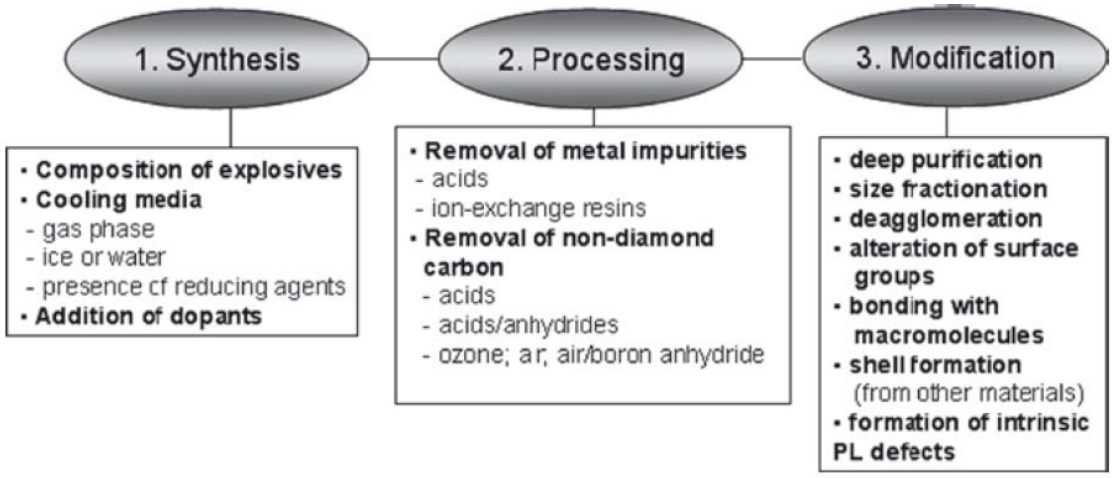

Figure 1.1. ***Three major steps of production of detonation nanodiamonds [6]***

1.1.1Synthesis

DNDs are most commonly synthesized through mixtures of trinitrotoluene (TNT) and 1,3,5-trinitro-1,3,5-*s*-triazine (RDX), though an assortment of other explosives may be used. The explosives are detonated in a chamber with a negative oxygen balance, so that a surplus of carbon remains in the system [7]. Upon detonation, the shockwave propagates at high pressures, 20 to 30 GPa, and high temperatures, 3500 to 4000 K, compressing the free carbon into 4-5 nm diamond particles [2, 8, 9]. The product of the explosion is "soot," in which the newly created diamond particles, termed *primary particles*, are present. To inhibit large amounts of graphite formation associated with the high temperatures of detonation, a non-oxidizing cooling medium must be in place during discharge. This may occur in "wet" or "dry" form, meaning the use of water or ice, or N_2, CO_2, or Ar gases. The rate of cooling should be at least 3000 K/min [10] as this rate is linked to the yield of diamond particles in the resulting soot [11, 12]. Diamond yields of 40 to 80 wt. % have been reported depending on detonation conditions [6], where diamond content can be determined through x-ray diffraction (XRD) analysis [13]. The remainder of the soot is comprised of incombustible impurities (1 to 8 wt. %) and non-diamond carbon (25 to 45 wt. %) that must be removed before use [14]. Though NDs produced via detonation synthesis require additional processing to remove the non-diamond remnants, DNDs have added advantages of being produced inexpensively and large, tons-quantities [10]. The average cost of DNDs is $1 to 2/gram for well purified polydispersed materials with a ~200 nm aggregate size and $10 to 20/gram for 20 nm particles. As a comparison 25 nm HPHT NDs cost on the order of $75/gram [6, 15].

DNDs are both interesting and complex in the fact that alterations to the manufacturing procedures lead to alterations in the resulting properties of the NDs [16]. Many of these characteristic variations come about during post-synthesis processing performed at the manufactures site. One of the primary goals during this step, as described in more detail below, is to remove impurities such as amorphous carbon and incombustible components, i.e., metallic components, formed from the metal chambers during detonation. NDs produced through detonation synthesis have higher impurity contents than NDs produced under other methods, for example, HPHT diamonds which are comprised of at least 96 % carbon. Alternatively, DNDs after conventional purification procedures have an atomic makeup of carbon (~80 to 89 %), oxygen (≤ ~10 %), nitrogen (~2 to 3 %), hydrogen (~0.5 to 1.5 %) and incombustible remnants (~0.5 % to 8 %). Of the carbon phase present approximately 90 to 99 % of it has a diamond structure [14]. Figure 1.2 represents the composition of detonation soot before and after post-synthesis procedures [6].

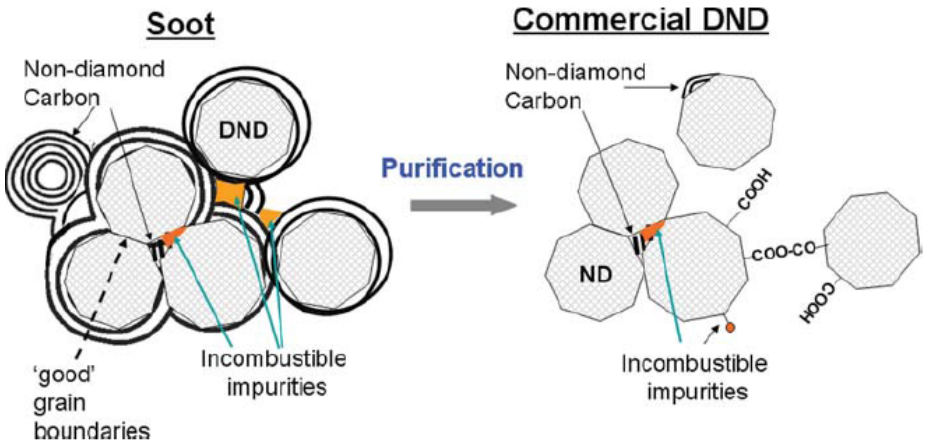

Figure 1.2. Tentative scheme of major structural components of detonation soot (left) and commercial DND product (right) [6].

1.1.2 Post-Synthesis Processing

Post-synthesis purification is an imperative step in preparing NDs for bioapplications. The Food and Drug Administration (FDA) places strict regulations on materials for medical and pharmaceutical use, thus, ND processing techniques aspire to meet the stringent regulations. A variety of techniques are used to extract NDs from the remainder of the soot impurities. While these techniques vary from vendor to vendor, the most regularly used process includes strong liquid oxidizers at elevated temperatures. In this process it is important to oxidize both the metallic content and non-diamond carbon from the exposed ND surface as well as in the internal cracks of the aggregates. As mentioned, NDs directly after detonation have primary particle sizes of 4 to 5 nm, however, immediately after synthesis the NDs aggregate to make larger particle sizes [2, 8, 9], as illustrated in Figure 1.2. The aggregates, which are made up of tightly and loosely bound parts, must be disintegrated for complete purification from incombustible and amorphous carbon impurities. Typically, metallic impurities are removed using sulfuric acid, sulfuric/nitric acid mixtures, hydrochloric acid and potassium dichromate in sulfuric acid [17, 18], whereas sp^2 remnants are extracted by use of KOH/KNO_3, Na_2O_2, CrO_3/H_2SO_4, $HNO_3/H2O_2$ under pressure, and sulfuric and perchloric acids mixtures [6, 14]. It has been shown that simultaneous removal of metallic impurities and sp^2 components can be completed by using high-temperature oxidation by a strong acid, such as nitric acid, under pressure [19]. In some cases additional treatment in ion-exchange resins may be necessary to remove any remaining non-carbon species [6]. X-ray absorption near-edge structure (XANES) [20] and x-ray diffraction (XRD)

[21] techniques can be applied to determine sp^2 versus sp^3 composition of the final product.

Separation techniques are not limited to the methods listed above, in fact, vendors are now leaning towards more economical and less hazardous practices. This includes the use of ozone air treatments at elevated temperatures [22]. Ozone oxidation, first introduced in 1991, has shown to effectively remove non-diamond carbon, while eliminating the need for corrosive liquid oxidizers that can make up to 40 % of manufacturing costs [6]. While oxygen has been used as an ozone substitute, it was shown to be less effective in oxidizing sp^2 carbon, consequently, industrial scale soot purification has turned exclusively to ozone oxidation for gas-phase treatments [6, 22, 23].

1.1.3 Modification

Up to this point all processing procedures took place at the site of the vendor, typically being located in Russia or China. NDs received from these vendors, even after preliminary purification, still show some residual impurities left over from the previous post-synthesis processing stage. Furthermore, as a result of the previous purification steps NDs aggregate into various particle sizes and are left covered with a wide range of surface groups. These non-homogeneities are not ideal for the desired application and often lead to poor colloidal stability when NDs are introduced to aqueous solutions. To achieve stable colloids, which are the preferred form for the majority of bioapplications, additional processing steps or modifications, must be completed. These steps may include deep purification, fractionation, de-aggregation, and/or surface functionalization. The modifications are usually

completed after purchasing from vendors, though manufactures may also choose to complete some of these steps on-site. Due to synthesis and post-synthesis steps being specific to individual vendors ND's properties will also vary, meaning different modification procedures may be necessary for NDs originating from different manufacturers. We briefly discuss several modification steps below.

Deep Purification

Deep purification is most important for introducing NDs into the biomedical segment. The purpose of deep purification is to remove any remaining incombustible impurity content from the NDs. To carry out this process, the use of liquid oxidizers is employed to lower the ash content and to increase colloidal stability. An example of this process can be seen in Table 1.1 where a standard ND sample, produced by the VNIITF center, Snezinsk, Ural region, Russia [24], was treated with a variety of liquid oxidizers (HCl, HCl/HNO_3, HF/HCl and H_2O_2-NaOH) to compare the resulting impurity content [6]. As seen, the most favorable purification process came from treatments with HF with subsequent treatments in HCl. In all cases, after purification of the original Ch-St sample, the impurity content was reduced and aggregate sizes were significantly decreased. As a result, these treatments lead to improved colloidal stability as compared to the unstable original sample. The most effective technique reported for lowering incombustible impurities has been with the use of hot nitric acid. While such a method has only been performed on a small scale, the results are promising, showing only a remaining 0.07 wt. % to 0.08 wt. % ash content [6].

Alternatively, deep purification has been demonstrated by heat treatments in air [6]. Such a technique has been shown to effectively remove any remaining sp^2 carbon content. In studies by Shenderova *et. al*. [25] oxidation of commercial Ch-St was completed using air at 400 to 450 degrees C, with results showing a significant increase in colloidal stability from the original sample. It was seen in other experiments that ND treatment in Cl_2 at 850 degrees C showed a considerable decrease in non-diamond content and lowered elemental contents, including Al, Cr, Si and Fe [26].

Table 1.1. Comparison of incombustible impurities content and average aggregate size for the same initial soot purified with either a wet oxidizer or ozone (rows 1 and 2 correspondingly) as well as for different additional purification treatments [6].

ND treatment	Incombustible Impurities, wt.%	Size in H2O, nm
Soot purified with CrO_3/H_2SO_4 (Ch-St ND)	1.5	300
Soot purified with O_3	0.9	190
Ch-St purified with air		210
Ch-St purified with HCl	1.2	177
Ch-St purified with HCl/HNO_3	0.9	175
Ch-St purified with HF/HCl	0.2	171
Ch-St purified with H_2O_2-NaOH	0.8	202

De-agglomeration

While deep purification has resulted in some aggregate size reduction, the final aggregate sizes are still too large to employ in most biomedical application. Quickly after detonation synthesis, larger particles form due to aggregation of 4 to 5 nm primary particles,

leading to micron sized NDs with poor colloidal stability [19, 27]. Commercially received NDs can be subjected to vigorous ultrasonication to break up the loosely aggregated portions of the particle. However, the tightly compacted segments remain held together and, as a result, ultrasonication typically leaves unbreakable particle sizes of 200 to 400 nm [28]. Refer to Figure 1.3 e-g for HRTEM images of ultrasonicated NDs with unbreakable aggregates.

De-agglomeration of these unbreakable aggregates to their primary 4 to 5 nm sizes is imperative for some biomedical applications (Figure 1.4). Current efforts and advances have been led by Osawa *et. al*. to use mechanical de-agglomeration through stirred media milling [23, 27] (Figure 1.5) or bead-assisted sonication disintegration of DNDs in suspensions [29]. Through their techniques ND suspensions consisting of individual 4 to 5 nm particles have been produced which contain only a very small fraction (less than 1 vol. %) of 30 nm particles [6, 29]. One downfall to this method is added contamination of the resulting DND particles due to introduction of zirconia beads [31], which break up the strong cohesive energies of the diamond at the sharp boundaries [15]. These sharp grain boundaries on the NDs are shown in Figure 1.3 c and d.

Other drawbacks include the creation of sp^2 layers of the ND surface [30]. To remove the sp^2 and zirconia contamination, researchers resort back to liquid oxidizers which re-agglomerate the primary particles [15]. Alternative methods use a NaOH solution in water to purify the material, but it yet to be determined if an acceptable degree of purification can be reached while keeping the NDs in their so called "single-digit" state [6]. The stage

progression of detonation soot to the final single-digit material is depicted in Figure 1.6. It is important to note that complete de-agglomeration of NDs should not always be the ultimate objective, given that there are numerous applications for NDs of sizes larger than the primary particles, as shown in Figure 1.4.

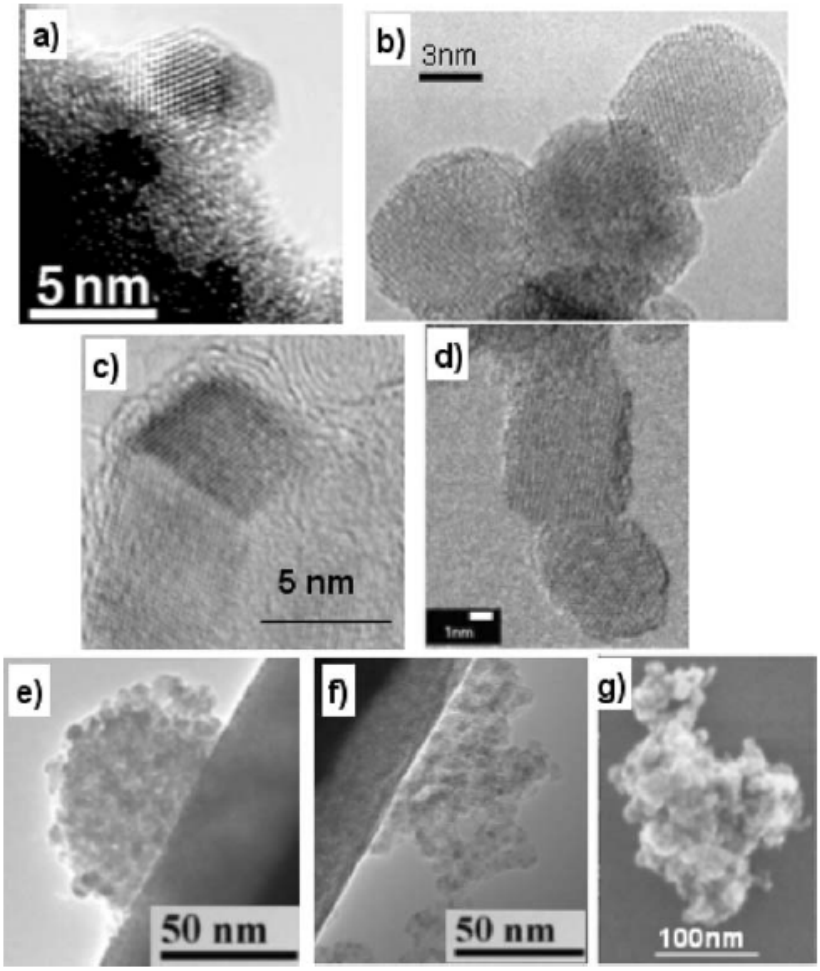

Figure 1.3. HRTEM images of primary DND particles (a, b), primary DND particles forming small agglomerates with atomically sharp grain boundaries (c, d); medium-size agglomerates with high (e) and low (f) DND packing density and a large aggregate with highly irregular shape (g) [6].

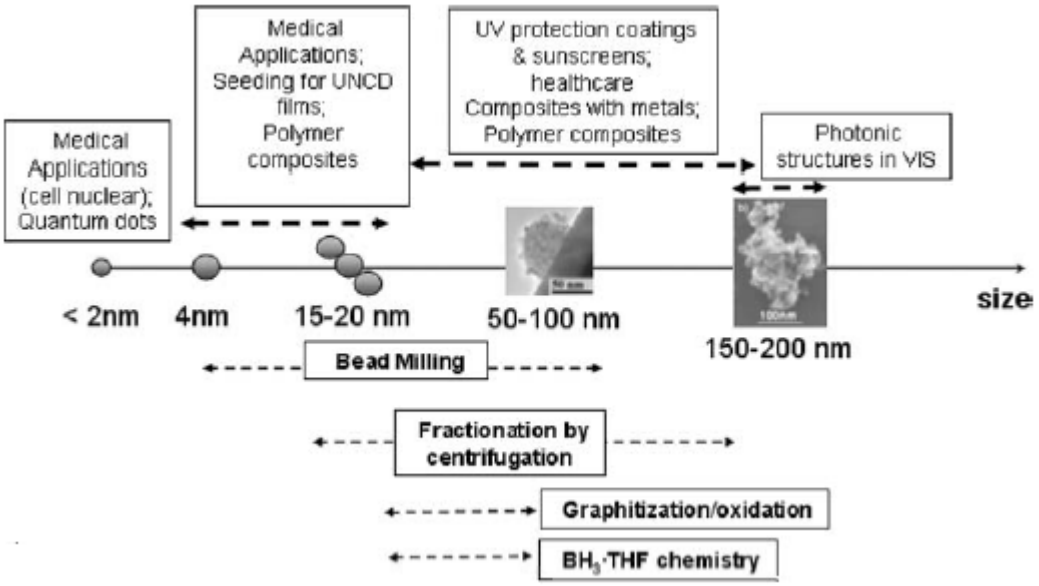

Figure 1.4. Schematics of the size ranges of DND primary particles and aggregates in relation to different possible areas of biomedical and healthcare applications as well as current approaches for obtaining DND product within these size ranges [6].

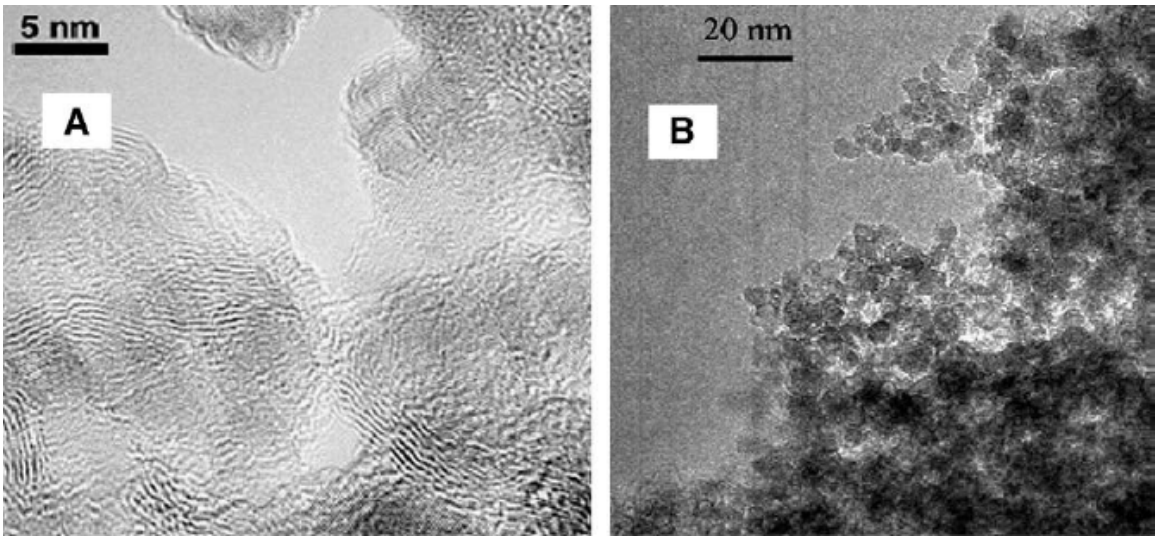

Figure 1.5. Typical TEM photographs of detonation nanodiamond before (A) and after (B) stirred-media milling with zirconia beads. A: particles may appear dispersed but are tight agglutinates. B: particles are partially aggregated but can be dispersed readily by sonication. The TEM photographs were taken by Dr. M. Ozawa [19].

Graphitization of detonation by-products through the use of N_2 at 1000 degrees C for 1 hour with subsequent oxidation in air for several hours at 450 degrees C have also been proposed as de-agglomeration procedures [32]. This method resulted in approximately 50 % of the total product as DNDs, with less than 50 nm ND particle sizes. DND treatments in atmospheric pressure plasma have also shown a reduction in DND aggregate size by roughly 20 % [6, 15]. It was recently revealed that temperatures of 400 to 430 degrees C, put in place over several hours, were best at removing large amounts of sp^2-bonded carbon from the ND while not affecting the sp^3 carbon [20].

Regardless of the method used, concerns are still present on whether or not the de-agglomerated materials will remain small upon drying or surface group modification. For example, it was discovered that upon silanization of DND materials, NDs agglomerated due to condensation reactions between the treated particles (however, further aggregation was not seen with reduction reactions) [33]. The dried ND suspensions, which were extracted from water or other solvents for storage or surface functionalization, showed a further increase in aggregate growth. To overcome this, new techniques developed by Puzyr *et. al*. propose using sonication assisted treatment in NaCl solution to incorporate sodium ions on the ND surface as well as purify the original material [34]. With such treatment, it is possible to dry the ND suspensions to a powder and re-suspend the material without agglomeration of the 40 nm particles [6].

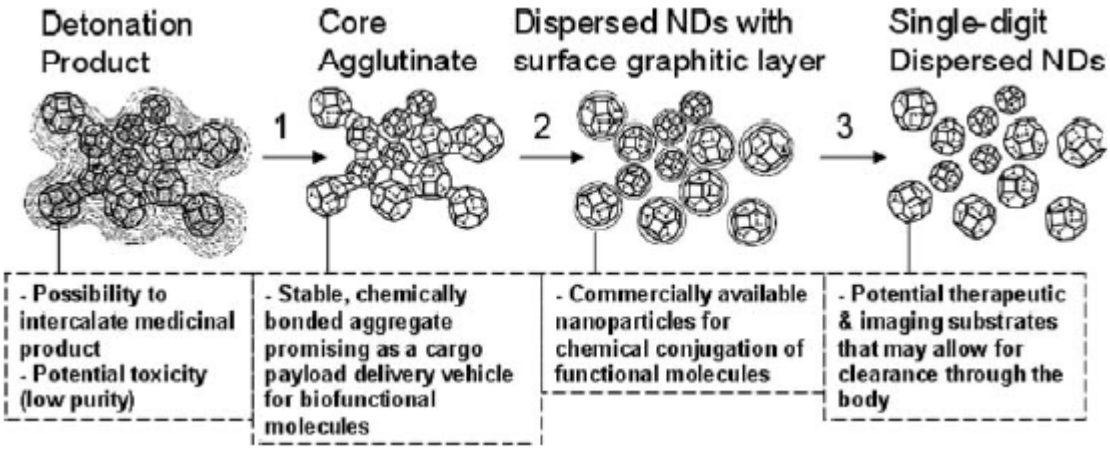

Figure 1.6. Detonation nanodiamond structural changes and proposed uses for controlled and sustained release of small molecules or medicinal products during different stages of purification: (1) Nitric acid oxidation, (2) Bead milling, and (3) Removal of graphitic surface layer [6].

Fractionation

An alternative method for obtaining small ND aggregates is completed using fractionation. In this method one extracts the smallest fractions, through centrifugation, from the larger unbreakable aggregates after ultrasonication treatment. Fractionation by centrifugation has several attractive features including no introduction of contaminates (as seen with the zirconia beads in beads-milling [30, 31]) and an approach that is recognized as being very inexpensive. Furthermore, one can separate the suspension into a variety of particles sizes with a very small size distribution [25, 35, 36]. As different applications require different sizes of ND aggregates, this technique is undoubtedly useful. Figure 1.6 above shows the aggregate sizes during different stages of processing and where each aggregate size may be the most practical.

The primary drawback of this technique is that NDs must possess colloidal stability before centrifugation, since it is nearly impossible to fractionate suspensions that immediately result in sedimentation. Figure 1.7 shows an unstable ND colloid unable to be centrifuged for fractionation along with several centrifugated pellet fractions from DND suspension (Figure 1.8).

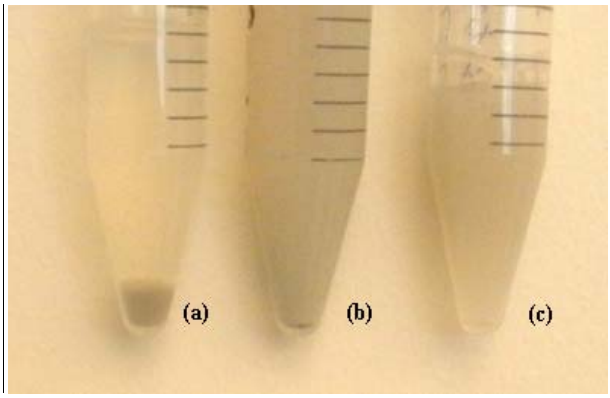

Figure 1.7. Photos unstable (a) moderately stable (showing some sedimentation) (b) and stable (c) versions of commercially available DND (Ch-St) in DI water.

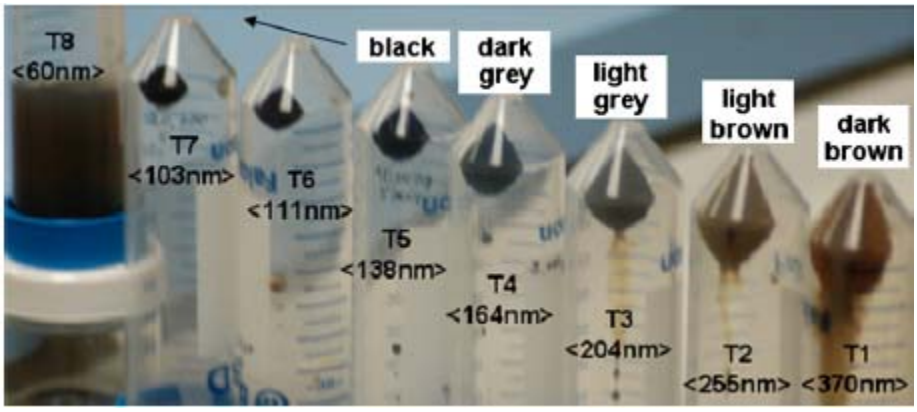

Figure 1.8. Photographic image of pellets and supernatant obtained by consecutive fractionation of 1 wt. % hydrosol of Ch-St ND oxidized in air (Ch-St-T) according to the data in Table 1.2 [25].

Increasing the number of centrifugation cycles increases the transparency and stability of the colloid as the average particle size is decreasing (Table 1.2). Suspensions with an average of 15 nm have been achieved from this method [6] and 4 nm particles have been extracted by using ultracentrifugation techniques [37]. Also noteworthy, is that small ND particles obtained by this method have a more uniform surface than seen in the beads milling process [6]. In fractionation by centrifugation small particles are extracted from the total volume, however, in beads-milling ND aggregates are broken revealing a "fresh" surface which can adsorb molecules from the surrounding environment [33, 38]. However, due to the use of centripetal force for sedimentation, the centrifugation method has limitations that are dependent on the particle shape, whether spherical or elongated chains (Figure 1.3g), which make sedimentation dependent on the aggregate size and shape rather than size alone [6].

Table 1.2. Centrifugation conditions, average particle sizes in different fractions based on the unimodal intensity analysis (third column), average volumetric size distribution (fourth column) and fraction yield for Ch-St-T ND fractionated by consecutive 5-min centrifugations [25].

Fraction	Centrifugation conditions (g)	Average intensity-based particle size[a] (nm)	Average volumetric particle size (nm)	Yield (wt.%)
Polydisperse	–	210	190	100
T1	1000[b]	370	360	23
T2	3000	255	245	15
T3	5000	204	200	13
T4	8000	164	140	10
T5	10,000	138	94	7
T6	12,000	111	80	6
T7	20,000	103	69	6
T8	Supernatant	58	30	20

Surface Functionalization

One of the most modern topics in ND research is surface functionalization of the material to tailor their properties for desired applications. DND materials have a wide variety of surface groups that are naturally present on the particles' surface due to detonation and post-detonation procedures [28]. As a result, NDs are unique among their larger carbon classification since they may contain a multifaceted collection of chemical groups, often including carboxylic acids, esters, ethers, lactones, amines and more (Figure 1.9) [15]. Because primary particles contain approximately 15 to 20 % of their carbon atoms on the surface, groups are found in high density and are easily accessible for chemical alterations [20, 28]. Surface modifications have been achieved using a wide variety of reactions.

One of the first modification techniques used radical based reactions under wet chemical treatments where the hydrogen atom was removed to create a free radical species for binding carboxylic acids, dicarboxylic acids and benzoyl peroxides, and NO_2 [6]. Dry methods of functionalization may also be used including chlorine, fluorine and hydrogen gas-phase treatment [39]. Additionally, NDs, which are already unique from the rest of the carbon class due to its natural hydrophilicity, can have their hydrophilic property improved by 20 fold though annealing the NDs with CCl_4/Ar mixtures [26].

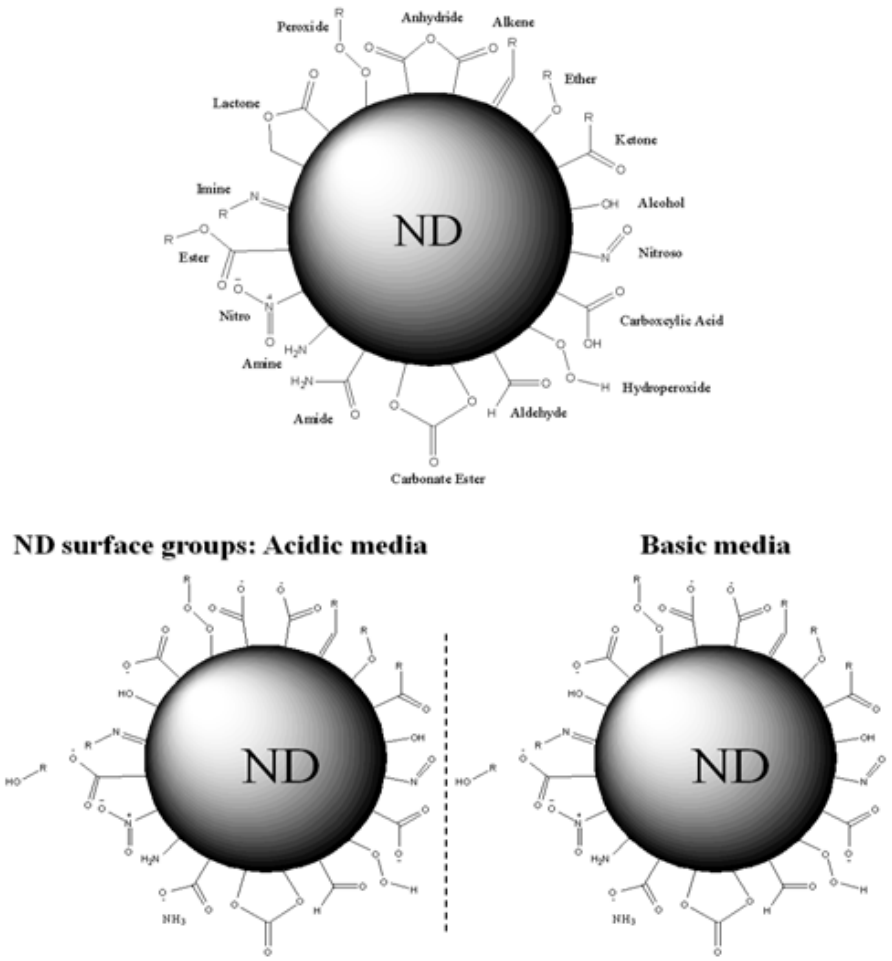

Figure 1.9. Schematics of surface groups reported for DND after different types of purification modification (**a**) and possible dissociation of these groups in acidic (HCl) and basic media (**b**) [15].

More recently, ND research has focused on chemical attachment of surface groups for biofunctionalization [40, 41]. Such a task begins by reducing the number of surface groups on the ND in order to decrease the initial number of chemical products formed after treatment. Krueger *et. al.* used borne treatment to remove oxygen containing groups, like the

readily found carboxylic acid. The result of this is a product with augmented OH surface groups (Figure 1.10) to which alkyl silanes may be attached. The presence of alkyl silanes on the ND surface allow for a covalent linkage of peptides [40]. Previously, only non-covalent interactions of the ND surface with biomolecules, like peptides, have been achieved via electrostatic interactions [42-44].

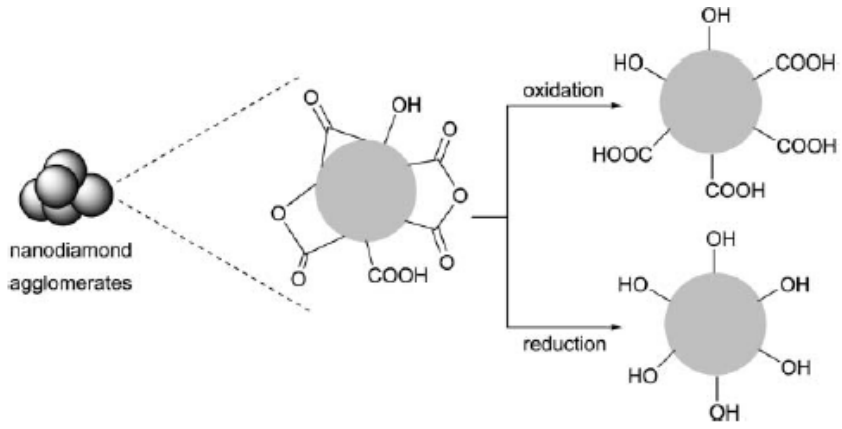

Figure 1.10. Existing functional groups on pristine detonation diamond and effects of oxidation (with O_3, conc. HNO_3, H_2SO_4 or $HClO_4$) or reduction (with BH_3-THF solution or $LiAlH_4$) [40].

In other efforts, oxidation of the ND surface was also attempted by Kruger, however, efforts failed to create surface group uniformity (Figure 1.10) and lead to only partially oxidized surfaces [40]. Today current efforts focus on saturating the ND surface with homogeneous surface groups to create uniformity for foreseen applications [31, 45, 46].

Zeta Potential

As a result of introducing NDs into liquid media, dissociation of the surface groups lead to various charges on the ND surfaces to which tightly and loosely bound counterions associate. The slip plane of the loosely bound ions can easily be read through electrophoretic measurements; this charge termed zeta potential (ZP) is imperative in sorption applications, where electrostatic interactions may dominate. Because of NDs previous chemical treatments during manufacturing and purification, NDs hold a variety of acidic and basic groups (Figure 1.9a), which gives rise to the positive and negative ZPs [14]. Moreover, the previous processing steps can create various degrees of charge on the ND, allowing the ZP measurement to also predict the colloidal stability of the ND suspension over time. Generally, values above +30 mV or below -30 mV have been termed stable [47, 48]. NDs introduced to acidic or basic media may disassociate in a manner that affects their inherent ZPs (Figure 1.9b) [16]. Though for many biological ND studies, the ND is used in rather neutral aqueous media.

A shared goal among ND researchers is classifying the origin of the surface charge on DNDs. It is widely accepted that the origin of the negative charge on the ND surface is from predominating carboxylic acid groups as a result of oxidation of ND soot using singlet oxygen in liquid media [32, 47], oxygen [50] or ozone [22] enriched air during manufacturing [16]. However, the source of the positive charge is unclear. It was formerly believed, via FTIR taken in air, that the positive charge was attributed to the protonation of amino groups in acidic media [51]. However, upon completing the same measurement in a

vacuum cuvette, an insignificant amount of amino groups were seen [16] as compared to aminated-ND signatures [52]. It is believed the spectra taken in air allowed for water moieties to obscure the true signature of the ND. Thus, one critically important topic being explored by ND researchers is exposing the source of the positive charge. Current thoughts focus on the possibility of alcoholic groups creating the positive ZPs [6, 51]. Several other theories contemplate the possibility of chromene structures, diketones, quinines, pyrone-like groups or the protons' electrostatic interactions with the π-electron system of the graphene structure to be the source of the positive charge [53, 54].

The pyrone-like structures, as illustrated in Figure 1.11, are comprised of mixtures of non-neighboring carbonyl and ether oxygen atoms at the edges of a graphene layer [55]. FTIR data helps to confirm this possibility with the presence of ketone and ether groups [16]. The stabilization of the protonated form of the pyrone-like structure through the π-electron conjugation throughout the sp^2 phase is said to be responsible for its basic nature [55, 56]. Though this model is determined for graphenes, it can be modified to DNDs with positive ZPs, since it is known that sp^2 carbon impurities may be present on the outer surface of the ND.

Recently, calculations by Barnard-Sternberg [57, 58] proposed that charge differences may exist on different facets of the ND. This model suggests there are ND facets with very strong positive electrostatic potential, where other facets may carry very strong negative electrostatic potentials and intermediate facets where the electrostatic potential falls between that of the other two. Such a model may explain self-organization of ND clusters and other

surface interactions, such as adsorption, on the ND. Similarly, binding energy calculations of different ND facets were calculated revealing different facets of the ND showing different binding energies [57]. Thus, during surface modifications it may be energetically preferential for different groups to bind to different surfaces of the ND. However, such conclusions require further investigations.

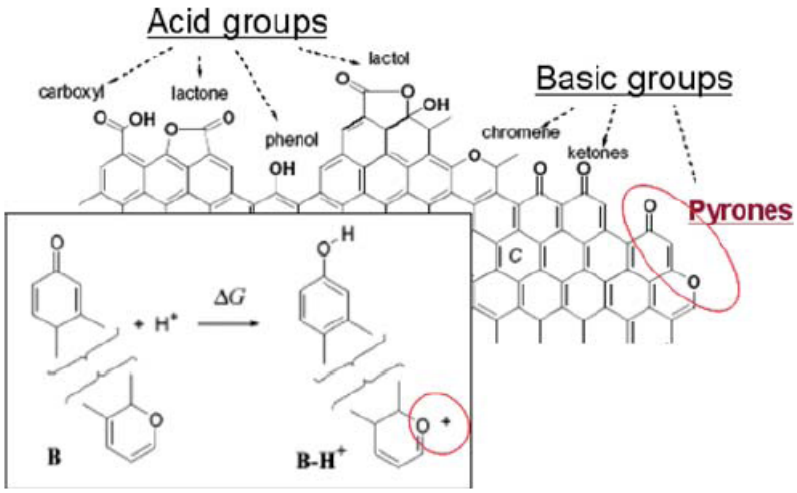

Figure 1.11. Illustration of acid and basic groups on the edge surface of graphene. Pyrones surface groups can be responsible for the positive zeta-potential of the DND possessing residual aromatic rings at the surface. The inset illustrates a model of the basicity of carbon surface attributed to pyrone-like structures [6].

1.1.4 NDs as Biomaterials

Though NDs remain to be one of the lesser known materials within the larger carbon based class, as scientists discover the advantageous properties of the NDs applications, particularly in the biomedical field, research is increasing exponentially. NDs have been proposed for use as materials in imaging [59-62], sensing [44], purification [63] and drug

delivery [64-66]. There are numerous biotechnical uses for NDs [6] and with time these applications are greatly increasing. Despite the many uses, this section will focus on bioapplications where NDs are utilized for their adsorption characteristics, wherein molecules, polymers or dyes may be fixated onto the ND surface for specific uptake, delivery or identification of substances.

Bioapplications

NDs have the ability to adsorb large amounts of substances due to their exceptionally large surface-to-volume ratios. ND's specific surface areas (SSA) are estimated to be on average 300-400 m^2/g, with the ability to extend beyond this range [20, 67]. NDs have been shown in non-specific adsorption to have a high affinity for adsorbing a variety of biological molecules [68, 69], however, with the ability to functionalize or modify the material's surface it is expected that scientists will be able to tailor the ND to adsorb specific materials. With this, NDs possess many promising qualities for new bioanalytical materials that may help advance pharmaceuticals. For example, with the growth of the pharmaceutical industry, drugs have become more potent. Accordingly, more sensitive and advanced biological assays are needed to precisely and reliably measure these molecules, which may include drugs or proteins, at lower concentrations.

Through a combination of physisorption and chemisorptions NDs were developed for cellular targeting [40, 43, 70]. In such development, negatively charged NDs were loaded with poly-L-lysine through physical adsorption mechanisms. Subsequently, the poly-L-

lysine's prominent amine groups allowed for chemical conjugation with succinimidyl conjugate dyes and proteins (Figure 1.12). In this case, it was also seen possible to chemically link free sulfhydryl groups on cytochrome c to sulfhydryl groups on one end of the heterobifunctional linker. The other end of this linker remained intact with the poly-L-lysine. It was estimated through UV-Vis, FTIR and IR spectroscopy that each 5 nm ND particle may carry up to two cytochrome c molecules [43].

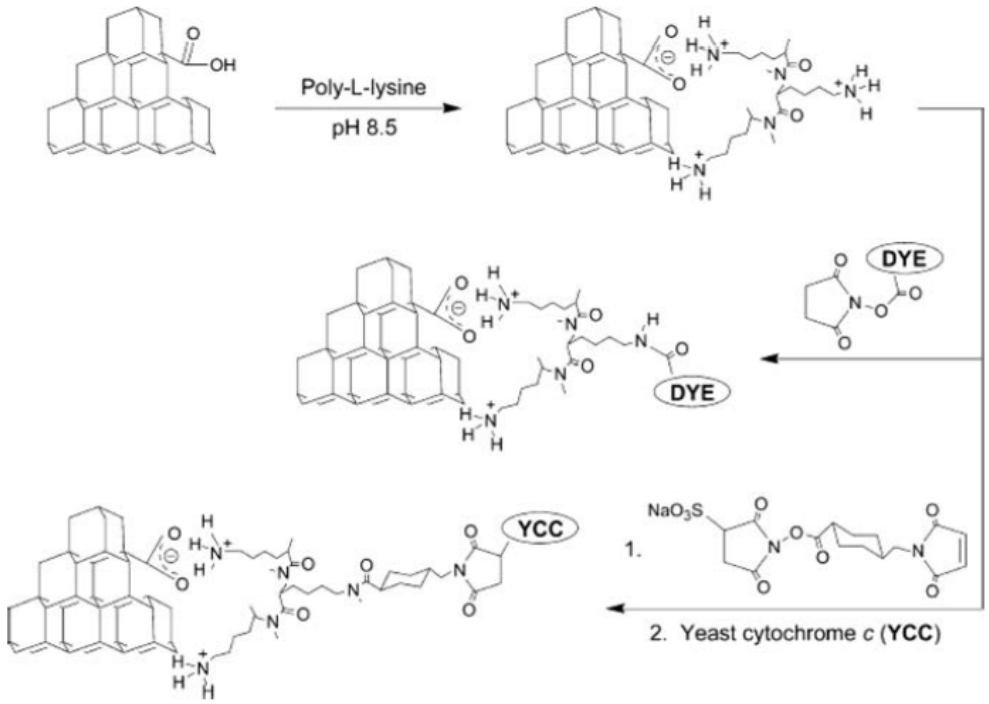

Figure 1.12. A schematic representation for the combination of indirect-direct conjugation of a dye and protein to ND surface. Poly-L-lysine is physisorbed onto the ND surface by charge-charge interactions, thus providing amine surface groups on the ND for conjugation to either a NHS-dye or -protein conjugate [43].

Currently, methods for direct chemical attachment of molecules to functionalized NDs are being recorded. One of the first cases of direct chemical attachment was demonstrated by Krueger *et al*. where a peptide was conjugated onto silanized ND [70]. Similarly, covalent attachment of the protein streptavidin was achieved on biotinylated NDs [52, 71]. The advantage of chemical attachment is the stronger, more reliable bond formed over that of more typical physical, electrostatic bonds. Additionally, chemical attachment of protein-specific probes onto the ND surface allows for targeting the adsorption of specific proteins within a biological matrix. Consequently, collection of the biomolecule can be achieved using electrophoresis to quantify the amount of protein within a biological sample.

In addition to the protein-ND conjugates seen above, NDs have also been shown to adsorb growth hormone [72], insulin [73], and a variety of enzymes, such as lysozyme [69, 74, 75]. It was seen that the attachment of the lysozyme enzyme creates potential applications for NDs as antibacterial coatings on implants. Lysozyme protein lyses bacterial cells' walls via hydrolysis of the sulfur backbone [76]. Studies using 100 nm carboxylated NDs electrostatically conjugated with lysozyme were shown to attach to *Escherichia coli* bacteria as opposed to the lysozyme-free NDs [75]. Such attachment of the conjugated ND to the bacteria was shown to disrupt the *E. coli's* outer membrane and as a result significantly decrease the number of bacterial colonies [76]. Supplementary studies using NDs within a sol-gel matrix to form epoxy-silicate coatings show promising results for microbial reduction against various fungi [77].

In an unrelated application the physical adsorption of insulin onto NDs was completed to assess time dependent drug delivery of the insulin by the ND substrate [73]. The key property in the ND's adsorption-desorption system is the role of electrostatic interactions between the ND's anionic end groups (COO-) and the polypeptide's protonated amino groups ($-NH_3+$). While attraction of opposite charges controls the initial interaction, the controlled release of insulin is created through pH alterations of the surrounding environment. As the pH of the solution media is increased through additions of NaOH the overall charge of the insulin becomes more negative thereby detracting itself from the ND. The amount of desorption was shown to be proportional with the increased pH of the surrounding solution. While the bulk of the release (31.3 %) was seen in the first day, slow release of the drug was observed over the remaining days to reach 45.8 % desorption at Day 5. While time-dependent release is a key concept in drug delivery, this study begins to show a good basis for ND development in pharmaceutical implants [73].

NDs are being increasingly considered as drug delivery agents. One of the largest media frenzies with ND particles came about with research showing the chemotherapy drugs, doxyrubin hydrochloride (DOX) and dexamethasone (Dex) can be attached to DNDs for effective, direct delivery of anti-cancer medications [64, 78, 79]. The drugs were electrostatically loaded onto 2- 8 nm NDs as well as 50 nm ND aggregates; with the help of NaCl higher loading capacities of the DOX could be achieved (< 0.5 wt. % versus 10 wt. % with salt). The introduction of Cl- ions helps to mediate adsorption by shifting the dominating repulsive interactions between the DOX-DOX molecules by balancing the

cations with Cl- ions to move to a more unified DOX-ND complex. Upon attachment to the ND substrate, DOX is found on the surface of the ND aggregate as well as in the internal pores of the aggregate (Figure 1.13). The distribution allows for rapid delivery of the surface bound molecules and slower release of the DOX within the ND's aggregates [79].

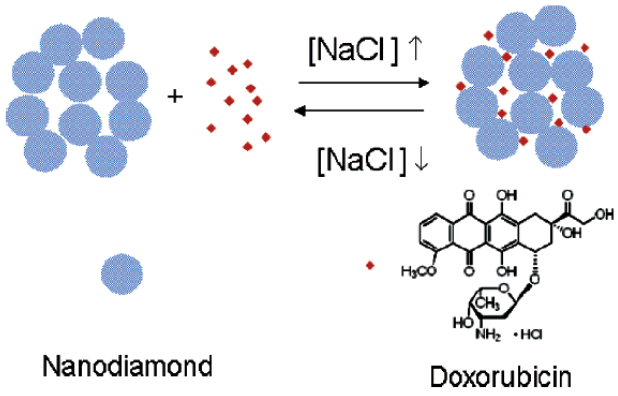

Figure 1.13. Schematic drawing of NaCl-mediated loading and release of doxorubicin hydrochloride. The addition of the salt induces functionalization of the drug onto the nanodiamond aggregate surface. Salt removal drives drug release. This mild switching process is amenable toward medically relevant processes [79].

Just as the addition of salt drives the binding of the drug on the ND surface, the removal of NaCl from the system triggers release of the drug from the substrate. Thus, controlled DOX uptake and release are determined through regulating the Cl- ion concentration within media [79]. It is important to control when and how much of the drug is released as DOX, as an apoptosis inducting drug should have little contact with normal cells and primary contact with malignant cells. This notion introduces the possibilities of ND's

cytotoxicity not only of this particular DOX-ND system, but all systems or applications where NDs are present.

Biocompatibility

Nanotoxicology has spent much of its focus in recent years observing the effects of carbon based fullerenes [80] and carbon nanotubes [81], with results showing signs of oxidative stress for both carbon materials, unless modifications to improve biocompatibility and toxicity are completed [82, 83]. This provides an opportunity for other carbon based alternatives, like DNDs. However, it is only necessary to speculate and explore the biocompatibility and toxicity of these ND materials. Though NDs, like diamond in general, appears to be a promising biomaterial, largely due to its chemical and biological stability, it has been recognized that materials which have good biocompatibility in their bulk phase may not retain this property when in their nano-form.

The aforementioned applications address the use of NDs in biological environments where there is direct interaction with cells and tissue. Accordingly, several biocompatibility assays have been underway to help identify how NDs are interacting and internalized by cells, as well as identifying the exit path the materials take to clear the body. Figure 1.14 addresses several ways that NDs may interact with mammalian cells to cause possible adverse interactions and hinder biocompatibility. In the following section various research efforts will briefly be addressed to help identify cell viability, immune response and the factors which affect these concerns.

The body's initial reaction to a foreign material's, like NDs, cause it to trigger a cascade of immune responses. Immune response, while complicated, can simply be described as the body's way of clearing unfamiliar organisms and objects from the body through the use of leukocytes, i.e., macrophages, monocytes, neutrophils, etc. Because these are some of the first cells that engulf ND they are usually studied first in biocompatibility studies.

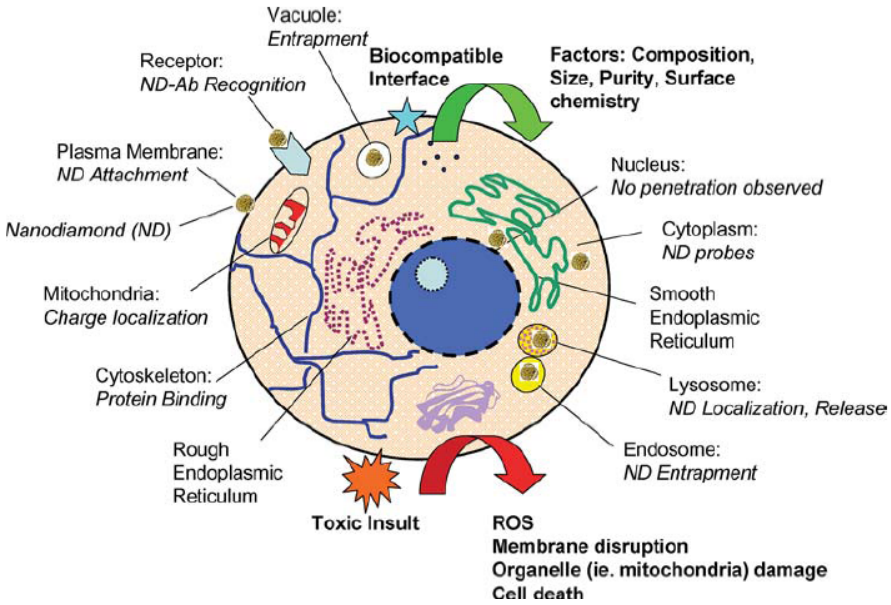

Figure 1.14. Schematic representation of a mammalian cell showing some possible interactions nanodiamond (ND) particles including biomolecular binding interactions, entrapment within organelles, and localization to areas within the cell resulting in biocompatibility or unforeseen toxic insults [6, 84].

One of the most descriptive ways of monitoring cell health after exposure to foreign materials is the production of reactive oxygen species (ROS). Though ROS are a normal by-product of cellular metabolism under stress inducing conditions, ROS levels can increase

drastically, in turn, causing substantial damage to the cell structure. This imbalance between ROS production and the ability for the cell to repair the resulting damage leads to conditions of oxidative stress where apoptosis, under conditions of moderate oxidation, or necrosis, with more intense stress, may occur [85, 86]. Thus, monitoring the ROS is one of the most common ways of determining biocompatibility of a material. Studies by Schrand *et. al*. [87] investigated the ROS of neuroblastoma cells and alveolar macrophages with NDs as well as with other more common carbon materials, single-wall and multi-wall carbon nanotubes (SWNT and MWNT) and carbon black (CB) (Figure 1.15).

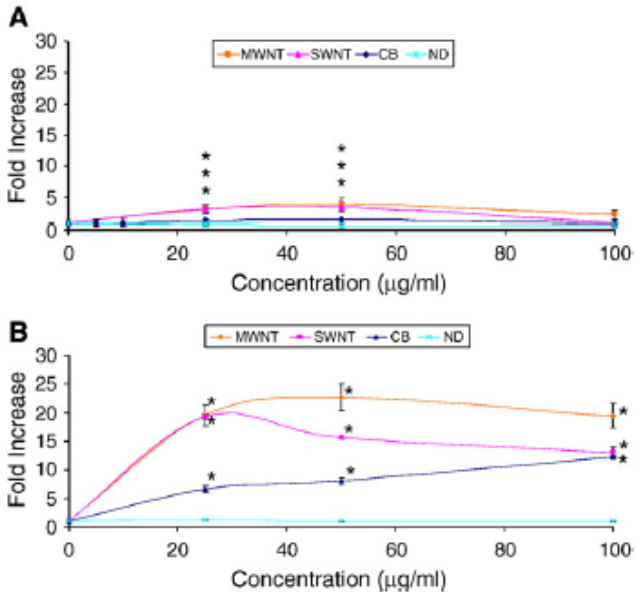

Figure 1.15. Generation of reactive oxygen species (ROS) determined by the hydrolysis of DCFH-DA after 24 hr of incubation with various carbon nanomaterials in (A) neuroblastoma cells and (B) macrophages. Note that macrophages produce approximately five times the ROS when exposed to the same nanomaterials at the same concentrations as neuroblastoma cells. All values were significantly different from the control ($p<0.05$) with the exception of the NDs (A, B) and 100 μg/ml concentrations in (A) [87].

In the study it was determined that the largest ROS response in both cell lines came from carbon nanotubes, particularly MWNTs followed by SWNTs due to the higher Fe content in the MWNTs over the SWNTs [88, 89]. Likewise, CB also produced more ROS than NDs; intriguingly, NDs showed no ROS response in either cell line, suggesting that ROS production may be triggered by impurity content, like Fe, on the carbon surface.

Comparisons of both cell types with non-diamond materials showed a large difference in ROS depending on the cells used. Macrophages generated up to five times the amount of ROS as compared to neuroblastoma cells after being exposed to the same carbon species. This result may be explained by the role each cell plays in immune responses and how they uptake the materials (phagocytosis versus endocytosis) [87]. For example, macrophages are programmed to internalize foreign structures, as opposed to neuroblastoma cells, and as a result, naturally generate higher levels ROS to eradicate bacteria that may be present [88].

One test that may be more popular than ROS identification in evaluating biocompatibility is the MTT assay, which predicts cell viability. The MTT assay is a colorimetric evaluation for measuring the enzymatic activity in the reduction of MTT dye, more properly identified as 3-(4,5-Dimethylthiazol-2-yl)-2,5-diphenyltetrazolium bromide, thereby turning the originally yellow dye purple. The reduction of MTT occurs only when reeducates enzymes are active; consequently the tests exclude the coloration of dead cells. Thus, the MTT assay is a measure or the living or viable cells [91, 92]. Schrand *et al.* conducted the MTT assay in addition to the ROS evaluation of carbon based nanomaterials.

In this study cadmium oxide (CdO) was chosen as a positive control, whereas CB remained the negative control. Trends were similar to those seen in the ROS studies; NDs were seen as having the highest biocompatibility of all the materials (Figure 1.16). Though dose-dependent viability was seen with non-diamond materials, NDs showed no significant cell viability changes with increased doses. Following NDs, CB shows to have the next highest viability followed by MWNT, SWNTs and, finally, CdO. Unlike other nanomaterials, NDs also showed no difference in cell viability between the lung and neuronal cell lines [87].

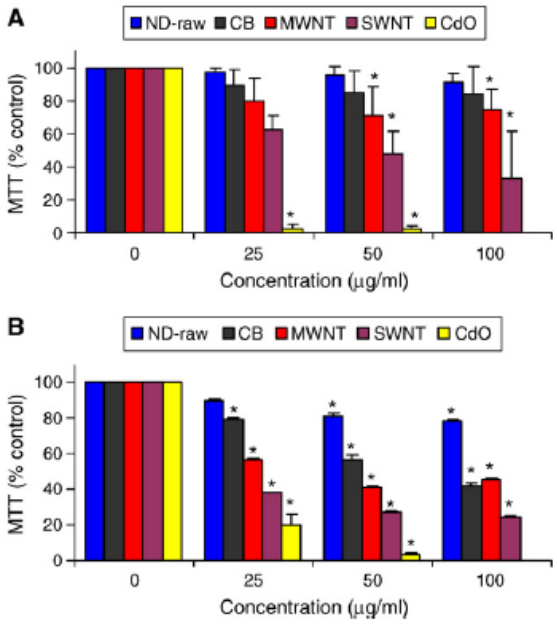

Figure 1.16. Cytotoxicity evaluation after 24 hr of incubation with various nanocarbons showing differential toxicity due to factors such as nanomaterial composition, size, or shape in (A) neuroblastoma cells or (B) macrophages. Note the similar trends in biocompatibility ND>CB>MWNT>SWNT>CdO for both neuroblastoma cells and macrophages, with the latter being more sensitive to the carbon nanomaterials. Values that were significantly different from the control ($p<0.05$) are denoted with asterisks (*) [87].

Additional methods to monitor cellular effects of nanoparticles have also been identified, these include alternative tetrazolium dyes, such as XTT, MTS and WSTs, trypan blue dye exclusion, propidium iodide staining, neutral red (NR) assay, thymadine uptake, morphological examinations, cell counts, cellular permeability breakdown (LDH assay), chemiluminescent luminole reaction (CLR) measurement, genetic analyses, protein expression, glutathione alterations, pro-inflammatory cytokine activation and mitochondrial membrane permeability (MMP, in which Schrand also showed no membrane leakage in the presence of NDs) [6, 92-94].

Whereas these studies show ND biocompatibility in various cell lines to be encouraging, blood cell studies show contradictory results where damage to leukocytes and erythrocytes was observed [95-100]. Blood studies hold significance in developing further biomaterials as hemolysis, the destruction of erythrocytes and the resulting hemoglobin release, must be evaluated. Puzyr *et. al*. indicated that NDs having 90 minute incubation times with whole human blood samples changed the reaction kinetics for active oxygen generation (AOG), which was directly related to cell death. Within this 90 minute time period, it was shown that 3 to 50 % of the erythrocytes hemolyze after the addition of the NDs. However, the effect could be lessened by pre-coating the NDs' surface with donor plasma blood proteins [95].

While up to this point only *in vitro* studies have been summarized, *in vivo* studies have even greater significance in understanding how NDs will affect humans. Though *in vivo* studies should help close the gap between simplistic *in vitro* studies and clinical trials, often

times, as in the case or carbon nanotubes, results can be inconsistent in their conclusions [80, 83, 87, 101-104]. Animal studies using white mice substituted their water for ND hydrosols of 0.002 to 0.05 wt. % over three to six months; the total concentration administered during sacrifice was between 16 and 450 mg per mouse [101]. Results showed neither deaths nor changes in weight of the liver, lung, heart, kidneys and pancreas [100, 101], nor did it interrupt the reproductive capabilities of the first three generations [96, 97, 101]. However, when blood cells and blood plasma chemistry were examined (Figure 1.17), there was an observed decrease in cholesterol content and a noteworthy decrease in bilirubin content. Conversely, this study showed elevated iron content after 1 month and protein concentrations in months 3 through 6 [6].

In this study, leukocyte content increased in the first month for 0.002 and 0.01 wt. % concentrations, but then declined over the next 6 months to normal levels, despite the sharp increase in the 0.05 wt. % sample at 2 months. It was hypothesized that this elevation was due to the non-specific immune reaction between the orally administered ND hydrosol and macrophages present in the gastrointestinal (GI) tract [6, 96, 100].

In intramuscular injections of rats, it was seen that the NDs localized as gelatinous clots at the injection sites with large amounts of proteins on their surface. Regardless, no signs of severe inflammation were detected [6, 96, 100]. The estimated median lethal dose (LD_{50}) in rats was confirmed at concentrations over 7000 mg/kg, whereas sodium chloride LD_{50} levels were of less than half that of the ND hydrosols [105]. Collectively, the experiments demonstrated adequate biocompatibility of ND particles.

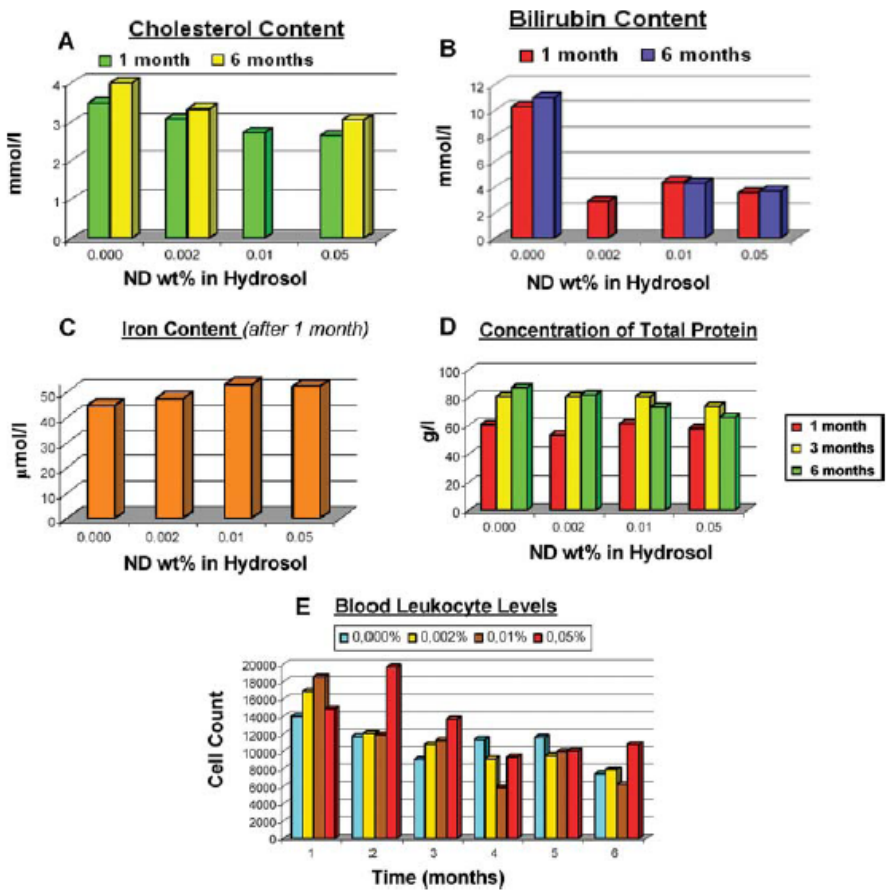

Figure 1.17. Dynamics of blood chemistry (A-D) and blood leukocyte levels (E) in experimental mice as a function of ND hydrosol concentration and time [6].

In each of the previous studies the effect of ND concentration was evaluated with little difference in its results. Studies have shown that carboxylated NDs (cNDs) of 5 and 100 nm were shown to have little to no cytotoxicity at concentrations up to 1000 µg/mL [106]. Nevertheless, other factors, aside from concentration, have been identified that may influence the biocompatibility of NDs. Additional factors include particle size, surface treatments and impurity content. Size related studies of NDs ranging from 2 to 100 nm, and produced under

a variety of different conditions, were all shown to be biocompatible [6]. Conversely, studies published by Liu *et. al*. found a slight decrease in cell viability in 5 nm NDs as compared to their larger 100 nm counterparts [107]. One of the reasons for this difference could be contributed to the smaller 5 nm ND having approximately 15 to 20 % of its carbon atoms located at the particles surface [20, 27], thereby possessing different properties than the larger 100 nm aggregate [108]. Under the same principle, micron sized NDs showed high biocompatibility with no effect of cytotoxicity or inflammatory response [109-111].

It is speculated, however, that surface chemistries and impurity content may cause a large inflammatory and cytotoxic response. One limitation in many of the biocompatibility studies is the lack of detail reported in the manufacturing and subsequent processing techniques of the NDs. As mentioned previously, DNDs show impurity contents associated with their manufacturing technique. In a study using ND powders, with elemental impurities of 0.05 wt. % Al, 0.05 wt. % Fe, 0.15 wt. % Si and 1.00 wt. % Zr, blood compatibility was analyzed. In this case, the low impurity concentrations on the NDs were not associated with hemolysis or cytotoxicity [110]. However, NDs which typically exhibit higher impurity contents may exhibit dissimilar results. For this reason, it is recognized that for NDs to be biocompatible they should go through a rigid purification process. This purification step is one reason why NDs may perform better than other carbon based materials.

In a previously discussed study [87] comparing NDs' cell viability to other carbon based materials, such as SWNT, MWNT and CB, NDs were pretreated with either strong acids or bases. Results showed no adverse affects as a result of either ND treatment as

evaluated by the 24 hour MTT assay on neuroblastoma and alveolar macrophages cell lines. However, with CNTs it was seen that the greatest ROS generation came from materials with the highest Fe impurity presence, due to the oxidative stress on the cell. This study follows previous studies on CNTs where toxicity and the resulting ROS production is related to impurity contents, like Fe, further stressing the importance of ND purification steps. Another reason for NDs' superior biocompatibility as compared to CNTs is due to NDs' structural configurations. The high aspect ratio of the CNTs allow them to easily penetrate cells [83, 112], which is advantageous for delivering membrane impermeable drugs, but may also give rise to the CNT's higher cytotoxicity.

The choice of cell lines may also show differences in biocompatibility. As seen with ND and CNT studies, completed by Schrand *et. al*. [87], different cell lines showed variations in the amount of material internalized, with macrophages internalizing more nanocarbons. To enhance these results, additional studies were completed to identify where the NDs are localized once uptake has occurred. NDs treated with the fluorescent dye rhodamine (T-NDs), were observed in both animal and human neuroblastoma cell lines [6, 84]. T-ND uptake did not lead to changes in the cells morphology, but showed internalization of the T-NDs increases with time. At 1 to 6 hours T-NDs were localized at endosomes and at lysosomes within 3 to 6 hours. After 24 hours aggregation of T-NDs in the cytoplasm was observed, signifying an endocytotic uptake mechanism. Other T-NDs were seen in the cell's vacuole (Figure 1.18) [6].

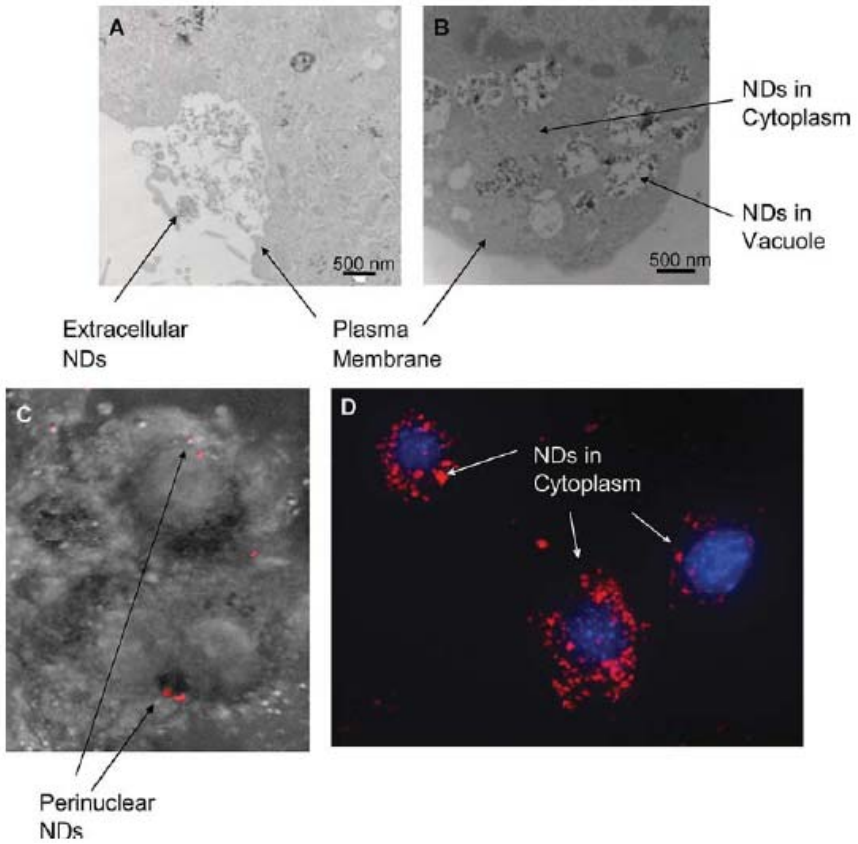

Figure 1.18. Internalization and localization of NDs in neuroblastoma (N2A) cells. (A, B) TEM images of thin sections of N2A showing NDs interfacing with the plasma membrane as well as internalized into the cytoplasm and vacuoles. (C, D) Confocal images of N2A cells incubated with T-ND taken with a 60x lens. (C) Overlay of transmitted light and rhodamine signal after incubated with 50 μg/mL of T-ND (*red*) for 1 hour showing perinuclear localization. (D) Demonstration of T-ND (*red*) accumulation over 24 hours into the cytoplasm after incubation with 25 μg/mL of T-ND and counterstaining of nuclei with Hoechst dye (*blue*). T-ND is a TAMRA-ND conjugate supplied by ITC, Inc [6].

A second study by Choa *et. al*. confirms the internalization of NDs inside the cytoplasm by using A549 human lung adenocarcinoma cells [106]. The experiments used carboxylated NDs. In their natural form, NDs exhibit fluorescent abilities, due to nitrogen vacancy (N-V) defects [60, 113, 114], thus, pre-labeling with florescent dyes could be eliminated. Interestingly, NDs which did not penetrate the cell were shown to adhere to the cells membrane even after repeated washing with PBS solution. This interaction is likely due to the interaction of COO^- groups found on the carboxylated NDs and the NH_3^+ groups on the outside to the cell's exterior. Penetration and localization of the NDs inside the cytoplasm were demonstrated through Raman and fluorescence experiments (Figure 1.19) [106].

While many studies are consistent in saying internalized NDs localize within the cytoplasm and do not permeate the nucleus [60-62, 84], there still remain many unanswered questions in fully determining if these materials are truly safe. At the cellular level, the pathways for internalization, degradation, and clearing the body are still unknown. Studies show NDs were not degraded by the cells, which bring up inquiries of uncertain whether internalized NDs will be released from the cell or cause cell death after long-term exposure [6]. With the natural ability for the human body to clear dead cells and some foreign matter, it the belief that small amounts of NDs may also be cleared through the natural cellular renewal process, without causing generation of ROS or other harmful side-effects [6, 15].

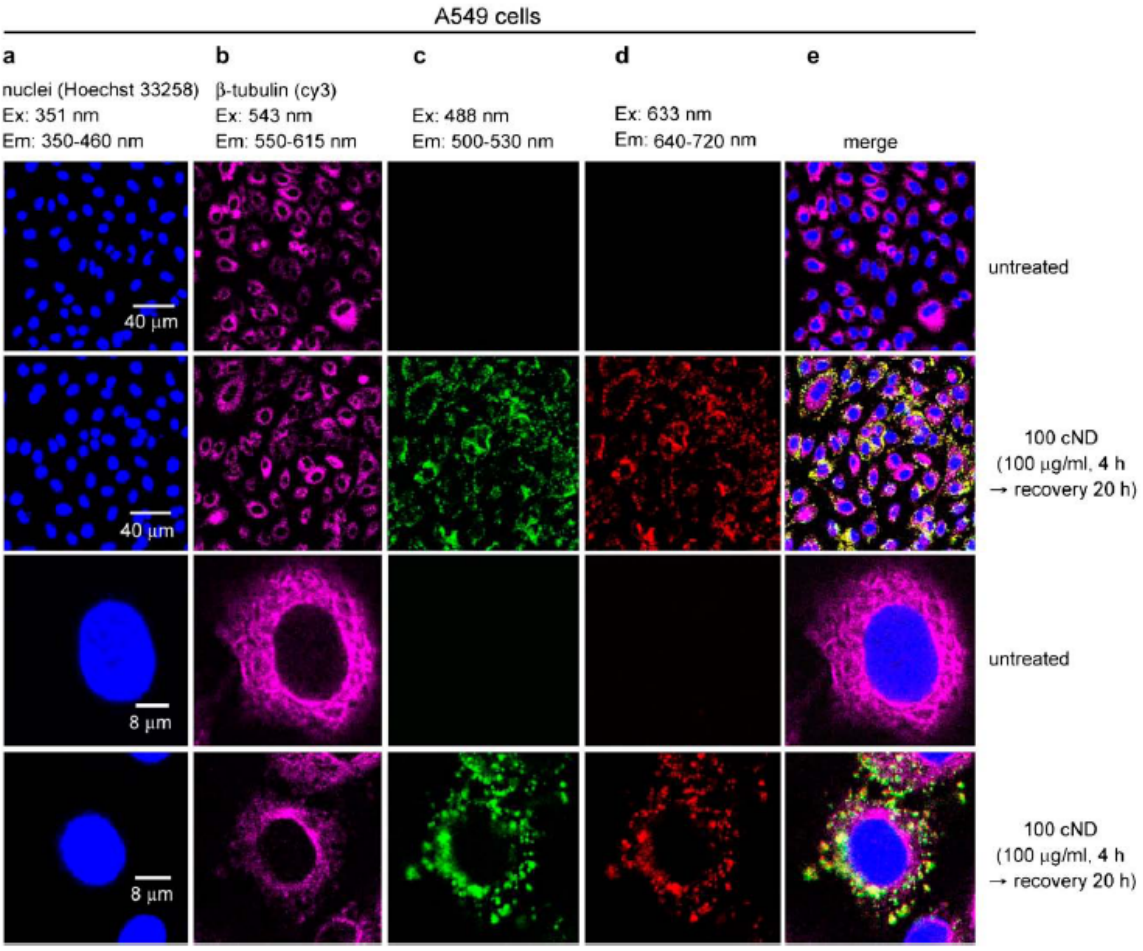

Figure 1.19. Confocal fluorescence images of an A549 cell and carboxylated 100 nm diamond. (a) The cell nuclei were dyed with Hoechst 33258 to reveal the position of the nucleus. (b) The cell tissue was dyed with anti-b-tubulin (Cy3) to reflect the cytoskeleton of the cells. (c) The cells were interacted with 100-nm cNDs and excited with 488-nm wavelength, and the emission was collected in the range of 500–530 nm. (d) Same as in c but exciting wavelength was 633 nm and emission was collected in the range 640–720 nm. (e) Merging the images of a–d [106].

1.2 Mycotoxin Enterosorbents

Mycotoxins are a group of secondary metabolites produced by fungi, which can grow on virtually any organic matter. Mycotoxins have been brought to worldwide attention within the past several decades due to their ability to contaminate foodstuff, bringing about economic setbacks [115, 116] and health hazards [117-120]. There are approximately 300 fungal metabolites, with more likely to be discovered, that have been identified with links to toxicity for humans and animals [121]. It has been reported that 25 % of the worlds cereal has been contaminated with mycotoxins [122, 123], causing it to enter the food chain through direct ingestion or consumption of an infected animal's by-products, such as its meat, milk and eggs [119, 123-125]. Direct and indirect consumption of mycotoxins has been linked to cancer [120, 126], mycotoxicosis, and, in extreme cases, death [127]. The variable degree of toxicity is dependent on the species that ingests the contaminated grains, due to differences in liver detoxification systems, age, sex, genetic makeup, physiological state or nutritional factors, and the type and amount of mycotoxin ingested [128]. While different mycotoxins have unique toxic effects, in general they are associated with strong suspicions of carcinogenicity, genotoxicity, teratogenicity, nephrotoxicity, hepatotoxicity, reproductive disorders, immunosuppression and, in some cases, incurable disease [123, 129]. This section will focus on two well-known mycotoxins, aflatoxin B1 (AfB1) and ochratoxin A (OTA).

1.2.1. Aflatoxin

Of the several types of mycotoxins, aflatoxin (Af) is the most widely studied and is classified as one the most potent naturally occurring compounds [130]. Af is most prominently produced by *Aspergillus flavus (A. flavus)* and *A. parasiticus* though other strains, such as *A. nominus, A. tamarii* and *A. pseudotamarii,* have been shown to produce aflatoxins [130-133]. These strains produce 18 types of Af, including AfB1, AfB2, AfG1, AfG2, and metabolized forms, AfM1 and AfM2. Under the entire mycotoxins class, AfB1 is the most common and most toxic [134]. AfB1 has been known to contaminate many crops; those which are frequently infected include cereals, tree nuts, oilseeds and spices. Under favorable environmental conditions, consisting of warm settings (30 to 35 degrees C) with high humidity (water activity of 0.90 to 0.99) fungus producing Af flourishes [135, 136]. Situations that place stress on the plant, such as drought, insect damage, or malnourishment, are known to host the funguses producing Af and allow them to thrive. Once Af is formed it remains stable and will not degrade during normal storage or milling processes [137]. In fact, contaminated peanut meal lead to the death of thousands of turkeys in the United Kingdom in the early 1960's, and ultimately, led to the identification of aflatoxins [138, 139] Since then, it has been found that aflatoxins are potent hepatotoxins, that lead to hepatocellular carcinoma (see Chapter 8) [140] and aflatoxicosis, a poisoning with symptoms that may include hemorrhaging, vomiting, weight reduction and suppression of the immune system [141].

Due to its severe health hazards, the World Health Organization (WHO) declared, in 1987 that Af should be classified as a group 1 carcinogen. Based on this declaration, the WHO and Food and Agriculture Organization (FAO) placed stringent regulations on the amount of aflatoxin, specifically AfB1, that may be present in food. The organization modestly set the upper limit at 30 μg of AfB1 per kg of food [142]. However, in 1998, The Commission of European Communities lowered this to 2 μg/kg for nuts, groundnuts, cereals and dried fruit that are intended for direct human consumption [143]. Similarly, other countries have lowered their tolerance levels for AfB1 in foodstuff. The maximum acceptable levels for Af are shown for select countries in Table 1.3. The United States, not shown, has lowered their maximum level to 20 μg/kg [135, 144].

Table 1.3. A selection of maximum tolerated levels of aflatoxin B1 in food (μg/kg), as stated by the Food and Agriculture Organization [142].

Country	Max. level ($\mu g\ kg^{-1}$)	Products
Argentina	0	Groundnuts, maize and products
Brazil	15	All foodstuffs
China	10	Rice and edible oils
Czech Republic	5	All foods
Hungary	5	All foods
India	30	All foods
Japan	10	All foods
Nigeria	20	All foods
Poland	0	All foods
South Africa	5	All foods
Zimbabwe	5	Foods

While many other countries have drastically lowered their aflatoxin tolerance levels, some counties, such as India, have remained at the predetermined level. Higher tolerance levels are expected in underdeveloped nations, where the danger of malnutrition outweighs the threat of aflatoxin; such rationalization was used in setting the original maximum acceptable level [145]. Even with these regulations, in countries where food is scarce, Af contaminated crops are often still consumed, as it is not feasible to destroy all infected foodstuff. Such situations require a method to decontaminate infected crops, thereby, eradicating or neutralizing the effect of Af.

There are three approaches to avoiding the detrimental effects of aflatoxin. These include (1) prevention of aflatoxin in pre-harvesting or in storage, (2) detoxification of aflatoxin containing harvests and (3) inhibiting the absorption of Af inside the GI tract [134]. For any of these processes to be successful they must be carried out in a realistic and economical manner. The FAO has stated that for a decontamination method to be suitable it must:

1. Destroy, inactivate or remove aflatoxins, including spores of the fungus that could proliferate and produce new toxins under favorable conditions;

2. Neither produce nor leave toxic and/or carcinogenic/mutagenic residues in the final products or in the byproducts of animals which have been fed the decontaminated feeds;

3. Not significantly alter the important technologic properties and sensory of the starting material;

4. It should preserve, as much as possible, the nutritive value and palatability of the starting material [146-149]

The most effective way of preventing aflatoxin infestation at the pre-harvesting stage is by using ideal agronomic practices in the pre-harvesting stage, some of which include using healthy seeds, adequate irrigation, preventing insect damage, and proper storage conditions [150]. While these attempts are ideal, it is next to impossible to prevent all aflatoxin formation. Thus, other pre-harvesting techniques are used, such as breeding aflatoxin resistant or tolerant crops [151, 152] or genetic engineering. After identifying genes and enzymes responsible for aflatoxin production, the genes, which encode resistant traits, can be transferred to crops to discourage the toxin's synthesis and produce crop resistant varieties [153]. However, since the resistance to fungal growth has shown to be a result of uncontrollable factors, including biochemical, physical and environmental factors, as well as storing conditions, Af may still form [134].

Attempts to control aflatoxin contamination at this pre-harvesting stage are plausible, but not yet achievable. Consequently, prospective tactics involve destroying the molecule once a fungal attack has occurred. Successful treatments to degrade the AfB1 molecule should take place by removing the double bond of the terminal furan ring or opening the lactone ring. Opening the lactone ring alters the ability of the terminal furan ring to bind to DNA or proteins [154] (discussed further in Chapter 8). The chemical structure of AfB1 can be seen in Figure 1.20.

To induce these structural changes one may use biological or enzymatic treatments, supply energy absorbable by the molecule, or use chemicals to eliminate or obstruct the active sites. In doing so, the toxic effect of AfB1 may be neutralized or lessened. Physical

methods of removal involve mechanical separation of tainted portions and destruction of the molecule by heating [155], cooking [156, 157], roasting [158] and radiation [159, 160]. The results of these methods vary in their effectiveness; however, none of these procedures are able to fully remove Af from the crop. One reason for the ineffectiveness is due to AfB1's hardy nature and thermal stability [161, 162], therefore, chemical methods are explored.

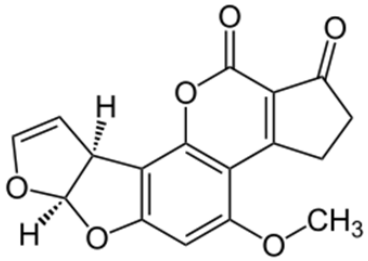

Figure 1.20. Chemical Structure of aflatoxin B1.

Several chemical procedures have been reported, these methods include the use of ammonia [163], sodium bisulfite, calcium hydroxide, formaldehyde [148], urea, sodium hypochlorite [164, 165] and ozone [133]. Ozone, a fairly recent method of treating AfB1 [166-168], is promising as it is also associated with low economical costs [169]. Unlike many of the previous chemical treatments, ozonation neither compromises the nutritional content of the produce [170], nor does it leave behind potentially toxic reaction products or residues [171, 172]. Ozone treatment can be utilized in either a gaseous phase or in a water solution to destroy mycotoxins. Aqueous ozone solutions, with only a 2 % concentration, have been shown to fully degrade AfB1, and furthermore, do so within 5 minutes [166]. Several studies, including maize [167], red peppers [168] and figs [173] show the efficacy this treatment by

reducing AfB1 contents up to approximately 93 %. The extent of AfB1 degraded depends on the treatment time, concentration of ozone used, and the moisture in the raw materials being handled [168, 173].

Due to lingering concerns of remaining residues and nutritional decomposition in chemical treatments, biological approaches to eradicate Af are also being considered. Microorganisms, such as bacteria, yeasts, molds and algae have all been shown to break down AfB1. For example, the bacteria, *Flavobacterium aurantiacum*, showed irreversible removal of AfB1 from solution [174]. The outcome was dependent on temperature, pH and population of the bacterial cells [175], and while the removal rate of living cells is higher, dead cells were also shown to adsorb some AfB1 [134], though, the presence of copper and zinc trace metal ions inhibited the degradation of Af [174, 176].

Similarly, probiotic bacterial strains *Lactobacillus acidophilus (L. acidophilus), L. bulgaricus, L. planatarum* [177] and *L. rhamnosus* strain GG [178] were shown to bind or degrade Af and/or prevent mold growth. More on these bacterial strains and their ability to adsorb AfB1 are seen in Chapter 8. Some bacterial strains, such as *Flavobacterium odoratum*, do not adsorb AfB1 and instead suppress its growth through biocompetitive inhibition [179]. Interestingly, it was also found that molds that are able to produce Af are also capable of destroying them [180]. While naturally occurring organisms, as those listed above, may destroy aflatoxin, there are concerns that the destruction process may release compounds that are equally or more virulent. For this reason, further research is needed

[134]. A summary of several physical, chemical and biological methods to destroy AfB1 are discussed in Table 1.4.

Table 1.4. Some Commonly used physical, chemical and biological methods for aflatoxin [134].

Methods	Condition	Destruction (%)	Authors	Comments
Physical				
Sunlight	Bright sunlight effective on liquid commodity	99	Shantha and Sreenivasamurthy(1977)	Not very much effective and dereriorates organoleptic qualities in most of the cases. No single process can detoxify all the toxin in liquid as well as solid infected commodity.
UV light	Chloroform solution of groundnut oil	45	------do------	
Microwave	6 KW, 4 min	95	Staron et al (1980)	
Autoclaving	121 °C, 4 hr	95	Coomes et al (1966)	
Cooking	Steaming/ puffing	50	Rehana and Basappa (1990)	
Roasting	180 °C, 30 min	80	Lee et al (1968)	
Pasteurization	80 °C, 45 sec	64	Purchase et al (1972)	
Dry heat	250 °C	Partial	Peers and Linsell (1975)	
Solvents	Specific for each solvent	80- 95	Aibara and Yano (1977)	
Chemical				Harmful chemical residues may be left after the detoxification and also more toxic compounds may be generated by the reaction process.
H_2O_2	6% H_2O_2, 30 min, 80 °C, alkaline pH	97	Sreenivasamurthy et al (1967)	
Ozone	2 h, 100°C, 22% moisture	100	Dwarakanath et al (1968)	
Ammonia	40 psig, 100°C, 4% NH_4OH, 30 min	99	Park et al (1984)	
Urea+ Urease	20% Urea, 2% soyflour, sunlight 14 h	85	Shantha et al (1986)	
Na-hypochlorite	15 mg Cl_2 gas per 100 mg AFB_1	100	Sen et al (1988)	
Na-bisulphite	0.4%, 5 min	45	Doyle et al (1982)	
Biological				It is expensive, if breeding of resistant varieties are tried they are time consuming and also infection of some more fungi and bacteria are not expected.
F. aurantiacum NRRL B 184	Aqueous reaction medium	100	Ciegler et al (1966)	
Tetrahymena pyriformis	Liquid reaction medium	Partial	Robertson (1970) H. K. Chaurasia (1995)	
Bacillus sp.	--------do--------			
Rhizopus sp.	--------do--------		Cole et al (1972)	

Aflatoxin Enterosorbents

While the formation of aflatoxin is unavoidable, subsequent methods to decontaminate crops and destroy the aflatoxin molecule must take place. The above methods discussed destruction of the AfB1 molecule on a large scale. This approach, while ideal, is not yet achievable, economical or time-effective. The most recent approach uses non-

nutritive materials, termed enterosorbents, which bind the toxins *in vivo* and reduce absorption into the body. This approach is currently deemed the most practical and promising as it safe, inexpensive, and can easily be administered as a feed or water additive [96, 181, 182]. For the adsorbent to be effective it must possess certain traits. These include:

1) Having high adsorption affinity for AfB1, as to form a strong bond with the molecule and prevent desorption in latter parts of the GI tract;

2) Have a high capacity for AfB1 to prevent saturation of the substrate and/or allowing less of the substrate to be administered [119, 183];

3) Be harmless or nontoxic to the body;

4) Selectively bind the aflatoxin molecule, as to not adsorb essential vitamins and minerals.

Several materials have been considered as substrates for AfB1 adsorption with many of them being commercially obtainable throughout the world [184]. However, not all adsorbents perform equally in their ability protect the consumer from AfB1. In fact, some enterosorbents have been shown to hinder the natural absorption of vital nutrients [185, 186]. The most common enterosorbent materials for Af are briefly explored below along with their effectiveness and mechanisms used in adsorbing the AfB1 toxin.

Activated Charcoal (AC): AC has long been utilized for the treatment of acute poisonings and to prevent the absorption of overdosed drugs and poisons in the GI tract [187]. AC is formed through pyrolysis of different organic materials. The process of "activating" the material increases the charcoals porosity and, therefore, the surface area of the material,

creating a substrate that is appropriate for adsorbing large quantities of material. Its success stems from its large specific surface area (SSA). Commercially available varieties may have SSA ranging from 500 to over 2,000 m^2/g [124]. One of the determining factors of the SSA is the initial material used to form the activated charcoal. ACs with lignin as the starting material have smaller SSAs as compared to ACs using oil as the starting material [188]. Aside from the SSA, the degree of adsorption is also dependent on the pore sizes, amount of charcoal administered, the chemical nature of the molecules being adsorbed, the pH and GI contents [124]. Additionally, particle size reduction and chemical modifications of the AC's base can influence the SSA. Such alterations, performed during the manufacturing process may provide SSAs of up to 3,500 m^2/g. These materials are commonly termed super activated charcoals [124, 183].

AC's high adsorption capabilities naturally led them to be considered for AfB1 enterosorbents. Several studies have been completed to test the efficacy of AC in binding AfB1. Studies were completed *in vitro* and *in vivo* settings using several animal species [183, 189-193], however, each has generated conflicting results, as seen in the summarized Table 1.5. Decker and Corby [192] used *in vitro* studies to first identify AC as an effective enterosorbent for AfB1. Two years later, Hatch *et. al.* [194] used AC to adsorb lethal doses (3 mg of AfB1/kg of body weight, corresponding to $LD_{90\text{-}100}$) of AfB1 in goats. Astoundingly, there treatments correlated to a 100 % survival rate and only 3 % hepatic destruction, where non-treated goats had seen 25 % destruction.

In other studies AC showed marginal [183, 195] or no significant gains [196] when introduced to animal feeds. One reason for AC's inability to effectively lessen the effects of Af ingestion is attributed to nonspecific adsorbing nature. Larger quantities of stomach contents may be adsorbed than Af, especially when non-Af contents significantly outweigh that of the Af [194, 197]. This non-specificity also demonstrates a disadvantage of AC, as chronic usage of the enterosorbent may cause uptake of critical vitamins and minerals leading to malnourishment of the species over time. To overcome AC's limitations, two strategies have been introduced: (1) The supplemental addition of essential nutrients that are shown to be excessively adsorbed onto AC or (2) modifying the AC during the activation process to have greater selectivity towards the targeted toxin [123].

The idea of modifying the AC brings to light the importance of the manufacturing process on the final AC product. The adsorption properties of AC, as stated previously, are a result of several factors, including the SSA and pore size. These values can greatly differ depending of the starting material, preparation methods and chemical treatments used to morph the initial product into the final form. Manufacturing differences may provide a good understanding on the discrepancies in ACs results on AfB1 adsorption [123, 124]. Because there is no standard method for preparing AC and no universal way of testing the adsorptive properties, authors suggest AC should only be selected for Af adsorption after full appraisal. Figure 1.21 proposes a methodological approach one may take for selecting AC for Af and other mycotoxins adsorption [123].

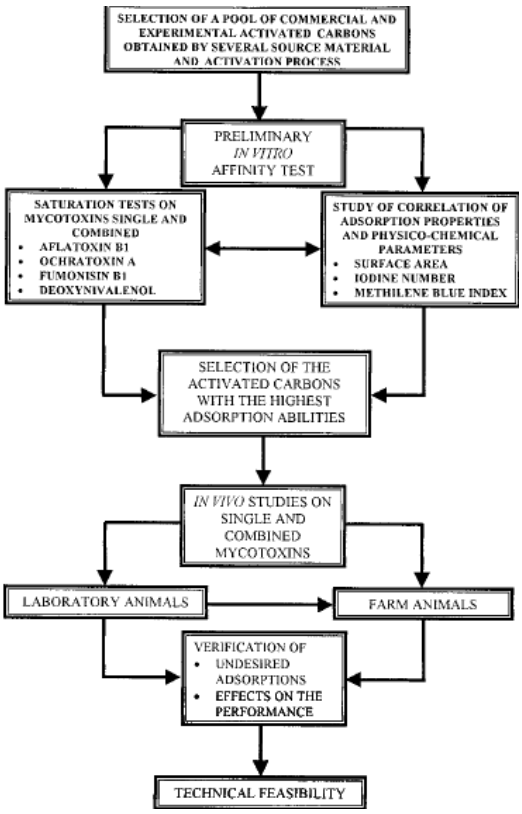

Figure 1.21. Methodological approach to the study of activated carbons as mycotoxin-sequestering agents [123].

Biological Binding Agents: Yeast and yeast cell walls, which have excellent nutritional values have also been shown to adsorb mycotoxins. Devegowa *et. al*. [122] showed *Saccharomyces cerevisiae* yeast adsorbed up to 77 % of Af and a modified form of *S. cerevisiae*, Mycosorb™, consisting only of yeast cell walls had an even greater capacity for binding Af. Mycosorb™ adsorbed approximated 95 % of Af in *in vitro* studies [121], with specificity for the toxin, giving it advantages over the common clay-based enterosorbents [198]. *In vivo* adsorption also successfully reduced the side effects of Af

ingestion in chicks [199, 200]. The cell walls embrace polysaccharides (glucan, mannan), proteins and lipids which allow for several different adsorption centers, allowing for various adsorption mechanisms, such as hydrogen bonding, ionic or hydrophobic interactions [197].

Some strains of lactic acid bacteria (LAB) are known to naturally adsorb aflatoxins in the GI tract. LAB, particularly *Lactobacillus rhamnosus* strains GG and LC-705, use a variety of mechanisms to bind AfB1 [201]. The cell walls of these bacterial cells are shown to have an inner layer of peptidoglycan and an surface layer of polysaccharides that contribute to toxin binding [202]. Because of the abundance and presence on the surface of the cell wall, polyscaccarides are said to be a predominant feature in AfB1 binding. In spite of this, hydrophobic interactions, resulting from lipoteichoic acids found in the gram positive cell, are shown to play a major role in binding as well as electrostatic interactions [201, 203]. Furthermore, recent studies show bacterial cells' surface is rich with a variety of proteins that may play roles in aflatoxin attraction [204]. Though the source of attraction for AfB1 to the LAB cells is complicated, research shows that upon binding to LAB there is a reduction in mycotoxin uptake and a natural decrease in its potency [205]. Upon recreating these natural interactions in *in vitro* experiments, LAB was able to remove AfB1 from liquid media rapidly and with high removal rates (~ 80 %) upon immediate contact [206].

Clays: Another strategy for reducing the exposure of Af in contaminated crops is the introduction of clays to the diet. Dietary clays for humans and animals have been observed for centuries [207] and consuming these clays is often considered "culturally acceptable

[208, 209]." In 1979, clay minerals became of interest for adsorbing AfB1 [210]. The introduction of non-nutrient clay minerals to contaminated food has demonstrated to reduce the bioavailability of the toxin and its distribution into the bloodstream as well as to the liver and other targeted organs [210-213]. Clay based sorbents are the largest and most complex class of Af enterosorbents. Below, we will introduce the three most studies clays for Af removal. These include zeolite, bentonite and hydrated sodium calcium aluminosilicate (HSCAS).

Zeolite- Zeolites are microporous, crystalline, hydrated aluminosilicate of alkali and alkaline-earth cations and contain a three-dimensional infinite structure of SiO_4 tetrahedra [211]. The minerals are characterized by their ability to reversibly gain and lose water and exchange constituent cations without compromising their basic structure [124, 214, 215]. The first work on zeolite for AfB1 adsorption was completed by Dvorak [216]. The *in vitro* studies showed that the clay was able to adsorb on average 60 % of the toxin in various liquid media. It was seen that in media containing nitrogen compounds the average retention was lower. In that same year, studies performing AfB1 adsorption in gastric content solution showed 58 to 74 % of the toxin was adsorbed [185], with dependencies on the type of zeolite used [124]. As seen by Piva *et. al*. [148], t he origin of the zeolite can highly influence the adsorption properties, due to differences in the pore size distribution. If the size of the pores is comparable, even in the case of synthetic and natural zeolites, comparable AfB1 uptake should occur. However, if the zeolite lacks intermediate-sized pores, adsorption may be low or not occur at all [123, 148].

Dissimilarity in pore sizes is perhaps the reason why *in vivo* studies using zeolite for AfB1 vary. In one study, by Fukal *et. al.* [217], boiler chickens given feed containing 2.5 mg AfB1 per kg feed were studied after 5 and 12 days. Poultry which received grain supplemented with 5 % zeolite showed no significant differences than the control group. Comparisons were based on weights of the pancreas, liver, spleen, glandular stomach, bursa fabricia and bone (tibiotarsus) strength [124]. However, in a highly comprehensive study, using the same experimental design, it was seen the inclusion of zeolite into an Af contaminated diet lessened the heterophilia and lymphopenia effects observed in the non-treated group. Lymphocytopenia, seen in the untreated group, is a feature of many antibody-deficiency syndromes and their increase in heterophils, a type of granulocyte, may signify a predisposition of the species to compensate for its decreased resistance. Nevertheless, the same study also showed that zeolite had no defensive properties against the acute alteration of the liver tissue [218]. Interestingly, a final study by Harvey *et. al*. [219] employed the use of five commercially available zeolite mixtures. The additive was administered at a 0.5 % concentration to observe the counteracting effects of the added 3.5 mg of Af (79 % AfB1, 16 % AfG1, 4 % AfB2, and 1 % AfG2) per kg of feed. The three week experiment of broiler chickens showed three of the zeolite compounds were not able to counteract the effects of the high concentrations of Af. However, the other two samples reduced toxicity by 29 % for SC Zeolite™ and 41 % for Zeomite™, with the latter also giving added protection of liver weights and serum metabolites [124].

Bentonite- Bentonite is a type of clay sorbent of a lamellar and crystalline microstructure that consists primarily of montmorillonite, a soft group of aluminosilicate minerals [123, 124]. The clay forms from the weathering of volcanic ash. Its final composition may vary from one deposit to another due to their interchangeable ions, such as sodium, potassium, calcium and magnesium, thereby terming the clays sodium bentonite, potassium bentonite, etc. [124]. These cations also provide bentonite with its well-known adsorption properties. Bentonite has been used as a versatile adsorbent in a variety of industries and for various applications, some of which include the clarifications of beverages and the discoloration of oils. The addition of water, as in many of its applications, lead to its characteristic swelling capabilities [220].

More recently bentonite has been considered for the adsorption of AfB1. In 1978, Masimango *et. al*. [221] demonstrated that bentonite was able to adsorb 94 to 100 % of AfB1. Several different types of bentonite were tested, with adsorption dependent of the nature of the clay. Ten years later, supplementary experiments, by Dvorak [216], showed that, aside from water, bentonite could continue to adsorb AfB1 in a variety of different liquid media, including saline solution, porcine blood serum and stomach fluid, and bovine rumen fluid. The average AfB1 uptake by bentonite in these different media was 66 %. Additionally, 2.5 % bentonite additions are able to adsorb Af to non-detectable amounts at low pH 2 [124].

In vivo studies using bentonite were not as promising. A porcine study using 0.5 % calcium bentonite in feed contaminated with 800 ppb AfB1 showed no benefit over the

control group, where the clay was omitted. Increasing the clay content to 1 to 2 % showed no substantial performance gains or improvement in blood serum levels [222]. Studies giving AfB1 contaminated feed (also 800 ppb) to pigs showed no additional benefits in increasing sodium bentonite clay concentrations more than 0.5 % [223]. Alternatively, other studies show the inclusion of bentonite at 0.5 % and 1.0 % show that growth inhibiting effects of broiler chickens diminish by 64 % and 84 %, respectively [195]. The effects of bentonite additions to animal diets may inhibit mineral metabolism. Schell *et. al.* [224] studied these effects using 1 % additions of sodium bentonite to pig diets. It was shown that the clay did not alter the absorption and retention of potassium, copper and manganese, but did have some affects on calcium, zinc, phosphorous, and iron. It was also seen that sodium and magnesium absorption was lowered with the additions of the clay. However, serum and liver mineral concentrations were generally unaltered.

HSCAS- HSCAS, which today can be more commonly be found under the name NovaSil™ is a form of natural zeolite, which was originally sold as an anti-caking agent for animal feeds [210, 211]. However, this aluminosilicate clay has positive-charge deficiencies that cause it to adsorb positively charged molecules [225]. This property led to its discovery, in 1987, of adsorbing AfB1 [124, 226]. To this day, HSCAS remains one of the most widely used materials for adsorption AfB1.

In vitro experiments performed using radio-labelled AfB1 revealed that of 38 sorbents tested, many of which included clays, HSCAS was the most stable AfB1 adsorbing substrate. It remained stable under various pH environments (pH 2, 7, and 10) and

temperatures (35 and 37 degrees C). Studies showed HSCAS had the ability to adsorb more than 80 % of the AfB1 present [227] and may reach equilibrium after only 30 minutes [228], though other studies show lower adsorption [185] and longer incubation times of up to 1 day are needed [229]. Binding calculations indicated that roughly a maximum of 200 to 232 nmol of AfB1 could be bound per mg of HSCAS [228]. *In vivo* assessments were also promising. HSCAS at a 0.5 % concentration also has been added to the diets of a variety of animals, including chickens, turkey [229], minks [231], pigs [222, 224], cows and lambs [232, 233], with or without AfB1 additions. Studies show that in all cases HSCAS abolished or lessened the related health hazards, as evaluated through animal performance and numerous biochemical and histopathlogical parameters [124]. Furthermore, HSCAS was able to reduce the secretion of metabolized AfB1, known as AfM1, in the milk of cows [233].

HSCAS's high affinity and high capacity for binding AfB1 cause for speculation of binding mechanisms as compared to other clays. Earlier studies testing the stability of AfB1-HSCAS complexes observed less than 10 % desorption with the addition of an elutropic series of solvents. The authors believed that a strong binding chemisorption had taken place [227]. However, in later years, it was proposed that the suggested mechanism of AfB1 sorption was due to an electron donor acceptor mechanism [210]. Layers of HSCAS clay are negatively charges resulting from isomorphic substitution. To balance this charge positively, charged molecules, or molecules with partially positive areas are attracted to the clay. In the case of AfB1, its dicarbonyl system is partially positive and has shown to be drawn to the

HSCAS. Additionally, with the exception of the terminal furan ring (Figure 1.20), AfB1 is a planar molecule. Therefore, special orientation is shown to play a role in how AfB1 is adsorbed. HSCAS is believed to favor an orientation where this furan ring is aligned away from the surface. The primary binding size of HSCAS is within the interlamellar region, thus, adsorption experiments on heat-collapsed HSCAS show that, if this area is compromised, AfB1 adsorption is greatly reduced since the external surface only accounts for a minor amount of the AfB1 adsorbed. Additionally, the stereochemistry is believed to be important in sorption. Aflatoxin analogues, which contained functional groups, making them larger than AfB1, may have their adsorption in the interlamellar region compromised by the stereochemical restrictive groups [210]. Other mechanisms may also be involved in the adsorption of AfB1, theses include potential chelation of interlayer cations, particularly Ca^{2+}, and attraction of the carbonyl system to uncoordinated edge-site metals, specifically aluminum ions [211, 213, 234-236].

Recent research studies the long term effects of HSCAS consumption. Suspicions of Ramos and Hernandez [119] state that, due to the physical binding of AfB1 to HSCAS, there is also a strong possibility of binding essential vitamins, minerals and amino acids present in the gut, thereby making these less available for natural absorption. However, short-term animal studies have showed no adverse effects when administering doses up 2 % in the diet [237]. Long-term exposure (6.5 months) of HSCAS was also completed with rats [238]. HSCAS dosage ranged from 0 to 2 %. Results showed no mortality or morbidity and no adverse affects on bodily or organ weights, feed conversion rations, gross anatomy and

histological appearance of major organs, hematology and serum biochemistry parameters. Select nutrients, vitamins A and E, iron and zinc were also studied and showed no deviations from normal levels, though previous studies showed zinc utilization was slightly reduced [186]. Because of HSCAS's high inclusion rates, there is still concern over other vitamins and minerals that may be adsorbed [239]. Overall, this outcome led to short-term phase I clinical trials for 50 healthy adult humans (ages 20 to 45) at Texas Tech University [240].

The study was carried out to examine the short-term safety and tolerance of HSCAS (NovaSil™) capsules in normal human subjects and to develop optimal protocols for human intervention studies. The study used a high dose (3 grams/day) and low dose (1.5 grams/day) group, which were extrapolated from previously published animal studies [211, 235, 238]. After 14 days it was determined that doses of both 1 and 3 grams/day were safe as determined through physical examination, biochemistry and hematology evaluations, including no statistical differences in the serum levels of vitamin A and E, iron and zinc present. These results further suggest that HSCAS has a biding specificity for AfB1 and allowed for further direction into phase IIa clinical trials [240].

Phase IIa clinical trials were completed in Ejura-Sekyedumase district, Ashanti Region, Ghana [241] to further evaluate the safety and tolerance of HSCAS pills for potential preventative use in countries where the risk of aflatoxicosis is high. The 3 month study was completed on 177 adults, in which 90 % completed the study and 99 % reported no side effects. Of those who experienced side effects, conditions were only mild to moderate and none appeared to be associated with HSCAS treatment. The outcome of the study reported no

significant different in hematology, liver and kidney functions and electrolytes. Additionally, serum biochemical analysis showed some isolated differences in a few parameters but no trends of association or dose-dependency. Furthermore, all differences fell within the normal physiological ranges. Overall, results show that inclusion of HSCAS, at the tested levels, were safe and support the application for HSCAS to be used as preventative maintenance against aflatoxicosis of humans who are acutely exposed. However, phase IIb and III trials must be performed to confirm safety and efficacy for prolonged therapy [210].

Nanodiamonds: NDs are the latest addition to potential aflatoxin enterosorbents. Though HSCAS clays seem promising in their removal of Af, there are still some questions and disadvantages relating to their use. For example, questions still remain on how quickly they can bind the toxin, while some experiments say 30 minutes [228] others report 24 hour incubation times [229]. Additionally, though it was shown not to inhibit natural adsorption of vitamin A and E, as well as iron and zinc, interference of other essential vitamins and minerals were not evaluated. Due to the high inclusion rate of aluminosilicate clays it is probable that other critical nutrients may be affected and such deficiencies may create problems with prolonged administration [197]. Lastly, methods of administering HSCAS become difficult *in situ* for livestock. *In vitro* experiments for enterosorbent materials mentioned earlier are commonly evaluated in liquid media. However, upon dosing *in vivo* both human and animal subjects are administered powered materials. Humans may take capsules without difficulty; however, for animal species administering the clay becomes

more difficult. Animals commonly receive dosing in their daily feed, which creates uncertainties in monitoring the exact dosage consumed by each animal. Real life situations will require an easy way of administering the enterosorbent on a day to day basis, which is not yet attainable by HSCAS.

NDs have to potential to overcome the failing attributes of HSCAS, while still adsorbing high quantities of Af. As stated previously, NDs have advantages of biocompatibility with low cytotoxicity, but additionally possess high colloidal stability and sorption capacity over a wide range of pH [16]. Their high aqueous stability has the possibility to make dosing animal subjects much simpler. Substitutions of aqueous ND solutions for pure water will allow for precise dosage of enterosorbents. Several studies have already indicated ND colloids as a substitute for water, shown no adverse effects in animal. Furthermore, because NDs stay stable over a wide range of pH they may be able to exhibit higher sorption capabilities in the GI tract due to their resistance to aggregation, which may block binding sites. Lastly, because NDs can be tailored with different functional groups during manufacturing and modification treatments, NDs may be able to selectively adsorb Af while excluding critical nutrients.

Though this work focuses on exploring the effectiveness of ND enterosorbents, a few studies have already been completed showing the effectiveness of ND substrates in AfB1 adsorption. Studies by Puzyr *et. al*. [182] showed that modified NDs (MND) have the ability to adsorb AfB1 within only 2-3 minutes, and increasing this time did not show elevated adsorption levels. Moreover, dry powder additions versus ND hydrosols showed no

differences in their ability to adsorb AfB1. However, the amount of ND added does influence AfB1 uptake. Results (Figure 1.22) show differences in adsorption percentages and capacities based on varying ND and AfB1 additions. In example, AfB1 adsorption reaches 60 % with 25 mg of ND (1 mL), however, the correlated adsorption capacity is low. By increasing the amount of AfB1, the capacity of the ND increases by one order of magnitude. Similarly, increasing the amount of ND increases the amount of bound toxin, but decreases the sorption capacity [182]. Other papers have reported 81 % of AfB1 can be adsorbed by NDs, based on spectral analysis, without specification of ND-AfB1 ratios [242]. Our most recent studies show that the ratio of NDs to AfB1 and the concentration of the ND suspensions critically influence the calculated capacities of the ND [243]. In agreement with Puzyr's studies, we also observed higher capacities with lower ND concentrations and lower ND to AfB1 ratios, though adsorption percentages are lower. This outcome is rationalized by the fact that more ND particles allow for greater adsorption of the AfB1 molecules, but there are not enough of these molecules to completely saturate the ND's surface.

Results of Puzyr's study illustrate that adsorption capacities and percentages as compared to other enterosorbents are not astonishing. However, this work only examines adsorption by one type of ND. Whereas, our studies illustrate selection of a different ND substrate, or modification of the ND, increases the ND's adsorption affinity for AfB1. Modified NDs (MNDs) used in Puzyr's studies were reduced in size from approximately 80 nm to 40 nm. ND concentrations were also reduced from 25 μg/mL to 1 μg/mL and showed a significant increase in adsorption capacity for AfB1 (from 0.011 μg/mg to 9.75 μg/mg).

Moreover, adsorption capacities were even higher (12.47 μg/mg) when using positively charged, 40 nm Ch-F6 ND. Though positively charged substrates show slight increases in AfB1, the dominating characteristic for AfB1 adsorption is reliant on the aggregate size of the NDs [243].

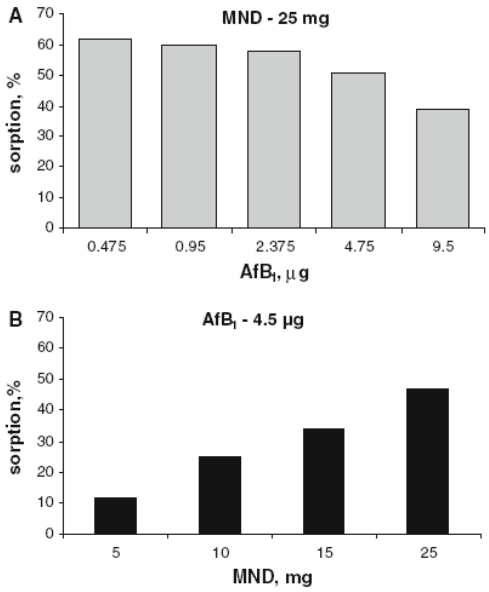

Figure 1.22. Modified ND (MND) sorption characteristics depending on the AfB1 content in specimen at a constant amount of nanoparticles (a) and depending on the content of nanoparticles in specimen at a constant amount of AfB1 (volume 1 mL) (b) [242].

NDs also show promising behaviors under different pH environments. Their experiments demonstrate that adsorption of AfB1 in acidic environments (pH 2) are identical to results at the natural pH (pH 6). However, in alkaline conditions (pH 9) the characteristic spectra of AfB1 changes as alkalinity begins to destroy the lactone ring, thereby degrading

the molecule. Even so, the addition of ND to Af at this pH resulted in greater changes to the spectrum indicating that NDs still continue to adsorb the toxin [182].

The authors' latest publications demonstrate the increased effectiveness of combining NDs with Af destruction techniques, i.e. ozonation [244]. Figure 1.23, below, shows results of their studies, including the effect of ozone solutions on AfB1 alone and paired with subsequent ND additions for adsorption of residual toxins. As reported, the combination treatment of both ozone hydrosols and NDs together are more effective than employing these techniques separately. In *in vivo* experiments, rats were examined for their hematological parameters and the state of the liver cells after orally administering AfB1 with and without ND substrates. As different species show varying resistance to AfB1's toxic and carcinogenic effects [245], rats were selected as they show greater sensitivity to the toxin than mice. Rats were giving 0.1 μg AfB1 per gram of body weight with some rats receiving additional ND hydrosols (0.4 wt. %). After the 35 day experiment, hematological parameters and state of the rat's liver cells show that the presence of ND substrates lessens the toxic effects of AfB1 on the animal. Leukocyte increases were seen in the presence of NDs alone, likely due to interaction with GI macrophages. However, ND in the presence of AfB1 lowered count to more normal levels. AfB1 with NDs showed normal platelet and erythrocyte levels. Ultrathin sections of liver cells were also analyzed in all rat groups. AfB1 in the presence of NDs showed higher amounts of lysosomes and lipid aggregates of low electron density, likely a result of compensatory response to NDs. Rats who received AfB1 alone showed hyperplasia of the smooth endoplasmic reticulum (EPM), possibly indicating

hyper-function. Most importantly, rats who received AfB1 with NDs showed no such changes, but did show some lysosome aggregates, indicative active degradation of foreign compounds and their elimination from the cell [242]. The hepatocyte ultrastructure taken by TEM imaging can be seen in Figure 1.24.

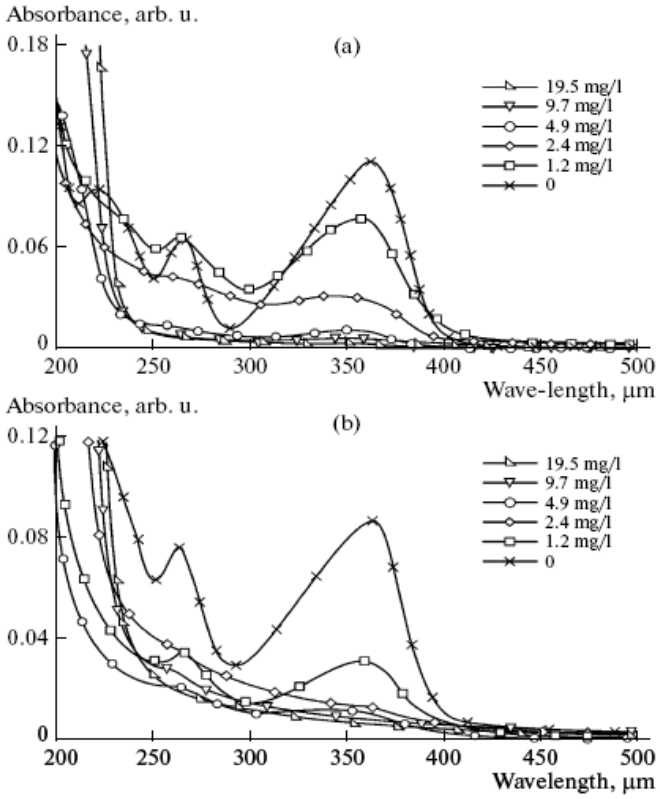

Figure 1.23. Absorption spectra of AfB1 water solutions for various ways of processing them: (a) processing with ozonized water with different concentrations of O3 and (b) posterior adsorption on MND (particle content is 2.5 mg) [244].

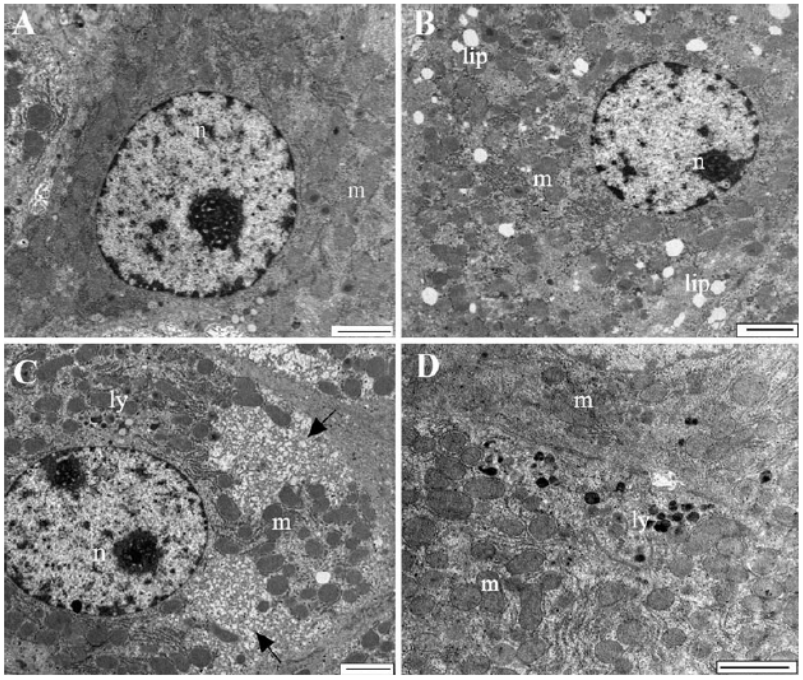

Figure 1.24. Ultrastructure of hepatocytes of animals: (a) rats that orally received water, (b) rats that orally received the MND hydrosol, (c) rats that orally received the AfB1 aqueous solution, (d) rats that orally received AfB1 with the MND hydrosol. Bar—2 μm. Arrows show hyperplasia of smooth endoplasmic reticulum in hepatocyte image. Note: n=nucleus, m=mitochondria, lip=lipid inclusions, ly=lysosomes [242].

Table 1.5. Summary of *in vitro* adsorption experiments of aflatoxins by different adsorbents.

Sorbent	Adsorption capacity (mg/g)	Reference
Activated Charcoal	10	[192]
Activated Charcoal	120	[193]
Mycosorb	0.204	[135]
Bentonite	45	[246]
HSCAS	62-103	[228]
Aluminosilicates (Ethacal®, Novasil™, perlite, zeobrite)	0.06–0.80 μg/g	[185]
RUDDM NDs	0.148- 9.75	[182, 243]
Ch-F6 NDs	12.47	[243]

1.2.2 Ochratoxin

Ochratoxin is another class of mycotoxins produced from *Penicillium verrucosum* and several *Aspergillus* strains, including *A. ochraceus*, *A. carbonarius*, and less commonly *A. niger*. There are several varieties of ochratoxin, including ochratoxin A, B and C and their various derivatives [247]. Of these, ochratoxin A (OTA) is the most commonly detected and most toxic. OTA is found in a variety of different food sources. Most regularly, OTA is found in grains but has also been known to affect many other commodities of plant and animal origin, including coffee, spices, herbs, cocoa, grapes, meat, milk, juices, beer, wine and vinegars [247, 248]. Unlike the funguses that produce aflatoxins, those that produce OTA can flourish under moderate temperature and humidity. Because of this OTA can be found in crops world-wide, however, the continents of primary concern are Africa, particularly Europe and North America [248, 249]. In fact, studies conducted in the early and mid-1990's show OTA to be widespread in Europeans' blood and breast milk [250, 251].

Evaluation of data by The Joint Expert Committee on Food Additives, the FAO and the WHO led to the conclusion that human ochratoxin exposure is primary gained through consumption of grains (58 % of the intake), wine (21 %), grape juice (7 %), coffee (5 %), and pork (3 %) [252]. Furthermore, the toxin is relatively heat stable, meaning baking or roasting contaminated foods will only reduce the toxin concentration by 20 %, where boiling [253, 254] and most other processing methods have no influencing effects [163, 247].

Ingestion of OTA has been associated as mutagenic, nephrotoxic, nephrocarcinogenic, teratogenic [255], immunosuppressive properties that may lead to the

development of certain disease, such as Balkan Endemic Nephropathy (BEN), the development of urinary tract tumors, and possibly connected with testicular cancers [247]. Based on sufficient evidence in humans, the International Agency for Research of Cancer (IARC), in 1993, classified OTA as a group 2B carcinogen, representing possible carcinogenic properties [256]. Because of this the maximum tolerance levels are set at 5 and 3 μg/kg for raw and processed cereals. However, several countries, including the United States [257] and European Union [255, 258], are currently reassessing this maximum.

Interestingly, unlike aflatoxin, not all animal species are affected by OTA. In fact, OTA is shown to have strong species- and sex- specific differences [255]. While humans and pigs have sensitivity to the toxin, cattle and other ruminants lack side-effects from OTA consumption. Ruminants natural flora in their rumen, used for microbial fermentation of ingested feed, naturally decompose the OTA so that it does not pass on throughout the remainder of their GI tract. Additionally, this means consuming the meat or milk of these animals is of no dire threat [247]. Sex-specific differences were also reported surrounding BEN disease, a kidney disease that primarily affects women [259] and whose final stage is characterized by renal failure and shrinkage of both kidneys. In rodent studies, male rats were far more likely to develop renal cell carcinoma or renal tumors than females. Reasons for this are not clear, however, it is known the OTA forms adducts with DNA and the levels of DNA-adducts appear higher in male rats. Uncertainty also surrounds OTA's mechanism used in cell death and antiproliferation of cells, despite the fact that OTA has been

extensively documented in laboratory animals [255]. Table 1.6 shows lethal doses, LD_{50}, and half lives, $t_{½}$, of several different animal species.

Table 1.6. Selected LD50 values and half-lives of OTA in relevant species following oral administration [255].

Species	Oral LD_{50} (mg/kg b.w.)	$t_{1/2}$ (po)
Human	n.d.	35.5 days
Monkey	n.d.	21 days
Pig	1.0–6.0	72–120 hrs
Rat	20–30	55–120 hrs
Mouse	48–58	40 hrs

Note. $t_{1/2}$ Varies considerably with the route of administration; n.d., no data available

As with aflatoxin prevention, it is stated that good agricultural practices, such as appropriate irrigation procedures, crop turnover, sufficient use of pesticides, and proper handling and storage may help minimize the production of OTA [247]. However, even with careful agricultural practices OTA may still develop due to the ability of the producing fungi to grow in cold climates (0 to 31 degrees C, 20 degrees C is optimum) and in a wide range of pH (pH 2 to pH 10, pH 6 to 7 is optimum) [260].To eliminate or counteract the toxin, physical, chemical and biological methods are employed. These chosen methods must satisfy several criteria including being cost effective, compatible with existing food safety legislations and the final quality of the product must remain unaltered [247, 261].

Physical decontamination methods, including cleaning, mechanical sorting, separation (though filtering, most commonly by activated carbon and potassium caseinate),

ultrasonication, irradiation, heating, roasting, frying and autoclaving, vary in their effectiveness to reduce the toxin [262]. These differences can be due to heat spiking methods, selectivity and sensitivity values, initial contamination level, inhomogeneous toxin, and treatment and drying conditions. Overall, roasting and fining agents appear to have the largest reductions in OTA showing up to 99.8 % of the toxin may be removed [247]. However, not all physical treatment methods are applicable for all applications. For example, some of the reported results were completed on contaminated liquids, which will not cure grains. While roasting may greatly reduce the toxin in grains, it is impractical to expect farmers will roast grain before feeding to their livestock.

Many chemical methods to remove ochratoxin have shown to be rather successful. Ammonization has received the most attention as it was shown to completely decompose OTA in corn, wheat and barley [263] without the formation and accumulation of toxic byproducts from the OTA molecule. After treatment, sensorial properties, such as the browning of cereals, and nutritional properties, including the decrease of lysine and sulfur-containing amino acids, may be altered [263, 264], thereby, compromising ozone's ability to treat contaminated feed [263]. Other methods, including ethyl acetate, dichloromethane, and methylene chloride supplemented with 2 % formic acid treatments, have shown to reduce OTA by 80 % in coffee beans. Additionally, alkaline treatments eliminate more than 98 % of OTA in cocoa, due to the opening of the lactone ring (molecule seen in Figure 1.25) [262]. Like aflatoxin decontamination, ozonization has also shown to be effective with some applications showing undetectable OTA remnants in grains, nuts and vegetables after

treatment [167]. Furthermore, ozone treatments can be completed quickly requiring only 15 treatment times with 10 wt. % concentrations. However, chemical treatments are not allowed within the European Union for products destined for human consumption. Chemical alternatives, i.e., biological decontamination methods, are then considered [262].

Biological treatments often use microbes or their enzymes for mycotoxins detoxification mimicking the natural biological processes found in some species. As previously mentioned, OTA degradation occurs in the GI tract of cows due to naturally occurring microbial flora in the rumen. Sheep, another in the ruminant family, also possess this ability to breakdown the OTA molecule [265]. Enzymes responsible for this decomposition are carboxypeptidase A and chymotrypsin [266]. The degradation of ochratoxin A by carboxypeptidase A into nontoxic byproducts is seen in Figure 1.25. This enzyme is also present in the caecum and large intestine of rats where a similar reaction occurs. Partial degradation of OTA was also observed by the microflora in human intestines [267], though not enough to fully protect the human from OTA consumption. This identifies two ways OTA can be destroyed. The first being the opening of the lactone ring and the second including breaking of the peptide bond of OTA into phenylalanine and ochratoxin α. Ochratoxin α is almost nontoxic [268] although genotoxicity has been indentified [269]. Of these two options, breaking of the peptide bond maybe more successful as the opening of the lactone ring is reversible and may be regenerated in acidic environments [247].

The majority of microbes degrading OTA have been able to do so by removing the phenylalanine moiety from OTA. It has been seen *Saccharomyces cerevisiae* and *Kloeckera*

apiculata yeast isolates were able to cause OTA degradation during alcoholic fermentation, and *Streptococcus salivarius*, *Bifidobacterium bifidum*, *Lactobacillus delbrueckii*, as well as yogurt bacteria have entirely degraded OTA levels in milk samples. Furthermore, in excess of 70 Aspergillus fungal isolates have also showed their ability to degrade OTA into the phenylalanine and ochratoxin α byproducts [262].

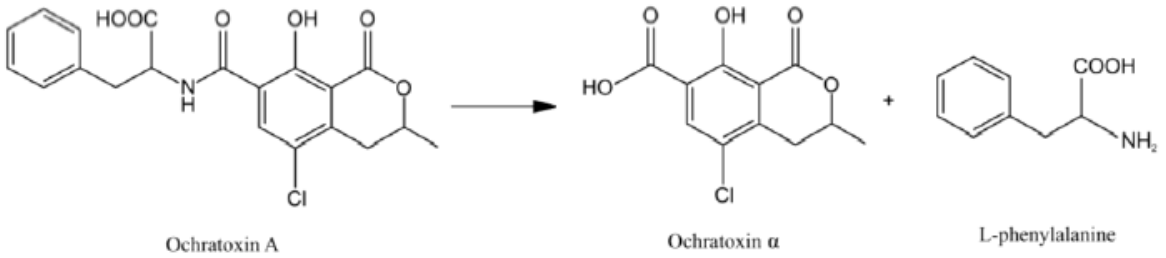

Figure 1.25. Degradation of ochratoxin A by carboxypeptidase A [262].

Researchers are studying other methods of inducing peptide cleavage in the OTA molecule. One molecule that shows much promise is aspartame, a common sugar substitute. Aspartame has a structural similarity to OTA and its breakdown products also include phenylalanine. Creppy *et. al.* [270] comprehensively explored the molecular mechanism responsible for the preventative measures of aspartame. Their conclusions arise to the fact that phenylalanine is cleaved at the peptide bond and the peptide directly affects the bending capacity and transport of the toxin *in vivo* and *in vitro*. These studies showed aspartame inhibited OTA from binding to plasma proteins *in vitro* and prevented genotoxicity and

nephrotoxicity when given to rats [123]. Many authors suggest that aspartame is the best candidate for preventing OTA induced toxicosis [264, 270]. However, the addition of aspartame to food substances can be detrimental to phenylketonurics, individuals who cannot properly metabolize the amino acid, phenylalanine. Phenylketonuria, commonly referred to as PKU, has been said to affect 1 out of every 1,000 to 2,000 humans [271]. Though this group is not large, alternative preventative measures to inhibit OTA toxicity are needed.

Ochratoxin Enterosorbents

Requirements listed earlier for aflatoxin enterosorbents must also be met for OTA adsorbing substrates. These included having a high capacity for the molecule, strong and selective binding of the molecule, and it must be safe for ingestion. Though OTA and AfB1 enterosorbents share the same requirements, substrates deemed appropriate for adsorbing one molecule may not perform equally in the case of the other, primarily due to structural and charge differences between the two molecules. It is well recognized that binding by substrates is reliant on the properties of mycotoxins, including shape, size, polarity, and solubility in water. In example, unlike rather neutrally charged AfB1, OTA dissociates to create a negatively charged molecule that may be heavily influenced by electrostatic interactions between OTA and the adsorbing substrate. Because different substrates may have distinct affinities for binding each toxin, enterosorbents listed in the previous section must be re-evaluated in the case of OTA. We describe several classes of enterosorbents most

commonly studied with OTA, along with their effectiveness for adsorbing the OTA molecule.

Yeast and Yeast Cell Walls: OTA biosorption with yeast has shown varying rates of success. Adsorption values ranging from 32 to 98 % have been reported depending on the type of yeast used and the toxin concentration [272]. In addition to this, other factors, such as pH have also shown to influence OTA adsorption. *In vitro* experiments using 40 % sterilized yeasts and 60 % residua of beer production were examined for adsorption at a pH of 3 and pH of 8. As seen, lower pH adsorbed greater amounts of OTA, specifically 8.6 mg of OTA per gram of yeast, whereas at a pH of 8 only 1.2 mg/g was adsorbed. However, i*n vivo* results were less promising showing the inclusion of feed supplements of 5 % yeast, given to pigs, insignificantly reduced OTA concentrations in blood plasma, bile and tissue samples [197]. However, when yeast cell walls were chosen over the whole cells, OTA adsorption may be elevated. The cell walls, as mentioned previously, have numerous and diverse adsorption centers allowing for adsorption though physical adsorption, chemical binding of ionic groups, ion exchange, and more [197]. Though biosorption mechanisms in some cases are still not very well understood, it is proposed that cell surface adsorption is a physio-chemical interaction between the toxin and cell's functional groups, which occur quickly and reversibly [272, 273]. Surface adsorption by yeast cells relies on physical adsorption ion-exchange and complexation, which is not dependent on metabolism. Cell walls, however, offer an abundant of functional groups, including carboxyl, hydroxyl, phosphate and amino

groups, polysaccharides, proteins, lipids, and hydrophobic adsorption sites such as aliphatic carbon chains and aromatic rings, which aid in the binding of toxins like OTA [273].

Activated Charcoal: AC has exhibited high *in vitro* affinity for OTA, with up to 121 μg of OTA adsorbed per milligram of sorbent [274, 275]. Rotter *et. al*. showed that 50 mg of AC was able to adsorb 90 % OTA (150 μg) [275]. However, the addition of charcoal to a complete diet did not significantly reduce the effects of OTA in chickens. Increasing charcoal supplementation to up to 10,000 ppm in chicken's diets also showed no additional gains. The authors speculate that AC additions are an impractical method to eradicate OTA toxicity in poultry, but state that diets with smaller OTA levels may be effectively protected with AC [119]. However, other studies show significant OTA reduction by AC in blood, bile and tissue samples of pigs [197]. Also, one must take into account the property differences in ACs based on manufacturing techniques and starting materials [274]. Other types of AC may be more effective at adsorbing OTA *in vivo* [123]. To determine this, several types of AC should be considered using the methodological approaches previously shown in Figure 1.21. It should also be noted that while ACs aren't very effective as an *in vivo* enterosorbent, AC as a fining agent for OTA contaminated wine is very effective, showing up to 99.8 % toxin reduction [247].

Clays: Clay research with OTA is very limited. While several studies have been completed with OTA, none hold high promises on OTA adsorption. While HSCAS clays were

extremely effective in the binding of AfB1, however, it holds no protective properties against OTA toxicosis [123, 124]. *In vitro* studies show 0 to 2.2 mg of OTA adsorbed per g of HSCAS show no significant reduction in OTA toxicosis in pigs. Bentonite, which demonstrates slightly higher adsorption in vitro (1.5 to 9 mg/g), also showed insignificant protection against pigs at both 1 and 10 % concentrations [197]. The ineffectiveness of the clays arises from their hydrophilic, negatively charged surfaces. OTA, which also carries a negative charge, likely demonstrates electrostatic repulsions with the clay substrates, thereby, preventing adsorption. Modification of the negatively charged minerals was carried out to control the surface properties and hydrophobicity by cation exchange of natural charge-balance cations, including Na^{+}, K^{+}, Ca^{2+}, Mg^{2+}, with high molecular weight quaternary ammonium ions. With modification of zeolites and organo-zeolites, by different amounts of organic cations, adsorption was significantly improved. The presence of long chain organic cations on the zeolite's surface resulted in up to 99 % adsorption of OTA. Authors suggest the increase in hydrophobicity of the mineral substrate plays a role in the newly improved adsorption, but the non-linear shape of constructed isotherms may indicate additional mechanisms are involved [276]. However, the effectiveness of these materials still needs to be evaluated *in vivo*.

Nanodiamonds: We report first studies of OTA adsorption by NDs substrates [243]. Outcomes of our studies show NDs have increased affinity for OTA over AfB1. This attraction is dominated by the electrostatic interactions of negatively charged OTA on

positively charged ND substrates. While the positively charged NDs showed the highest adsorption capacities (up to 25.2 μg/mg), negatively charged NDs also showed adsorption of the molecule, indicating adsorption mechanisms are not purely electrostatic. Other influences on OTA adsorption capacities include aggregate size reduction, though not as influential as in AfB1 studies, and surface chemistry modifications, with hydroxylated NDs showed highest adsorption.

Table 1.7. Summarized *in vitro* experiments for ochratoxin A by various sorbents.

Sorbent	Adsorption capacity (mg/g)	Reference
Activated Charcoal	100	[197]
Activated Charcoal	124	[274]
Yeast	1.2-8.6	[197]
Bentonite	1.5-9.0	[197]
HSCAS	0-2.2	[197]
Modified Organo-zeolites	1.48	[276]
Hydroxylated ND	25.23	[243]

1.3 Dye Models

Due to the toxic nature of the mycotoxins, dye models were initially used to develop methodologies and better understand the adsorption properties of the ND as it relates to surface modifications, including electrostatic interactions, surface chemistry differences, and aggregate sizes. Three fluorescent dye molecules were chosen for initial experiments. Each of these dyes were selected for their well-characterized properties and for their fluorescent

ability, making it easy to detect the amount of bound versus unbound molecules on the ND substrates through spectroscopy.

The first dye, propidium iodide (PI, Figure 1.26), was chosen as it is a positively charged molecule used widely in microbiology for distinguishing necrotic (sudden cell death), apoptotic (programmed cell death), and normal cells [277, 278]. In simpler terms, it can be used to stain dead cells in a large population. Additionally, PI allows for the determination of the DNA content of each cell and the percentage of cells in each phase of the cell cycle population by simply staining the cell's nuclei or the entire cell [279-281].

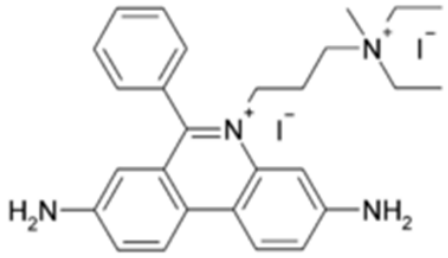

Figure 1.26. Molecular Structure of positively charged fluorescent dye molecule propodium iodide (PI).

Propidium iodide functions by binding to nucleic acids and intercalating between bases of DNA or RNA. In double stranded DNA, intercalation of the dye occurs with a density of roughly one dye molecule per every 4-5 base pairs. Binding is facilitated by the charge interaction of the positively charged dye with the negatively charged nucleic acid. However, the dye can only go into late apoptotic and necrotic cultured cells without sequence preference [282, 283] and is prohibited from penetrating live cells due to its positive charge

[284]. Propidium iodide, when bound to nucleic acids enhances its fluorescence 20-30 fold and absorption maximum shifts approximately 30 to 40 nm to 535 nm (red shift). Additionally, fluorescence emission maximum shifts roughly 15 nm to 617 nm (blue shift) [280-283].

As a comparison to the positively charged dye, and to observe the role of electrostatic interactions with various ND substrates, two negatively charged models were also chosen, this being 8-Hydroxypyrene-1,3,6-trisulfonic acid (pyranine) and 2,2'-azino-bis(3-ethylbenzthiazoline-6-sulphonic acid) ABTS (Figure 1.27). Pyranine is a small, hydrophilic fluorophore that has been shown to have many industrial uses, including as a coloring agent in dyes and cosmetics [285], biological stain, and an optical detecting reagent for bile acids [286]. However, pyranine is most commonly known for its pH detecting properties. While pyranine is capable of measuring intracellular pH, it is not membrane permeable [287]. However, due to its sensitivity, it is often used for monitoring the pH of liposomes. This use of pyranine was first introduced in 1978 by Kano & Fendler. The authors discovered the three sulfonate groups on pyranine completely ionize and are repelled from the negatively charged interior of the liposomes. The interior of these liposomes contain water molecules that are acidic in nature and gave rise to pH detection. Conversely, the anionic nature of pyranine allows for its attraction to positively charged portions of the liposome and as a result also provides information on the surface charge of the cell [288].

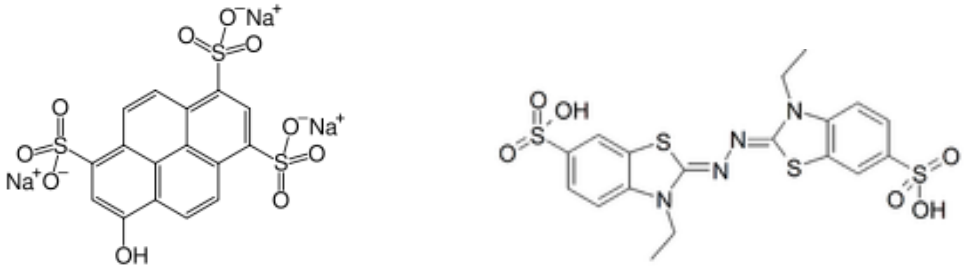

(a) (b)

Figure 1.27. Molecular structure of negatively charged fluorescent dyes Pyranine (a) and ABTS (b).

Pyranine, which has been shown to have a pH-dependent absorption maxima at 380, 400, and 450 nm, undergoes a large excitation shift, at 510 nm, when the molecule becomes protonated and in turn results in a distinct isobestic point. The isobestic point is an important contributor in to pyranine's ability to accurately identify pH by taking the ratio of the two absorption intensities at each side of the isobestic point [287, 289].

The second dye, ABTS, was selected also due to its anionic nature. ABTS has conventional use in observing the kinetic reactions of certain enzymes. It is a stable and nontoxic dye that can be easily dissolved in water. Oxidation of ABTS, through the removal of an electron, results in a solution of a vibrant blue-green hue [290]. The resulting radical cation is reactive towards most antioxidants, including phenolics, thiols and Vitamin C [291], thus it is often used in the food industry to measure the antioxidant capacities of food. After completing the reaction ABTS returns back to its neutral state and colorless form,

which is observed through spectrophotometry [292]. Other applications of ABTS include estimating glucose levels in blood serum. The reaction requires two molecules of glucoseoxidized ABTS for each oxidized glucose molecule [290].

The use of these dyes will not only divulge the absorbing nature of the ND substrates, but the easy coupling of these dyes to ND substrates may also expand the applications of NDs in the area of biosensors.

References

1. Danilenko, V.V., *On the history of the discovery of nanodiamond synthesis.* Physics of the Solid State, 2004. **46**(4): p. 595-599.

2. Shenderova, O.A., V.V. Zhirnov, and D.W. Brenner, *Carbon nanostructures.* Critical Reviews in Solid State and Material Science, 2002. **27**(3-4): p. 227-356.

3. Hall, H.T., *Sintered diamond: a synthetic carbonado* in *Science*. 1970. p. 868-869.

4. Gruen, D.M., *Nanocrystalline diamond films.* Annual Review of Materials Science, 1999. **29** p. 211-259.

5. Carlson, R.M.K., J.E.P. Dahl, and S.G. Liu, *Diamond molecules found in petroleum*. Synthesis, properties, and applications of ultrananocrystalline diamond, ed. D.M. Gruen, A.Vul, and O.A. Shenderova, Vol. 192. 2005: Springer Netherlands. 63-78.

6. Schrand, A.M., S.A. Chiftan Hens, O.A. Shenderova, *Nanodiamond Particles: Properties and Perspectives for Bioapplications.* Critical Reviews in Solid State and Materials Sciences, 2009. **34**: p. 18-74.

7. Dolmatov, V.Y., *Detonation-synthesis nanodiamonds: synthesis, structure, properties and applications* Russian Chemical Reviews, 2007. **76**(4): p. 339-360.

8. Danilenko, V.V., *Shock-wave sintering of nanodiamonds.* Physics of the Solid State, 2004. **46**(4): p. 711-715.

9. Aleksenskii, A.E., M.V. Baidakovam A.Y. Vul', V.I. Siklitskii. *The structure of diamond nanoclusters.* Physics of the Solid State, 1999. **41**(4): p. 668.

10. Vereschagin, A.L., *Detonation Nanodiamonds*. 2001, Altai State Technical University (in Russian): Barnaul, Russia.

11. Baidakova, M.V., A.Y. Vul', V.I. Siklitskii, N.N. Faleev. *Fractal structure of ultradisperse-diamond clusters.* Physics of the Solid State, 1998. **40**(4): p. 715-718.

12. Iakoubovskii, K., et al., *Structure and defects of detonation synthesis nanodiamond* Diamond and Related Materials, 2000. **9**(3-6): p. 861-865.

13. Donnet, J.B., E. Fousson, T.K. Wang, et al. *Dynamic synthesis of diamonds.* Diamond and Related Materials, 2000. **9**: p.877-892.

14. Dolmatov, V.Y., *Detonation synthesis ultradispersed diamonds: properties and applications.* Russian Chemical Reviews, 2001. **70**(7): p. 607-626.

15. Shenderova, O.A. and S.A. Chiftan Hens, *Detonation nanodiamond particles processing, modification and bioapplications*, in *Nanodiamonds: Applications in Biology and Nanoscale Medicine*, D. Ho, Editor. 2010, Springer. p. 79-116.

16. Gibson, N., O. Shenderova, T.J.M. Luo, S. Moseenkov, V. Bondar, A. Puzyr, K. Purtov, Z. Fitzgerald, D.W. Brenner. *Colloidal stability of modified nanodiamond particles.* Diamond and Related Materials, 2009. **18**(4): p. 620-626.

17. Pichot, V., M. Comet, E. Fousson, C. Baras, A. Senger, F. Le Normand, D. Spitzer. *An efficient purification method for detonation nanodiamonds.* Diamond and Related Materials, 2008. **17**(1): p. 13.

18. Petrov, I., O. Shenderova, *History of Russian patents on detonation nanodiamonds*, in *Ultrananocrystalline diamond*, O. Shenderova and D. Gruen, Editor. 2006, William-Andrew: Norwich, UK.

19. Dolmatov, D.Y., *Synthesis and post-synthesis treatment of detonation nanodiamonds*, in *Ultrananocrystalline diamond: synthesis, properties, and applications*, D.M. Gruen and O.A. Shenderova, Editor. 2006, William Andrew Publishing: Norwich, NY. p. 360.

20. Osswald, S., G. Yushin, V. Mochalin, S.O. Kucheyev, Y. Gogotsi. *Control of sp2/sp3 carbon ratio and surface chemistry of nanodiamond powders by selective oxidation in air.* Journal of The American Chemical Society, 2006. **128**(35): p. 11635-11642.

21. Huang, F., Y. Tong, S. Yun, *Synthesis mechanism and technology of ultrafine diamond from detonation.* Physics of the Solid State, 2004. **46**(4): p. 616-619.

22. Petrova, I., O. Shenderova, V. Grishko, et al. *Detonation nanodiamonds simultaneously purified and modified by gas treatment.* Diamond and Related Materials, 2007. **16**(12): p. 2098-2103.

23. Pavlov, E.V., and J.A. Skrjabin, *Method for removal of impurities of non-diamond carbon and device for its realization*. 1994: Russia.

24. Mochalin, V., Y. Gogotsi, *Wet chemistry route to hydrophobic blue fluorescent nanodiamond.* Journal of The Amerian Chemical Society, 2009. **131**(12): p. 4594.

25. Shenderova, O. I. Petrov, J. Walsh, V. Grishko, et al., *Modification of detonation nanodiamonds by heat treatment in air.* Diamond and Related Materials, 2006. **15**(11-12): p. 1799-1803.

26. Spitsyn, B., J.L. Davidson, M.N. Gradoboev, et al. *Inroad to modification of detonation nanodiamond.* Diamond and Related Materials, 2006. **15**(2-3): p. 296-299.

27. Krüger, A., F. Kataoka, M, Ozawa, et al., *Unusually tight aggregation in detonation nanodiamond: Identification and disintegration.* Carbon, 2005. **43**(8): p. 1722-1730.

28. Kulakova, I., *Surface chemistry of nanodiamonds.* Physics of the Solid State, 2004. **46**(4): p. 636-643.

29. Ōsawa, E. *Synthesis, properties and applications of ultrananocrystalline diamond*. in *Proceedings of the NATO Advanced Research Workshop on Ultrananocrystalline Diamond*. 2004. St. Petersburg, Russia: Springer, Dortrecht.

30. Ōsawa, E., *Recent progress and perspectives in single-digit nanodiamond.* Diamond and Related Materials, 2007. **16**(12): p. 2018-2022.

31. Ōsawa, E., *Disintegration and Purification of Crude Aggregates of Detonation Nanodiamond: A Few Remarks on Nano Methodology*, in *NATO Science Series II: Mathematics, Physics and Chemistry, 2005*. 2005, Springer: St. Petersburg, Russia.

32. Ku, J., Q.J. Xue, *Deaggregation of ultradispersed diamond from explosive detonation by a graphitization-oxidation method and by hydriodic acid treatment.* Diamond and Related Materials, 2007. **16**(2): p. 277-282.

33. Krueger, A., M. Ozawa, G. Jarre, et al., *Deagglomeration and functionalisation of detonation diamond.* physica status solidi (a): applications and materials science, 2007. **204**(9): p. 2881–2887.

34. Puzyr, A.P., V.S. Bondar, *Method of production of nanodiamonds of explosive synthesis with an increased colloidal stability*. 2003: Russia.

35. Chukhaeva, S.I., *Synthesis, properties, and applications of fractionated nanodiamonds.* physics of the Solid State, 2004. **46**(4): p. 625-628.

36. Shenderova, O., I. Petrov, J. Walsh, V. Grichko, et al., *Modification of detonation nanodiamonds by heat treatment in air.* Diamond and Related Materials, 2006. **15**(11-12): p. 1799-1803.

37. Morita, Y., T. Takimoto, H. Yamanaka, et al., *A facile and scalable process for size-controllable separation of nanodiamond particles as small as 4 nm.* Small, 2008. **4**(12): p. 2154-2157.

38. Zhu, Y., F. Xu, J. Shen, et al., *Study on the modification of nanodiamond with DN-10.* Journal of Material Science and Technology, 2007. **23**(5): p. 599-603.

39. Loktev, V.F., et al., *Surface modification of ultradispersed diamonds.* Carbon, 1991. **29**(7): p. 817-819.

40. Krüger, A., Y. Liang, G.J., J. Stegk, *Surface functionalisation of detonation diamond suitable for biological applications.* Journal of Materials Chemistry, 2006. **16**(24): p. 2322-2328.

41. Yeap, W.S., Y.Y. Tan, and K.P. Loh, *Using detonation nanodiamond for the specific capture of glycoproteins.* Analytical Chemistry, 2008. **80**(12): p. 4659-4665.

42. Chung, P.H., E. Perevedentseva, et al., *Spectroscopic study of bio-functionalized nanodiamonds.* Diamond and Related Materials, 2005. **15**(4-8): p. 622-625.

43. Huang, L.C.L. and H.C. Chang, *Adsorption and immobilization of cytochrome c on nanodiamonds.* Langmuir, 2004. **20**(14): p. 5870-5884.

44. Huang, T.S., et al., *Immobilization of antibodies and bacterial binding on nanodiamond and carbon nanotubes for biosensor applications.* Diamond and Related Materials, 2004. **13**(4-8): p. 1098-1102.

45. Liu, Y., Z. Gu, J.L. Margrave, et al., *Functionalization of nanoscale diamond powder: fluoro-, alkyl-, amino-, and amino acid-nanodiamond derivatives.* Chemistry of Materials, 2004. **16**(20): p. 3924-3930.

46. Khabashesku, V.N., J.L. Margrave, and E.V. Barrera, *Functionalized carbon nanotubes and nanodiamonds for engineering and biomedical applications.* Diamond and Related Materials, 2005. **14**(3-7): p. 859-866.

47. Riddick, T.M., ed. *Control of colloid stability through zeta potential*. ed. T.M. Riddick. 1968, Creative Press: New York, NY. 138.

48. Zm-75, Zeta Meter Operating Manual. 1968, Zeta-Meter, Inc.: 1720 First Avenue, New York, N.Y. 10028. p. 43.

49. Bondar, V.S. and A.P. Puzyr, *Nanodiamonds for biological investigations.* Physics of the Solid State, 2004. **46**(4): p. 716.

50. Xu, N.S., J. Chen, and S.Z. Deng, *Effect of heat treatment on the properties of nano-diamond under oxygen and argon ambient.* Diamond and Related Materials, 2002. **11**(2): p. 249-256.

51. Xu, X., Z. Yu, Y. Zhu, et al., *Effect of sodium oleate adsorption on the colloidal stability and zeta potential of detonation synthesized diamond particles in aqueous solutions.* Diamond and Related Materials, 2005. **14**(2): p. 206-212.

52. Hens, S., G. Cunningham, T. Tyler, et al., *Nanodiamond bioconjugate probes and their collection by electrophoresis.* Diamond and Related Materials, 2008. **17**(11): p. 1858-1866.

53. Boehm, H.P., *Surface oxides on carbon and their analysis: a critical assessment.* Carbon, 2002. **40**(2): p. 145-149.

54. Fuente, E., J.A. Menendez, D. Suarez, et al., *Basic surface oxides on carbon materials: a global view.* Langmuir, 2003. **19**(8): p. 3505-3511.

55. Montes-Morán, M.A., D. Suarez, J.A. Menéndez, E. Fuente, *On the nature of basic sites on carbon surfaces: An overview.* Carbon, 2004. **42**(7): p. 1219-1225.

56. Raty, J.Y., et al., *Quantum confinement and fullerene like surface reconstructions in nanodiamonds.* Physical Review Letters, 2003. **90**(3): p. 037401-1-037401-4.

57. Ōsawa, E., D.H., H. Huang, M.V. Korobov, N.N. Rozhkova, *Consequences of strong and diverse electrostatic potential fields on the surface of detonation nanodiamond particles.* Diamond and Related Materials, 2009. **18**(5-6): p. 904-909.

58. Barnard, A.S., M. Sternberg, *Crystallinity and surface electrostatics of diamond nanocrystals.* Journal of Materials Chemistry, 2007. **17**(45): p. 4811-4819.

59. Chang, Y.R., H.Y. Lee, K. Chen, et al., *Mass production and dynamic imaging of fluorescent nanodiamonds.* Nature Nanotechnology, 2008. **3**: p. 284-288.

60. Yu, S.J., K.M. Kang, H.C. Chang, et al., *Bright fluorescent nanodiamonds: no photobleaching and low cytotoxicity.* Journal of The Amerian Chemical Society, 2005. **127**(50): p. 17604-17605.

61. Fu, C.C., H,Y. Lee, K. Chen, et al., *Characterization and application of single fluorescent nanodiamonds as cellular biomarkers.* Proceedings of the National Academy of Sciences, 2007. **104**(3): p. 727-732.

62. Neugart, F., A. Zappe, F. Jalezko, et al., *Dynamics of diamond nanoparticles in solution and cells.* Nano Letters, 2007. **7**(12): p. 3588-3591.

63. Bondar, V.S., I.O. Pozdnyakova, and A.P. Puzyr, *Applications of nanodiamonds for separation and purification of proteins.* Physics of the Solid State, 2004. **46**(4): p. 758-760.

64. Huang, H., E. Pierstorff, E. Osawa, et al., *Active nanodiamond hydrogels for chemotherapeutic delivery.* Nano Letters, 2007. **7**(11): p. 3305-3314.

65. Xing, Y. and L. Dai, *Nanodiamonds for nanomedicine.* Nanomedicine, 2009. **4**(2): p. 207-218.

66. Liu, K.K., W.W. Zheng, et al., *Covalent linkage of nanodiamond-paclitaxel for drug delivery and cancer therapy.* Nanotechnology, 2010. **21**(31): p. 1-14.

67. Portet, C., G. Yushin, and Y. Gogotsi, *Electrochemical performance of carbon onions, nanodiamonds, carbon black and multiwalled nanotubes in electrical double layer capacitors.* Carbon, 2007. **45**(13): p. 2511-2518.

68. Kong, X.L., L.C.L. Huang, C.M. Hsu, et al., *High-Affinity Capture of Proteins by Diamond Nanoparticles for Mass Spectrometric Analysis.* Analytical Chemistry, 2005. **77**(1): p. 259-265.

69. Nguyena, T.T.B., H.C. Changa, and V.W.K. Wu, *Adsorption and hydrolytic activity of lysozyme on diamond nanocrystallites.* Diamond and Related Materials, 2007. **16**(4-7): p. 872-876.

70. Krueger, A., *New Carbon Materials: Biological Applications of Functionalized Nanodiamond Materials.* Chemistry: A European Journal, 2007. **14**(5): p. 1382–1390.

71. Krueger, A., J. Stegk, et al., *Biotinylated nanodiamond: simple and efficient functionalization of detonation diamond.* Langmuir, 2008. **24**(8): p. 4200-4204.

72. Cheng, C.Y., E. Perevedentseva, J.S. Tu, et al., *Direct and in vitro observation of growth hormone receptor molecules in A549 human lung epithelial cells by nanodiamonds labeling.* Applied Physics Letters, 2007. **90**(16): p. 163903-163906.

73. Shimkunas, R.A., E. Robinson, et al., *Nanodiamond–insulin complexes as pH-dependent protein delivery vehicles.* Biomaterials, 2009. **30**(29): p. 5720-5728.

74. Perevedentseva, E., C.Y. Cheng, P.H. Chung, et al., *The interaction of the protein lysozyme with bacteria E. coli observed using nanodiamond labelling.* Nanotechnology, 2007. **18**(31): p. 315102.

75. Wu, V.W.K., *Adsorption reaction constants between nanosilica/nanodiamond and lysozyme molecule at pH=11.0.* Chemistry Letters, 2006. **35**(12): p. 1380.

76. Ibrahim, H.R., M. Yamada, K. Matsushita, et al., *Enhanced bactericidal action of lysozyme to Escherichia coli by inserting a hydrophobic pentapeptide into its C terminus.* Journal of Biological Chemistry, 1994. **269**(7): p. 5059-5063.

77. Shilova, O.A., T. Khamova, et al. *Sol-gel synthesis and investigation nanocomposite protective biostable coatings*. in *Nanodiamond 2008,* 2008. St. Petersburg, Russia.

78. Chen, M., E.D. Pierstorff, R. Lam, et al., *Nanodiamond-Mediated Delivery of Water-Insoluble Therapeutics.* ACS Nano, 2009. **3**(7): p. 2016-2022.

79. Houjin H., E. Pierstorff, E. Osawa, D. Ho, *Functionalized nanodiamonds as efficient transmembrane drug carriers*. in *Proceedings of the 7th IEEE International Conference on Nanotechnology*. 2007. Hong Kong.

80. Oberdörster, E., *Manufactured nanomaterials (fullerenes, C60) induce oxidative stress in the brain of juvenile largemouth bass.* Environmental Health Perspectives, 2004. **112**(10): p. 1058-1062.

81. Bellucci, S., *Carbon Nanotubes Toxicity*. Nanoparticles and Nanodevices in Biological Applications, ed. A.W. Z.M. Wang, G. Salamo, N. Kishimoto Vol. 4. 2009, Berlin: Springer-Verlag. 47-67.

82. Sayes, C.M., C.M. Gobin, A.M. Ausman, et al., *The differential cytotoxicity of water-soluble fullerenes.* Nano Letters, 2004. **4**(10): p. 1881-1887.

83. Bianco, A., et al.,. *Biomedical applications of functionalised carbon nanotubes*. Medicinal Chemistry and Pharmacological Potential of Fullerenes and Carbon Nanotubes, ed. F. Cataldo and T. Da Ros. Vol. 1. 2008, Springer. 23-50.

84. Schrand, A.M., *Characterization and in vitro biocompatibility of engineered nanomaterials*, in *The School of Engineering, University of Dayton*. 2007: Dayton, OH.

85. Simon, H.U., A. Haj-Yehia, and F. Levi-Schaffer, *Role of reactive oxygen species (ROS) in apoptosis induction.* Apoptosis, 2000. **5**(5): p. 415-418.

86. Lennon, S.V., S.J. Martin, T. G. Cotter, *Dose-dependent induction of apoptosis in human tumour cell lines by widely diverging stimuli.* Cell Proliferation, 1991. **24**(2): p. 203-214.

87. Schrand, A.M., L. Dai, et al., *Differential biocompatibility of carbon nanotubes and nanodiamonds.* Diamond and Related Materials, 2007. **16**(2): p. 2118-2123.

88. Kagan, V.E., Y.Y. Tyruina, et al., *Direct and indirect effects of single walled carbon nanotubes on RAW 264.7 macrophages: role of iron.* Toxicology Letters, 2006. **165**(1): p. 88-100.

89. Pulskamp, K., S. Diabaté, and H.F. Krug, *Carbon nanotubes show no sign of acute toxicity but induce intracellular reactive oxygen species in dependence on contaminants.* Toxicology Letters, 2007. **168**(1): p. 58-74.

90. Sherwood, L., *Human physiology: from cells to systems 7th edition*, ed. M. Arbogast. 2008, Belmont: Brooks/Cole.

91. Mosmann, T., *Rapid colorimetric assay for cellular growth and survival: application to proliferation and cytotoxicity assays* Journal of Immunological Methods, 1983. **65**(1-2): p. 55-63.

92. Berridge, M.V., P.M. Herst, and A.S. Tan, *Tetrazolium dyes as tools in cell biology: new insights into their cellular reduction.* Biotechnology Annual Review, 2005. **11**: p. 127-152.

93. Murdock, R.C., L. Braydich-Stolle, A.M. Schrand, et al., *Characterization of nanomaterial dispersion in solution prior to in vitro exposure using dynamic light scattering technique.* Toxicological Sciences, 2007. **101**(2): p. 239-253.

94. Schrand, A.M., J. Johnson, L. Dai, et al., *Cytotoxicity and genotoxicity of carbon nanomaterials*, in *Safety of nanoparticles: from manufacturing to clinical applications*, T. Webster, Editor. 2008, Springer: Providence, RI.

95. Puzyr, A.P., D.A. Neshumayev, et al., *Destruction of human blood vells in interaction with detonation nanodiamonds in experiments in vitro.* Diamond and Related Materials, 2004. **13**(11-12): p. 2020-2023.

96. Puzyr, A.P., et al., *Results of studies of possible applications of detonation nanodiamonds as enterosorbents.* Siberian Med. Obozrenie (Siberian Medical Review), 2004. **25**(2-3).

97. Bondar, V. and D. Baron, *Changes in bio-chemical parameters of blood plasma at administration of nanodiamond to laboratory animals.* Bull. Siberian Medi. (in Russian), 2005. **4**: p. 182.

98. A.P. Puzyr, V.S. Bondar, Z.Y. Selimkhanova, et al., *Results of in vitro and in vivo studies using detonation nanodiamonds/complex systems under extreme conditions.* Bull. Siberian Medi. (in Russian), 2005. **4**: p. 185.

99. Puzyr, A.P., A.V. Baron, K.V. Purtov, et al., *Nanodiamonds with novel properties: a biological study.* Diamond and Related Materials, 2007. **16**(12): p. 2124-2128.

100. Puzyr, A.P., et al., *Results of in vitro and in vivo studies using detonation nanodiamonds/complex systems under extreme conditions.* KSC SB RAS, Krasnoyarsk, 2005. **229**.

101. Puzyr, A.P., V.S. Bondar, and S.E. Al, *Dynamics of the selected physiological responses in laboratory mice under the prolonged oral administration of*

nanodiamonds suspensions. Siberian Med. Obozrenie (Siberian Med. Rev.) (in Russian), 2004. **4**: p. 19.

102. Vermeeren, V., N. Bijnens, S. Wenmackers, et al., *Towards a real-time, label-free, diamond-based DNA sensor.* Langmuir, 2007. **23**(26): p. 13193–13202.

103. Holt, K.B., C. Zeigler, D. Caruana, et al., *Redox properties of undoped 5 nm diamond nanoparticles.* Physical Chemistry Chemical Physics, 2008. **10**(303-310): p. 303.

104. Donaldson, K., R. Aitken, et al., *Carbon nanotubes: a review of their properties in relation to pulmonary toxicology and workplace safety.* Toxicological Sciences, 2006. **92**(1): p. 5-22.

105. Dolmatov, V.Y., *Application of detonation nanodiamond*, in *Ultra nanocrystalline diamond: synthesis, properties, and applications*, D.G. O. Shenderova, Editor. 2006, William Andrew Publishing: Norwich, NY, USA. p. 513.

106. Chao, J.I., E. Perevendensteva, P.H, Chung, et al., *Nanometer-sized diamond particle as a probe for biolabeling.* Biophysical Journal, 2007. **93**(6): p. 2199-2208.

107. Liu, K.K., et al., *Biocompatible and detectable carboxylated nanodiamond on human cell.* Nanotechnology, 2007. **18**(32): p. 325102.

108. Tu, J.S., et al., *Size dependent surface CO stretching frequency investigations on nanodiamond particles.* The Journal of Chemical Physics, 2006. **125**: p. 174713.

109. Schmidt, J.A., et al., *Silica-stimulated monocytes release fibroblast proliferation factors identical to interleukin 1. A potential role for interleukin 1 in the pathogenesis of silicosis.* The Journal of Clinical Investigation, 1984. **73**: p. 1462-1472.

110. Dion, I., et al., *Blood haemolysis by ceramics.* Biomaterials, 1993. **14**(2): p. 107-110.

111. Nordsletten, L., et al., *Human monocytes stimulation by particles of hydroxyapatite, silicon carbide and diamond: in vitro studies of new prosthesis coatings.* Biomaterials, 1996. **17**(15): p. 1521-1527.

112. Kostarelos, K., et al., *Cellular uptake of functionalized carbon nanotubes is independent of functional group and cell type.* Nature Nanotechnology, 2007. **2**(108): p. 108-113.

113. Sonnefraud, Y., et al., *Diamond nanocrystals hosting single nitrogen-vacancy color centers sorted by photon correlation near-field microscopy.* Optics, 2008. **33**(6): p. 611-613.

114. Gruber, A., et al., *Scanning confocal optical microscopy and magnetic resonance on single defect centers.* Science, 1997. **276**(5321): p. 2012-2014.

115. Wua, F., J.D. Miller, E.A. Casman, *The Economic Impact of Bt Corn Resulting from Mycotoxin Reduction.* Toxin Reviews, 2004. **23**(2-3): p. 397-424.

116. Schaafsma, A.W., *Economic changes imposed by mycotoxins in food grains: case study of deoxynivalenol in winter wheat.* Advances in Experimental Medicine and Biology, 2002. **504**: p. 271-276.

117. Robbins, C.A., et al., *Health effects of mycotoxins in indoor air: a critical review.* Applied Occupational and Environmental Hygiene, 2000. **15**(10): p. 773-784.

118. Speijers, G. J. A., M.H.M. Speijers, *Combined toxic effects of mycotoxins.* Toxicological Letters, 2004. **153**(10): p. 91-98.

119. Ramos, A.J. and E. Hernández, *In vitro aflatoxin adsorption by means of a montmorillonite silicate. A study of adsorption isotherms.* Animal Feed Science and Technology, 1996. **62**(2): p. 263-269.

120. Gradelet, S., et al., *Dietary carotenoids inhibit aflatoxin B1-induced liver preneoplastic foci and DNA damage in the rat: role of the modulation of aflatoxin B1 metabolism.* Carcinogenesis, 1998. **19**: p. 403-411.

121. Devegowda, G., M.V.L.N. Raju, and H.V.L.N. Swamy., *Mycotoxins: novel solutions for their counteraction.* Feedstuffs, 1998. **70**(50): p. 12-17.

122. Devegowda, G., B.I.R. Aravind, and M.G. Morton. *Saccharomyces cerevisiae and mannanoligosaccharides to counteract aflatoxicosis in broilers*. in *Australian Poultry Science Symposium*. 1996.

123. Galvano, F., et al., *Dietary strategies to counteract the effects of mycotoxins: a review* Journal of Food Protection, 2001. **64**(1): p. 120-131.

124. Ramos, A.J., J. Fink-Gremmels, and E. Hernandez, *Prevention of toxic effects of mycotoxins by means of nonnutritive adsorbent compounds.* Journal of Food Protection, 1996. **59**(6): p. 631-641.

125. Bryden, W.L., *Mycotoxins in the food chain: human health implications.* Asia Pacific Journal of Clinical Nutrition, 2007. **16**(1): p. 95-101.

126. Gradelet, S., et al., *Modulation of aflatoxin B1 carcinogenicity, genotoxicity and metabolism in rat liver by dietary carotenoids: evidence for a protective effect of CYP1A inducers.* Cancer Letters, 1997. **114**: p. 221-223.

127. Hussein, H.S. and J.M. Brasel, *Toxicity, metabolism, and impact of mycotoxins on humans and animals.* Toxicology, 2001. **167**(2): p. 101-134.

128. Ramsdell, H.S. and D.L. Eaton, *Species susceptibility to aflatoxin B1 carcinogenesis.* Cancer Research, 1990. **50**(3): p. 615-620.

129. Haubruge, E., et al., *The prevalence of mycotoxins in kashin-beck disease.* International Orthopedics, 2001. **25**(3): p. 159-161.

130. Squire, R.A., *Ranking animal carcinogens: a proposed regulatory approach.* Science, 1981. **214**(4523): p. 877-880.

131. Kurtzman, C.P., B.W. Horn, and C.W. Hesseltine, *Aspergillus nomius, a new aflatoxin-producing species related to aspergillus flavus and aspergillus tamarii.* Antonie Van Leeuwenhoek, 1987. **53**(3): p. 147-158.

132. Goto, T., et al., *Mycotoxin production ability of aspergillus tamari.* Mycotoxins, 1997. **44**: p. 17-20.

133. Ito, Y., et al., *Aspergillus pseudotamarii, a new aflatoxin producing species in aspergillus flavi.* Mycological Research, 2001. **105**(2): p. 233-239.

134. Mishra, H.N. and C. Das, *A review on biological control and metabolism of aflatoxin.* Critical Reviews in Food Science and Nutrition 2003. **43**(3): p. 245-264.

135. Rensburg, C.V., *The ameliorating effect of oxihumate on aflatoxicosis in broilers*, in *Animal and Wildlife Sciences*. 2005, University of Pretoria: Pretoria.

136. Wood, A.M., *Fungal diseases*, in *Poultry Diseases*, P.M. M. Pattison, J.M. Bradbury, D. Alexander, Editor. 2008, Saunders Elsevier. p. 428.

137. Brown, T., *Fungal Diseases*, in *Poultry Diseases*, M.P. F.T.W. Jordan, Editor. 1996, W.B Saunders Company Ltd.

138. Spensley, P.C., *Aflatoxin, the active principle in turkey'X'disease.* Endeavour, 1963. **22**(75-79): p. 75.

139. Bradburn, N., R.D. Coker, and G. Blunden, *The aetiology of turkey 'x' disease* Phytochemistry, 1994. **35**(3): p. 817.

140. Rheal A. Towner, H. Hashimoto, P.M. Summers, *Non-invasive in vivo magnetic resonance imaging assessment of acute aflatoxin Bl hepatotoxicity in rats.* Biochimica et Biophysica Acta (BBA) 2000. **1475**(3): p. 314-320.

141. Miller, D.M. and D.M. Wilson, *Veterinary diseases related to aflatoxins*, in *The Toxicology of Aflatoxins: Human Health, Veterinary and Agricultural Significance*, J.D.G. D.L. Eaton, Editor. 1994, Academic Press: San Diego, CA. p. 347–364.

142. Moss, M.O., *Risk assessment for aflatoxins in foodstuffs.* International Biodeterioration & Biodegradation, 2002. **50**(3-4): p. 137-142.

143. Anon, *Official Journal of the European Communities*. 1998, Commission Regulation (EC). p. 43–46.

144. Adams, M. and Y. Motarjemi, *Basic food safety for health workers*. Foodborne Hazards. 1999: World Health Organization

145. Anon, *Alarm about aflatoxin.* Nature, 1966. **212**(5070): p. 1512.

146. (FAO), *FAO Food and Nutrition Paper 2.* 1977.

147. FAO-WHO-UNEP, *Global perspective on mycotoxins*, in *MYC Document of 4" Conference on Mycotoxins*. 1977: Nairobi, Kenya.

148. Piva, G., et al., *Detoxification methods of aflatoxins: a review.* Nutritional Research, 1995. **15**(5): p. 767-776.

149. Sinha, K.K., *Detoxification of mycotoxins and food safety*, in *Mycotoxins in Agriculture and Food Safety*, D.B. K. K. Sinha, Editor. 1998, Marcel Dekker: New York, NY. p. 381-406.

150. Santha, T. *Effectiveness of control methods of aflatoxin.* in *Proceedings of 3rd International Food Convention (IFCON), CFTRI*. 1993. Mysore, India.

151. Windstrom, N.W., D.M. Wilson, W.W. McMillan *Ear resistance of maize inbreds to field aflatoxin contamination.* Crop Science, 1984. **24**(6): p. 1154–1157.

152. Mixon, A.G., *Reducing aflatoxin contamination in peanut genotypes by selection and breeding.* Journal of the American Oil Chemists' Society 1981. **58**: p. 961A–966A.

153. Cary, J.W., B.G. Montalbano, and K.C. Ehrlich, *Promoter elements involved in the expression of the Aspergillus parasiticus aflatoxin biosynthesis pathway gene avnA.* Biochimica et Biophysica Acta (BBA), 2000. **1491**(1-3): p. 7-12.

154. Basappa, S.C. and T. Santha, *Methods for detoxification of aflatoxins in foods and feeds—a critical appraisal.* Journal of Food Science and Technology, 1996. **33**(2): p. 95-107.

155. Farag, R.S., M.M. Rashed, A.A. Amel, *Aflatoxin destruction by microwave heating.* International Journal of Food Sciences and Nutrition, 1996. **47**(3): p. 197-208.

156. Park, J.W. and Y.B. Kim, *Effect of pressure cooking on aflatoxin B1 in rice.* Journal of Agricultural and Food Chemistry, 2006. **54**(6): p. 2431-2435.

157. Hwang, J.H. and K.G. Lee, *Reduction of aflatoxin B1 contamination in wheat by various cooking treatments.* Food Chemistry, 2006. **98**(1): p. 71-75.

158. Yazdanpanah, H., et al., *Effect of roasting on degradation of aflatoxins in contaminated pistachio nuts.* Food and Chemical Toxicology, 2005. **43**(7): p. 1135-1139.

159. Nine de Bruyn, I., *The application of high dose food irradiation in South Africa* Radiation Physics and Chemistry, 2000. **57**(3-6): p. 223-225.

160. Herzallah, S., K. Alshawabkeh, and A.A.L. Fataftah, *Aflatoxin decontamination of artificially contaminated feeds by sunlight, gamma-radiation, and microwave heating.* Journal of Applied Poultry Research, 2008. **17**: p. 515-521.

161. Bullerman, L.B. and A. Bianchini, *Stability of mycotoxins during food processing.* International Journal of Food Microbiology, 2007. **119**(1-2): p. 140-146.

162. Raters, M. and R. Matissek, *Thermal stability of aflatoxin B1 and ochratoxin A.* Mycotoxin Research, 2008. **24**(3): p. 130-134.

163. Weng, C.Y. and D.L. Park, *Efficacy and permanency of ammonia treatment in reducing aflatoxin levels in corn.* Food Additives & Contaminants: Part A, 1994. **11**(6): p. 649-658

164. Yang, C.Y., *Comparative studies on the detoxification of aflatoxins by sodium hypochlorite and commercial bleaches.* Applied Microbiology, 1972. **24**(6): p. 885-890.

165. Castegnaro, M., et al., *Problems related to the use of sodium hypochlorite in the detoxification of aflatoxin B 1* American Industrial Hygiene Association Journal, 1981. **42**(5): p. 398-401

166. McKenzie, K.S., et al., *Oxidative degradation and detoxification of mycotoxins using a novel source of ozone.* Food and Chemical Toxicology, 1997. **35**(8): p. 807-820.

167. Prudente, A.D., J.M. King, *Efficacy and Safety Evaluation of Ozonation to Degrade Aflatoxin in Corn.* Journal of Food Science 2002. **67**(8): p. 2865-2872.

168. Inan, F., M. Pala, and I. Doymaz, *Use of ozone in detoxification of aflatoxin B1 in red pepper.* Journal of Stored Products Research, 2007. **43**(4): p. 425-429.

169. (CAST) *Mycotoxins: Risks in Plant, Animal, and Human Systems.* The Science Source for Food, Agricultural, and Environmental Issues, 2003(Task Force Report).

170. Moerch, K.E., et al., *Aflatoxin destruction in corn using sodium bisulfite, sodium hydroxide and aqueous ammonia.* Journal of Food Protection, 1980. **43**(571-574): p. 571.

171. Park, D.L., et al., *Review of the decontamination of aflatoxins by ammoniation: current status and regulation.* Journal of the Association of Official Analytical Chemists, 1988. **71**(4): p. 685-703.

172. Akbas, M.Y. and M. Ozdemir, *Effect of different ozone treatments on aflatoxin degradation and physicochemical properties of pistachios.* Journal of the Science of Food and Agriculture, 2006. **86**(13): p. 2099-2104.

173. Zorlugenç, B., et al., *The influence of gaseous ozone and ozonated water on microbial flora and degradation of aflatoxin B1 in dried figs.* Food Chemistry and Toxicology, 2008. **46**(4): p. 3593–3597.

174. D'Souza, D.H. and R.E. Brackett, *Aflatoxin B1 degradation by Flavobacterium aurantiacum in the presence of reducing conditions and seryl and sulfhydryl group inhibitors.* Journal of Food Protection, 2000. **64**: p. 268-271.

175. Ciegler, A., et al., *Microbial detoxification of aflatoxin.* Applied Microbiology, 1966. **14**(6): p. 934-939.

176. D'Souza, D.H. and R.E. Brackett, *The role of trace metal ions in aflatoxin B1 degradation by flavobacterium aurantiacum.* Journal of Food Protection, 1998. **61**(12): p. 1666-1669.

177. Karunaratne, A., E. Wezenberg, and L.B. Bullerman, *Inhibition of mold growth and aflatoxin production by lactobacillus species.* Journal of Food Protection, 1990. **53**: p. 230-234.

178. Kankaapaa, P., et al., *Binding of aflatoxin B1 alters the adhesion properties of lactobacillus rhamnosus strain GG in a caco- 2 model.* Journal of Food Protection, 2000. **63**: p. 412-414.

179. Chaurasia, H.K., *Kernel infection and aflatoxin production in peanut (Arachis hypogaea L) by Aspergillus flavus in presence of geocarpospheric bacteria.* Journal of Food Science and Technology, 1995. **32**(5): p. 459-464.

180. Hamid, A.B. and J.E. Smith, *Degradation of aflatoxin by aspergillus flavus.* Journal of General Microbiology, 1987. **133**: p. 2023-2029.

181. Ledoux, D.R. and G.E. Rottinghaus, *In vitro and in vivo texting of adsorbents for detoxifying mycotoxins in contaminated feedstuffs*, in *Biotechnology in the Feed Industry. Proceedings of Alltech's 15th Annual Symposium*, K.A.J. T.P. Lyons, Editor. 1999, Nottingham University Press.

182. Puzyr, A.P., K.V. Purtov, O. A. Shenderova, M. Luo, D. W. Brenner, and V. S. Bondar, *The Adsorption of Aflatoxin B1 by Detonation-Synthesis Nanodiamonds.* Doklady Biochemistry and Biophysics, 2007. **417**(1): p. 299-301.

183. Edrington, T.S., L.F. Kubena, R. B. Harvey, G.E. Rottinghaus, *Influence of a Superactivated Charcoal on the Toxic Effects of Aflatoxin or T-2 Toxin in Growing Broilers1.* Poultry Science, 1997. **76**: p. 1205-1211.

184. Diaz, D.E., et al., *Aflatoxin binders I: in vitro binding assay for aflatoxin B1 by several potential sequestering agents.* Mycopathologia, 2002. **156**: p. 223-226.

185. Scheideler, S.E., *Effect of various types of aluminosilicates and aflatoxin on aflatoxin toxicity, bird performance and mineral status.* Poultry Science, 1993. **72**(2): p. 282-288.

186. Chung, T.K., J.W. Erdman, and D.H. Baker, *Hydrated sodium calcium aluminosilicate: effects on zinc, manganese, vitamin A, and riboflavin utilization.* Poultry Science, 1990. **69**(8): p. 1364-1370.

187. Holt, L.E. and P.H. Holz, *The black bottle.* The Journal of Pediatrics, 1963. **63**: p. 306-314.

188. Diamadopoulus, E., P. Samaras, and G.P. Sakellaropoulus, *The effect of activated carmon properties on the adsorption of toxic substances.* Water and Science Technology, 1992. **25**: p. 153-160.

189. Ademoyero, A.A. and R.R. Dalvi, *Efficacy of activated charcoal and other agents in the reduction of hepatotoxic effects of a single dose of aflatoxin B1 in chickens.* Toxicological Letters, 1983. **16**: p. 153-157.

190. Abdelhamid, A.M., et al., *Effect of low level of dietary aflatoxins on baladi rabbits.* Archives of Animal Nutrition, 1990. **40**: p. 517-537.

191. Dalvi, R.R. and C. McGowan, *Experimental induction of chronic aflatoxicosis in chickens by purified aflatoxin B1 and its reversal by activated charcoal, phenobarbital and reduced glutathione.* Poultry Science, 1984. **63**(485-491): p. 485.

192. Decker, W.J. and D.G. Corby, *Activated charcoal adsorbs aflatoxin B1.* Veterinary and Human Toxicology, 1980. **22**(6): p. 388-389.

193. Galvano, F., et al., *Activated carbons: in vitro affinity for aflatoxin B1 and relation of adsorption ability to physicochemical parameters.* Journal of Food Protection, 1996. **59**(5): p. 545-550.

194. Hatch, R.C., et al., *Induced acute aflatoxicosis in goats: treatment with activated charcoal or dual combinations of oxytetrachycline, stanozolol and activated charcoal.* American Journal of Veterinary Research, 1982. **43**: p. 644-648.

195. Jindal, N., S.K. Mahipal, N.K. Mahajan, *Toxicity of aflatoxin B1 in broiler chicks and its reduction by activated charcoal.* Research in Veterinary Science, 1994. **56**(1): p. 37-40.

196. Kubena, L.F., et al., *Efficacy of a hydrated sodium calcium aluminosilicate to reduce the toxicity of aflatoxin and T-2 toxin.* Poultry Science, 1990. **69**: p. 1078-1086.

197. Huwig, A., et al., *Mycotoxin detoxication of animal feed by different adsorbents.* Toxicological Letters, 2001. **122**(2): p. 178-188.

198. Newman, K., ed. *The biochemistry behind esterified glucomannans- titrating mycotoxins out of the diet*. Biotechnology in the feed Industry: Proceedings of Alltech's 16th Annual Symposium, ed. T.P. Lyons and K.A .Jacques. 2000, Nottinghan University Press. 369-382.

199. Savage, T.F., P.F. Cotter, and E.I. Zakrzewsja, *Performance of male turkeys to 8 weeks of age when fed on oligosaccharide derived from yeast cells.* Poultry Science, 1995. **74**(1): p. 53.

200. Stanley, V.G., et al., *The use of saccharomyces cerevisiae to suppress the effects of aflatoxicosis in broiler chicks.* Poultry Science, 2000. **72**: p. 1867-1872.

201. Haskard, C.A., et al., *Surface binding of aflatoxin B1 by lactic acid bacteria.* Applied and Environmental Microbiology, 2001. **67**(7): p. 3086-3091.

202. Schär-Zammaretti, P. and J. Ubbink, *The cell wall of lactic acid bacteria: surface constituents and macromolecular conformations.* Biophysical Journal, 2003. **85**(6): p. 4076-4092.

203. Haskard, C., C. Binnion, and J. Ahokas, *Factors affecting the sequestration of aflatoxin by lactobacillus rhamnosus strain GG.* Chemico-Biological Interactions, 2000. **128**(1): p. 39-49.

204. B. Sáncheza, P. Bressollier, S. Chaignepainb, J.M. Schmitterb and M.C. Urdacia, *Identification of surface-associated proteins in the probiotic bacterium lactobacillus rhamnosus GG.* International Dairy Journal, 2009. **19**(2): p. 85-88.

205. El-Nezami, H., et al., *Ability of lactobacillus and propionibacterium strains to remove aflatoxin B1 from the chicken duodenum.* Journal of Food Protection, 2000. **63**(4): p. 549-552.

206. El-Nezami, H., et al., *Ability of dairy strains of lactic acid bacteria to bind a common food carcinogen, aflatoxin B1.* Food and Chemical Toxicology, 1998. **36**: p. 321-326.

207. Carretero, M.I., *Clay minerals and their beneficial effects upon human health.* Applied Clay Science, 2002. **21**(3): p. 155-163.

208. Johns, T. and M. Duquette, *Detoxification and mineral supplementation as functions of geophagy.* American Journal of Clinical Nutrition, 1991. **53**(2): p. 448-456.

209. Diamond, J.M., *Evolutionary biology: dirty eating for healthy living.* Nature, 1999. **400**(6740): p. 120-121.

210. Phillips, T.D., et al., *Reducing human exposure to aflatoxin through the use of clay: a review.* Food Additives & Contaminants: Part A, 2008. **25**(2): p. 134-145.

211. Phillips, T.D., S.L. Lemke, and P.G. Grant, *Characterization of clay-based enterosorbents for the prevention of aflatoxicosis.* . Advances in Experimental Medicine and Biology, 2002. **504**: p. 157-71.

212. Phillips, T.D., A.B. Sarr, and P.G. Grant, *Selective chemisorption and detoxification of aflatoxins by phyllosilcate clay.* Natural Toxins, 1995. **3**(4): p. 204-213.

213. Phillips, T.D., et al., *The potential of aflatoxin sequestering clay*, in *The Mycotoxin Fact Book*, D. Barug. D. Barug, H. Van Egmond, J. Van der Kamp, W. Van Osenbruggen, A. Visconti,, Editor. 2006, Wageningen Academic Publishing: Wageningen. p. 329-346.

214. Ming, D.W. and F.A. Mumpton. *Zeolite in soils*. in *Minerals in Soil Environments* 1989. Madison, WI: Soil Society of America.

215. Mumpton, F. A., P.H. Fishman, *The application of natural zeolites in animal science and aquaculture.* Journal of Animal Science, 1977. **45**: p. 1188-1203.

216. Dvorak, M., *Ability of bentonite and natural zeolite to absorb aflatoxin from liquid media.* Veterinary Medicine, 1989. **34**: p. 307-316.

217. Fukal, L., et al., *The effect of a high aflatoxin B1 concentration in feed on the weights of organs and strength of bones in grown-up chickens.* Biol. Chem. Vet. (Praha), 1990. **26**: p. 187-191.

218. Sova, Z., et al., *Hematological and histological response to the diet containing aflatoxin B1 and zeolite in broilers of domestic fowl* Acta Veterinaria Brno, 1991. **60**: p. 31-40.

219. Harvey, R.B., et al., *Efficacy of zeolitic ore compounds on the toxicity of aflatoxin growing broiler chickens.* Avian Diseases, 1993. **37**: p. 67-73.

220. Grim, R.E. and N. Guven, *Bentonites: geology, mineralogy, properties and uses*. Developments in Sedimentology 24. 1978, Amsterdam: Elsevier Scientific.

221. Masimango, N., J. Remacle, and J.L. Ramaut, *The role of adsorption in the elimination of aflatoxin B1 from contaminated media.* Applied Microbiology and Biotechnology, 1978. **6**(1): p. 101-105.

222. Schell, T.C., M.D. Lindemann, E.T. Kornegay, D.J. Blodgett and J.A. Doerr *Effectiveness of different types of clays for reducing the detrimental effects of aflatoxin-contaminated diets on performance and serum profiles of weanling pigs.* Journal of Animal Science, 1993. **41**(5): p. 1226-1231.

223. Lindemann, M.D., D.J. Blodgett, E.T. Kornegay and G.G. Schurig *Potential ameliorators of aflatoxicosis in weanling/growing swine.* Journal of Animal Science, 1993. **71**(1): p. 171-178.

224. Schell, T.C., et al., *Effect of feeding aflatoxin-contaminated diets with and without clays to weanling and growing pigs on performance, liver function, and mineral metabolism.* Journal of Animal Science, 1993. **71**(1): p. 1209-1218.

225. Theng, B.K.G., *The chemistry of clay organic reactions*. Clay and Clay Minerals, ed. J.W. Jordan. 1974, London: Halsted Press.

226. Davidson, J.N., et al., *Hydrated sodium calcium aluminosilicate decreases the bioavailability of aflatoxin in the chicken.* Poultry Science, 1987. **66**(1): p. 89.

227. Phillips, T.D., et al., *Hydrated sodium calcium aluminosilicate: a high affinity sorbent for aflatoxin.* Poultry Science, 1988. **67**(2): p. 243-247.

228. Phillips, T.D., et al., *Detection and detoxification of aflatoxins: prevention of aflatoxicosis and aflatoxin residues with hydrated sodium calcium aluminosilicate.* Veterinary and Human Toxicology, 1990. **32**: p. 15-19.

229. Grant, P.G., T.D. Phillips, *Isothermal adsorption of aflatoxin B1 on HSCAS clay.* Journal of Agricultural and Food Chemistry, 1998. **46**(2): p. 599-605.

230. Kubena, L.F., et al., *Effects of a hydrated sodium calcium aluminosilicate on growing turkey poults during aflatoxicosis.* Poultry Science, 1991. **70**(8): p. 1823-1830.

231. Bonna, R.J., et al., *Efficacy of hydrated sodium alumino silicate and activated charcoal in reducing the toxicity of dietary aflatoxin to mink.* Archives of Environmental Contamination and Toxicology, 1991. **20**: p. 441-447.

232. Harvey, R.B., et al., *Diminution of aflatoxin toxicity to growing lambs by dietary supplementation with hydrated sodium calcium alumino silicate.* American Journal of Vetrinary Research, 1991. **52**(1): p. 152-156.

233. Harvey, R.B., et al., *Effects on aflatoxin M1 residues in milk by addition of hydrated sodium calcium alumino silicate to aflatoxincontaminated diets of dairy cows.* American Journal of Vetrinary Research, 1991. **52**(9): p. 1556-1559.

234. Sarr, A.B., B.A. Clement, and T.D. Phillips, *Effects of molecular structure on the chemisorption of aflatoxin Bl and related compounds by hydrated sodium calcium aluminosilicate.* Toxicologist, 1990. **60**: p. 163.

235. Phillips, T.D., *Dietary clay in the chemoprevention of aflatoxin-induced disease.* Toxicological Sciences, 1999. **52**(1): p. 118-126.

236. Grant, P., *Investigation of the mechanism of aflatoxin B1 adsorption to clays and sorbents through the use of isothermal analysis*. 1998, Texas A&M University College Station, TX.

237. Wiles, M., et al., *Toxicological evaluation and metal bioavailability in pregnant rats following exposure to clay minerals in the diet.* Journal of Toxicology and Environmental Health, 2004. **67**(11): p. 863-874.

238. Afriyie-Gyawu, E., et al., *Chronic toxicological evaluation of dietary novasil clay in sprague-dawley rats.* Food Additives & Contaminants: Part A, 2005. **22**(3): p. 259-269.

239. Akande, K.E., et al., *Nutritional and health implications of mycotoxins in animal feeds: a review.* Pakistan Journal of Nutrition, 2006. **5**(5): p. 398-340.

240. Wang, J.S., et al., *Short-term safety evaluation of processed calcium montmorillonite clay (NovaSil) in humans.* Food Additives and Contaminants 2005. **22**: p. 270-279.

241. Afriyie-Gyawu, E., et al., *NovaSil clay intervention in ghanaians at high risk for aflatoxicosis, part I: study design and clinical outcomes.* Food Additives & Contaminants: Part A, 2008. **25**(1): p. 76-87.

242. Mogilnaya, O.A., A.P. Puzyr, A.V. Baron, V.S. Bondar, *Hematological Parameters and the State of Liver Cells of Rats After Oral Administration of Aflatoxin B1 Alone and Together with Nanodiamonds.* Nanoscale Research letters, 2010. **5**: p. 908-912.

243. Gibson, N.M. T.J.M. Luo, O. Shenderova, and D.W. Brenner, *Aflatoxin B1 and Ochratoxin A Adsorption by Modified Nanodiamonds.* Chapter 7.

244. Puzyr, A.P., A.E. Burov, V. S. Bondar and Yu. N. Trusov, *Neutralization of aflatoxin B1 by ozone treatment and adsorption by nanodiamonds* Nanotechnologies in Russia, 2010. **5**(1-2): p. 137-141.

245. Hengstler, J.G., et al., *Interspecies differences in cancer susceptibility and toxicity.* Drug Metabolism Reviews, 1999. **31**(4): p. 917-970.

246. Rosa, C.A.R., et al., *Evaluation of the efficacy of bentonite from the south of argentina to ameliorate the toxic effects of aflatoxin in broilers.* Poultry Science, 2001. **80**(2): p. 139-144.

247. Soriano, J.M., et al., *Control and decontamination of ochratoxin A in food processing: the key of tracability*, in *New Issues in Food Policy, Control and Research*, A.P. Riley, Editor. 2007, Nova Science: New York, NY.

248. Denli, M. and J.F. Perez, *Ochratoxins in feed, a risk for animal and human health: control strategies.* Toxins, 2010. **2**: p. 1065-1077.

249. WHO, *Environmental Health Criteria*. 1990, Geneva. 105.

250. Breitholtz-Emanuelsson, A., et al., *Ochratoxin A in cow's milk and in human milk with corresponding human blood samples* Journal of the Association of Official Analytical Chemists 1993. **76**: p. 842.

251. Miraglia, M., et al., *Ochratoxin A levels in human milk and related food samples: an exposure assessment.* Natural Toxins, 1995. **3**: p. 436.

252. Murphy, P.A., et al., *Food mycotoxins: an update.* Journal of Food Science and Technology, 2006. **71**(5): p. R51-R65.

253. Berry, L., *The pathology of mycotoxins.* Journal of Pathology, 1988. **154**(4): p. 301–311.

254. Puntarić, D., et al., *Ochratoxin A in corn and wheat: geographical association with endemic nephropathy.* Croatian Medical Journal, 2001. **42**(2): p. 175-180.

255. O'Brien, E. and D.R. Dietrich, *Ochratoxin A: the continuing enigma.* Critical Reviews in Toxicology, 2005. **35**(1): p. 33-60.

256. IARC, *Some naturally occurring substances: food items and constituents, heterocyclic aromatic amines and mycotoxin*, in *WHO*, I.a. WHO, Editor. 1993, IARC, WHO: Lyon. p. 489.

257. Park, D.L. and T.C. Troxell, *U.S. perspective on mycotoxin regulatory issues* in *Mycotoxins and Food Safety*, M.W.T. J.W. DeVries, L.B. Jackson, Editor. 2002, Kluwer Academic/Plenum: Summit Arga. p. 277.

258. Commission, E., *Assessment of dietary intake of ochratoxin A by the population of EU member states*. 1997, Reports of Task Force on Scientific Co-operation.

259. Atkins, D. and J. Norman, *Mycotoxins and food safety.* Nutrition & Food Science, 1998. **98**(5): p. 260-266.

260. Pitt, J.I., et al., *Mycotoxins and toxigenic fungi.* Medical Mycology, 2000. **38**(Supplement 1): p. 41-46.

261. Alldrick, A.J., *The effects of processing on the occurrence of ochratoxin A in cereals.* Food Additives & Contaminants, 1996. **13**: p. S27-S28.

262. Varga, J., et al., *Chemical, physical and biological approaches to prevent ochratoxin induced toxicoses in humans and animals.* Toxins, 2010. **2**: p. 1718-1750.

263. Scott, P.M., *Effects of processing and detoxification treatments on ochratoxin A: introduction.* Food Additives & Contaminants, 1996. **13**(Suppl.): p. 19-21.

264. M. Peraica, A.M. Domijan, Z. Jurjevic, B. Cvjetkovic, *Prevention of exposure to mycotoxins from food and feed.* Arh Hig Rada Toksikol 2002. **53**: p. 229–237.

265. Hult, K., A. Teiling, and S. Gatenbeck, *Degradation of ochratoxin A by a ruminant.* Applied and Environmental Microbiology, 1976. **32**: p. 443-444.

266. Pitout, M.J., *The hydrolysis of ochratoxin A by some proteolytic enzymes.* Biochemical Pharmacology, 1969. **18**(2): p. 485-491.

267. Akiyama, H., et al., *The degradation of several mycotoxins by human intestinal microflora cultured by continuous flow culture system.* Mycotoxins 1997. **44**: p. 21-27.

268. Bruinink, A., T. Rasonyi, and C. Sidler, *Differences in neurotoxic effects of ochratoxin A, ochracin and ochratoxin-alpha in vitro.* Natural Toxins, 1998. **6**: p. 173-177.

269. Follmann, W., et al., *Sister chromatid exchange frequency in cultured isolated porcine urinary bladder epithelial cells (PUBEC) treated with ochratoxin A and alpha.* Archives of Toxicology, 1995. **69**: p. 280-286.

270. Creppy, E.E., I. Baudrimont, and A.M. Betbeder, *How aspartame prevents the toxicity of ochratoxin A.* Journal of Toxicological Sciences, 1998. **2**: p. 165-172.

271. Baker, A., *State will expand tests that find defects in newborns*, in *The New York Times*. 2004: Albany.

272. Ringot, D., B. Lerzy, J.P. Bonhoure, E. Auclair, E. Oriol, Y. Larondelle, *Effect of temperature on in vitro ochratoxin A biosorption onto yeast cell wall derivatives.* Process Biochemistry, 2005. **40**: p. 3008-3016.

273. Ringot, D., et al., *In vitro biosorption of ochratoxin A on the yeast industry by-products: comparison of isotherm models.* Bioresource Technology, 2007. **98**: p. 1812-1821.

274. Galvano, F., et al., *Activated carbons: in vitro affinity for ochratoxin A and deoxynivalenol and relation of adsorption ability to physicochemical parameters.* Journal of Food Protection, 1998. **61**: p. 469-475.

275. Rotter, R.G., A.A. Frohlich, and R.R. Marquardt, *Influence of dietary charcoal on ochratoxin a toxicity in leghorn chicks.* Canadian Journal of Veterinary Research, 1989. **53**: p. 449-453.

276. Tomasevic-Canovic, M., et al., *Surfactant modified zeolites—new efficient adsorbents for mycotoxins.* Microporous and Mesoporous Materials, 2003. **61**: p. 173-180.

277. Yang, W., O. Auciello, J.E. Butler, W. Cai, J.A. Carlisle, J.E. Gerbi, D.M. Gruen, T. Knickerbocker, T.L. Lasserter, J.N. Russell, L.M. Smith, and R.J. Hamers. *DNA-*

modified nanocrystalline diamond thin-films as stable, biologically active substrates Nature Materials, 2002. **1**: p. 253–257.

278. Foglieni, C., C. Meoni, and A.M. Davalli, *Fluorescent dyes for cell viability: an application on prefixed conditions.* Histochemistry and Cell Biology, 2001. **115**(3): p. 223-229.

279. Gitig, D.M. and A. Koff, *Cdk Pathway: cyclin-dependent kinases and cyclin-dependent kinase inhibitors.* Molecular Biotechnology, 2001. **19**(2): p. 179-188.

280. Waring, M.J., *Complex formation between ethidium bromide and nucleic acids.* Journal of Molecular Biology, 1965. **13**(1): p. 269-282.

281. Waring, M., *Variation of supercoils in closed circular DNA by binding of antibiotics and drugs: evidence for molecular models involving intercalation.* Journal of Molecular Biology, 1970. **54**: p. 247-279.

282. Arndt-Jovin, D.J. and T.M. Jovin, *Fluorescent labeling and microscopy of DNA.* Methods of Cell Biology, 1989. **30**: p. 417-448.

283. Lecoeur, H., *Nuclear apoptosis detection by Flow Cytometry: Influence of Endogenous Endonucleases* Experimental Cell Research, 2002. **277**(1): p. 1-14.

284. Schmid, I., W.J. Krall, C**.**H. Uittenbogaart, J. Braun, and V. Giorgi *Dead cell discrimination with 7-amino-actinomcin D in combination with dual color immunofluorescence in single laser flow cytometry.* Cytometry Part A, 1992. **13**(2): p. 204-208.

285. Otterstätter, G., *Coloring of food, drugs, and cosmetics*. 1999, New York: : Marcel Dekker.

286. Camara, J.N., et al., *Boronic acid substituted viologen based optical sugar sensors: modulated quenching with viologen as a method for monosaccharide detection.* Tetrahedron Letters, 2002. **43**(7): p. 1139-1141.

287. Gan, B.S., et al., *Loading pyranine via purinergic receptors or hypotonic stress for measurement of cytosolic pH by imaging.* American Journal of Physiology: Cell Physiology, 1998. **275**(4): p. 1158-1166.

288. Kanoa, K. and J.H. Fendlera, *Pyranine as a sensitive pH probe for liposome interiors and surfaces: pH gradients across phospholipid vesicles.* Biochimica et Biophysica Acta (BBA) - Biomembranes, 1978. **509**(2): p. 289-299.

289. Giuliano, K.A. and R.J. Gillies, *Determination of intracellular pH of BALB/c-3T3 cells using the fluorescence of pyranine.* Analytical Biochemistry, 1987. **167**(2): p. 362-371.

290. R.C. Bateman Jr, J.A. Evans, *Using the glucose oxidase/peroxidase system in enzyme kinetics.* Journal of Chemical Education, 1995. **72**(12): p. A240-241.

291. Walker, R.B. and J.D. Everette, *Comparative reaction rates of various antioxidants with ABTS radical cation.* Journal of Agricultural and Food Chemistry, 2009. **57** (4): p. 1156–1161.

292. Huang, D., B. Ou, and R.L. Prior, *The chemistry behind antioxidant capacity assays.* Journal of Agricultural and Food Chemistry, 2005. **53**(6): p. 1841-1856.

Chapter 2

Nanodiamonds for Detoxification

Published in the Technical Proceedings of the 2007 NSTI Nanotechnology Conference and Trade Show (2007)

Nanodiamonds for Detoxification

N. Gibson [1], O. Shenderova [2, 1], A. Puzyr [3], K. Purtov [3], V. Grichko [2], T. J. M. Luo [1], Z. Fitzgerald [1], V. Bondar [3], D. Brenner [1]

[1] Department of Materials Science and Engineering, NC State University, Raleigh, NC
[2] International Technology Center, Research Triangle Park, NC
[3] Institute of Biophysics, Russian Academy of Sciences, Krasnoyarsk, Russia.

Abstract

Identifying new biocompatible enterosorbents that bind aflatoxins is an active area of research. One particular enterosorbent of interest is nanodiamond particles. We report the first experiments on using nanodiamonds (NDs) as enterosorbents for aflatoxin (Af) adsorption. Because nanodiamonds exhibit low colloidal stability, modification techniques and ways of stabilizing these structures over various pH environments are essential. Analysis of colloidal stability of ND suspensions that have undergone different surface modifications is presented based on measurements of their zeta potentials and on titration experiments.

***Keywords*:** nanodiamonds, bioapplications, aflatoxins, enterosorbents, nanoparticles.

2.1 Introduction

Mycotoxins, low molecular weight metabolites produced by fungi, are potential carcinogens. Aflatoxins, a group of mycotoxins, are invisible to the naked eye and may affect humans directly or indirectly by ingestion of moldy foods or infected animal products. Enterosorbents, structures that bind toxins in the gastrointestinal tract, are an effective way to remove mycotoxins. Requirements for a successful enterosorbent include biocompatibility, good dispersivity during ingestion and excellent selectivity as to not interfere with the adsorption of critical nutrients needed in the diet [1]. Furthermore, they should be relatively cheap and abundant, as well as easily transported and administered. Previous studies have shown that hydrated sodium calcium aluminosilicate (HSCAS) clay as a feed additive [1] serves as an effective enterosorbent for the binding of aflatoxins. While HSCAS is effective towards aflatoxin adsorption, it has a low selectivity, which motivates the discovery of more suitable enterosorbents.

Nanodiamonds (NDs) are among one of the materials being researched for enterosorbent applications. ND particles have attractive physicochemical properties that include very high surface densities (300-400 m^2/g), rich surface chemistries, and permanent surface charges. Previous studies indicate that these diamond nanoparticles are biocompatible and non-toxic [2, 3]. Such properties are critical for their biomedical use. Biocompatibility and non toxicity issues were demonstrated in white mice by substituting ND hydrosols (0.002-0.5 wt. %) for water over a period of 3-6 months [2]. No significant weight changes, problems in reproduction (over 5 generations) or deaths were observed as a result of this

study. However, with extended substitution, leukocyte counts were increased, with the level dependent on the concentration of NDs in the hydrosol [2, 3]. A second study using intramuscular injection showed no tissue inflammation at the area of injection [3]. Outcomes from these studies encourage further research and indicate that the use of diamond nanoparticles may be promising for binding particular classes of mycotoxins in both animal and potentially human use.

While their physicochemical properties make them attractive candidates as enterosorbents, selection of the appropriate NDs for mycotoxin binding is not straight forward, primarily due to a wide variety of ND types. In general, NDs produced by detonation of carbon-containing explosives were purified from the soot and metallic impurities were removed by a wide variety of methods at an industrial scale. This results in different aggregates size and surface chemistry, which leads to various levels of dispersivity and stability among ND particles. Colloidal stability among vendor received, unmodified nanodiamonds in most cases is quite low. Appropriate surface modification significantly increases ND colloidal stability [4]. Additional processing may include fractionation [5] and treatment in atmospheric plasma [6] to produce target surface structures that alter chemical and physical properties that in turn change both the hydrophilic/hydrophobic and dispersivity characteristics.

With an end goal to develop the optimal enterosorbent, such characteristics as particle size, surface chemistry, and zeta potential across different pH levels have been studied for

several types of NDs and are reported below. Preliminary results on binding aflatoxin by ND particles are also discussed.

2.2 Experimental Details

The ND used in this work was synthesized by the detonation of a mixture of trinitrotoluene (TNT) and 1,3,5-trinitro-1,3,5-*s*-triazine (RDX). The sample denoted Ch-St was purchased from "New Technologies", Chelyabinsk, Russia. This sample was generated by a detonation soot purification process using a mixture of sulfuric acid with chromic anhydride treatment, washed with water, and dried. Sample Ch-St was then additionally purified using ion-exchange resins, heat treated in an air atmosphere and fractionated by centrifugation. This modified sample is called Ch-I6 in the experiments below. Samples denoted Kr-Black and Kr-Grey were produced at the Krasnoyarsk Research Center, Russia by explosion of TNT/RDX in a CO_2 atmosphere and oxidized in air in the presence of boric anhydride. The samples were then modified, as given in reference [4], resulting in a significant increase of the ND dispersivity and hydrosol stability. Sample RUDDM was purchased from Real-Dzerzinsk, LTD. This product was also modified according to the method in reference [4], fractionated and dried. The polydispersed powder (RUDDM) was fractionated to 2 fractions with ND agglomerate size within the 0-250nm range (RUDDM 1) and the 150-400nm range (RUDDM 2). Prior to zeta-potential and particle size measurements, the ND suspensions were sonicated. The sonicator was equipped with a tapered titanium horn with a tip diameter of 3 mm (Cole-Parmer® 750-Watt Ultrasonic

Homogenizer EW-04711-60, 20 kHz), which was directly immersed into the sample. The output power was 10 W and the output intensity was ~100 W/cm [3]. Size distributions of the NDs in their hydrosols were measured by dynamic light scattering using a Beckman-Coulter N5 submicron particle size analyzer and Malvern ZetaSizer Nano ZS. Zeta potential values were measured using laser doppler velocimetry (ZetaSizer Nano ZS, Malvern Instruments). The pH titrations of 0.1 wt. % ND suspensions were conducted in several manners: from pH of 12 to 1; from pH of 1 to 12 and, additionally, from the 'natural' pH of suspensions to 1 or to 12. To conduct the pH titration, 0.1M HCl and 0.1M NaOH were used. De-ionized (DI) water with a resistivity of 18 MΩ·cm was used to prepare the samples.

Aflatoxin B_1 (Af) was purchased from VNIIVSGE (Russia). A suspension of Af (5 μg/ml) in DI water was mixed with a ND hydrosol (10 mg/ml) in the ratio 1:1. After a 5 min incubation time, Ca^+ ions (5 mM) were added to the mixture to promote ND coagulation. After separating the NDs with adsorbed Af using centrifugation (Eppendorf Mini Spin Plus centrifuge), the concentration of the Af in the supernatant was measured and compared with the concentration of the stock Af solution. Adsorption capacity was calculated as the difference between the initial and final concentrations of Af. The concentration of Af in suspensions was measured by two methods: from fluorescence spectra collected with SpectronicUnicam (USA) and by High performance liquid chromatography (HPLC) with a Milichrom A-02 (EcoNova, Novosibirsk). It was noticed that fluorescence of Af nonlinearly depended on a variety of factors such as irradiation time, Af concentration as well as

presence of the traces of NDs in the suspension. These factors made interpretation of the results challenging.

2.3 Results and Discussion

2.3.1 Zeta Potential

The zeta potential is the electrostatic potential (or the net charge) at the particle-slipping plane. The slipping plane is the boundary of a hypothetical sphere enclosing a particle (where loosely bound ions form a stable state and move together with a particle). It is generally stated that colloids with zeta potential values above 30 mV or below -30 mV are considered stable suspensions because particles electrostatically repel each other and do not agglomerate.

It was important that the sample preparation procedures provide reproducible results. Thus, we studied several factors that can potentially influence readings of the zeta potential, namely the role of the sample sonication and ND concentration. To study the role of sonication time, suspensions of 0.1 wt. % I6 in DI water were prepared and sonicated for 0, 1, 2, 3, 5 or 10 minutes. The zeta potential of the suspension without agitation was also measured. The ND zeta potential result was the average of six consecutive measurements with a standard deviation (STD) about 1-2 mV. The results of this study are illustrated in Figure 2.1. It can be concluded that sonication time has little affect on the zeta potential readings.

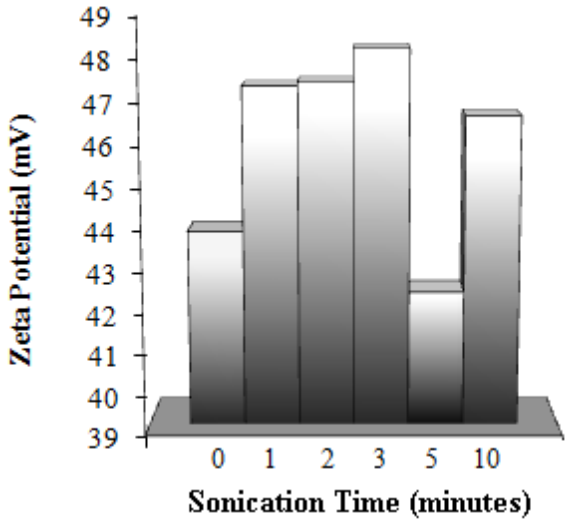

Figure 2.1. Zeta Potential as a function of sonication time for 0.5 wt. % I6 ND.

The dependence of zeta potential on sample concentration was also studied for the I6 ND suspension (Figure 2.2). An increase in the absolute value of the zeta potential by several mV was observed as the sample was diluted from ~0.1 wt. % to ~0.01 wt. %. A similar tendency was observed for several other ND types. To avoid a number of variables, a standard procedure for performing zeta potential measurements on samples with 0.1 wt. % was used in further experiments. The results most likely indicate that the number of dissociating surface groups responsible for the surface charge of the ND is concentration dependent.

A second study by Choa *et. al*. confirms the internalization of NDs inside the cytoplasm by using A549 human lung adenocarcinoma cells [106]. The experiments used carboxylated NDs. In their natural form, NDs exhibit fluorescent abilities, due to nitrogen vacancy (N-V) defects [60, 113, 114], thus, pre-labeling with florescent dyes could be

eliminated. Interestingly, NDs which did not penetrate the cell were shown to adhere to the cells membrane even after repeated washing with PBS solution. This interaction is likely due to the interaction of COO^- groups found on the carboxylated NDs and the NH_3^+ groups on the outside to the cell's exterior. Penetration and localization of the NDs inside the cytoplasm were demonstrated through Raman and fluorescence experiments (Figure 1.19) [106].

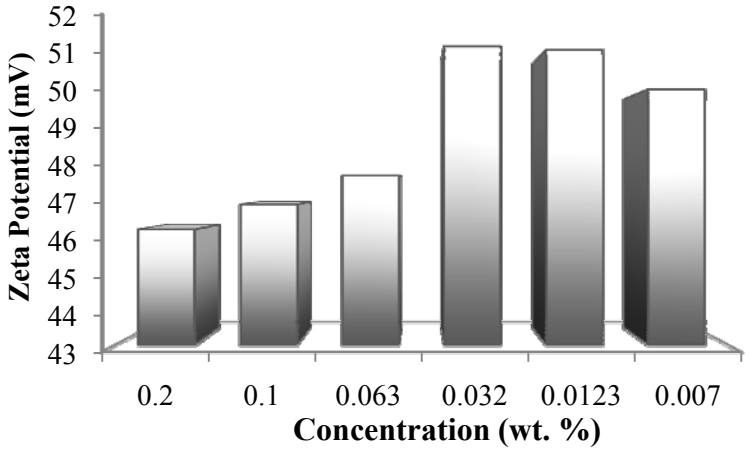

Figure 2.2. Dependence of zeta potential on ND concentration, using I6-ND.

Table 2.1 below summarizes agglomerate sizes and zeta potentials of several types of NDs. The size result is the average of six consecutive measurements with a standard deviation (STD) of ~3-4 nm. All samples, except Ch-St, demonstrate a high zeta potential, in correspondence with the high colloidal stability of these samples. Both positive and negative zeta potentials for the studied samples were observed. In principle, this can be important for adsorption of charged toxins by means of electrostatic interactions. The different zeta potential signs for the two groups of samples (Ch-St and I6) and (Kr and RUDDM) are caused by different types of the chemical groups at the surface of the particles. These

chemical groups originate from different stages of sample purification/modification and, possibly, due to residual metal ions that are incorporated to the particles during synthesis. In the present paper we do not proceed with a detailed discussion of the origin of the sign of zeta potentials of the samples. Nonetheless, it is worth mentioning that the modification [4] itself does not change the zeta potential sign; Ch-St, modified by the method in reference [4], demonstrates a zeta-potential of ~ +40 mV. It should be noted also that there is no correlation between aggregate size and zeta potential in the studied samples.

Table 2.1. Agglomerate size (nm) and zeta potential (ZP, mV) for 0.1wt% ND suspensions in DI water.

ND (0.1 wt. %)	ZP (mV)	ZP STD	Size (nm)
Ch-I6 (I6)	+46.8	0.9	185
Ch-St	+17.4	0.4	300
Kr-Black	-47	2.1	80
Kr-Grey	-44.7	0.6	397
RUDDM 1	-49.3	1.9	75

2.3.2 Titration of ND Suspensions

Titration studies were carried out to determine the stability of ND suspensions at various pH levels. Due to the proposed end use of ND as gastrointestinal (GI) nanoenterosorbents, the selected pH range was broad enough to simulate conditions in cow GI tract. It has been observed that zeta potential values vary depending on the starting point of the titration. For the five samples under study the titration curves were first taken from

initial pH to 1 and initial pH to 12 for 0.1 wt. % ND suspensions (two independent titrations). The initial pH values of these samples ranged within pH 5-6 (pH of the DI water was ~5.8). The titration curves of these samples are plotted in Figure 2.3.

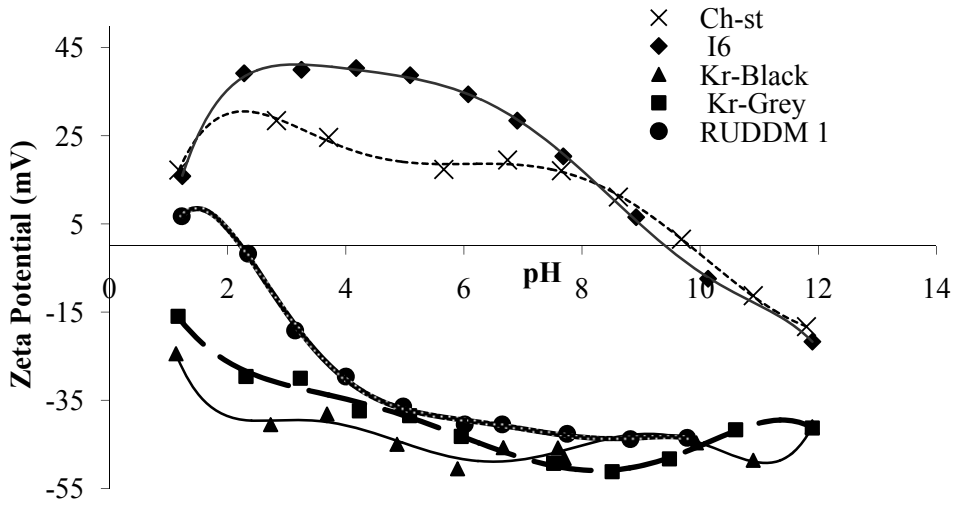

Figure 2.3. Zeta potential vs. pH for five NDs (0.1 wt. %). Titration was carried out starting at initial pH toward either pH 1 or pH 12 in each case.

During this experiment it was observed that the stability over pH environments depends on the charge of the nanodiamond particle. Those nanodiamonds that were negatively charged showed a decrease in colloidal stability as pH approaches 1 (shown quite prominently for RUDDM 1). RUDDM 1, which under normal conditions was shown to be the most stable of the nanodiamond types, possesses an isoelectric point (point of least stability) at a pH of ~2.4, and noted to be the least stable of all negatively charged nanodiamonds. For those samples that hold a positive charge, as pH was increased the stability was quickly diminished reaching an isoelectric point around a pH of 9.5 and 10.

This experiment suggested that Kr-Black was the most stable among the all nanodiamonds titrated.

As previously mentioned, the shape of the titration curve and the stability of the colloid was influenced by the starting pH. Consequently, titration was performed to show the influence of the starting pH. Samples of Kr-Black and Kr-Grey were prepared at a concentration of 0.1 wt. %. These samples were then titrated over various 'trajectories' that included: initial pH to 1, initial pH to 12, pH of 1 to 12, and a pH of 12 to 1. The results of this experiment are given in Figure 2.4.

The outcome of the concentration verses zeta potential reported in Section 2.3.1 allowed for further experimentation on concentration versus zeta potential under various pH. Full titration (taken from pH 1 to 12 and 12 to 1) was performed for the Kr-Black sample at 0.1 wt. % and 0.01 wt. % (Figure 2.5). Similar to the data found in Section 2.3.1, the concentration does have a notable effect on the zeta potential. Wherein Figure 2.2 the zeta potential for positively charged I6 increased with deceasing concentration, the opposite held true for negatively charged Kr-Black; when concentration was decreased the absolute value of the zeta potential decreased. These experiments suggested that both the direction of the titration and the concentration of the sample have a great affect on zeta potential and, therefore, colloidal stability.

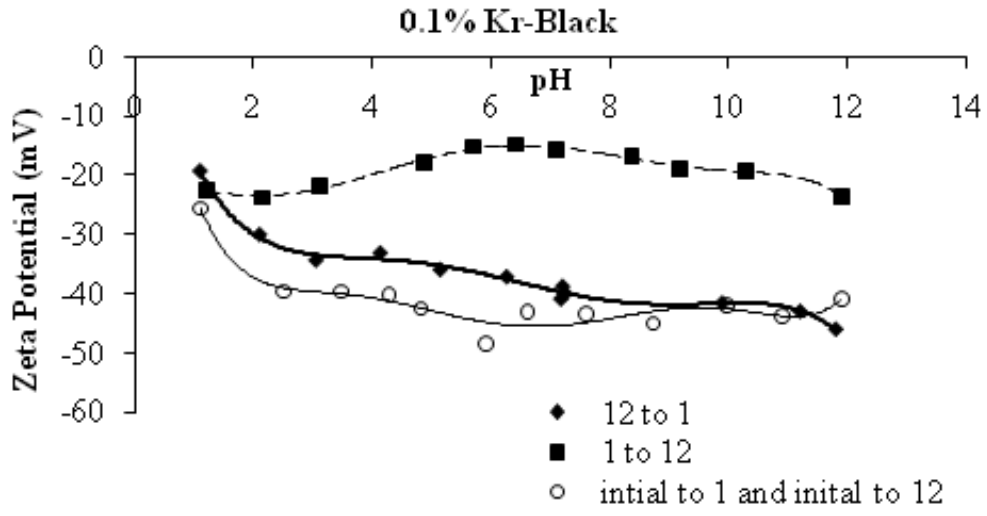

(a)

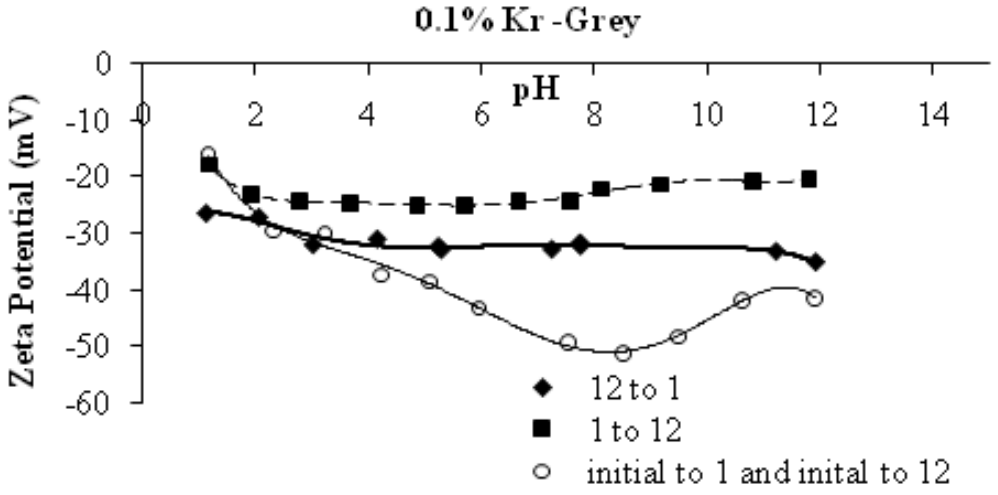

(b)

Figure 2.4. Effect of titration direction on zeta potential of Kr-Black (a) and Kr-Grey (b).

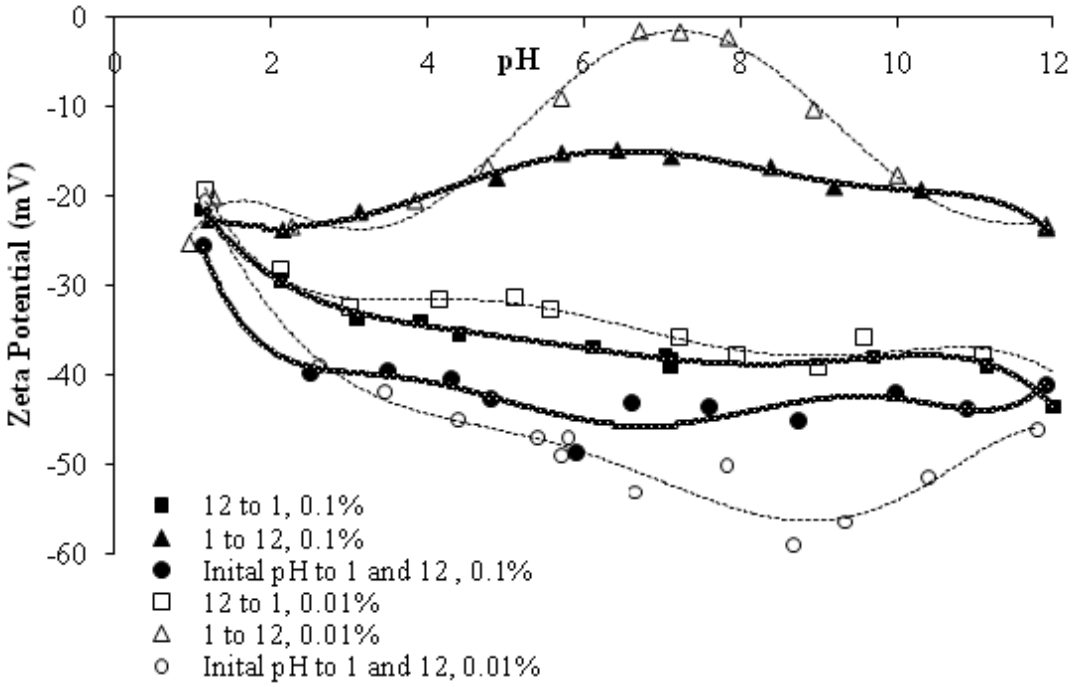

Figure 2.5. Titration curves for 0.1 and 0.01 wt% of Kr Black.

2.3.3 Aflatoxin Adsorption by ND

Polydispersed ND RUDDM and its two fractions with different particle sizes as well as the Ch-St and I6 samples were studied for Af adsorption. An aim of the experiments was to elucidate the role of the sign of the zeta potential (surface chemistry) and influence of particle size (surface area available for binding) on adsorption. Results of the experiments on sorption capacity of the ND samples defined by two independent methods (fluorescent spectroscopy and HPLC) are given in Table 2.2. Results of the two independent methods of measurements are consistent.

Table 2.2. Sorption capacity of AfB1 by different types of ND (mg of AfB1 per kg of ND).

ND	Fluorescence Spectroscopy	HPLC method
RUDDM	45	42.5
RUDDM 1	55	75
RUDDM 2	63	45
Ch-St	132	112
Ch-I6	123	106.25

The NDs preserved colloidal stability in the presence of Af. A fast adsorption rate is essential for enterosorbents. In our experiments we studied both addition of ND hydrosols and dry powders to Af suspensions (details are not reported). The ability to use enterosorbents either as dried powders or hydrosols is important from a practical viewpoint. Using dried sorbents is most common because for some enterosorbents the presence of water in pores prevents Af penetration to the pores [7]. At the same, time dispersivity in water of the sorbents is higher.

As follows, from Table 2.2, NDs with a positive zeta potential demonstrate higher adsorption toward Af as compared to a group of NDs with a negative surface charge in an aqueous media. In principle, Af has both positively and negatively charged groups within the molecule, thus, both types of NDs can electrostatically interact with Af. We can also preliminarily conclude that the size of ND aggregates within both groups of NDs does not play an essential role in the Af sorption capacity.

2.4 Conclusion

Two groups of NDs with positive and negative zeta potentials in neutral media were selected and thoroughly characterized. Titration of the samples demonstrated that for some samples relatively high zeta potentials can be preserved over a wide pH range, indicating high colloidal stability in these conditions. Initial experiments on Af adsorption by NDs demonstrated their ability to adsorb Af. At the same time, NDs from different vendors processed and modified under different conditions demonstrated different sorption capacity toward Af. This suggests that ND surface chemistry can be modified in a controlled manner such that the Af sorption is increased.

Acknowledgements

The authors acknowledge the financial support of the Materials World Network program of the National Science Foundation (Grant DMR-0602906) and Fundamental Research Foundation of Russian Academy of Sciences (Grant 06-04-90234). V. Vorobiev is acknowledged for the providing RUDDM 1 sample and I. Petrov for providing Ch-I6 ND sample. The authors thank G. Baram and I. Azarova (ZAO Institute of chromatography "EcoNova", Novosibirsk) for their help in the experiments with HPLC.

References

1. Grant, P.G. and T.D. Phillips, *Isothermal adsorption of aflatoxin B1 on HSCAS clay.* Journal of Agriculture and Food Chemistry, 1998. **46**: p. 599-605.

2. Puzyr, A.P., V.S. Bondar, and A. Selimhanova, *Dynamics of the selected physiological responses in laboratory mice under the prolonged oral administration of nanodiamond suspensions.* Siberian Med. Obozrenie (Siberian Med. Rev.) (in Russian), 2004. **4**: p. 19-23.

3. Varga, J., et al., *Chemical, physical and biological approaches to prevent ochratoxin induced toxicoses in humans and animals.* Toxins, 2010. **2**: p. 1718-1750.

4. Bondar, V.S. and A.P. Puzyr, *Nanodiamonds for biological investigations.* Physics of the Solid State, 2004. **46**(4): p. 716.

5. Shenderova, O., et al., *Modification of detonation nanodiamonds by heat treatment in air.* Diamond and Related Materials, 2006. **15**(11-12): p. 1799-1803.

6. Ray, M.A., et al., *Cold plasma functionalization of nanodiamond particles* Diamond and Related Materials, 2006. **15**(11-12): p. 1809-1912.

7. Lemke, S.L., et al., *Development of a multi-tiered approach to the in vitro prescreening of clay-based enterosorbents.* Animal Feed Science and Technology, 2001. **93**(1): p. 17-29.

Chapter 3

Colloidal Stability of Modified Nanodiamond Particles

Published in Diamond and Related Materials (April 2009)

Colloidal Stability of Modified Nanodiamond Particles

N. Gibson [1], O. Shenderova [1, 2], T.J.M. Luo [1], S.Moseenkov[4], V. Bondar [3], A. Puzyr [3], K. Purtov [3], Z. Fitzgerald [1], D. Brenner [1]

[1] Department of Materials Science and Engineering, NC State University, Raleigh, NC

[2] International Technology Center, Research Triangle Park, NC

[3] Institute of Biophysics, Siberian Branch of Russian Academy of Sciences, Krasnoyarsk, Russia.

[4] Boreskov Institute of Catalysis SB RAS, Novosibirsk, Russia

Abstract

Colloidal stability is one of the critical factors for the use of nanodiamonds as potential enterosorbents. Although nanodiamonds are believed to be a promising enterosorbent, colloidal stability in hydrosols of raw polydispersed nanodiamonds produced by detonation is typically low. Surface modification and fractionation significantly improves colloidal stability of nanodiamond suspensions within the physiological pH range. The modification of nanodiamonds can be completed either by physical means, i.e., plasma treatments, or by chemical methods. In the current paper an analysis of the colloidal stability of detonation nanodiamonds hydrosols, which have undergone different surface modifications, is presented based on zeta potential measurements and titration experiments.

***Keywords**:* Biomaterial; Nanoparticle; Nanodiamond; Surface Modification; Colloid Stability.

3.1 Introduction

Nanodiamond (ND) research has extended into the biomedical field with recent *in vitro* and *in vivo* animal studies that demonstrate NDs are biocompatible and non-toxic [1-10]. Recent *in vitro* studies demonstrated the absence of cytotoxicity in ND particles [6-9], suggesting the use of NDs as biolabels and drug delivery vehicles [6-11]. *In vivo* studies included oral, subcutaneous, intramuscular and intravenous administration of sterile detonation ND (DND) hydrosols [1-5]. No significant weight changes, reproduction problems (over 5 generations) or deaths were observed as a result of substituting DND hydrosols (0.002-0.5 wt. %) for water in the ration of white mice [2]. Such encouraging results allow for the expansion of DNDs into biomedical applications, one possible use is in the area of enterosorbents [1, 12, 13]. Enterosorbents are compounds that bind toxins in the gastrointestinal (GI) tract thereby neutralizing the effect of these toxins. Our preliminary studies, using DNDs in enterosorbent applications, focused on the binding of aflatoxin B1 [12, 13], one of the low molecular weight products of mold growth. Aflatoxins, produced by certain strains of *Aspergillus flavus* and *Aspergillus parasiticus,* are known to cause hepato- and pneumo- carcinogenicity [14, 15], suppression of the immune system, and aflatoxicosis when consumed by humans or animals [16].

Neutralization of these toxins requires an effective enterosorbent that possesses properties of biocompatibility, chemical inertness (chemically non-toxic), high dispersivity during ingestion, and high selectivity toward the toxin to avoid adsorption of essential nutrients and vitamins [14]. Nanodiamonds possess chemically inert cores, very high surface

areas (300-400 m^2/g for DND), a wide variety of surface groups, and facile surface functionalization. Based on these properties, it has been suggested that DNDs can be tailored to a specific surface structure to promote toxin binding, making them an attractive candidate for enterosorbent applications [1, 12, 13]. Although DNDs are attractive for this particular biomedical use, detonation synthesis of NDs followed by ND purification from soot produces a rather *heterogeneous* material with various cluster sizes and surface chemistries. While the sizes of primary DND particles are typically 4-5 nm, with a narrow size distribution, during synthesis and purification DND primary particles form tightly and loosely bound aggregates with average sizes up to several hundred nanometers [17, 18]. In addition, NDs, as received from vendors, exhibit insufficient colloidal stability [19] such that the particles in suspension do not have the ability to resist flocculation or aggregation over an extended period of time (e.g. several months). To achieve stability, sufficient repulsive forces must exist between the particles while in a suspension. Therefore, to obtain a stable suspension from commercial DNDs, further aggregate size reduction and surface modification to increase repulsive forces between nanoparticles must take place. Reduction of the average aggregate size in a suspension can be achieved, for example, through beads milling [20], sonication and fractionation using centrifugation [19]. Greater repulsive forces between particles can be accomplished through surface modification methods such as atmospheric plasma treatment [21], gas-phase treatment [22], or wet chemistry reactions [23]. Additional removal of non-diamond carbon also improves colloidal stability of DND [19].

In the current study, the colloidal stability of hydrosols of DNDs that have undergone different surface modifications has been analyzed. Several methods of DND modification have been used, including atmospheric plasma treatments in nitrogen or oxygen plasmas, treatment with NaCl [24,25] and additional purification using ion-exchange resins [26]. All of these modification methods posses unique features. Technologically simple atmospheric pressure plasma allows for nanoparticle functionalization to be performed within minutes, and in gram quantities, while avoiding costly vacuum conditions [21]. Oxygen and nitrogen based plasma treatments were performed based on the consideration that oxygen and nitrogen containing surface groups typically facilitate colloidal stability. The attractive feature of the NaCl-treatment method of ND modification [24, 25] is the ability to dry NDs from a hydrosol to powder form and subsequently re-suspend them in liquid without agglomeration. Modification of the ND surface based on sonication of DND in a NaCl solution [24, 25] results in purification of the NDs and possibly incorporation of Na^+ ions onto the ND surface. The treatment of DNDs with ion-exchange resins (deionization) [26] removes metal contaminates, which significantly increases DND surface charge. Since surface charge can be evaluated through zeta potential values of the colloids, stability was evaluated based on data collected from zeta potential measurements. Suspensions of the modified DNDs were titrated to examine their behavior over various pH environments. The chosen pH range was wide enough to simulate conditions in the GI tract (2-8 pH range).

3.2 Experimental Details

3.2.1 Types of Nanodiamonds (NDs)

The NDs used in this work, so called *detonation NDs*, were synthesized by the detonation of a mixture of trinitrotoluene (TNT) and 1,3,5-trinitro-1,3,5-*s*-triazine (RDX). A process of ND *purification* from detonation soot is typically performed using liquid or gas-phase oxidizers. Purposes of this procedure include the oxidation of the largest bulk of non-diamond carbon and reduction of the metallic impurity content. Further processing, tentatively called *modification*, can still be aimed at the reduction of non-diamond carbon content, but mostly provides deliberate changes to the composition and content of ND surface groups. The types of NDs used in our experiments are summarized in Table 3.1.

Table 3.1. Processing (type of oxidation from soot, modification, fractionation) and properties of the studied detonation NDs. Zeta potential (ZP, mV), and average unimodal intensity-based diameter (nm) of ND particles in aqueous suspension are provided.

ND, 0.1wt%	ZP, mV	Size, nm	Processing
Ch-st	17.4±0.4	300	CrO_3 in H_2SO_4
Ch-st F1	44.7±0.5	101	CrO_3 in H_2SO_4; NaCl; FC*
Ch-st F2	37±0.4	225	CrO_3 in H_2SO_4; NaCl; FC
Ch-st F3	33.2±0.2	1380	CrO_3 in H_2SO_4; NaCl; FC
Ch-F6 (Ch-I6)	46.8±0.9	185	CrO_3 in H_2SO_4; $NaOH+H_2O_2$; ion-exchange resin; FC
Ch-F6-O_2 plasma	44.6±1.18	157	Ch-F6 treated in O_2 plasma
Ch-F6-N_2 plasma	52.2±0.3	157	Ch-F6 treated in N_2 plasma
Kr Black	-47±2.1	80	O_2 in the presence of B_2O_3; NaCl; FC
Kr Grey	-45.5±0.6	397	O_2 in the presence of B_2O_3; NaCl; FC
RUDDM 1	-49.3±1.9	75	Singlet O in NaOH; HNO_3; NaCl; FC

Table abbreviations: *FC – fractionated by centrifugation

In the study, the sample Ch-st purchased from "New Technologies", Chelyabinsk, Russia, was obtained by the detonation explosion of a mixture TNT/RDX in ice cooling media, followed by a soot purification process using a mixture of sulfuric acid with chromic anhydride, washed with water, and dried. It contains up to 1.6 wt. % of incombustible impurities. Further modification of the Ch-st sample was performed at the vendor's site. Specifically, the sample Ch-st was purified from metal impurities by boiling in a $NaOH/H_2O_2$ mixture, washing in deionized (DI) water, treating with ion-exchange resins and fractioning by centrifugation. This modified sample is called Ch-F6 in the experiments below. The incombustible impurity content in this sample is 0.6 wt. %. The modified samples Ch-st F1, Ch-st F2 and Ch-st F3 were obtained by sonication-assisted treatment of Ch-st in a NaCl solution [24, 25], washed with DI water and fractionated by centrifugation. NDs Kr-Black and Kr-Gray were produced at the Krasnoyarsk Research Center, Russia by explosion of TNT/RDX in a CO_2 atmosphere followed by soot oxidation by high temperature treatment in air in the presence of B_2O_3. The DND sample was then modified by sonication-assisted treatment in a NaCl solution [24, 25], washed with DI water and fractionated by centrifugation to obtain the Kr-Black and Kr-Gray fractions of NDs. Sample RUDDM1 was obtained from Real-Dzerzinsk, LTD, Russia. The purification from soot included treatment with singlet atomic oxygen in the base environment, followed by treatment in nitric acid. This product was also modified according to the method in [24, 25], then fractionated and dried.

The average primary particle size is 4 nm for the Ch-st and Ch-F-series samples and 3.5 nm for the Kr-series samples. The average aggregate sizes of the samples after sonication assisted dispersion in water as measured using dynamic light scattering technique are provided in Table 3.1.

3.2.2 ND Hydrosol Preparation

Water suspensions were prepared using DI water at a pH of 5.8 and water resistivity of 18 MΩ·cm. ND suspensions were made at various concentrations and then sonicated with a Cole-Parmer 750-Watt ultrasonic homogenizer EW-04711-60 with a tapered titanium horn tip having a 3 mm diameter. The tip was placed directly into the polypropylene centrifuge tubes containing the sample suspension. Sonication of the samples was carried out over various times (listed below) with an output power of 10 W and output intensity of 100 W/cm^2. The as prepared ND colloids had a pH ranging from 5 to 6.

3.2.3 Atmospheric Plasma Treatment

In addition to the ND types listed above, Ch-F6 ND was plasma treated using an oxygen atmospheric plasma to generate ozone-related reactive species, for 3, 5, 15 and 30 minutes or with a nitrogen plasma treatment for 5, 15 and 30 minutes. Plasma treatments were conducted using the atmospheric pressure glow discharge plasma (APGDP) system, developed at the International Technology Center [21]. At the beginning of the treatment Ch-F6 ND powder was placed on the bottom electrode. The top electrode operated under

short positive pulses throughout the treatment, where the bottom electrode was held at ground. During the course of treatment the powder separated and stuck to the top and bottom electrodes. The powder collected from both electrodes was kept separate for further analysis. These samples were then labeled "top-electrode" and "bottom-electrode" as is indicated in the following sections. The treated NDs were then suspended at a 0.1 wt. % concentration using previously described techniques.

3.2.4 Characterization of ND Surface Groups

FTIR analysis of the composition of the surface groups for selected ND samples, specifically for samples with positive zeta potentials, was performed using a Shimadzu FTIR-8300 spectrometer. It is known [27] that peaks attributed to OH stretching and bending vibrations of adsorbed water obscure signatures of other moieties. Thus, in addition to the spectra taken in the air environment, the raw material Ch-st and two its modifications, ND Ch-F6 and Ch-st F1, were analyzed using a vacuum IR cuvette to avoid strong absorbance of adsorbed water. A 25 mg ND sample was mixed with 800 mg of KBr powder and pressed into plates 0.5-0.7 mm thick with pressures up to 150 kg/cm^2. The tablets were placed in an IR vacuum cell and heated at different temperatures below 100°C under vacuum (1×10^{-2} torr) for 3 hours to remove traces of water. Following this procedure, FTIR spectra were recorded without exposing the samples to air to avoid the influence of atmospheric water on the spectra.

3.2.5 Particle Size and Zeta Potential Measurements

Particle size distributions (PSD) were determined with dynamic light scattering technique using the Beckman Coulter N5 submicron particle size analyzer and/or the ZetaSizer NanoZS, Malvern Instruments. In general, samples of NDs were diluted by adding 10 μL of the 0.1 wt. % ND suspensions to approximately 1 mL of DI water. Unimodal intensity-based sizes (Z-average size in Malvern's terminology) are reported in the present work. Zeta potential measurements were conducted on the ZetaSizer instrument using approximately 2 mL of a 0.1 wt. % ND suspension. The reported results for both the PSD and zeta potential are averaged over 3 measurements performed at 25 ^{o}C.

3.2.6 Automatic Titration

Titration experiments were conducted on an MPT-2 Multipurpose Titrator, Malvern Instruments, using 0.1 M HCl, and 0.1 M NaOH titrants (Fischer, USA). ND samples for titration were prepared using the sonication method aforementioned where all samples had a concentration of 0.1 wt. %. Titration was performed by examining a wide pH range and different directions of titration, from pH 12 to pH 1, and from pH 1 to pH 12. Alternative titrations were also performed by gradually changing the original pH of the suspensions in DI water to a final pH 1 or pH 12.

3.3 Results and Discussion

3.3.1 FTIR Studies

Shown in Fig.1 are FTIR spectra taken in air and in vacuum of the original, raw ND powder, Ch-st, as well as samples Ch-st F1 and Ch-F6, which were additionally purified and modified according to the procedures described above (see also Table 3.1). The samples demonstrated oxygen containing groups, represented by vibrations at specific frequencies: ≥C-OH (3200-3600 cm^{-1} for ν_{O-H} in water, hydroxyl groups in carboxylic acid or alcohols), ≥C-O-C≤ (ν 1100-1370 cm^{-1} for ethers, acid anhydrides, lactones, epoxy groups), >C=O group (1700-1865 cm^{-1} for ketones, carboxylic acids, acid anhydrides, esters and lactones). Aliphatic C-H stretching vibrations at 2800-3000 cm^{-1} are also present with significant abundance on the Ch-st and Ch-F6 sample. It is important to note that adsorbed water provides strong absorption bands in the 3500-3300 (max 3420 cm^{-1} ν_{OH}) and 1620-1630 cm^{-1} (bending mode) regions. As can be seen from Fig.1 for the dehydrated samples, adsorbed water related peaks are strongly diminished and leave a low intensity broad band with a peak at 3258 cm^{-1} for Ch-F6 and peaks at 3229 cm^{-1} for Ch-st and Ch-st F1 samples, which can be attributed to hydroxyl groups in carboxylic acid species or tertiary alcohols. The peak at 1630 cm^{-1} also diminishes in the dehydrated sample but does not completely disappear even with heating at 200^{o}C in vacuum (spectrum not shown). This residual peak can be attributed to other functionalities on the carbon surface such as amide related bands as assigned by Jiang et al. [28] or stretching vibrations of aromatic C=C bonds, which are polarized by oxygen atoms bound near one of the C atoms [29]. The strong and acute peak at 1118.45

cm^{-1} of Ch-st may be connected with inorganic sulfate ions that originated from purification using sulfuric acid [30]. This peak disappears in the higher purity samples (Figure 3.1b and c). A peak at 2086 cm^{-1} in the Ch-F6 sample can be tentatively attributed to ketenes [31]. Small peaks at 2370 cm^{-1} originate from vibrations of CO_2 adsorbed on the external cuvette walls.

Peaks for oxygen-containing groups for Kr-Gray and Kr-Black samples taken in air (spectra not shown) are located at 3435, 1774, 1634, 1319 and 1240 cm^{-1}. The peak that can be related to the carbonyl group within carboxylic acid at 1774 cm^{-1} is well pronounced. Because spectra were taken in air, it is difficult to identify the origin of the 3435 cm^{-1} peak, which to a large extent can be due to adsorbed water. It should be mentioned that FTIR spectra of DND fractions produced at FGP Altay, Biisk, Russia of similar sizes to the Ch-F6 and Ch-st F1 samples were also taken in vacuum by Larionova et al. [32] using the same experimental set up as in the present study. The samples from Altay have negative zeta potentials [32]. Their FTIR spectra taken in vacuum demonstrated apparent peaks at 3140 cm^{-1} that are related to hydroxyl groups in carboxylic acid species (see Figure 3.1 in [32]), as opposed to the spectra of Ch-F6 and Ch-st F1 DND where a peak at 3200-3600 cm^{-1} region is weakly pronounced (Figure 3.1).

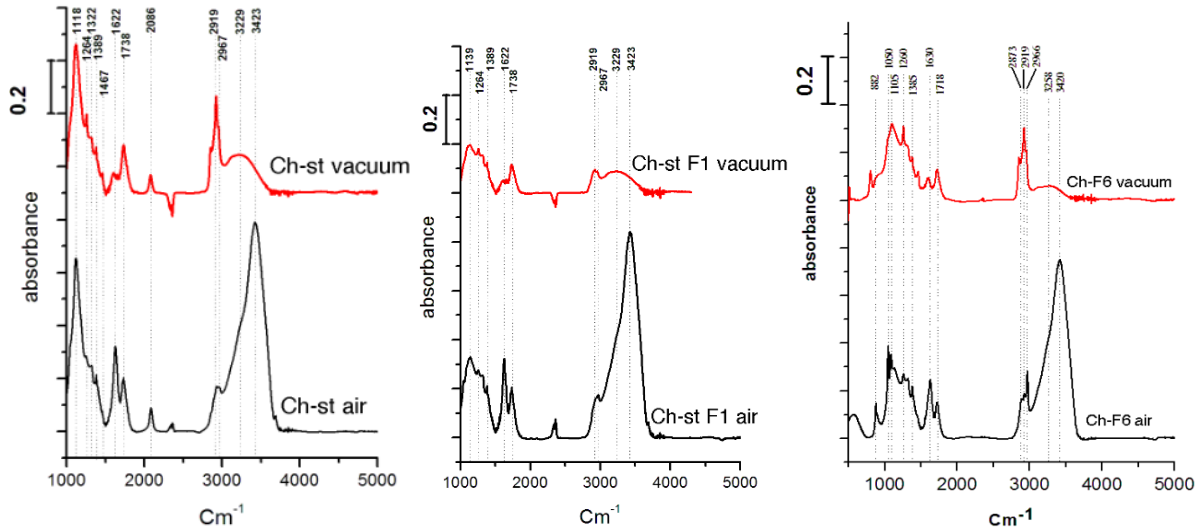

Figure 3.1. FTIR spectra of (a) Ch-st, (b) Ch-st F1, and (c) Ch-F6 ND samples under vacuum and ambient conditions. Spectra were taken using ND-blended K-Br pellet followed by exposure to air (bottom figures) or treatment in IR cuvette under vacuum conditions at 100°C to remove adsorbed water (top figures).

3.3.2 Zeta Potential

As previously mentioned colloidal stability can be measured quantitatively through the zeta potential. Suspensions that have a measured zeta potential above 30 mV or below -30 mV are considered stable because these particles will presumably maintain their repulsive forces while dispersed [33].

Preparation of ND colloids for detoxification purposes requires the development of precise protocols that will allow for highly reproducible zeta potential values. Factors that may influence the zeta potential are sonication and ND concentration. To examine the effect of sonication, 0.1 wt. % suspensions of Ch-F6 were prepared and sonicated for 0, 1, 2, 3, 5

and 10 minutes. The resulting data (not shown) revealed that there was little variation in the sonication time versus zeta potential. Such results suggest that 'typical' sonication regimes do not alter the ND surface groups.

The concentrations of the suspension and its effects on the zeta potential are also addressed in the present study using Ch-F6 suspensions. The samples were prepared at concentrations of 0.2, 0.1, 0.063, 0.032, 0.0123 and 0.007 wt. %. The result of this study, presented in Figure 3.2, indicated that as the sample was diluted a slight increase in zeta potential was observed. While a standard deviation of 5 mV in measuring zeta potentials is considered insignificant, the continuing trend during this experiment may indicate that the zeta potential is influenced by agglomeration. Similar behavior was observed for other ND suspensions.

For all DND types processed under different manufacturing methods, the zeta potential and agglomerate size were measured and compared (Table 3.1). It is well known that primary DND particles are 4 to 5 nm in diameter [34]. However, during synthesis and purification from the soot, these 4-5 nm particles agglomerate. While DND agglomerates can be de-aggregated to primary particles using beads milling methods [20], DND agglomerates are the primary focus of the present study as for the potential use as enterosorbents. The reason behind studying agglomerates is that once subjected to the GI tract, NDs will quickly form aggregates. It is in this form that toxin adsorption will take place.

The chosen concentration when measuring these samples was 0.1 wt. % as this is presumably the concentration that will be used in future animal trials. All NDs, excluding

Ch-st, show high stability, relating to the high absolute zeta potential values (Table 3.1). Importantly, there are classes of NDs with positive and negative zeta potential values. The type of charge the nanoparticles acquire in colloids becomes imperative in the development of enterosorbents. Toxins may have localized charges in suspensions and, thereby, may be attracted to and adsorbed by Van der Waals or electrostatic interactions with the NDs.

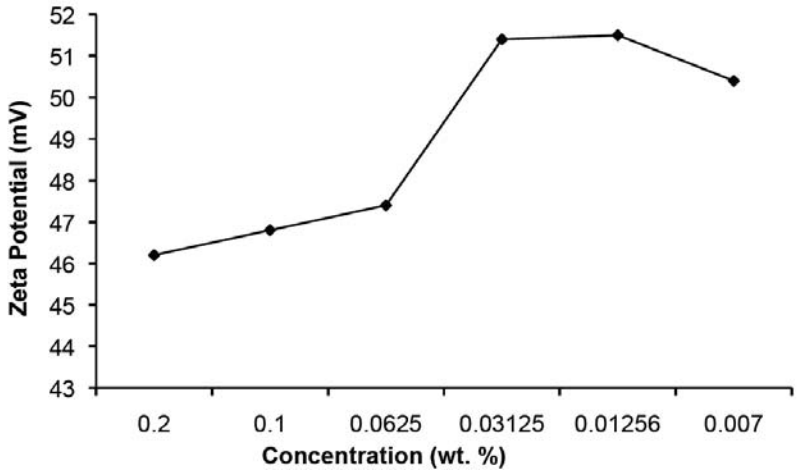

Figure 3.2. Zeta potential (mV) shown as a function of concentration (wt. %) for Ch-F6 ND suspensions in water.

The opposing zeta potentials for the ND samples under study are a consequence of various chemical surface groups. The different groups, both acidic and basic, present on the surface of the NDs were formed during chemical treatment of the nanomaterial at the time of purification and/or modification. NDs processed with soot oxidation using either bubbling with singlet oxygen (RUDDM) or air treated in a presence of a catalyst (Kr-series) have negative zeta potentials, while NDs oxidized from soot using a mixture of CrO_3/H_2SO_4 (Ch-

st) followed by oxidation and purification in a $NaOH/H_2O_2$ mixture (Ch-F6) have positive zeta potentials. At the same time, oxidation of the Ch-st sample in air, [19] as opposed to the treatment in liquid oxidizers, results in a material with a high negative zeta potential, -45 mV. It is important to note that NaCl-based modification of the ND [24, 25] does not change the type of charge associated with the ND in suspension, but increases the absolute value of the zeta potential, thus making the colloid more stable; i.e., Ch-st converted to Ch-st F1 (Table 3.1). It should also be noted that while smaller fractions of Ch-st modified with NaCl treatment have higher zeta potentials (Table 3.1), fractions of Kr ND have similar zeta potentials for both 80 nm and 400 nm fractions. For all the ND suspensions prepared and sonicated under the conditions stated previously, reasonable reproducibility with regard to size and zeta potential measurements was observed.

Thus, it might be suggested that some processes of oxidation of soot or further oxidation of ND containing non-diamond carbon, such as using singlet oxygen in liquid media or oxygen or ozone [35] in a gas phase, results in rather deep oxidation with predominant carboxylic acid groups on the ND surface. When the ND is dispersed in DI water, dissociated acidic groups cause a negative charge on the ND surface. As illustrated in the previous section, the amount of carboxylic acid species on the surface of dehydrated ND with negative or positive zeta potentials causes the major dissimilarity in FTIR spectra for these groups of NDs.

Revealing the origin of the positive zeta potentials of NDs is more complicated. Previously, it was thought that positive charges on ND surfaces can be attributed to

protonation of amino groups on the ND surfaces of NDs in acidic media [30]. The spectra [30] were taken in air, so the signatures attributed to amines could originate from the presence of adsorbed water. However, FTIR spectra taken in a vacuum cuvette, in the present study, revealed a negligible amount of amino groups on the surface of Ch-series NDs with positive zeta potentials (Figure 3.1). For confirmation, FTIR spectra of aminated Ch-F6 taken in vacuum produced a very pronounced peak at 3420 cm^{-1} clearly related to amines [36]. At the same time, the amount of alcohol groups that might be also responsible for positive zeta potentials is also small. From numerous studies of the nature of oxygen-containing groups on the surface of carbons [29, 37] two families of surface groups had been identified relative to their acidic or basic characteristics in aqueous solutions. Carboxyl groups, lactones, phenol and lactol groups contribute to the acidic character of carbon materials. Several models of basic oxygen-containing functionalities are still being debated, including chromene structures, diketone or quinone groups, pyrone-like groups and electrostatic interaction of protons with the π-electron system of the graphene structures [29, 37]. Quantum chemical calculations on a large series of polycyclic pyrone-like model compounds demonstrated high relevance of the model to carbon basicity [37, 38]. Pyrone-like structures are combinations of non-neighboring carbonyl and ether oxygen atoms at the edges of a graphene layer. Signatures for both ketone and ether groups are present in FTIR spectra of ND (Figure 3.1) (peaks in the 1100-1370 cm^{-1} region are related to ethers and peaks in the 1700-1865 cm^{-1} region are related to ketones). The underlying reason for the basicity of pyrone-like structures is the stabilization of the protonated form via the electronic

π-conjugation throughout the sp^2 skeleton [38]. In principle, this model of the basicity of carbon surface attributed to pyrone-like structures can be adapted to nanodiamonds with positive zeta potentials. It is known that a sp^2-like carbon shell might be present at the surface of the ND as well as graphitization of (111) surfaces, which can take place on the surface of nanodiamond [39], providing a π-conjugated system. HRTEM images (not shown) revealed the presence of sp^2 carbon on the surface of the Ch-F6 sample, similar to typical HRTEM images of DND [34]. In principle, one of the possible assignments of the peak at 1630 cm^{-1} can be related to stretching vibrations of aromatic C=C bonds, which are polarized by oxygen atoms bound near one of the C atoms [29]. The presence of sp^2- and sp^3-type oxygen had been also observed in FTIR spectra, making the presence of pyrone-like structures plausible at the nanodiamond surface.

3.3.3 Plasma Treated Samples

Two sets of measurements were conducted with plasma treated samples to examine the effects of a gas generating the plasma and duration of a treatment on DND agglomerate size and zeta potential. Each plasma treated sample was sonicated at 1.5 minutes before measuring its properties. First, influence of plasma treatment on PSD of DND was examined. The results of the measurements clearly indicate that the plasma treatment decreased the size of the ND particles by approximately 10-20 % (Figure 3.3).

The most prominent de-agglomeration after plasma treatment was observed in the nitrogen 5-minute-bottom-electrode (~15 %) and nitrogen 15-minute-top-electrode samples

(~17 %). Observations specify that the duration of treatment influences the particle size. It appeared that shorter treatment times, in almost all cases (except nitrogen 15-minute-top-electrode samples), produced smaller sized particles than longer treatment times. It is hypothesized that longer treatment times can cause condensation reactions to take place, thereby increasing the agglomerate sizes from the initial smaller particles formed by preliminary mechanical means within the plasma.

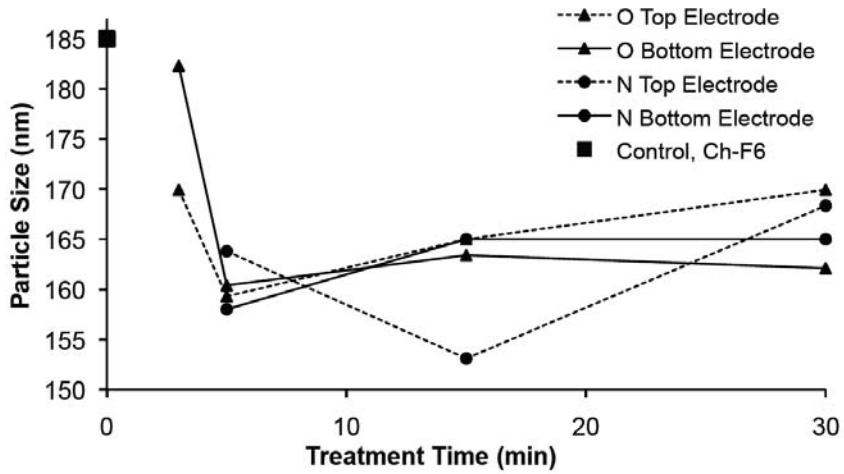

Figure 3.3. Particle size (nm) of 0.1 wt. % Ch-F6 ND samples vs. various reaction times (min) of plasma treatment in oxygen and nitrogen. Samples on both top and bottom electrodes were collected for measurement and labeled as "Top Electrode" and "Bottom Electrode," respectively. Particle sizes of plasma treated NDs are smaller compared to that of the untreated Ch-F6 ND.

Zeta potentials were also measured for each of these plasma treated Ch-F6 colloids. The zeta potential of the Ch-F6 control, as discussed earlier, is approximately 47 mV. In all cases, (except bottom-electrode samples treated for 5 and 15 minutes) zeta potential values of plasma treated samples were in less contrast with the control sample (Figure 3.4). The decrease in zeta potential of the oxygen plasma treated samples was expected given that the

oxygen containing groups originated from oxidation with gas-phase oxygen causing a negatively charged local area decreasing overall positive zeta potential. From the present results, it can be concluded that ND de-agglomeration during plasma treatment can be optimized. Additionally, treatment in oxygen plasma should be considered best only for negatively charged NDs. Such reasoning stems from the fact that the oxygen groups will increase the negativity of the already negative surface and, thereby, increase the repulsion and stability of the ND colloid.

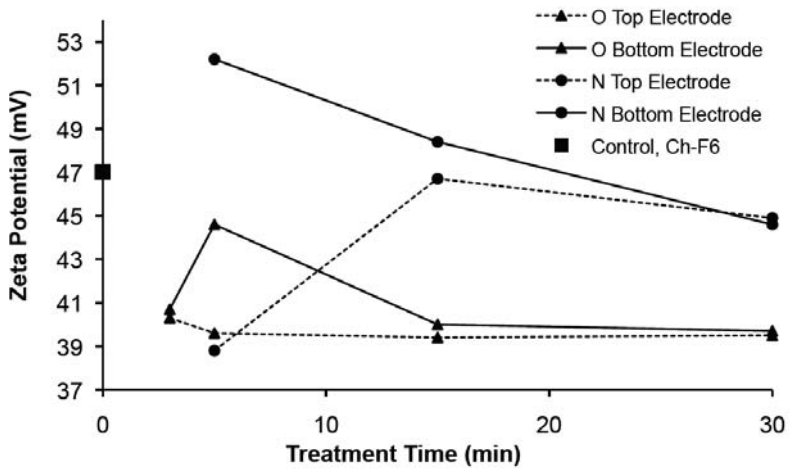

Figure 3.4. Zeta potential (mV) values of 0.1 wt. % Ch-F6 ND vs. various reaction times (min) of plasma treatment in oxygen and nitrogen. Samples on both top and bottom electrodes were collected for measurement and labeled as "Top Electrode" and "Bottom Electrode," respectively. Oxygen plasma treated NDs exhibit less positive zeta potential values compared to the untreated Ch-F6 ND.

3.3.4 Titration

All previous samples, up to this point, had zeta potential measurements taken only at their natural pH. Therefore, titration studies were performed to assess the stability of ND suspensions over a broad pH range. The range chosen was wide enough to simulate the

physiological pH in the GI tract of a cow. It is important to note that titration results are influenced by the starting pH of the suspension because zeta potentials depend on the ionic strength. When the concentration of the counter ions is increased the electrical double layer, which forms the slip plane for zeta potential readings, is compressed and thereby creates an increase in the potential gradient. Consequently, the direction of titration is important. To evaluate all conditions, titration was read from a pH of 1 to 12, pH 12 to 1, and two independent titrations from initial (or natural pH) to pH 1 or initial to pH 12. The initial pH values of all eight colloids were within a pH of 5 to 6, where the pH of DI water is approximately 5.8.

Titration experiments were conducted with eight ND suspensions of 0.1 wt. % concentration. Titration curves of all eight samples from their initial pH to the pH corresponding to highly acidic and highly basic systems are illustrated in Figure 3.5a and Figure 3.5b.

Data collected showed the colloid's stability over the pH range depends on the nature and charge of the ND particle. NDs that carry a positive charge have surfaces most likely enhanced with pyrone-like groups, because FTIR spectra indicated a negligible amount of amino groups that are typically considered to be responsible for positive zeta potentials [30].

These include the entire Ch-st series and Ch-F6. It was reported that pK_a for pyrone-like groups on carbon surfaces can span within a wide pH range, depending on the number of carbon rings and the placement of sp^2- and sp^3-type oxygen [37, 38], with a shift to higher pK_a as the number of carbon rings increases.

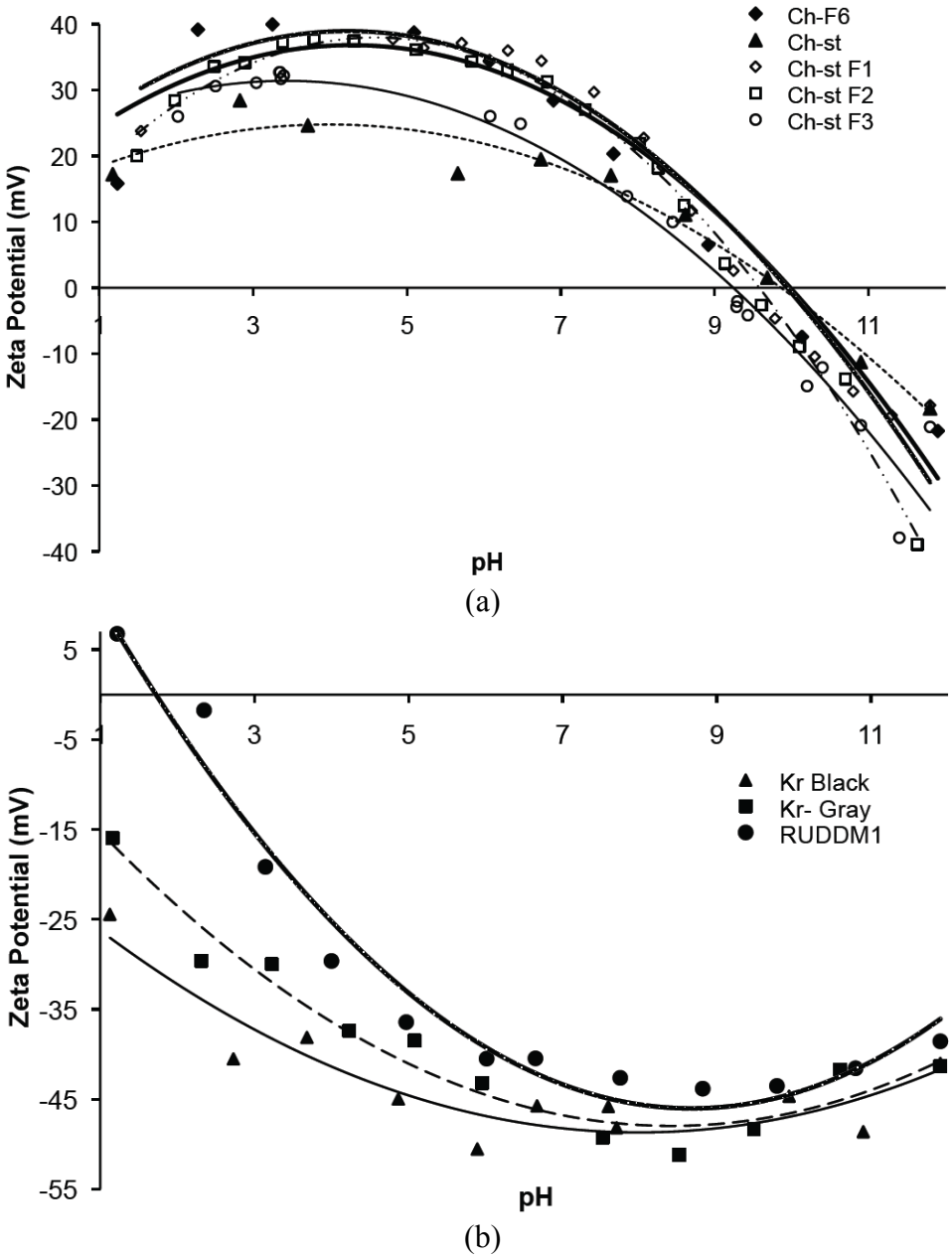

Figure 3.5. Titration curves of (a) positive and (b) negative ND samples illustrating zeta potential (mV) under various pH conditions. Samples were titrated from initial pH values (ranging from 5-6) to pH 1 and, in a separate measurement, samples were titrated from initial pH to pH 12.

In the case of the Ch-st and Ch-F6 NDs, as the pH approached the pK_a of the groups, the colloid stability quickly decreased until it reached the isoelectric point; the point at which no charge was associated with the particle. For these samples, the isoelectric point was reached around pH 9.5 to 10. Negative charges on NDs RUDDM1, Kr-Gray, and Kr-Black NDs arise primarily from the carboxyl groups on their surface. When the pH of these suspensions fell below the pK_a value of the carboxyl group, a decrease in colloidal stability was observed. In this group of negatively charged NDs, only the RUDDM1 sample had an observed isoelectric point, which was at pH 2.4. Among all studied samples in both the positive and negative zeta potential groups, Kr-Black was shown to have the highest stability where precipitation was not observed for an extended period of time, with Kr-Gray only having a slightly lower stability.

As mentioned previously, zeta potentials are influenced by the ionic strength. To illustrate how titration was influenced by the starting pH of the suspension, 0.1 wt. % Kr-Black and Kr-Gray were also titrated from pH 1 to 12 and pH 12 to 1. These in combination with related curves in Figure 3.5b are shown in Figure 3.6. In addition, Figure 3.7 illustrates the dependence of zeta potential on the direction of titration for a more dilute Kr-Black sample, with concentration 0.01 wt. %.

From Figure 3.6 and Figure 3.7 it can be concluded that the direction of titration can significantly influence the stability of the system (absolute value of the zeta potential). Titration from the initial pH in DI water toward low or high pH corresponds to the system with the highest stability, or the most negative zeta potential.

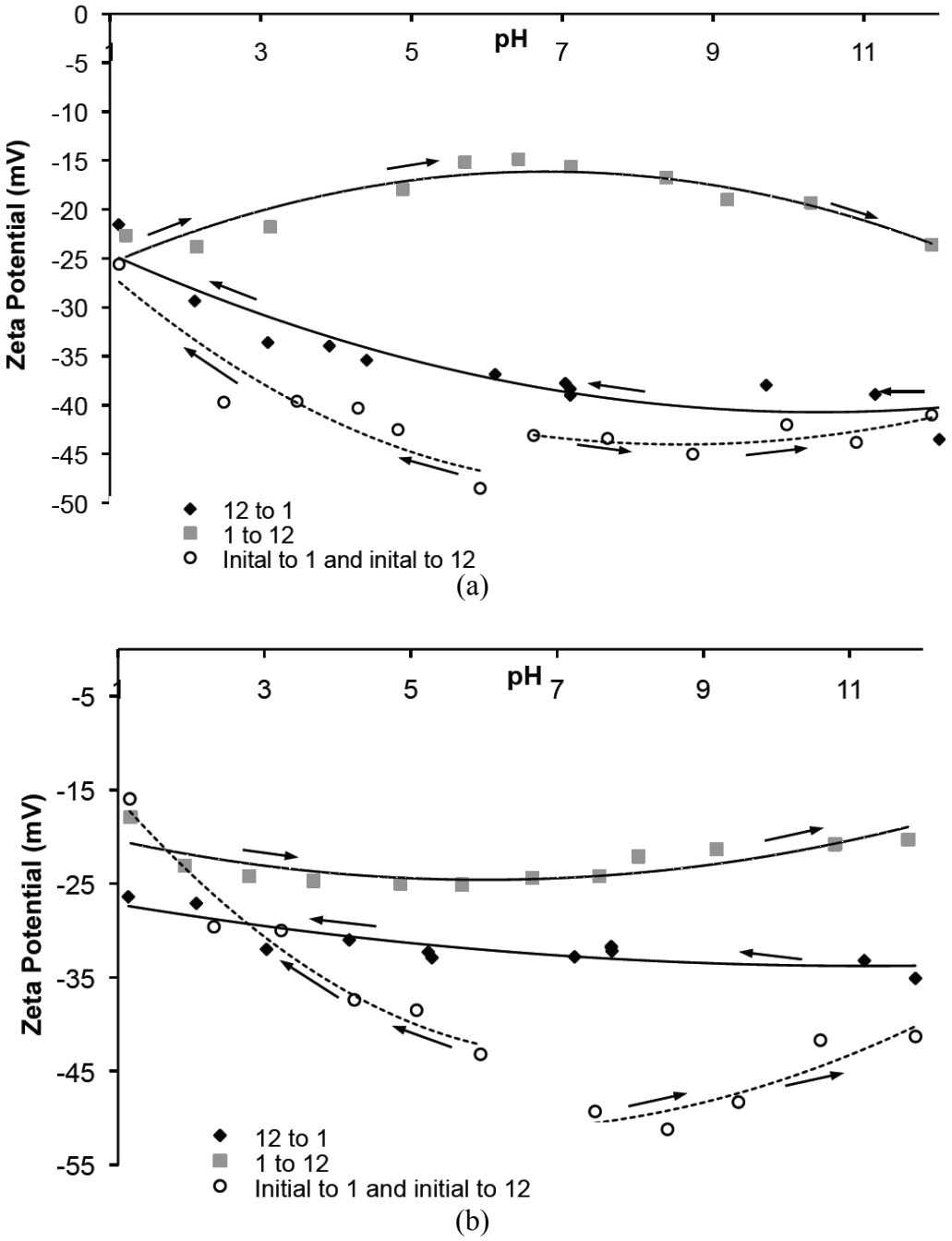

Figure 3.6. Influences of starting pH and direction of titration on ND zeta potential for (a) Kr-Black and (b) Kr-Gray colloids. Samples were titrated from initial pH values (ranging from 5-6) to pH 1, initial pH to pH 12, pH 1 to pH 12 and pH 12 to pH 1 (four separate experiments).

It was also shown that the least stable systems begin at a highly acidic region followed by the addition of NaOH to achieve a final pH of 12 (Figures 3.6 and 3.7). Path dependence effects observed on both ND samples indicate irreversible agglomeration at low pH regimes, as can be seen from the less negative zeta potentials. Once agglomerates were formed, raising the pH did not return the zeta potentials to their previous values, suggesting the Kr class NDs should never be preserved in very low pH solutions. Titration curves for the suspensions starting from basic regions and moving toward acidic regions have stabilities that fall between the previously described curves. An interpretation of above results can be made in the context of pK_a. There is no dissociation of carboxylic acid groups at a pH lower than the related pK_a for the groups, the charge density is low and repulsive forces between NDs are very small leading to irreversible agglomeration. An increase of pH, and the possibility of dissociation of the carboxylic groups on a surface of large agglomerates, does not improve the stability significantly because agglomerates are too large to form colloidal suspensions.

In contrast, starting titration from a high pH, much higher than pK_a value for carboxylic acid, promotes dissociation of the carboxylic acid groups. Thus, colloidal stability of the initial suspensions is high (Figure 3.6 and 3.7). Suspension stability remains high almost through the entire titration region and theoretically begins to decrease when the pKa is approached.

Also noticed, there is no significant difference in titration curves for titration directions from pH 1 to pH 12 (and vice versa) between Kr-Black and Kr-Gray samples

(Figure 3.6 a and b), which are fractions separated from the same modified polydispersed DND and, correspondingly, demonstrate average aggregate sizes of 80 nm and 400 nm. At the same time, the absolute zeta potential value is 5-10 mV higher for the smallest fraction (Kr-Black) over the entire pH range during titration experiments beginning at a natural pH and moving towards basic or acidic regions (Figure 3.6). Although the Kr-Gray sample has a high zeta potential in water suspensions, its resistance to sedimentation is low due to the large average aggregate size.

Previously, it was discussed that concentration has some influence on zeta potential values of DND dispersed in DI water (Figure 3.2). The influence of concentration on titration experiments was studied using 0.01 wt. % and 0.1 wt. % suspensions of Kr-Black samples. Results collected from experiments with different titration directions are shown in Figure 3.7. The titration curves, like the previous study, also exhibit path dependent effects. Figure 3.7 demonstrates that concentrations over various pH values have a significant effect on the zeta potential, thus suggesting that concentration has a substantial effect on colloidal stability.

Additional experiments were conducted to evaluate the influence of incubation time for various pH points along the titration curve. In this experiment, Ch-F6 was prepared to a 0.1 wt. % concentration and titrated along the four path directions previously indicated. While titration occurred, ND suspensions were taken to a specific pH along their path then held at this concentration for two days. After this time, the suspension was taken from the new pH value to another specified pH along the path where it was again left untouched for

two days. The process was repeated until the final pH value was reached. Zeta potential measurements were taken both before and after the two day incubation period. The pH values at which two days of incubation was performed were 12, 8, 4, and 1 for the acidic-to-basic and basic-to-acidic titration directions. For the path direction from natural pH to acidic, the pH points for incubation were 5, 3 and 1. Finally, for the titration direction going from the initial pH to a pH of 12, the suspension was incubated at pH values 6, 8 and 12. No significant difference was observed between the two day incubation time and the autotitration results collected within several hours on the Zetasizer.

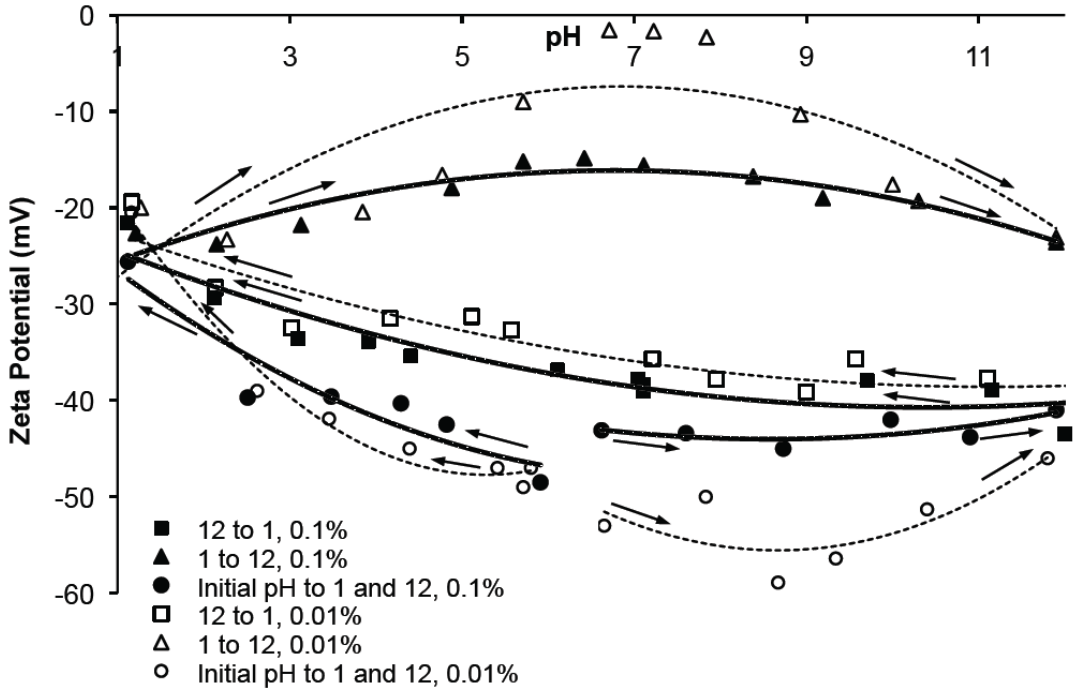

Figure 3.7. Zeta potential (mV) vs. pH for Kr-Black suspensions of 0.1 wt. % and 0.01 wt. % under four different titration directions (initial pH to pH 1, initial pH to 12; pH 12 to pH 1, and pH 1 to pH 12).

3.4. Conclusion

Results of the studies have several important practical implications. First, it was shown that commercial DNDs can be modified to form stable colloidal suspensions without aggregating and sedimenting for prolonged periods of time. To achieve these goals, DND particles in suspensions must have high zeta potentials and relatively small sizes (< ~100 nm in diameter). Centrifugal fractionation can be used to obtain suspensions of small DND sizes. To increase the zeta potential, DND samples should be separated from metal and amorphous carbon impurities and their surfaces should be enriched with surface groups that readily dissociate in water.

Studies of the particle size distribution respective to zeta potentials of surface-modified DNDs also suggest procedures to prepare stable DND colloids. It was demonstrated that commercial DNDs of low colloidal stability (e.g. Ch-st sample) can be further treated to result in stable hydrosols (Ch-F6 and Ch-st F1), in which the origin of the positive zeta potential has been attributed to the presence of pyrone-like structures. It was also demonstrated that DND treatment in atmospheric pressure plasma can result in a 20 % decrease of the average aggregate size.

Finally, for DND applications as enterosorbents, the present titration studies prove that the modified DNDs (both with negative and positive zeta potentials in DI water) preserve colloidal stability over the physiologically important pH range (2-8 pH).

Acknowledgements

The authors acknowledge the financial support of the Materials World Network program of the National Science Foundation (Grant DMR-0602906) and Fundamental Research Foundation of Russian Academy of Sciences (Grant 06-04-90234). Drs. V. Kuznetsov, S. Hens, G. Cunningham, V. Grichko, I. Petrov are acknowledged for helpful discussions. Mark Ray is acknowledged for the plasma treatment of the samples, and Dr. V. Vorobyev is acknowledged for providing the RUDDM1 nanodiamond samples.

References

1. Puzyr, A.P., V.S. Bondar, Z.Y. Selimhanova, A.G. Tyan, E.V. Bortnikov, E.V. Injevatkin, *Results of studies of possible applications of detonation nanodiamonds as enterosorbents.* Siberian Med. Obozrenie (Siberian Med. Rev.) (in Russian), 2004. **2-3**: p. 15.

2. Puzyr, A.P., V.S. Bondar, and A. Selimhanova, *Dynamics of the selected physiological responses in laboratory mice under the prolonged oral administration of nanodiamond suspensions.* Siberian Med. Obozrenie (Siberian Med. Rev.) (in Russian), 2004. **4**: p. 19-23.

3. Puzyr, A.P., V.S. Bondar, A.G. Selimkhanova, E.V. Tyan, Inzhevatkin, V.S. Bondar, and D. Baron, *Physiological parameters of laboratory animals at oral administration of nanodiamond hydrosols.* Siberian Med. Obozrenie (Siberian Med. Rev.) (in Russian), 2005. **4**: p. 185.

4. Puzyr, A.P., E.V. Bortnikov, N.N. Skobelev, A.G. Tyan, Z. Yu, G.G. Selimkhanova, G.G. Manashev, and V.S. Bondar, *A possibility of using of intravenous administration of sterile colloids of modified nanodiamonds.* Bull. Siberian Medi. (in Russian), 2005. **1**: p. 20.

5. Puzyr, A.P., A.V. Baron A.V., K.V. Purtov, E.V. Bortnikov, N.N. Skobelev, O.A. Mogilnaya, V.S. Bondar, *Nanodiamonds with novel properties: A biological study.* Diamond and Related Materials, 2007. **16**(12): p. 2124-2128.

6. Schrand, A.M., H.J., Huang, C. Carlson, J. Schlager, E. Osawa, S. Hussain. L. Dai, *Are diamond nanoparticles cytotoxic?* Journal of Physical Chemistry, 2007. **111**(1): p. 2-7.

7. Liu, K.K., C.L. Cheng, C.C. Chang, J.I. Chao, *Biocompatible and detectable carboxylated nanodiamond on human cell***.** Nanotechnology, 2007. **18**(32): p. 325102.

8. Yu, S.J., M.W. Kang, H.C. Chang, K.M. Chen, Y.C. Yu, *Bright fluorescent nanodiamonds: No photobleaching and low cytotoxicity.* Journal of the American Chemical Society**,** 2005. **127**(50): p. 17604-17605.

9. Chao, J.I., E. Perevedentseva, P.H. Chung, K.K. Liu, C.Y.Cheng, C.C. Chang, C.L. Cheng, *Nanometer-sized diamond particle as a probe for biolabeling.* Biophysical Journal**,** 2007. **93**(6): p. 2199-2208.

10. Bakowicz, K., and S. Mitura, *Biocompatibility of NCD***.** Journal of Wide Bandgap Materials**,** 2002. **9**(4): p. 261-272.

11. Grichko, V., V. Grishko, O. Shenderova, *Nanodiamond bullets and their biological targets.* Nanobiotechnology**,** 2007. **2**(1-2): p. 37-42.

12. Gibson, N., O. Shenderova, A. Puzyr, K. Purtov, V.Grichko, T.J.M. Luo, Z. Fitzgerald, V. Bondar, D. Brenner, *Nanodiamonds for detoxification.* **NSTI** Nanotechnology Conference and Trade Show - NSTI Nanotech 2007, Technical Proceedings, 2007. **2**: p. 713-716.

13. Puzyr, A.P., K.V. Purtov, O.A. Shenderova, M.Luo, D.W. Brenner, V.S. Bondar, *The adsorption of aflatoxin B1 by detonation-synthesis nanodiamonds.* Doklady Biochemistry and Biophysics, 2007. 417(1): p. 299-301.

14. Grant, P.G., T.D. Phillips, *Isothermal adsorption of aflatoxin B_1 on HSCAS clay.* Journal of Agricultural and Food Chemistry, 1998. 46(2): p. 599-605.

15. Kelly, J.D., F.P. Euengerich, R.A. Coulombe Jr., *Aflatoxin B_1 activation in human lung.* Toxicology and Applied Pharmacology, 1997. **144**(1): p. 88-95**.**

16. Pier, A.C., *Major biological consequences of aflatoxicosis in animal production.* Journal of Animal Science, 1992. **70**(12): p. 3964-3967.

17. Chiganova**,** G.A., *The effect of particle hydration on the aggregation stability of ultradispersed diamond hydrosols.* Colloid Journal of the Russian Academy of Sciences: Kolloidnyi Zhurnal, 1997. **59**(1): p. 87-89.

18. Chiganova**,** G.A., *Aggregation of particles in ultradispersed diamond hydrosols.* Colloid Journal of the Russian Academy of Sciences: Kolloidnyi Zhurnal, 2000. **62**(2): p. 238–243.

19. Shenderova, O., I. Petrov, J. Walsh, V. Grichko, V, Grishko, T. Tyler, G. Cunningham, *Modification of detonation nanodiamonds by heat treatment in air.* Diamond and Related Materials, 2006. **15**(11-12): p. 1799-1803.

20. Kruger, A., F. Kataoka, M. Ozawa, T. Fujino, Y. Suzuki, A.E. Aleksenskii, A.Y. Vul, E. Osawa, *Unusually tight aggregation in detonation nanodiamond: Identification and disintegration.* Carbon, 2005. **43**(8): p. 1722-1730.

21. Ray, M.A., O. Shenderova, W. Hook, *Cold plasma functionalization of nanodiamond particles.* Diamond and Related Materials, 2006. **15**(11-12): p. 1809-1912.

22. Liu, Y., Z. Gu, J.L. Margrave, V. N. Khabashesku, *Functionalization of nanoscale diamond powder: fluoro-, alkyl-, amino-, and amino acid-nanodiamond derivatives.* Chemistry of Materials, 2004. **16**(20): p. 3924-3930.

23. Kruger, A., Y.J. Liang, G. Jarre, J. Stegk, *Surface functionalisation of detonation diamond suitable for biological applications.* Journal of Materials Chemistry**,** 2006. **16**(24): p. 2322-2328.

24. Bondar, V.S. and A.P. Puzyr, *Nanodiamonds for biological investigations.* Physics of the Solid State, 2004. **46**(4): p. 716-719.

25. Puzyr, A.P., V.S. Bondar, *Method of production of nanodiamonds of explosive synthesis with an increased colloidal stability.* RU Patent 2252192. Priority date 26.06.2003.

26. Petrov, I., P. Detkov, J. Walch, O. Shenderova, *Polydispersed detonation nanodiamond and approaches for its fractioning.* NSTI Nanotechnology Conference and Trade Show - NSTI Nanotech 2006 Technical Proceedings**,** 2006. **1**: p. 150-153.

27. Ji, S. T Jiang, K Xu, S Li, *FTIR study of the adsorption of water on ultradispersed diamond powder surface.* Applied Surface Science**,** 1998. **133**(4): p. 231-238.

28. Jiang, T., K. Xu, *FTIR study of ultradispersed diamond powder synthesized by explosive detonation.* Carbon**,** 1995. **33**(12): p. 1663-1671.

29. Boehm, H.P., *Surface oxides on carbon and their analysis: a critical assessment.* Carbon**,** 2002. **40**(2): p. 145-149.

30. Xu, X., Z. Yu, Y. Zhu, B. Wang, *Effect of sodium oleate adsorption on the colloidal stability and zeta potential of detonation synthesized diamond particles in aqueous solutions.* Diamond and Related Materials**,** 2005. **14**(2): p. 206-212.

31. Fanning, P.E., M.A. Vannice, *A DRIFTS study of the formation of surface groups on carbon by oxidation.* Carbon**,** 1993. **31**(5): p. 721-730.

32. Larionova, I., V. Kuznetsov, A. Frolov, O. Shenderova; S. Moseenkov; I. Mazov, *Properties of individual fractions of detonation nanodiamond.* Diamond and Related Materials**,** 2006. **15**(11-12): p. 1804-1808.

33. Riddick, T.M., Zeta-Meter Operating Manual zm-75, Zeta-Meter, Inc., New York, 1968.

34. Shenderova, O., and D. Gruen (Eds.) Ultra-Nanocrystalline *Diamond*: Syntheses, Properties and Applications, William-Andrew, 2006.

35. Petrov, I., O. Shenderova, V. Grishko , V. Grichko, T. Tyler, G. Cunningham, G. McGuire, *Detonation nanodiamonds simultaneously purified and modified by gas treatment***.** Diamond and Related Materials, 2007. **16**(12): p. 2098-2103.

36. Hens, S., G. Cunningham, T. Tyler, S. Moseenkov, V. Kuznetsov, O. Shenderova, *Nanodiamond bioconjugate probes and their collection by electrophoresis.* Diamond and Related Materials**,** 2008. **17**(11): p. 1858-1866.

37. Fuente, E., J.A. Menendez, D. Suarez, M.A. Montes-Moran, *Basic surface oxides on carbon materials: a global view.* Langmuir, 2003. **19**(8): p. 3505-3511.

38. Montes-Moran, M.A., D. Suarez, J.A. Menendez, E. Fuente, *On the nature of basic sites on carbon surfaces: an overview.* Carbon**,** 2004. **42**(7): p. 1219-1224.

39. Raty, J.Y., G. Galli, *Ultradispersity of diamond at the nanoscale.* Nature Materials**,** 2003. **2**(12): p. 792-795.

Chapter 4

Fluorescent Dye Adsorption on Nanocarbon Substrates through Electrostatic Interactions

Published in Diamond and Related Materials (2010)

Fluorescent Dye Adsorption on Nanocarbon Substrates through Electrostatic Interactions

N. M. Gibson [1], T.J.M. Luo [1], O. Shenderova [1, 2], Y.J. Choi [1], Z. Fitzgerald [1], D.W. Brenner [1]

[1] Department of Materials Science and Engineering, NC State University, Raleigh, NC

[2] International Technology Center, Research Triangle Park, NC

Abstract

Nanodiamonds (NDs) with modified surface functional groups and surface characteristics are an attractive model to understand adsorption mechanisms of molecules and on substrates. The research described in this paper illustrates the binding mechanisms of fluorescent dyes to ND surfaces as these interactions are extremely useful in many biomedical ND applications. A thorough study of binding and release mechanisms was completed using an assortment of carbon based nanoparticles, including NDs, onion-like carbon, and single-wall nanohorns. Surface charge interactions were studied in combination with surface areas, configurations, and modifications in order to determine which is responsible for the largest adsorption capacity and strongest binding. Adsorption studies were carried out using UV-Vis measurements followed by maximum binding capacity determination using the Langmuir isotherm and related transform equations. Langmuir and transform calculations further reveal the specific surface area covered by adsorbents for select nanocarbon materials. In addition, cyclic voltammetry measurements confirm that dye adsorbed onto NDs exhibit equal electrochemical properties as in its unbound state.

4.1 Introduction

Nanodiamonds (NDs) have received heightened attention in nanotechnology and biomedicine as a result of their nontoxicity [1-5], chemical inertness, biocompatibility [6-9], and biological stability. Detonation NDs possess high specific surface areas (typically 300-400 m^2/g) that can readily be functionalized with a broad range of surface groups to enhance binding selectivity toward target chemicals. Proven to be absent of cytotoxicity [7-9], NDs can be used in a variety of applications, including as carriers for active molecules [10], drug delivery agents [7-9, 11], biosensors [12], and more recently enterosorbent applications for toxin deactivation [13, 14]. Each stated application requires attachment of a biological molecule to the ND during the course of utilization. Consequently, conjugation of biomolecules to NDs is an essential step in forming successful ND-biomolecule complexes.

The different surface properties of NDs make them good models for understanding adsorption mechanisms of molecules on a substrate. Binding mechanisms of fluorescent dyes to ND surfaces is illustrated in the following research as this assembly is extremely useful in many ND applications. Initial experiments use propidium iodide (PI), a nucleic acid stain and the target molecule; given that it's positive charge [15] clearly displays electrostatic interactions with NDs. Through the process of adhering PI onto the ND surface a drug delivery vehicle is simulated that could lead to the development of an adsorbent that releases a molecule when inside the targeted cells. In the case of PI, successful delivery can be observed through DNA coloration [16, 17] as a biolabeling application.

Here we report a study of binding and release mechanisms that were accomplished through surveying a wide variety of carbon based nanoparticles. These nanoparticles included nanodiamonds, onion-like carbon and single-wall nanohorns. Interactions between the dye and substrate were studied based on surface areas, surface charge, configurations and additional ND treatments (modification) with the goal of determining which factor is responsible for the adsorption capacity and binding. To examine electrostatic interactions, the research also incorporates the negatively charged fluorescent adsorbates pyranine (PY) and 2,2'-azino-bis(3-ethylbenzthiazoline-6-sulphonic acid) (ABTS). Experiments were conducted using UV-Vis measurements followed by maximum binding capacity determination using the Langmuir isotherm and four different transform equations. Cyclic voltammetry (CV) measurements were also completed to further validate the adsorption results of the UV-Vis spectroscopy. Both methods reveal the critical role of surface charges and the effects of the functional groups in adsorption mechanisms, and confirm that fast and effective adsorption of target molecules can be achieved with appropriate selection of the nanocarbon substrate.

4.2 Experimental Details

The nanocarbons (NCs) explored in this paper can be categorized into (a) nanodiamonds, (b) onion-like carbon (OLC) and (c) single wall nanohorns (SWNH). Table 4.1 lists the NC materials and their processing methods. Complete details of the processing and hydrosol preparations are given in references [14] and [18]. Zeta potential (ZP) and size measurements were completed with colloid concentrations of 0.1 wt. % in deionized (DI)

water [14]. The OLC sample was obtained from the Institute of Catalysis, Novosibirsk, Russia. Single wall nanohorns (SWNHs) were purchased from Nanocraft, Inc., Renton, WA.

Table 4.1. Nanocarbons used in adsorption experiments with general processing methods and resulting diameter size measurements (nm) and zeta potentials (ZP, mV).

ND, 0.1wt%	ZP, mV	Size, d.nm	Processing
Ch-F6 (I6)	46.8 ±0.90	185	CrO3in H2SO4; NaOH+H2O2; ion-exchange resin; FC*
RDDM1	-46.1 ±0.14	176	Graphite precursors; FC
RDDM 2	-35.1 ±0.61	232	Graphite precursors; FC
RDDM 3	-33.8 ±0.73	370	Graphite precursors; FC
RUDDM	-44.1 ±0.66	260	Singlet O in NaOH; HNO3;
RUDDM 1	-49.3 ±1.90	75	Singlet O in NaOH; HNO3; NaCl; FC
OLC Db2	47.1 ±0.65	189	Ch-F6 heat treated at 1600 K
SWNH	13.9 ±0.15	4305	Nanocraft, Inc. Renton, WA

*FC: Fractionation by centrifugation

The initial PI experiments used dye concentrations of 0.01 and 0.03 wt. % in DI water for the preliminary detection of dye adsorption. To 0.7 mL of PI suspension, 0.3 mL of NC solution (0.5 wt. %) was added and incubated over 30 minutes while shaking. Centrifugation was used to collect the supernatant, which was read on the UV-Vis Lambda 35, Perkin Elmer. RUDDM 1 showed high adsorption of PI and was further investigated over several additional PI concentrations in efforts to construct the Langmuir isotherm. (Note: PI is a potential carcinogen and mutagen; hence careful methods should be taken to dispose of the material [15]).

The Langmuir isotherm was obtained using PI concentration from 0.0025 wt. % up to a 0.07 wt. % in DI water, where adsorption was read in the same manner mentioned above. Adsorption percentages were converted to capacities (μg PI/mg sorbent) and plotted against the calculated PI equilibrium (μg PI/mL sorbent). Separate transform calculations (i.e., Eadie-Hofstee, Lineweaver-Burk, Reciprocal Line, and Scratchard) were employed to give rise to additional information such as the maximum capacity of the sorbent and its binding constants. PY and ABTS dyes were both tested on Ch-F6 and RUDDM 1 NDs to determine their adsorption. However, due to the different absorption coefficients of the dyes, PY was observed from 0.00125 to 0.03 wt.% and ABTS was observed from 0.00025 to 0.0025 wt. %.

The specific surface area (surface area per gram) covered by adsorbates was calculated by taking into account the maximum capacity and estimated cross-sectional area of the molecule. The "planar" cross-sectional area of each dye was determined by first relaxing the molecule using the PM6 semi-empirical electronic structure method as implemented in MOPAC [19]. The Connolly surface of the relaxed structure was then generated using the Visual Molecular Dynamics code [20] with a probe size of 1.5 Å. The image was then output to ImageJ where a measurement of 87.7 $Å^2$ was calculated for PY [18]. The cross-sectional value for PI was 128.7 $Å^2$. The Langmuir results were compared to BET experiments, which measured the true specific surface area by nitrogen adsorption at 77 K (Quadrasorb from Quantachrome).

Cyclic voltammetry (CV) was performed on a Faraday MP potentiostat (Obbligato Objectives Inc.). The electrochemical cell consisted of a working electrode constructed of

NDs (0.5 wt. %) coated onto a fluorine doped tin oxide (FTO) electrode, a platinum counter electrode and a silver/silver chlorine (Ag/AgCl) reference electrode. The working electrode was pretreated in nitrogen and oxygen plasma for 3 minutes before coating with NDs. The electrolyte for Ch-F6 experiments was phosphate buffered saline (PBS) that contained ABTS concentration at 0.002 mg/mL. Repeated scanning took place at a scan rate of 50 mV/s for 30 minutes to observe time-dependent adsorption of the dye. After scanning the samples were removed, rinsed thoroughly in DI water and rescanned in PBS solution to observe adsorbed dye.

4.3 Results and Discussions

Several NCs were studied to gain complete knowledge of surface charge, particle size, configuration, and sp^2 versus sp^3 hybridized surface influences. Size measurements indicated that processing methods can largely affect the aggregate size of ND particles. The creation of NDs via detonation results in primary particle sizes of 4-5 nm that quickly agglomerate during synthesis and purification from the detonation soot. While it is possible to reduce ND sizes back to the initial 4-5 nm it is found unnecessary in the current applications as ND suspensions will immediately return to the aggregated state when introduced inside the body due to the pH change and naturally occurring salts (though some NDs indicate high stability at the bodily pH [14]). As indicated, the surface of NDs can be either positively or negatively charged depending on the manufacturing and treatment processes. Zeta potential (ZP) values show that modification does not change the type of

charge, but instead changes the degree of the charge, i.e., to increase or decrease the positivity of an already positively charged ND. Additionally, particle size is not the sole influence on ZP, however, within each ND type decreasing size does cause some increase in ZP values (as seen with RUDDM and RDDM class NDs).

Each modification method led to considerable differences in adsorption capacities for each NC type. Experiments show that positively charged NDs do not adsorb the positively charged PI molecule. This is true of Ch-F6 and all its modified counterparts, i.e., those treated in oxygen and nitrogen plasma or coated in a positive or negative silane (not shown). The exceptions to these were positively charged SWNH and OLC, which both showed small amounts of PI adsorption, likely due to the internal cavity of the horn and the graphitic nature of the OLC sample. Conversely, all negatively charged NDs showed at least some adsorption of PI (Figure 4.1). The relationship between ZP and the amount of PI adsorbed was not strong between ND types, leading to the understanding conclusion that the processing methods, and thus surface chemistries, significantly influence adsorption. However, NDs processed under the same methods with differences in only size fractionation, and as a result ZP differences, show a correlation of increased PI adsorption with decreased size and increased ZP. Such a case can be seen in RUDDM and RDDM subclasses.

Construction of the Langmuir isotherm and its related transforms were completed by measuring adsorption of RUDDM 1, one of the largest adsorbers of PI, over an extensive range of concentrations. The Langmuir curve reached a plateau once saturation of the available binding sites was reached (Figure 4.2). RUDDM 1 reached a maximum at

concentrations of PI equaling ~130 μg/mL. Initially, adsorption capacities appear to be 85 μg/mg of ND based on the Langmuir isotherm.

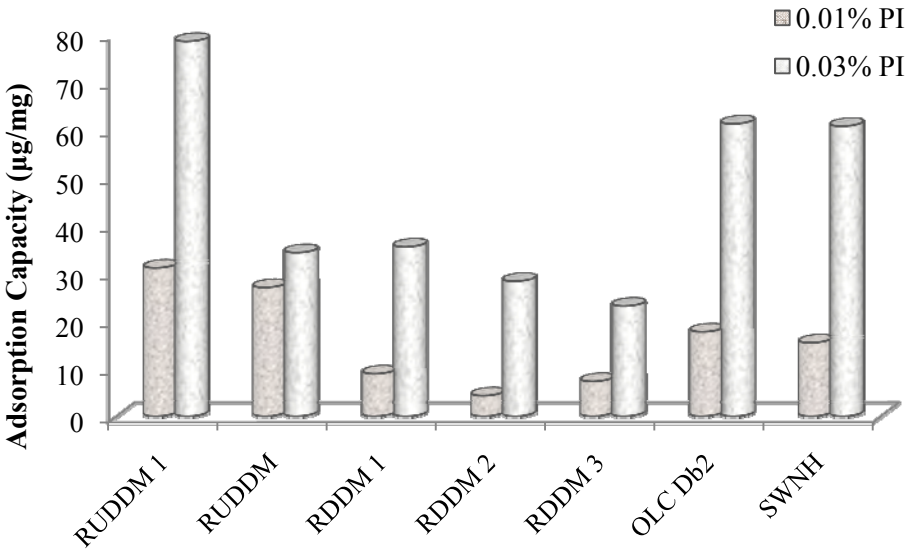

Figure 4.1. Nanocarbon substrates illustrating adsorption capacities (μg/mg) of 0.01 wt. % and 0.03 wt. % propidium iodide (PI) in DI water.

In contrast to the typical Langmuir curve, the plateau does not remain but instead falls over a given range of PI concentrations. This occurrence has been described by the concept [21] that dye micelles form and have a greater affinity to the dye that the ND substrate. The secondary increase reveals the conflicting nature of the PI to complete the first adsorption layer. Certain dyes and detergents have exhibited this presence based on surface impurities on the substrate and micelle formation of the molecule to be adsorbed [21].

Calculations for maximum capacity, Q_{max}, and binding constants, K_d, were completed by using data only up to the maximum point, as points included beyond this caused deviation

from linearity in the transform construction. The transform calculations gave maximum capacity values nearly twice higher than seen on the isotherm (Table 4.2). However, RUDDM 1 showed a relatively low binding constant, which may leave it susceptible to greater desorption under the influence of environmental stimuli, i.e., pH and salts, a property that could be advantageous if controllability in releasing the substance can be preformed.

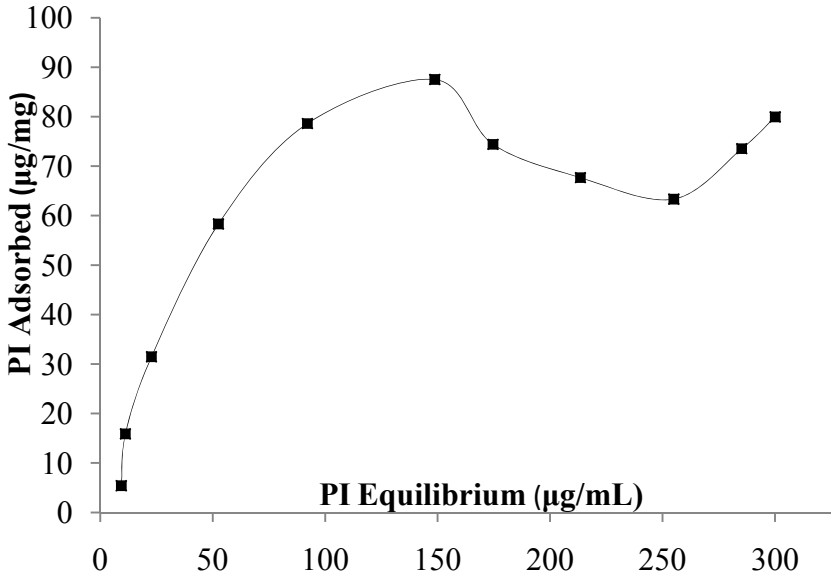

Figure 4.2. Langmuir isotherm for RUDDM 1 on propidium iodide (PI) adsorption.

Table 4.2. Maximum capacity and binding constants of RUDDM 1 based on four Langmuir transform equations.

RUDDM 1		
Transforms	Q_{max} (µg/mg)	K_d (mg/µg)
Eadie- Hofstee	**143.63**	**0.011989**
Lineweaver-Burk	**172.41**	**0.009195**
Reciprocal Langmuir	**136.99**	**0.012992**
Scratchard Transform	**149.99**	**0.011200**

PY and ABTS dyes, both negative in nature, were used to illustrate charge interactions with ND substrates, particularly those possessing a positive ZP. Ch-F6 was used to construct the Langmuir isotherm (Figure 4.3) and its transforms. RUDDM 1 samples, previously tested in PI experiments, were also observed for interactions with PY and ABTS. As expected, RUDDM 1 did not adsorb any of the negatively charged dyes. Observations made from the Langmuir isotherm showed a plateau effect at much lower adsorption values than that of PI and negatively charged NDs. PY dye may also have the ability to form micelles at larger concentrations, as seen by the dip in the last point. Transform calculations confirmed the lower maximum capacity of the Ch-F6 ND (Table 4.3).

CV experiments were performed to assess the electrochemical properties of the bound dye molecule. ABTS alone showed good reversibility and consistent peak placement over many cycles, allowing for simplicity in testing and continuous scanning cycles. ABTS paired with Ch-F6 showed an intensified signal (Figure 4.5) as compared to ABTS without ND. Preliminary experiments, not shown, also show increased signal due to adsorption of PI on RUDDM 1. Furthermore, both Ch-F6 and RUDDM1 are electrochemically inert during CV measurements so their signals can be neglected. Ch-F6 attracts ABTS dye and showed an increased signal over several cycles, then reached a saturation point after 30 minutes of reaction. Upon thoroughly washing the ABTS-ND complex with DI water, a CV signal was still observed, signifying that Ch-F6 does in fact strongly bind ABTS dye as indicated by UV-Vis experiments. Furthermore, bound dye remains electrochemically active, suggesting that NDs can physically bind to molecules without affecting their electrochemical properties.

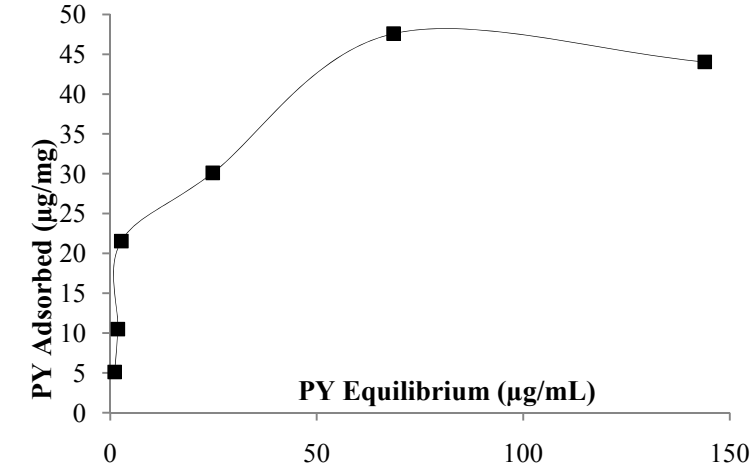

(a)

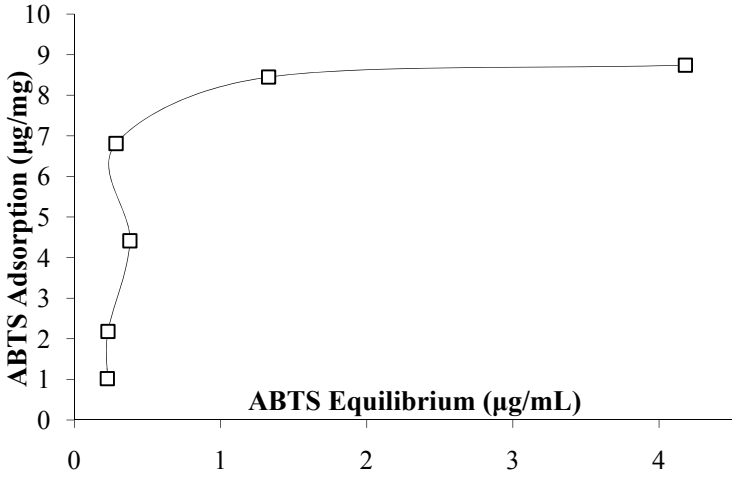

(b)

Figure 4.3. Ch-F6 ND illustrating the adsorption isotherm of pyranine, PY, (a) and ABTS (b) dyes.

Table 4.3. Langmuir transform equations showing differences in maximum capacities (Q_{max}) and binding constants (K_d) of Ch-F6 ND based on pyranine and ABTS dyes.

	Pyranine		**ABTS**	
Transforms	Q_{max} (µg/mg)	K_d (mg/µg)	Q_{max} (µg/mg)	K_d (mg/µg)
Eadie-Hofstee	35.13	0.3044	8.96	11.11
Lineweaver Burk	36.63	0.2877	8.70	11.39
Reciprocal Langmuir	40.65	0.1821	8.91	12.20
Scratchard Transform	35.66	0.2931	8.97	11.09

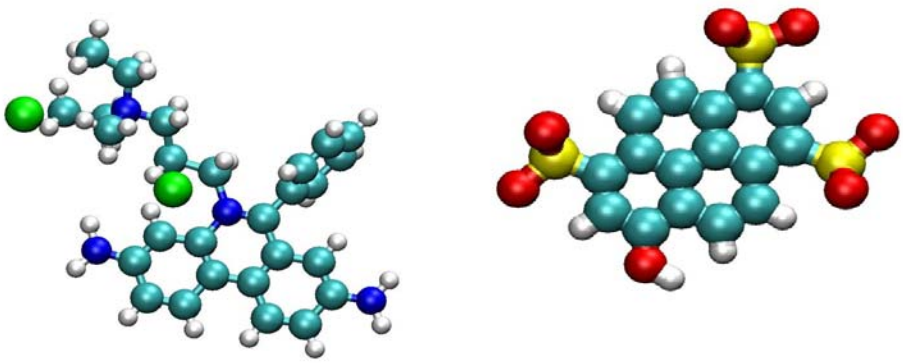

(a) (b)

Figure 4.4. Propidium iodide (a) and Pyranine (b) structures illustrating the top-down view of each molecule used to estimate the cross-sectional area.

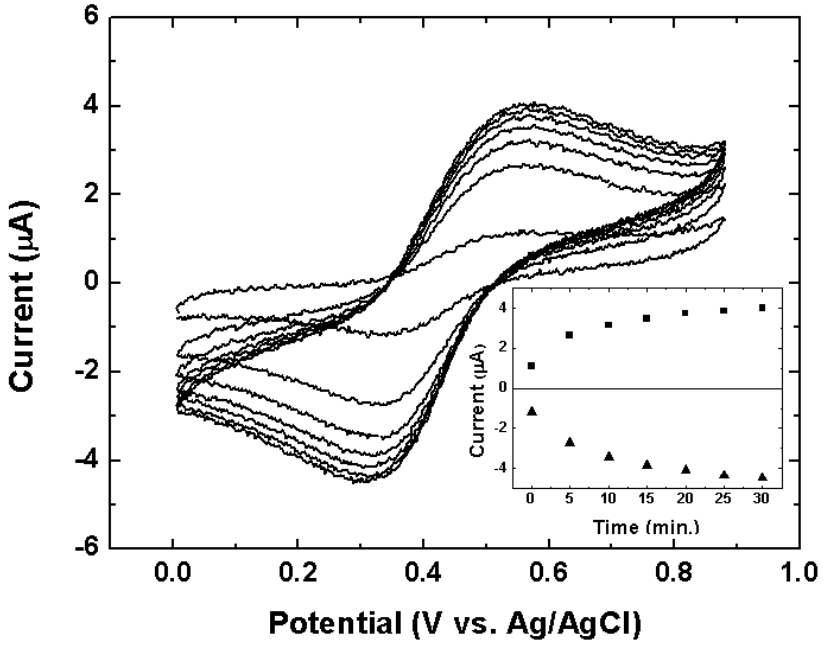

Figure 4.5. Cyclic Voltammetry results showing dye adsorption indicated by a signal increase over 30 min for ABTS on Ch-F6.

4.4 Conclusions

While NDs appear to be good adsorbers for many molecules the choice of ND substrate is critical in gaining high degrees of adsorption. Experimental assay has confirmed that electrostatic interactions play a large role in adsorption characteristics of each ND. Beyond charge, functional groups of the ND and binding partialities based on packing arrangements of each dye molecule determine how much of each substance is capable of being adsorbed. Negatively charged ND, e.g. RUDDM 1, was shown to effectively adsorb positively charged propidium iodide with reasonable capacities based on Langmuir calculations. Ch-F6, a positively charged ND, was shown to adsorb negatively charged ABTS and pyranine. However, the large differences in maximum capacities and binding constants of the dyes are possibly due to different preferential binding sites of each dye on the ND surfaces. Furthermore, specific surface areas covered by the dyes show complicated packing arrangements and preferential binding sites of PY and PI on the ND surfaces. Although dyes show a different preferential position, CV experiments provide a direct proof of dye adsorption and show that the bound dye remains electrochemically active.

Acknowledgements

This material is based upon work supported by the National Science Foundation under Grant No DMR-0602906. The authors would like to recognize Dr. V. Kuznetsov, Boreskov Institute of Catalysis, Novosibirsk for providing onion-like carbon samples, Dr. V. Vorobyev

for supplying RUDDM samples, Dr. Yury Gogotsi, Department of Materials Science and Engineering, Drexel University for BET analysis.

References

1. Puzyr, A.P., A.V. Baron A.V., K.V. Purtov, E.V. Bortnikov, N.N. Skobelev, O.A. Mogilnaya, V.S. Bondar, *Nanodiamonds with novel properties: A biological study.* Diamond and Related Materials, 2007. **16**(12): p. 2124-2128.

2. Schrand, A.M., H.J., Huang, C. Carlson, J. Schlager, E. Osawa, S. Hussain. L. Dai, *Are diamond nanoparticles cytotoxic?* Journal of Physical Chemistry, 2007. **111**(1): p. 2-7.

3. Liu, K.K., C.L. Cheng, C.C. Chang, J.I. Chao, *Biocompatible and detectable carboxylated nanodiamond on human cell.* Nanotechnology, 2007. **18**(32): p. 325102.

4. Yu, S.J., M.W. Kang, H.C. Chang, K.M. Chen, Y.C. Yu, *Bright fluorescent nanodiamonds: No photobleaching and low cytotoxicity.* Journal of the American Chemical Society, 2005. **127**(50): p. 17604-17605.

5. Chao, J.I., E. Perevedentseva, P.H. Chung, K.K. Liu, C.Y.Cheng, C.C. Chang, C.L. Cheng, *Nanometer-sized diamond particle as a probe for biolabeling.* Biophysical Journal, 2007. **93**(6): p. 2199-2208.

6. Chao, J.I., E. Perevedentseva, P.H. Chung, K.K. Liu, C.Y. Cheng, C.C. Chang and C.L. Cheng, *Biocompatibility of chemical-vapour-deposited diamond.* Biomaterials, 1995. **16**(6): p. 483-488.

7. Grill, A., *Diamond-like carbon coatings as biocompatible materials - An overview.* Diamond and Related Materials, 2003. **12**(2): p. 166-170.

8. Hauert, R., *A review of modified DLC coatings for biological applications.* Diamond and Related Materials, 2003. **12**(3-7): p. 583-589.

9. Schrand, A.M., L. Dai, J.J. Schlager, S.M. Hussain, E. Osawa, *Differential biocompatibility of carbon nanotubes and nanodiamonds.* Diamond and Related Materials, 2007. **16**(12): p. 2118-2123.

10. Kossovsky, N., A. Gelman, H.J. Hnatyszyn, A. Rajguru, R.L. Garrell, S. Torbati, S.S.F. Freitas, M.G. Chow, *Surface-modified diamond nanoparticles as antigen delivery vehicles.* Bioconjugate Chemistry**,** 1995. **6**(5): p. 507-511.

11. Kossovsky, N., A. Gelman, H.J. Hnatyszyn, A. Rajguru, R.L. Garrell, S. Torbati, S.S.F. Freitas, M.G. Chow, *Surface-modified diamond nanoparticles as antigen delivery vehicles.* Bioconjugate Chemistry**,** 1995. **6**(5): p. 507-511.

12. Grichko, V., V. Grishko, O. Shenderova, *Nanodiamond bullets and their biological targets.* Nanobiotechnology**,** 2007. **2**(1-2): p. 37-42.
13. Poh, W.C., K.P. Loh, W.D. Zhang, S. Triparthy, J.S. Ye, F.S. Sheu, *Biosensing properties of diamond and carbon nanotubes.* Langmuir**,** 2004. **20**(13): p. 5484-5492.

14. Puzyr, A.P., K.V. Purtov, O.A. Shenderova, M.Luo, D.W. Brenner, V.S. Bondar, *The adsorption of aflatoxin B1 by detonation-synthesis nanodiamonds.* Doklady Biochemistry and Biophysics, 2007. **417**(1): p. 299-301.

15. Gibson, N., O. Shenderova, T.J.M. Luo, S. Moseenkov, V. Bondar, A. Puzyr, K. Purtov, Z. Fitzgerald, D.W. Brenner, *Colloidal stability of modified nanodiamond particles.* Diamond and Related Materials, 2009. **18**(4): p. 620-262.

16. Schmid, I., W.J. Krall, C.H. Uittenbogaart, J. Braun, V. Giorgi*, Dead cell discrimination with 7-amino-actinomycin D in combination with dual color immunofluorescence in single laser flow cytometry.* Cytometry, 1992. **13**(2): p. 204-208.

17. Waring, M.J., *Complex formation between ethidium bromide and nucleic acids.* Journal of Molecular Biology, 1965. **13**(1): p. 269-282.

18. Gibson, N.M., T.J.M Mark Luo, O. Shenderova, Z. Fitzgerald, D.W. Brenner. *Propidium Iodide Adsorption and Binding by Nanodiamond and Nanocarbon Particles*. Chapter 5.

19. MOPAC2009, J.J.P. Stewart, Stewart Computational Chemistry, Version 8.318M web: http://OpenMOPAC.net

20. Humphrey, W., A. Dalke, K. Schulten, *VMD: Visual molecular dynamics.* Journal of Molecular Graphics, 1996. **14**(1): p. 33-38.

21. Giles, C.H., D. Smith, A. Huitson, *A general treatment and classification of the solute adsorption isotherm. I. Theoretical.* Journal of Colloid and Interface Science, 1974. **47**(3): p. 755-765.

Chapter 5

Propidium Iodide Adsorption and Binding by Nanodiamond and Nanocarbon Particles

Propidium Iodide Adsorption and Binding by Nanodiamond and Nanocarbon Particles

N.M. Gibson[1]*, T.J.M. Luo [1], O. Shenderova [1,2], A.P. Koscheev [3] and D.W. Brenner [1]

[1] Department of Materials Science and Engineering, North Carolina State University, 911 Partners Way, Raleigh, NC, USA 27695

[2] International Technology Center, P.O. Box 13740 Research Triangle Park, NC, USA 27617

3 State Scientific Center of Russian Federation, Karpov Institute of Physical Chemistry, ul. Vorontzovo Pole, 10, Moscow, Russia 105064

Abstract

Binding constants, loading capacities and rates were determined for propidium iodide (PI) interacting with several types of nanodiamonds (NDs), nanometer-scale onion-like carbon (OLC), single-wall nanohorns (SWNHs), and activated charcoal. Adsorption and desorption was characterized using ultraviolet-visible spectroscopy followed by binding capacity determination using Langmuir isotherms and transforms. Langmuir and transform calculations further allowed for estimates of the specific surface areas covered by the adsorbate for select nanocarbon materials. All NDs with a negative zeta potential were found to adsorb PI, while the type of surface functionalization greatly influenced the degree and capacity of the PI adsorbed. Ozone-purified NDs had the highest capacity for PI adsorption, due to its greater density of oxygen containing groups, i.e. acid anhydrides and carboxyls, as assessed by TDMS and TOF-SIMS. However, the binding strengths of all NDs studied was low, which allowed for desorption of PI at increased dye concentrations attributable to micelle formation of PI. SWNHs and OLC were found to adsorb PI regardless of their zeta

potential; this is likely due to π bonding between the aromatic rings of PI and the graphitic surface of the materials and the internal cavity of the horns. Preliminary studies indicate that the adsorption of PI can be reversed under the influence of salt solutions.

5.1 Introduction

Nanodiamonds (NDs) have recently attracted tremendous attention in the fields of nanotechnology and biomedicine due to their biocompatibility [1-4], nontoxicity [5-14], chemical inertness and environmental stability. NDs, which have high specific surface areas (SSAs) (typically 300-400 m^2/g for NDs produced by detonation synthesis), can be easily functionalized with a variety of surface groups to enhance binding selectivity toward target molecules. Because NDs are absent of cytotoxicity, as established from *in vitro* studies [10-13], possible applications include carriers for active molecules [15-16], drug delivery agents [10-13, 17], biosensors [18-20], and more recently enterosorbents [5, 21-23] for toxin binding. Biomolecules attached to NDs have included proteins, such as obelin [24], cytochrome c [25] and glycoproteins, ovalbumin and fetuin [26], as well as DNA [16, 17, 27, 28] and fluorescent dyes [17, 29]. Conjugation of biomolecules to NDs was shown to take place via chemisorptions [29, 30] or physisorption [25] for a variety of applications [31].

Conjugation of molecules to NDs is a critical step in the development of successful nanobiotechnology applications. NDs are complex in the fact that they possess many different types of surface groups. Dissociation of these groups in solution produces strong electrostatic potentials, which can dominate the adsorption process. To evaluate electrostatic

interactions of NDs' propidium iodide (PI) was chosen as a charged molecule model. PI was selected as it is a well characterized dye, used widely in the field of microbiology to indentify dead cells [28, 32, 33]. PI carries a strong positive charge, which prevents it from penetrating the membrane of live cells [34].

To fully understand PI adsorption we explore mechanisms beyond electrostatic interactions. A thorough study was completed to investigate the effect of graphitized surfaces, surface areas, surface configurations and surface modification methods. This was accomplished by using several types of NDs, each processed under different manufacturing techniques and modifications, and various graphitic carbon nanostructures, these included nanometer-scale onion-like carbon (OLC), nanometer-scale single wall nanohorns (SWNH) and activated charcoal.

Adsorption and desorption studies were characterized using ultraviolet-visible (UV-Vis) spectroscopy followed by development of the Langmuir isotherms and related transform calculations to determine the substrate which provides the largest adsorption capacity, strongest binding and greatest control in releasing PI. Maximum capacities obtained from transform calculations further allowed for estimates of the specific surface area (SSA) covered by the adsorbate for select NDs. Surface characterization using TDMS and TOF-SIMS were also completed to help determine surface groups responsible for PI adsorption.

5.2 Experimental Details

5.2.1 Types of Carbon Species

An extensive selection of carbon species were used to understand the effects of surface charge, particle size, surface configuration and sp^2 versus sp^3 surface hybridization on PI binding. The complete list of species is given in Table 5.1. Four classes of carbon species were used: (a) nanodiamonds, (b) OLC nanoparticles, (c) SWNHs and (d) activated charcoal. NDs, the prime focus of this paper, were further subdivided into two classes, those carrying a positive charge and those carrying a negative charge, which depends on manufacturing and treatment processes. For these NDs the role of particle size and surface treatment was also explored. OLC, obtained by annealing NDs, were classified based on annealing temperature and initial type of ND used. Both factors also affect the dispersivity in water and the amount of sp^2 coverage on the sorbent.

Nanodiamonds. NDs were produced through detonation using a mixture of trinitrotoluene (TNT) and 1,3,5-trinitro-1,3,5-*s*-triazine (RDX), which results in "detonation nanodiamonds" (DNDs). DNDs were purified from non-diamond carbon in the soot using liquid or gas phase oxidizers. With purification, the removal of metallic impurities and oxidation of non-diamond carbon was achieved. Additional processing methods were used to further reduce the non-diamond carbon content and provide intentional modifications to the ND's surface group content and composition. The sample $ND^{+}180$ ("New Technologies," Chelyabinsk, Russia) served as the standard positively charged ND. The material contained an incombustible impurity content of 0.6 wt. %. Details of the detonation,

purification, and modification process were recently reported [23]. Several negatively charged NDs were used, these included nanodiamonds processed under wet-phase (NDW^-) and gas-phase (NDG^-) techniques. NDW^- (Real-Dzerzinsk, LTD, Russia) was purified from soot using singlet oxygen in NaOH and HNO_3 [22, 23, 35]. A portion of NDW^- was treated in NaCl solution and size fractionated through centrifugation to achieve NDW^-75. NDG^- ("New Technologies") was purified by oxidizing soot with ozone at 200°C. NDG^- was also size fractionated by centrifugation to achieve NDG^-80, which had a smaller, more uniform particle size.

Table 5.1. Size (diameter for ND and OLC, nm), zeta potentials (ZP, mV) and processing methods of all nanocarbon aggregates used in the adsorption experiments.

Nanocarbon	ZP, mV	Size, d.nm	Processing
ND^+180 (Ch-F6)	46.8 ±0.9	185.59 ±0.25	CrO_3 in H2SO4; NaOH+H_2O_2; ion-exchange resin; FC*
NDW^- (RUDDM)	-44.1 ±0.7	260.1 ± 1.75	Singlet O in NaOH; HNO_3;
NDW^-75 (RUDDM 1)	-49.3 ±1.9	75.0 ± 0.35	Singlet O in NaOH; HNO_3; NaCl; FC
NDG^- (ND-OZ)	-48.5 ±0.2	139.2 ±0.59	Soot oxidized with Ozone
NDG^-80 (OZ-Bl)	-51.2 ±0.5	80.5 ±0.99	Soot oxidized with Ozone; FC
OLC	47.1 ±0.65	189.2 ±0.92	ND^+180 heated in vacuum at 1600 K
SWNH	13.9 ±0.15	4305.0 ±252	Nanocraft, Inc. Renton, WA
Activated Charcoal	0	20/40 mesh	Supelco Bellefonte, PA

FC*: Fractionation by Centrifugation

Onion-like carbon, Single wall nanohorns and Activated Charcoal. The OLC sample Institute of Catalysis, Novosibirsk, Russia), produced by annealing $ND^{+}180$ at a temperature of 1600 K, was chosen due to its superior colloidal stability based on a high zeta potential (ZP) and small size characteristics. SWNHs (Nanocraft, Inc., Renton, WA.) and activated charcoal (Supelco Inc., 20/40 mesh size) were used as received.

5.2.2 Hydrosol Preparation

All ND suspensions were prepared using deionized (DI) water (pH = 5.8 and water resistivity = 18 MΩ·cm) followed by sonication with a Cole-Parmer 750-Watt ultrasonic homogenizer (EW-04711-60). Its tapered titanium horn (3 mm diameter) was directly immersed into the polypropylene centrifuge tubes containing the sample suspension. Sonication occurred for 2-4 min at an output power of 10 W and output intensity of 100 W/cm^2. All solutions were prepared to a 0.1 wt. % concentration for ZP, size and pH measurements while a 0.5 wt. % concentration was prepared for adsorption measurements. The ND colloids had a natural pH ranging from 5 to 6, related to the 0.1 wt. % suspension concentration. OLC and SWNH suspensions were prepared in the same manner but with sonication times of 8-10 min. The natural pH of OLC was measured as 5.7; SWNHs were more acidic with a pH close to 4.6.

5.2.3 Particle Size and Zeta Potential Measurements

Particle size was measured using the N5 submicron particle size analyzer (Beckman Coulter Inc.) and the ZetaSizer NanoZS (Malvern Instruments). To prepare samples for particle size measurements, ND suspensions were diluted by adding approximately 10 μL of the concentrated suspension to 3 mL of DI water. Each sample was measured three times and the average particle sizes were calculated based on unimodal intensity. It is worth noting the ZetaSizer is able to measure particle sizes accurately without diluting the suspension below 0.1 wt. %. ZP measurements were completed solely on the ZetaSizer by using 0.1 wt. % ND suspensions that were transferred into specialized Malvern zeta cells. Again, three measurements were taken at room temperature; averaged results are reported.

5.2.4 Propidium Iodide Adsorption

All Nanocarbon Types. Propidium iodide (PI) from Sigma Aldrich was dissolved in DI water to prepare a 0.07 wt. % stock solution. All ND adsorption experiments were carried out first by mixing the desired concentration of PI solution and a 0.5 wt. % ND suspension at a 7:3 volume ratio. Initial adsorption experiments used final PI concentrations of 0.01 and 0.03 wt. %. A ND suspension with 0 wt. % PI was used as the control sample. The mixtures were incubated on an orbital shaker at room temperature for 30 min followed by centrifugation (14,000 RPM, 25 min). The remaining PI in each supernatant was measured on a UV-Vis spectrophotometer (Lambda 35, Perkin Elmer). Due to ND's very high colloidal stability, there is a remaining ND in the supernatant after centrifugation. To eliminate these

effects, the spectra of these residual NDs were subtracted from all ND-PI spectra that used PI concentrations below 0.015 wt. %. PI concentrations above this concentration caused complete coagulation of the residual NDs. The percentage of unbound PI was determined based on a PI standard absorption curve and this concentration was converted to ND adsorption capacity (μg PI/mg ND). Because SWNH and OLC samples do not form a pellet during centrifugation, microcentrifugal regenerated cellulose filters (Sigma-Aldrich, MWCO 100 kDa) were used to separate nanocarbons from unbound PI. To reduce non-specific binding of PI on the cellulose membrane, all filters were washed with 0.04 wt. % PI and DI water twice before performing adsorption experiments.

Activated Charcoal. PI is an effective and widely used dye, but it also carries many harmful health hazards as it is a possible carcinogen and mutagen [36, 37]. For disposal, we compare NDs to traditional techniques which call for PI to be poured through activated charcoal and filter paper followed by incineration of the charcoal [37] or charcoal filters for simpler, faster methods of disposal [36]. To complete experiments activated charcoal (6 or 3.5 mg) was added to 1 mL PI suspensions of 0.005 to 0.025 wt. % concentrations. Individual mixtures were vortexed for 1 min and then placed on the orbital shaker for 15 min, 1 hr, 24 hrs, and 28 hrs. Control samples included PI concentrations in absence of activated charcoal. After incubation, charcoal was removed and the amount of unbound PI was measured spectroscopically.

5.2.5 Langmuir Isotherm

Langmuir isotherms were constructed for the $ND^{+}180$, $NDW^{-}75$ and $NDG^{-}80$ samples by including an adsorption studies at several different PI concentrations ranging from 0.0025 to 0.07 wt. %. To obtain the Langmuir curve adsorption percentages were converted to capacities as micrograms of PI adsorbed per milligram of sorbent and plotted against the concentration of equilibrium PI (μg/mL). From this data the maximum capacity (Q_{max}) and the binding constants (K_d) of the sorbents were extracted by linear regression curve fitting using four transform equations: Eadie-Hofstee, Lineweaver-Burk, Reciprocal Line and Scratchard.

5.2.6 Specific Surface Area

SSAs (surface area per gram of ND) covered by PI were calculated based on $Q_{max,}$ obtained through transform equations, and the cross sectional area of the adsorbed molecule ($Å^2$). The cross-sectional area of PI (128.7 $Å^2$) was obtained on a PI molecule whose energy was previously minimized on MOPAC using the PM6 semi-empirical method [38]. The relaxed structure was added with the Connolly surface using a probe size of 1.5 Å on the Visual Molecular Dynamics program [39]. By outputting the image to ImageJ the cross-sectional value was determined. Results based on the Langmuir model were compared to true SSAs measured by the Brunauer, Emmett and Teller (BET) method, which used nitrogen adsorption at 77 K (Quadrasorb from Quantachrome).

5.2.7 Propidium Iodide Desorption.

Desorption studies were conducted to detect the controllability of releasing PI from the ND substrates. $ND^{+}180$, $NDW^{-}75$ and $NDG^{-}80$ pellets, saved from previous adsorption experiments, were used. In the first stage individual pellets were redispersed into 1 mL of DI water followed by vortexing (2 min) and placing on an orbital shaker (20 min). Redispersed samples were then centrifuged (14,000 RPM, 25 min) and supernatants collected for UV-Vis detection. In the second stage redispersion occurred in 5 mg/mL NaCl solution or 5 mg/mL $CaCl_2$ solution with all remaining steps the same. This stage was repeated a second time to have a total of 3 redispersion cycles for each ND sample.

5.2.8 Surface Characterization

Mass Spectroscopy. A portion (4.4 ±0.1 mg) of ND powder was placed into the Ni-envelope (pre-cleaned ultrasonically in acetone and water and dried) and introduced in the high-temperature vacuum oven. The sample was then degassed under evacuation by ion pump for one day at room temperature. The residual pressure at the end of degassing was in the range of 10^{-7} Torr. TDMS analysis was performed by measuring the mass spectra of gases released from the sample under programmed heating with constant rate 10^{o}C/min up to 1100^{o}C. Mass spectrometer was a quadrupole MX7304 with electron multiplier with mass range 10-120 amu (up to 700^{o}C) and 2-50 amu (700-1150^{o}C). MS scan rate was 1 min per scan (or 10^{o}C per scan). The evolved gases were pumped permanently with the rate ~1l/s (relative to nitrogen). In this case the measured partial pressures of gases were proportional

to desorption rates at every moment. The total pressure in the vacuum chamber during heating was measured by ionization gauge. The obtained mass spectra were analyzed and handled to calculate the intensities of characteristic ion fragments at different temperatures, their temperature profiles, and the relative amounts of released species.

In complementary analysis, TOF-SIMS was used. The instrument was equipped with a Bi_n^{m+} (n = 1 - 5, m = 1, 2) liquid metal ion column. The analysis chamber pressure was maintained below 5.0 x 10^{-9} mbar to avoid surface contamination. The primary Bi^+ ions had a kinetic energy of 25 keV and were contained within a ~10 μm diameter probe beam. For high mass resolution spectra, the Bi^+ ion beam was rastered across a 500 x 500 μm^2 area divided into 128 x 128 pixels. The electron flood gun was used to neutralize the charge accumulated on the sample surface while acquiring the spectrum. The total accumulated primary ion dose used to acquire spectra was less than 1 x 10^{12} ions/cm^2, which is within the static SIMS regime. The secondary ions were extracted at 2 keV and mass analyzed using a TOF mass spectrometer. Secondary ions were post accelerated to 10 keV prior to impacting the detector. At least three areas of each sample were analyzed. Positive secondary ion mass spectra are calibrated using H^+, C^+, CH^+, CH_2^+, CH_3^+, $C_2H_3^+$, $C_2H_5^+$, $C_4H_9^+$ and negative spectra were calibrated using C^-, O^-, OH^-, and various C_n^- secondary ions. Peak intensities were reproducible to within 10 % from scan to scan. Mass resolution of ~5000 M/ΔM (50 % valley definition) at m/z 29 was obtained throughout. Results from TOF-SIMS studies are described in the Supplementary Data.

5.3 Results and Discussion

5.3.1 Size and Zeta Potential

Particle size measurements showed that different processing and treatment methods had largely impacted the aggregate size of the NDs. The size of the primary ND particles is known to be between 4 and 5 nm; however, the primary particles quickly aggregate during synthesis [40]. While beads milling could have been used to reduce the aggregate size back down to the primary size range [40], for the purposes of this research significant size reduction was not desired, since high colloidal stability of small NDs difficult to pellet. PI additions at high concentrations to ND suspensions cause immediate and rapid precipitation; this may cause additional PI confinement within ND agglomerates. Independent objectives were placed on revealing the possible role of pores within the aggregates of primary particles, as these pores may promote internal diffusion and trapping of PI molecules within the aggregates.

ZP measurements indicated that the modification methods used did not alter the sign, but instead altered the magnitude of the charge. The results also indicated that the influence of particle size on the ZP is insignificant. When comparing the non-fractionated NDG^- to NDW^-75 it was shown that NDG^- was nearly twice the size of NDW^-75 (139 nm versus 75 nm), however, the ZPs of these two samples were virtually the same (-49 mV). Such a result shows the importance of surface chemistry; NDG^- has a greater density of negative surface groups which gives rise to higher ZPs. Nevertheless, NDs, processed under identical

conditions, can be manipulated to have slightly higher ZP values by decreasing size through fractionation by centrifugation (Figure 5.1).

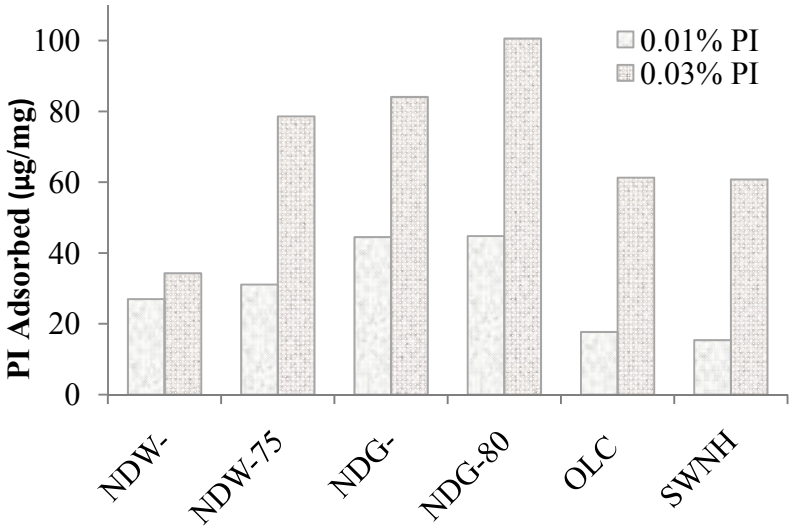

Figure 5.1. Adsorption capacities (µg/mg) of 0.01 wt. % and 0.03 wt. % PI in DI water on various nanocarbon substrates (1.5 mg/mL).

5.3.2 Propidium Iodide Adsorption for All Samples at 0.01 % and 0.03 % PI

Nanodiamond. The adsorption studies show drastic differences in adsorption capacities for each NC type (Figure 5.1). More interestingly, NDs themselves show notable changes in their adsorption capacity depending on their modification method. The data indicates that positively charged NDs do not adsorb the PI, which is also positively charged in DI water (Figure 5.2a), due to electrostatic repulsion. However, all negatively charged NDs showed adsorption of PI, though the amount each ND adsorbed was drastically different depending on the modification and treatment procedures. As an example, the adsorption

spectrum of NDW-75 is illustrated in Figure 5.2b. It was also concluded that ZP is not a direct indicator of adsorption capacities, as seen with NDW^- and NDW^-75. Both NDs had comparable ZPs but vary drastically in the amount of dye adsorbed. More examples of this face were provided in previous work [41]. It is understood that surface chemistry of the ND has the greatest influences on adsorption. However, adsorption capacity of NDs can be increased by using fractions of ND with smaller sizes, obtained, for example, by centrifugation. Using NDs with smaller average aggregate sizes resulted in increased ZPs and subsequently increased adsorption quantities. This result can be seen for both the NDW^- and NDG^- series (Figure 5.1).

SWNH and OLC. Positive ZPs exist for SWNHs (+14 mV) and OLC (+47 mV), yet unlike observations with positively charged NDs these carbon based particles show adsorption of PI, although the amount of adsorption is low. Both samples adsorbed roughly equal amounts of PI, suggesting that adsorption extends beyond surface functional groups. Annealing ND^+180 in vacuum at high temperatures generates the sp^2 surface of the OLC derivative. The sp^2 graphitic surface of the OLC and the SWNH has a greater, though not excellent, ability to adsorb the PI molecule likely due to π bonding between the aromatic rings of PI and the graphitic surface of the materials. The SWNH also has an internal cavity accessible to PI, which allows entrapment of the molecule and contributes to its increased adsorption characteristics. In each case defects or non-uniformities on the surface may also play a role in PI adsorption.

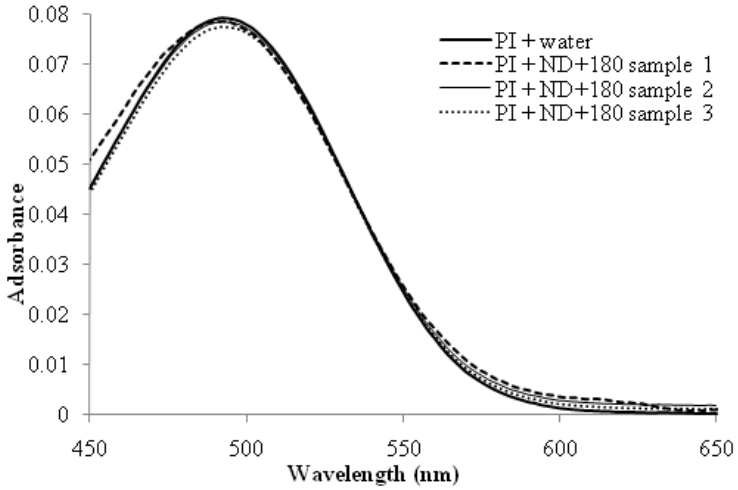

(a)

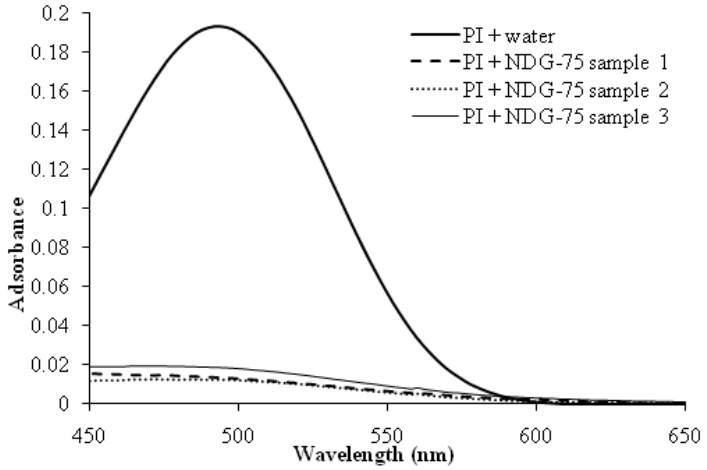

(b)

Figure 5.2. UV-Vis absorbance spectra of ND-PI supernatants after incubation and centrifugation as compared to the reference PI concentration (PI + water): $ND^{+}180$ with 0.009 wt. % PI (a) and $NDW^{-}75$ with 0.01 wt. % PI (b).

Activated Charcoal. Activated charcoal has been used as a PI adsorbent in disposal protocols [38, 39] and is therefore an important standard with which to compare the results of the other carbon structures in the present study. It was found that the activated charcoal adsorbed PI at a much slower rate than NDs even though the charcoal concentration was 6

mg/mL as compared to 1.5 mg/mL of ND samples (Figure 5.3). For activated charcoal, the amount of adsorbed PI linearly increased from 15 min incubation to 24 hr incubation, while for ND samples the adsorption reached 82 % in 30 min and only increased by 5 % at the end of the 24 hr period. Therefore, it was concluded that 30 min incubation times for all ND samples are sufficient.

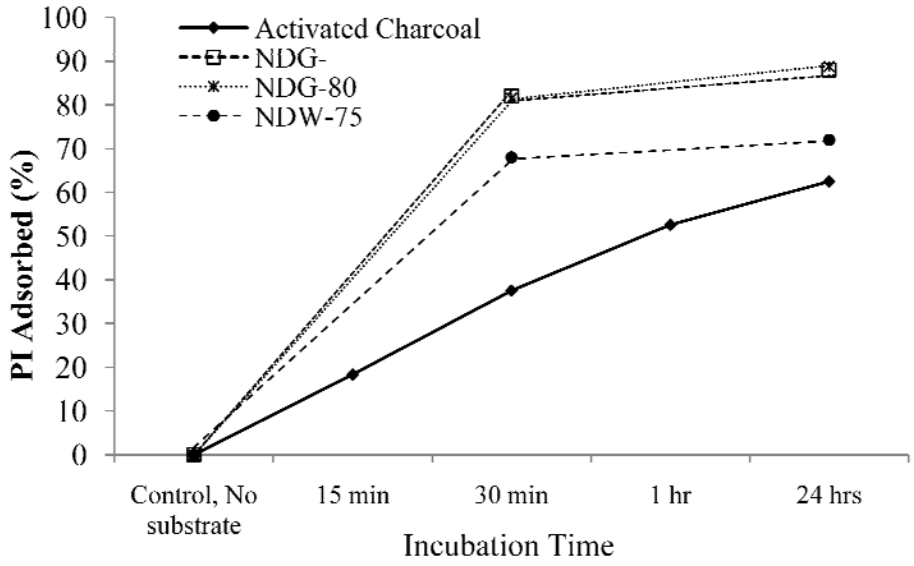

Figure 5.3. Total percentage of 0.005 wt. % PI adsorbed on activated charcoal (6 mg/mL) as compared to NDW$^-$75, NDG$^-$ and NDG$^-$80 (1.5 mg/mL) substrates during 0.25, 0.5, 1 and 24 hour incubation times.

In another experiment, the amount of activated charcoal was reduced by almost half (3.5 mg/mL) and results of the PI adsorption were compared to the previously used 6 mg/mL. The experiment was completed using 0.025 wt. % PI with incubation times of 15 min, 1 hr, 24 hrs and 28 hrs. The two samples performed similarly until 1 hr, after this time the 6 mg/mL sample began adsorbing more PI than the 3 mg/mL sample. Remarkably, a noticeable

amount of adsorption was seen in the time interval between 24 and 28 hrs and was significantly higher for the higher concentration of charcoal. Overall, the amount of PI adsorbed over 28 hrs was about 44 % for 6 mg/mL and 21 % for 3.5 mg/mL of activated charcoal. For both studies the total amount of PI adsorbed by activated charcoal, which had a SSA of 1040 m^2/g, adsorbed far less PI than NDs, consequently, opening up new possible applications for NDs.

5.3.3 Langmuir Studies

Langmuir isotherms shapes for NDW$^-$75, NDG$^-$ and NDG$^-$80 (Figure 5.4) deviate from the typical isotherms demonstrating a plateau indicating saturation of the substrate's adsorption sites. In all cases, it was initially observed that as the amount of PI increased there still remained available active sites for other PI molecules to bind, denoted by the gradual slope early on in the curve. However, at higher concentrations of PI a turning point exists where some sites become free, corresponding to desorption of the dye ("valleys" on the curves, Figure 5.4). Such a phenomenon had been previously described by Giles [42], who attributed desorption of dye adsorbates to micelle formations, due to dyes having a stronger affinity for itself than to the adsorbing substrate. Concentrations of PI used in this experiment were very high making micelle formation plausible. However, detection of PI at their micelle formation is still needed. The NDW$^-$75 and NDG$^-$80 samples with smaller sizes show a maximum adsorption or a turning point between adsorption and desorption at PI concentrations of nearly 150 μg/mL. The NDG$^-$ curve shows a continuous increase that does

not reach a maximum until beyond 150 µg/mL. NDG⁻'s aggregates, which are larger, may allow for diffusion of the dye into pores and, thus, it may be able to capture more dye before desorption at the surface begins.

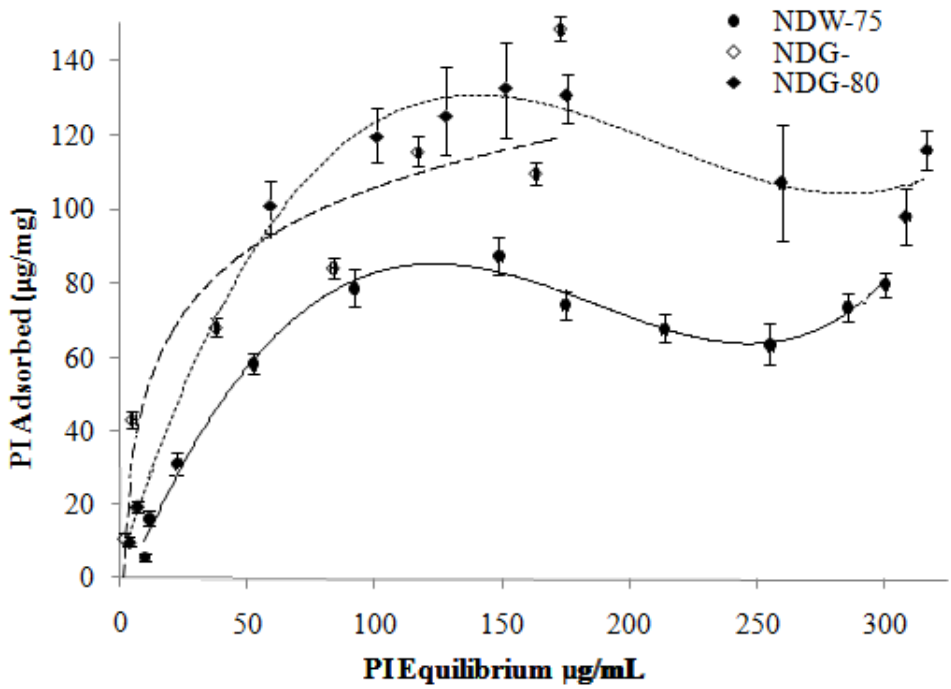

Figure 5.4. Langmuir Isotherm plot for adsorption PI to NDW⁻75, NDG⁻ and NDG⁻80.

As the concentration of PI is increased further a secondary increase of adsorbed PI is observed. Such behavior illustrates the conflicting ability for the material to complete the first monolayer, as the PI molecules are adsorbed, desorbed and reabsorbed onto the ND substrate. Giles' theory [42] suggests that this pattern should continue if PI concentrations were further increased and furthermore states that the exhibited behavior, seen in certain dyes and detergents, may be caused by the presence of surface impurities.

The maximum capacity and binding constants of all three NDs were calculated using the four transforms listed in Section 5.2.5. Four transforms were selected as each shows different error sensitivities and have biases towards fitting data at low or high concentration ranges. Data beyond the PI concentration corresponding to the adsorption/desorption turning point were excluded because linearity must be achieved to calculate the maximum capacity and binding constants. The transform calculations showed the highest capacity for NDG$^-$80 (~200 μg/mg) followed by NDW$^-$75 (Table 5.2). As previously mentioned, both NDs have roughly the same aggregate size and ZPs in water. In order to understand 25 % difference in the sorption capacity, detailed surface characterization of the ND samples was performed (Section 5.3.6). Besides differences in types of surface groups, internal pores, which contribute to a larger surface-to-volume ratio may contribute to NDG$^-$80's higher maximum capacity. Therefore, we characterized pores size and total volumes with BET methods (Table 5.3). As seen, NDG$^-$80 has a larger average pore size and nearly double the pore volume than NDW$^-$75, which helps explain the larger loading capacity.

Despite differences in maximum capacities, the binding constant of both NDs were similar (Table 5.2). The weak binding of PI to the ND substrates is a reason for the observed desorption at higher PI concentrations on the isotherms. If the binding strength of the dye to the ND was increased the decrease from maximum could potentially be reduced or eliminated. Interestingly, NDG$^-$, which possessed the lowest maximum capacity, had the highest binding constant. Its smaller surface area, as a result of larger aggregate sizes, may heavily influence the lower capacity values.

Table 5.2. Transforms used in the calculation of maximum capacity and binding constant for PI on (a) NDW-75, (b) NDG- and (c) NDG-80.

Transforms	Max Capacity (µg/mg)	K_d (mg/µg)	r^2
Eadie-Hofstee	143.63	0.011989	0.9354
Lineweaver-Burk	172.41	0.009195	0.9968
Reciprocal Line	136.99	0.012992	0.9819
Scratchard	149.99	0.011200	0.9354
Average	*150.76*	*0.011344*	*0.9624*

(a)

Transforms	Max Capacity (µg/mg)	K_d (mg/µg)	r^2
Eadie-Hofstee	136.59	0.026355	0.9208
Lineweaver-Burk	135.14	0.026696	0.9981
Reciprocal Line	140.85	0.024200	0.9689
Scratchard	141.33	0.024300	0.9208
Average	*138.48*	*0.025388*	*0.9522*

(b)

Transforms	Max Capacity (µg/mg)	K_d (mg/µg)	r^2
Eadie-Hofstee	189.91	0.016324	0.9611
Lineweaver-Burk	232.56	0.012349	0.9956
Reciprocal Line	185.19	0.017159	0.9921
Scratchard	194.05	0.015700	0.9611
Average	*200.43*	*0.015383*	*0.9775*

(c)

Table 5.3. Comparisons of calculated SSAs, m^2/g, covered by PI based on maximum capacity computations, in relationship to the true SSA, m^2/g (BET). Average pore size, nm, and pore volume were also obtained through BET measurements.

Nanodiamonds	SSA from Langmuir*	SSA from BET	Average Pore Size (nm)	Pore Volume (cc/g)
NDW-75	174.72	319.5	6.52	0.599
NDG-	160.49	244.9	12.3	0.868
NDG-80	232.29	426.4	8.5	1.105

*Calculations carried out using the following relationships:
Specific Surface Area= $(Q_{max}*N_A*A)/MW_{PI}$
N_A: Avogadro's number, A: cross-sectional area of the adsorbed molecule ($Å^2$), MW_{PI}: Molecular weight of the adsorbed molecule.

5.3.4 Specific Surface Areas

SSAs covered by the dye reveal that NDG$^-$80 had the largest SSA (Table 5.3) though NDG$^-$80 and NDW$^-$75 had similar aggregate sizes. As expected, comparisons between NDG$^-$ and NDG$^-$80 indicate that as aggregate particle sizes decrease the SSA covered by PI increases. Compared to the true SSA, found by BET measurements, the Langmuir results underestimate the area covered by PI as compared to the BET SSA by approximately 85 to 195 m^2/g. NDG$^-$80 exhibited the highest areas covered by PI from the Langmuir calculations (174.7 m^2/g) as well as SSA from BET measurements (426.4 m^2/g), which follows the previous trend showing it also had the highest capacity. The lowest SSA came from NDG$^-$ due to its larger particle sizes. Discrepancies between the measured and calculated areas can be attributed to PI having preferred binding sites on each ND where once these sites are filled no more PI is adsorbed. Additionally, during adsorption PI may lay on the ND surface in preferred orientations that may not allow for ordered, high density packing of PI. Inaccuracies in the estimated size of the PI may also contribute to this error.

5.3.5 Desorption Experiments

The three ND samples used in the adsorption experiments were also examined for desorption of PI. NDG$^-$80 and NDG$^-$ sample pellets showed no release of PI under the influence of water. NDW$^-$75, however, showed approximately 5 % of the dye was removed with the addition of water (Figure 5.5). This result is explained by the weaker calculated binding constants of NDW$^-$75 as compared to the ozonated samples.

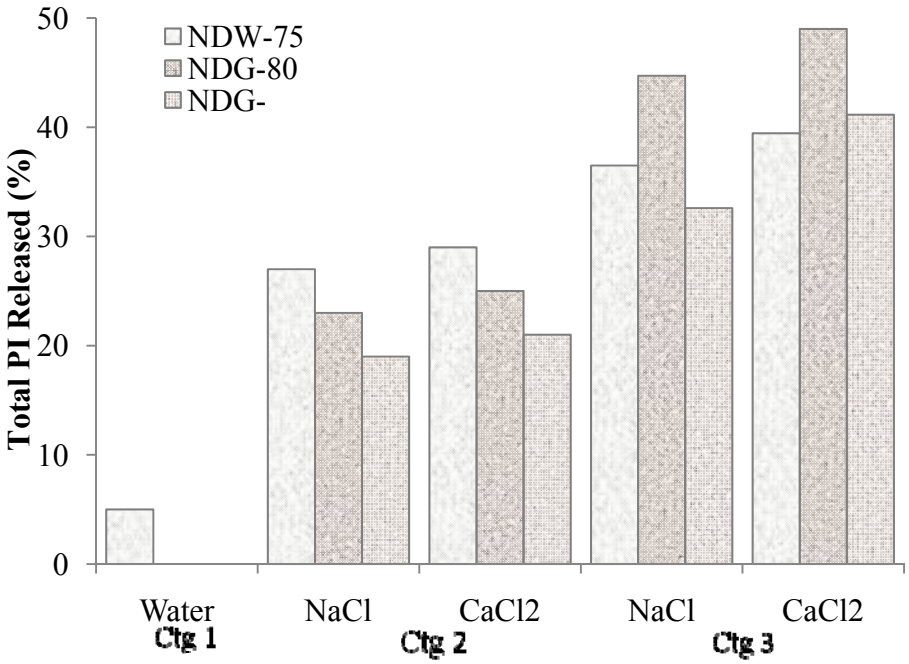

Figure 5.5. Total percentage of PI released from ND substrates, NDW$^-$75, NDG$^-$80 and NDG$^-$, during three centrifugation cycles in water (Ctg 1) followed by redispersion and centrifugation in NaCl or $CaCl_2$ (Ctg 2 and 3).

Samples under the influence of NaCl and $CaCl_2$ all showed PI desorption. NDG$^-$80 pellets showed ~23 % of PI was released under the influence of NaCl and a 25 % release under the influence of $CaCl_2$. NDG$^-$ showed slightly lower desorption rates at 19 % release with NaCl and 21 % with $CaCl_2$, which is attributed to the somewhat higher binding constant. For NDW$^-$75 an additional 21 % with NaCl and 23 % with $CaCl_2$ was released after the 5 % in water. NDW$^-$75 samples in which water desorption was not first completed showed a 27 % PI release when introduced to NaCl and almost a 29 % PI release with $CaCl_2$. In performing the experiments a second time it was seen the amount of PI released for all

samples was comparable to the first salt solution redispersion. The total amount of PI desorbed was 45 % and 49 % in NaCl and $CaCl_2$ for NDG^-80 and 33 % and 41 % in NaCl and $CaCl_2$ for NDG^- after all desorption rounds. For NDW^-75 the total amount of PI released was 37 % and 40 % in NaCl and $CaCl_2$, taking into account the 5 % washed out initially with DI water. NDG^-80 exhibited the highest desorption rate due to the weak binding constant and higher density of surface charges, i.e., surface groups, which are effected by salt additions. Results also show that NaCl and $CaCl_2$ are equally effective on removing PI from NDW^-75, while $CaCl_2$ removed more PI from NDG^- and NDG^-80 samples than NaCl indicating there exists negatively charged functional groups on the ozonated surface that preferentially bind to Ca^{2+}.

5.3.6 Surface Characterization

Samples NDW^-75 and NDG^- have similar average aggregate sizes and negative zeta potentials similar in value. However, the NDG^- sample possesses higher sorption capacity, which might originate from the difference in surface groups. It has previously been observed that NDG^- is the most acidic of all currently known ND due to its larger concentration of oxygen containing groups originating from treatment in ozone [43, 44]. In the present work, mass spectroscopy techniques which both included TOF-SIMS and TDMS were used to reveal details of the surface groups on the ND samples.

The main differences between NDG^- and NDW^-75 are the shape and intensities of TDMS profiles of H_2O, CO CO_2 and C_xH_y (spectra for CO and CO_2 are shown in Figure 5.6).

The measured profiles allowed the estimation of the amounts of desorbed species calculated as the area under the curve. The total amount of $CO+CO_2$ was highest for NDG^- indicating surface oxidation was highest for this sample. The complex shape of CO_2 and CO release curves indicates the presence of several types of C-O bonds on the ND surface giving rise to CO and CO_2 evolution under heating at different temperatures. According to the published data on the thermal decomposition of oxygen containing species on the surface of diamond and carbon materials one can suggest the next simplified explanation of observed release pattern: Region 1 (below 400^{o}C, CO_2 only) – carboxyl groups; region 2 (500-600^{o}C, CO_2+CO) – carboxylic anhydride; region 3 (600-700^{o}C) – lactone (CO_2 release) and hydroxylic groups (CO release); region 4 (above 700^{o}C, CO only) – ether and/or carbonyl groups. It was concluded that majority groups on NDG^- are carboxylic acid anhydride species [43], while carboxylic groups prevail on the surface of NDW^-75 sample. TOF-SIMS revealed presence of Na^+ peak in sample NDW^-75 (Supplementary Data Figure 1). The presence of Na originates from the treatment procedures on the ND, which used NaCl with a purpose of increased colloidal stability at the vendor site [22, 23]. The presence of positively charged Na ions on the ND surface can be one of the reasons of the lower adsorption capacity of this sample, since these sites became unavailable for PI adsorption.

TOF-SIMS and TDMS were also performed for ND^+180 ND with positive zeta potential (see Supplementary Data for results on TOF-SIMS). ND^+180 has a much lower level of surface oxidation as compared to NDW^-75 and NDG^- (Figure 5.6) It's concentration of carboxyl groups is very low, with the main oxygenated surface species belonging to

carbonyl groups. Additionally, $ND^{+}180$ showed to have a large presence of hydrocarbon residues (Figure 5.2, Supplementary Data) probably due to ion exchange treatment, which is a part of the procedure at a vendor site. Their presence may also inhibit high adsorption capacities in cases where electrostatic charges are not the dominant mechanism of adsorption.

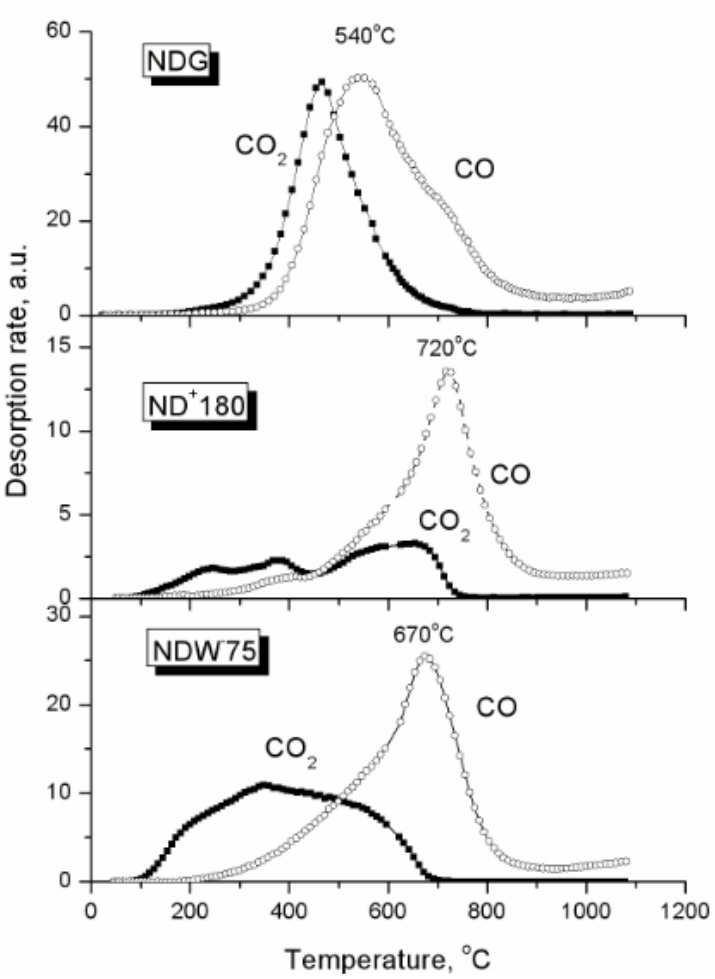

Figure 5.6. TDMS profiles CO and CO_2 desorbed from NDG-, $ND^{+}180$ and $NDW^{-}75$.

5.4 Conclusion

Extensive studies on PI adsorption onto various ND substrates indicate that NDs with a negative ZP adsorb PI, while the type of surface functionalization greatly determines the degree and capacity of the PI adsorbed. By reducing surface area through size fractionation PI adsorption capacity on the ND can be further increased. Small-sized ozone-purified ND was shown to have the highest capacity for PI adsorption, although the binding strengths of all NDs studied were low. The Langmuir curves indicate a decrease of PI adsorption at increased PI concentrations that is likely caused by micelle formation of PI and subsequent desorption from the NDs. It was also revealed that SWNHs and OLC adsorb PI regardless of their positive ZPs due possibly to the nanohorns' internal cavities and π bonding between the aromatic rings of PI and the graphitic surface of the OLCs. Activated charcoal, which also adsorbs PI, is shown to do so at a much lower rate and much higher concentrations than that needed for certain ND samples. Calculations of SSAs covered by the adsorbate gave the same trends as BET measurements but at a reduced overall capacity. This discrepancy in capacity may be due to preferential binding sites for PI compared to the nitrogen used in the BET measurements, as well as uncertainties in the effective size of the PI used in calculating the SSAs. Preliminary studies indicate that the adsorption of PI can be reversed under the influence of salt solutions. Lastly, surface characterization methods using TOF-SIMS and TDMS indicate a large presence of all oxygen containing groups, especially carboxyls (ND oxidized using atomic oxygen) and anhydrides (ND oxidized using ozone), on the negatively

charged NDs. The case of positively charged NDs is more complex showing an abundance of carbonyls and hydrocarbons.

Acknowledgements

This research is supported by the Materials World Network program of the National Science Foundation under Grant No DMR-0602906. O.S. acknowledges the partial support through Air Force Office of Scientific Research under grant N66001-04-1-8933. In addition, we thank V. Kuznetsov, of the Boreskov Institute of Catalysis, Novosibirsk for providing onion-like carbon samples, V. Vorobyev for providing NDW^- samples, Yury Gogotsi, Department of Materials Science and Engineering and Nanomaterials Group at Drexel University, for the BET analysis, Elaine Chuanzhen Zhou at the Analytical Instrumentation Facility for TOF-SIMS experiments and Zachary Fitzgerald, Department of Materials Science and Engineering at North Carolina State University for his modeling of the PI molecule. Any opinions, findings, and conclusions or recommendations expressed in this material are those of the authors and do not necessarily reflect the views of the National Science Foundation.

References

1. Schrand, A.M., et al., *Cytotoxicity and genotoxicity of carbon nanomaterials*, in *Safety of nanoparticles: from manufacturing to clinical applications*, T. Webster, Editor. 2008, Springer: Providence, RI.

2. Schrand, A.M., et al., *Differential biocompatibility of carbon nanotubes and nanodiamonds.* Diamond and Related Materials, 2007. **16**(2): p. 2118-2123.

3. Shenderova, O.A. and S.A.C. Hens, *Detonation nanodiamond particles processing, modification and bioapplications*, in *Nanodiamonds: Applications in Biology and Nanoscale Medicine*, D. Ho, Editor. 2010, Springer. p. 79-116.

4. Vaijayanthimala, V. Y.K. Tzeng, H.C. Chang and C.L. Li, *The biocompatibility of fluorescent nanodiamonds and their mechanism of cellular uptake.* Nanotechnology, 2009. **20**(42): p. 425103.

5. Puzyr, A.P., et al., *Results of studies of possible applications of detonation nanodiamonds as enterosorbents.* Siberian Med. Obozrenie (Siberical Medical Review), 2004. **25**(2-3).

6. Xing, Y. and L. Dai, *Nanodiamonds for nanomedicine.* Nanomedicine, 2009. **4**(2): p. 207-218.

7. Zhu, Y., W. Li, Q. Li, Y. Li, Y. Li, X. Zhang and Q. Huang, *Effects of serum proteins on intracellular uptake and cytotoxicity of carbon nanoparticles.* Carbon, 2009 **47**(5): p. 1351-1358.

8. Puzyr, A.P., V.S. Bondar, Z.Y. Selimkhanova, A.G. Tyan, E.V. Inzhevatkin, E.V. Bortnikov, *Results of in vitro and in vivo studies using detonation nanodiamonds/complex systems under extreme conditions.* Bull. Siberian Medi. (in Russian), 2005. **4**: p. 185.

9. Puzyr, A.P., A.V. Baron, K.V. Purtov, E.V. Bortnikov, N.N. Skobelev, O.A. Mogilnaya, V.S. Bondar, *Nanodiamonds with novel properties: a biological study.* Diamond and Related Materials, 2007. **16**(12): p. 2124-2128.

10. Schrand, A.M., H.J. Huang, C. Carlson, J. Schlager, E. Osawa, S. Hussain, L. Dai, *Are diamond nanoparticles cytotoxic?* Journal of Physical Chemistry, 2007. **111**(1): p. 2-7.

11. Liu, K.K., et al., *Biocompatible and detectable carboxylated nanodiamond on human cell.* Nanotechnology, 2007. **18**(32): p. 325102.

12. Yu, S.J., et al., *Bright fluorescent nanodiamonds: no photobleaching and low cytotoxicity.* Journal of The Amerian Chemical Society, 2005. **127**(50): p. 17604-17605.

13. Chao, J.I., et al., *Nanometer-sized diamond particle as a probe for biolabeling.* Biophysical Journal, 2007. **93**(6): p. 2199-2208.

14. Bakowicz, K. and S. Mitura, *Biocompatibility of NCD*. Journal of Wide Bandgap Materials, 2002. **9**(4): p. 261-272.

15. Grichko, V., V. Grishko, and O. Shenderova, *Nanodiamond bullets and their biological targets.* NanoBioTechnology, 2006. **2**(1-2): p. 1551-1294.

16. Kossovsky, N., A. Gelman, H.J. Hnatyszyn, A. Rajguru, R.L. Garrell, S. Torbati, S.S.F. Freitas and M.G. Chow, *Surface-modified diamond nanoparticles as antigen delivery vehicles.* Bioconjugugate Chemistry, 1995. **6**(5): p. 507-511.

17. Chen, M., E.D. Pierstorff, R. Lam, S.Y. Li, H. Huang, E. Osawa, D. Ho, *Nanodiamond-Mediated Delivery of Water-Insoluble Therapeutics.* ACS Nano, 2009. **3**(7): p. 2016-2022.

18. Huang, T.S., et al., *Immobilization of antibodies and bacterial binding on nanodiamond and carbon nanotubes for biosensor applications.* Diamond and Related Materials, 2004. **13**(4-8): p. 1098-1102.

19. Raina, S., W.P. Kang, J.L. Davidson, *Nanodiamond macro- and microelectrode array bio-sensor.* 2009 IEEE Sensors Conference, 2010. p. 1780-1783.

20. Chung, P.H., E. Perevedentseva, J.S. Tu, C.C. Chang, and C.L. Cheng, *Spectroscopic study of bio-functionalized nanodiamonds.* Diamond and Related Materials, 2005. **15**(4-8): p. 622-625.

21. Gibson, N., O. Shenderova, A. Puzyr, K. Purtov, V.Grichko, T.J.M. Luo, Z. Fitzgerald, V. Bondar, D. Brenner, *Nanodiamonds for detoxification.* NSTI Nanotechnology Conference and Trade Show - NSTI Nanotech 2007, Technical Proceedings**,** 2007. **2**: p. 713-716.

22. Puzyr, A.P., K.V. Purtov, O.A. Shenderova, M.Luo, D.W. Brenner, V.S. Bondar, *The adsorption of aflatoxin B1 by detonation-synthesis nanodiamonds.* Doklady Biochemistry and Biophysics, 2007. **417**(1): p. 299-301.

23. Gibson, N., O. Shenderova, T.J.M. Luo, S. Moseenkov, V. Bondar, A. Puzyr, K. Purtov, Z. Fitzgerald, D.W. Brenner, *Colloidal stability of modified nanodiamond particles.* Diamond and Related Materials, 2009. **18**(4): p. 620-262.

24. Puzyr, A.P., I.O. Pozdniakova, and V.S. Bondar, *Design of a luminescent biochip with nanodiamonds and bacterial luciferase.* Physics of the Solid State, 2004. **46**(4): p.761-763.

25. Huang, L.C.L. and H.C. Chang, *Adsorption and immobilization of cytochrome c on nanodiamonds.* Langmuir, 2004. **20**(14): p. 5870-5884.

26. Yeap, W.S., Tan, Y.Y., and Loh, K.P. *Using Detonation Nanodiamond for the Specific Capture of Glycoproteins.* Analytical Chemistry, 2008. **80**(12): p. 4659-4665.

27. Ushizawa, K., Y. Sato, T. Mitsumory, T. Machinami, T. Ueda and T. Ando, *Covalent immobilization of DNA on diamond and its verification by diffuse reflectance infrared spectroscopy.* Chemistry and Physics Letters, 2002. **351**(1-2): p. 105-108.

28. Yang, W., O. Auciello, J.E. Butler, W. Cai, J.A. Carlisle, J.E. Gerbi, D.M. Gruen, T. Knickerbocker, T.L. Lasserter, J.N. Russell, L.M. Smith, and R.J. Hamers. *DNA-modified nanocrystalline diamond thin-films as stable, biologically active substrates* Nature Materials, 2002. **1**: p. 253–257.

29. Hens, S., G. Cunningham, T. Tyler, S. Moseenkov, V. Kuznetsov, O. Shenderova, *Nanodiamond bioconjugate probes and their collection by electrophoresis.* Diamond and Related Materials, 2008. **17**(11): p. 1858-1866.

30. Krueger, A., *New Carbon Materials: Biological Applications of Functionalized Nanodiamond Materials.* Chemistry: A European Journal, 2007. **14**(5): p. 1382–1390.

31. Schrand, A.M., S.A.C. Hens, O.A. Shenderova, *Nanodiamond Particles: Properties and Perspectives for Bioapplications.* Critical Reviews in Solid State and Materials Sciences, 2009. **34**: p. 18-74.

32. Foglieni, C., C. Meoni, and A.M. Davalli, *Fluorescent dyes for cell viability: an application on prefixed conditions.* Histochemistry and Cell Biology, 2001. **115**(3): p. 223-229.

33. Gitig, D.M. and A. Koff, *Cdk Pathway: cyclin-dependent kinases and cyclin-dependent kinase inhibitors.* Molecular Biotechnology, 2001. **19**(2): p. 179-188.

34. Schmid, I., W.J. Krall, C.H. Uittenbogaart, J. Braun, and V. Giorgi, *Dead cell discrimination with 7-amino-actinomcin D in combination with dual color immunofluorescence in single laser flow cytometry.* Cytometry Part A, 1992. **13**(2): p. 204-208.

35. Puzyr, A.P., V.S. Bondar, *Method of production of nanodiamonds of explosive synthesis with an increased colloidal stability*. 2003: Russia.

36. Menozzi, F.D., A. Michel, H. Pora, and A.O.A. Miller, *Absorption method for rapid decontamination of solutions of ethidium bromide and propidium iodide.* Chromatographia, 1990. **29**(3-4): p. 167-169.

37. Waring, M.J., *Complex formation between ethidium bromide and nucleic acids.* Journal of Molecular Biology, 1965. **13**(1): p. 269-282.

38. MOPAC2009, J.J.P. Stewart, Stewart Computational Chemistry, Version 8.318M web: http://OpenMOPAC.net

39. Humphrey, W., A. Dalke, K. Schulten, *VMD: Visual molecular dynamics.* Journal of Molecular Graphics, 1996. **14**(1): p. 33-38.

40. Chiganova, G.A., *Aggregation of particles in ultradispersed diamond hydrosols*. Colloid Journal, 2000. **62**: p. 238-243.

41. Gibson, N.M., T.J.M. Luo, O. Shenderova, Y.J. Choi, and D.W. Brenner. *Modified Nanodiamonds for Adsorption of Propidium Iodide and Aflatoxin.* MRS Fall 2009 Proceedings, available online. Paper #1236-SS09-05.

42. Giles, C.H., D. Smith, A. Huitson, *A general treatment and classification of the solute adsorption isotherm. I. Theoretical***.** Journal of Colloid and Interface Science, 1974. **47**(3): p. 755-765.

43. Petrov, I., O. Shenderova, V. Grishko, V. Grichko, T. Tyler, G. Cunningham and G. McGuire, *Detonation nanodiamonds simultaneously purified and modified by gas treatment.* Diamond and Related Materials, 2007. **16**(12): p. 2098-2103.

44. Cunningham, G., A.M. Panich, A.I. Shames, I. Petrov and O. Shenderova, *Ozone-modified detonation nanodiamonds.* Diamond and Related Materials, 2008. **17**(4-5): p. 650-654.

Chapter 6

Modified Nanodiamonds for Adsorption of Propidium Iodide and Aflatoxin

Published in Fall 2009 MRS Technical Proceedings (2010)

Modified Nanodiamonds for Adsorption of Propidium Iodide and Aflatoxin

N.M. Gibson [1], T.J.M. Luo [1], O. Shenderova [1, 2], Y.J. Choi [1] and D.W. Brenner [1]

[1] Department of Materials Science and Engineering, North Carolina State University, 911 Partners Way, Raleigh, NC 27695

2 International Technology Center, P.O. Box 13740, Research Triangle Park, NC 27709

Abstract

Nanodiamonds (NDs) have desirable chemical, physical and biological properties that lend them to a wide range of applications. ND's facile surface chemistry, for example, can be used to create a high affinity for adsorbing various biological molecules. However, NDs, which are commercially available from multiple vendors, show inconsistencies with surface groups, aggregate sizes and impurity contents that may limit adsorption. We explore adsorption mechanisms of molecules to NDs in efforts to expand ND applications to drug delivery agents, bio-labels and enterosorbents. In doing so, several types of NDs and modification methods are evaluated to increase adsorption capacity and selectivity of propidium iodide and aflatoxin B1. Capacities and binding strengths of target molecules are assessed by Langmuir isotherms and transform calculations. UV-Vis spectroscopy shows our modification treatments are successful in increasing ND adsorption capacities. Additionally, cyclic voltammetry measurements, used to monitor in-situ adsorption, show electrochemical detection even after binding

6.1 Introduction

Detonation nanodiamonds (NDs) represent an emerging class of diamond material. The interest in NDs stems from their large specific surface areas (300-400 m^2/g) and rich surface chemistry, which can be easily manipulated for specific applications. NDs have recently been shown to be biocompatible and noncytotoxic [1], opening up their applications to biology and medicine. Previously, NDs have been explored as carriers for active molecules and drug delivery agents [2]. Here, we explore adsorption mechanisms of molecules to the surface of NDs in an effort to develop new applications for NDs in drug delivery, bio-labeling and as enterosorbents.

Propidium iodide (PI) was selected as a charged molecule model. PI is used widely in biology because its positive charge prevents penetration into positively charged cell membranes, so that only staining of dead cells is facilitated [3,4]. Because this dye has been extensively studied, we look to it for observing initial behaviors of positively charged molecules with ND aggregates. PI's fluorescence is easy to detect with UV-Vis spectroscopy, meaning simple and time efficient measurements. Basic knowledge of electrostatic interactions between the molecule and NDs will allow for future development of NDs as drug delivery carriers and bio-labels.

Aflatoxin B1 (AfB1), a carcinogenic and mutagenic product of mold growth found in crops and feedstuff [6], was selected as a neutral charged molecule model. Currently, hydrated sodium calcium aluminosilicate (HSCAS) clays are the most common enterosorbents for AfB1 adsorption [6]. However, these clays show nonspecific adsorption

that can lead to binding of essential nutrients [6] and may saturate the active binding sites for AfB1. Thus, there is a need to engineer an alternative substrate that will specifically bind AfB1. NDs are candidates for such substrates because of their high adsorption capacity, non-toxicity and availability of a wide range of methods to modify its surface [2].

Both experiments use vendor supplied NDs, which show an inhomogeneity of surface groups, large aggregate sizes and the presence of impurities (e.g. non-diamond carbon and incombustible content) that may hinder adsorption. Thus, several modification techniques were explored to augment adsorption selectivity and capacity on several purchased NDs. To evaluate the success of these treatments, Langmuir isotherms and related transform calculations were used to analyze adsorption capacities and binding strengths. In addition, cyclic voltammetry (CV) methods were developed as a direct and in-situ monitoring tool for molecule adsorption.

6.2 Experimental Details

6.2.1 ND Preparation and Modification

Vendor supplied NDs were suspended in water to a 0.1 wt. % solution and then ultrasonicated for 2-4 minutes [7]. Select NDs were also size fractionated by centrifugation (FC) to obtain the zeta potentials (ZPs) and aggregate sizes (Malvern ZetaSizer) listed in Table 1. The positivity charged modified standard ND (ND^{+}Mst, New Technologies, Chelyabinsk, Russia), was further treated with plasma at the International Technology Center [8]. Separate ND^{+}Mst samples were introduced to oxygen atmospheric pressure plasma to

generate ozone reactive species or treated with nitrogen plasma for 5 minutes [9]. Separate ND^{+}Mst samples were silane coated using 50 μL of tetramethylorthosilicate (TMOS) or 100 μL of N,N'-bis[(3trimethoxysilyl) propyl]-ethylenediamine (enTMOS) for every 5 mL of ND (0.7 wt. %).

The negatively charged standard (ND^{-}st) and its modified fraction (ND^{-}Mst) were obtained from Real-Dzerzinsk, LTD, Russia [10]. ND^{-}GP, (Real-Dzerzinsk) was produced by detonation of graphite precursors mixed with RDX and fractionated by centrifugation to several fractions (ND^{-}GP 1, 2 and 3). Ozonated ND (ND^{-}Oz, New Technologies) was created by treating detonation soot with ozone at 200 ˚C. ND^{-}MOz, obtained through centrifugation, represents the smaller fractions of the ND^{-}Oz sample. AfB1 studies further fractionated ND^{+}Mst and ND^{-}Mst suspensions by centrifugation to obtain 40 nm sizes; these are termed ND^{+}Mst40 and ND^{-}Mst40.

6.2.2 Propidium Iodide Studies

Dye concentration from 25 to 700 μg/mL in DI water were mixed with 0.5 wt. % ND solution (7:3 ratio) and incubated for 30 min on a shaker before being centrifuged (25 minutes, 14,000 RPM) [11,12]. Supernatants were analyzed on a UV-Vis spectrophotometer (Lambda 35, Perkin Elmer). The Langmuir isotherm was constructed for ND^{-}MOz and transform calculations determined maximum capacities, Q_{max}, and binding strengths, K_d, of the sorbent.

CV measurements were performed using a Faraday MP potentiostat (Obbligato Objectives Inc.) using a scanning rate of 50 mV/s. The electrochemical cell consisted of a fluorine doped tin oxide (FTO) working electrode, a platinum counter electrode and an Ag/AgCl reference electrode. The FTO electrode was spin coated with 0.5 wt. % ND^-Mst in methanol. A syringe pump continuously dropped the suspension onto the spinning electrode (3,000 RPM) at 200 μL/min. Once dried, PI solution (200 μg/mL) was left to sit on the electrode for five minutes before rinsing thoroughly in DI water and taking measurements in phosphate buffered saline solution. The irreversible electrochemical reaction of PI prevented multiple cycles or long scanning times on the same sample. Thus, adsorption with time was observed on separate samples for time periods ranging from five to 30 minutes in five minute intervals.

6.2.3 Aflatoxin B1 Studies

AfB1 powder (Sigma Aldrich) was dissolved in acetonitrile and then introduced to DI water to form a stock solution of 10 μg/mL. Adsorption experiments were carried out using ND^+Mst40 and ND^-Mst40 of 0.1 and 0.5 wt. %. AfB1 (8 μg/mL) and ND were mixed in a 7:3 ratio and incubated on a shaker at 150 RPM followed by centrifugation at 15,000 RPM for 15 minutes. Incubation times of 5, 15, 30 minutes and 20 hours were used. The influence of salt was studied by adding 162 μL of NaCl or $CaCl_2$ to samples before centrifugation. Salts were prepared in DI water at concentrations of 5, 16 and 33 μg/mL for NaCl and 5 and 10 μg/mL for $CaCl_2$.

ND^{+}Mst and its 40 nm fraction were first surveyed for adsorption using 2 and 10 μg/mL AfB1 concentrations and 30 minute incubation times. Immediately before centrifugation, 162 μL of NaCl (33 μg/mL) was added. AfB1 concentrations of 0.5-10 μg/mL were used to construct isotherms and determine capacities.

6.3 Results & Discussion

6.3.1 ND Modification

Processing and modification methods can significantly influence aggregate sizes and ZPs (Table 1). ZP analysis indicates that positive and negative classes of NDs exist depending on manufacturing treatments. Modification by size reduction (sonication and fractionation), plasma treatments and silane coatings altered the magnitude of this charge but not the polarity. Similar results were found when applying a negatively charged TMOS coating to ND surfaces. TMOS and positively charged enTMOS, in the absence of NDs, carried very small ZPs in water, but a ND coating notably changed the ND's ZPs. Electrostatic binding of TMOS to the ND increased ZPs and prevented any NDs from re-aggregating after sonication. enTMOS coatings reduced aggregate sizes and ZPs. ND^{+}Mst may have localized charges that attract enTMOS to some areas and repel it from positive sections, leading to a non-uniform coating on the ND surface.

Plasma treatments also decrease aggregate sizes and influence ZPs. Nitrogen plasma increased the positivity and stability of ND suspensions. In contrast, introducing oxygen species made the ND's surface more negative, although the accompanied change in the ZP is

trivial. Studies reveal that ZPs are not solely affected by aggregate size, but more directly influenced by treatment type. However, if NDs are treated under the same methods ZPs can be improved by reducing particle size (ND^-Mst and ND^-GP classes). NDs were not reduced down to their primary particle size of 4 to 5 nm in efforts to examine the pores created by aggregates and if these openings play a role in increasing adsorption.

Table 6.1. Size, zeta potentials (ZP) and processing methods of ND aggregates.

ND, 0.1wt. %	**ZP, mV**	**Size, nm**	**Processing**
ND^+st (Ch-st)	17.4 ±0.40	300	CrO_3 in H_2SO_4
ND^+Mst (Ch-F6)	46.8 ±0.90	185	ND^+st with $NaOH+H_2O_2$; ion-exchange resin; FC*
ND^+Mst40	50.1 ±0.90	40	ND^+Mst; FC
ND^+O_2 (Ch-F6-O_2 plasma)	44.6 ±1.18	157	ND^+Mst treated in O_2 plasma
ND^+N_2 (Ch-F6-N_2 plasma)	52.2 ±0.30	157	ND^+Mst treated in N_2 plasma
ND^+TMOS	52.8 ±1.09	132	ND^+Mst coated with TMOS
ND^+enTMOS	38.3 ±0.18	148	ND^+Mst coated with enTMOS
ND^-GP 1	-46.1 ±0.14	176	Graphite precursors; FC
ND^-GP 2	-35.1 ±0.61	232	Graphite precursors; FC
ND^-GP 3	-33.8 ±0.73	370	Graphite precursors; FC
ND^-st (RUDDM)	-44.1 ±0.66	260	Singlet O in NaOH; HNO_3;
ND^-Mst (RUDDM 1)	-49.3 ±1.90	75	ND^-st treated with NaCl; FC
ND^-Mst40	-53.3 ±1.30	40	ND^-Mst; FC
ND^-Oz (OZ-ND)	-48.5 ±0.20	139	Soot oxidized with ozone
ND^-MOz (OZ-Bl)	-51.2 ±0.50	80	ND^-Oz; FC

*FC: Fractionated by centrifugation

6.3.2 Propidium Iodide Studies

NDs explored for PI adsorption showed drastic differences in their capacities as a result of different treatment procedures (Table 2). ND^{+}Mst and its counterparts modified via plasma and silane did not adsorb any PI owing to the electrostatic repulsion between PI and the ND. All NDs with negative ZPs adsorbed PI to varying degrees. ND capacities are based on surface chemistry differences arising from various treatments; however, trends show capacities can be increased via size reduction and increased ZP (ND^{-}st and ND^{-}GP series).

Table 6.2. Adsorption capacities (μg/mg) of PI on NDs (0.5 wt. %).

PI Concentration	ND^{-} st	ND^{-} Mst	ND^{-} Oz	ND^{-} MOz	ND^{-} GP 3	ND^{-} GP 2	ND^{-} GP 1	ND^{+} Mst
1 μg/mL	27.0	31.1	44.5	44.8	7.3	4.3	8.9	0
3 μg/mL	34.3	78.6	84.1	100.6	23.1	28.3	35.5	0

PI adsorption to ND^{-}MOz occurred until all the ND binding sites were filled, which is indicated by a plateau in the isotherm (Figure 1). Interestingly, as the concentration of PI increased desorption occurred due to PI having a greater affinity to itself than the ND. Transform calculations reveal relatively weak binding of PI to ND which may facilitate desorption (Table 3). This may be favorable for bio-labeling and drug delivery where the target molecule must be released from the ND substrate; with PI this can be triggered by introducing NaCl or $CaCl_2$ [11]. Estimates also reveal ND^{-}MOz's high loading capacities for PI making it an optimal substrate for PI adsorption. Comparisons with other NDs suggest that

the greater density of oxygen containing groups on the surface of ND-MOz make it more preferential for binding PI.

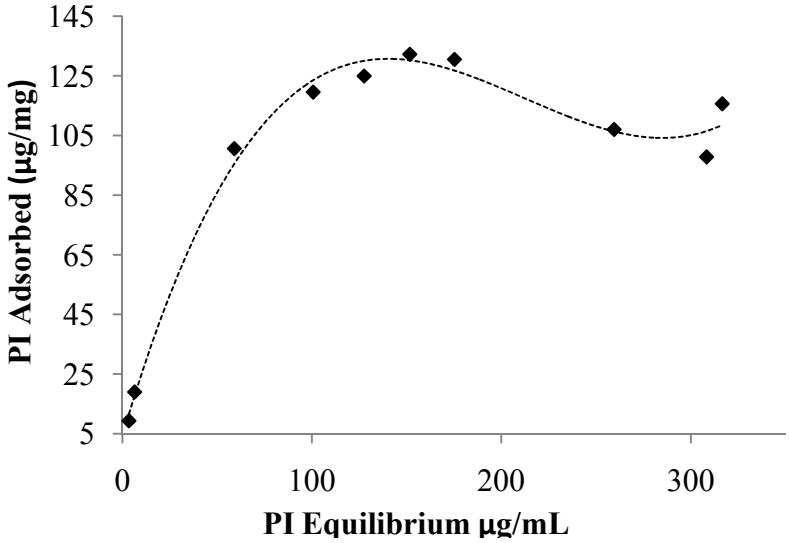

Figure 6.1. Langmuir Isotherm for PI on ND-MOz.

Table 6.3. Transform calculations used to calculate maximum capacity, Q_{max}, and binding strengths, K_d, on ND-MOz.

Transforms	Q_{max} (µg/mg)	K_d (mg/µg)	r^2
Eadie-Hofstee	189.91	0.01632	0.9611
Lineweaver-Burk	232.56	0.01235	0.9956
Reciprocal Line	185.19	0.01716	0.9921
Scratchard	194.05	0.01570	0.9611
Average	***200.43***	***0.01538***	***0.9775***

Detection methods discussed above measured unbound dye left in the supernatant. Thus, CV measurements were developed to directly observe dye adsorption via changes in current density before and after PI adsorption. Because measurements show ND-Mst is

electrochemically inert its signal can be neglected in the combined PI-ND$^-$Mst system. As more PI was adsorbed onto the ND an increasing oxidation current was apparent (Figure 6.2). This current increase was observed within five minutes of adsorption and the point of saturation (~25 minutes). These intense signals remained after thoroughly washing in DI water, which signifies strong binding between PI and ND$^-$Mst. CV measurements also showed that adsorbed dye remained electrochemically detectable; thus, the properties of PI are unaltered by physical binding.

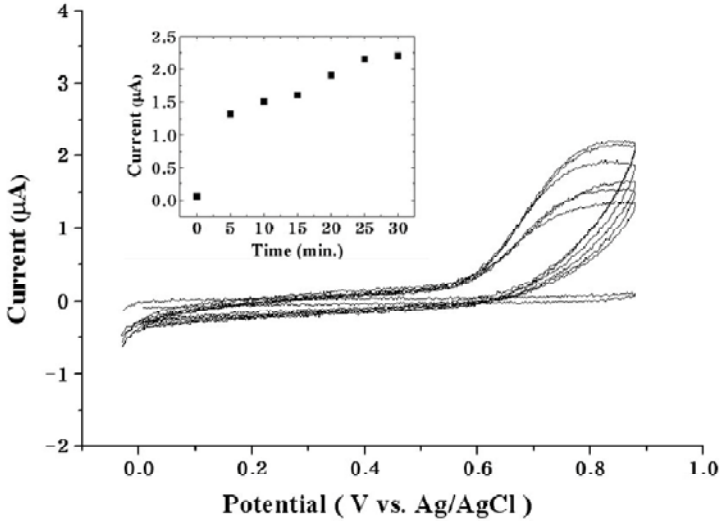

Figure 6.2. CV experiments show adsorption of PI on ND$^-$Mst from 5 to 30 min reaction times.

6.3.3 Aflatoxin B1 Studies

Although ND$^+$Mst40 showed only ~38 % adsorption of AfB1, adsorption begins immediately after introduction of the two materials (Figure 3). ND's maximum adsorption capability is reached within 5 minutes of incubation, whereas HSCAS clays require long

incubation times of several hours to bind AfB1 [13]. Introducing salt solutions to NDs does not significantly influence AfB1 adsorption independent of whether the solution is NaCl or $CaCl_2$ (Figure 4). Both salts were successful in sedimenting small ND particles to aid in pellet formation during centrifugation. Without salt, pellet formation of small ND particles is nearly impossible, which complicates UV-Vis spectrums as background NDs remain in the supernatant.

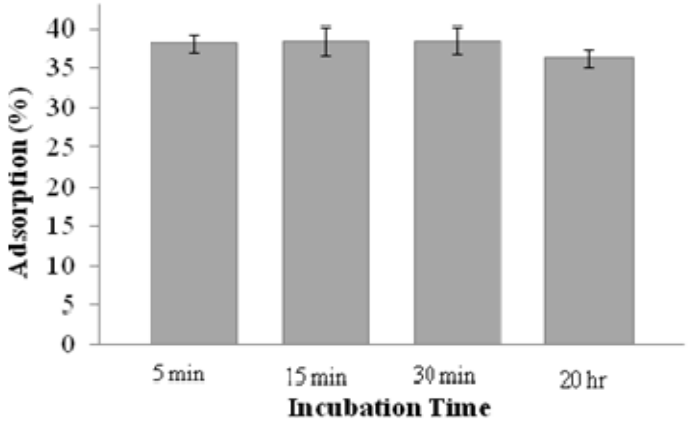

Figure 6.3. AfB1 adsorption on ND^{+}Mst40 showing the influence of incubation time.

Aggregate sizes influence adsorption. For example, by decreasing particle size from the original ND^{+}Mst (at ~185 nm) to 40 nm there is a 14 % increase in aflatoxin adsorbed. Therefore, the 40 nm NDs were used to construct the Langmuir isotherm (Figure 5). Transform calculations revealed that AfB1 capacity on both ND^{-}Mst40 and ND^{+}Mst40 are quite low (Table 4). However, the size reduction and ZP increase of ND^{-}Mst40 showed improvement over previously reported ND^{-}Mst that had a Q_{max} of 0.2536 μg/mg and binding constant of 0.2249 mg/μg [10]. ND^{+}Mst40 adsorbed even greater amounts of AfB1 and had

stronger binding. AfB1's slight negative charge may aid in minor electrostatic adsorption mechanisms.

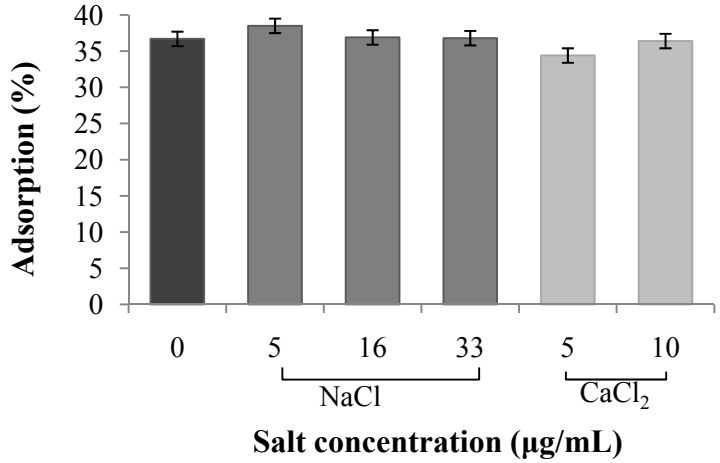

Figure 6.4. AfB1 adsorption on ND^{+}Mst40 showing salt influences.

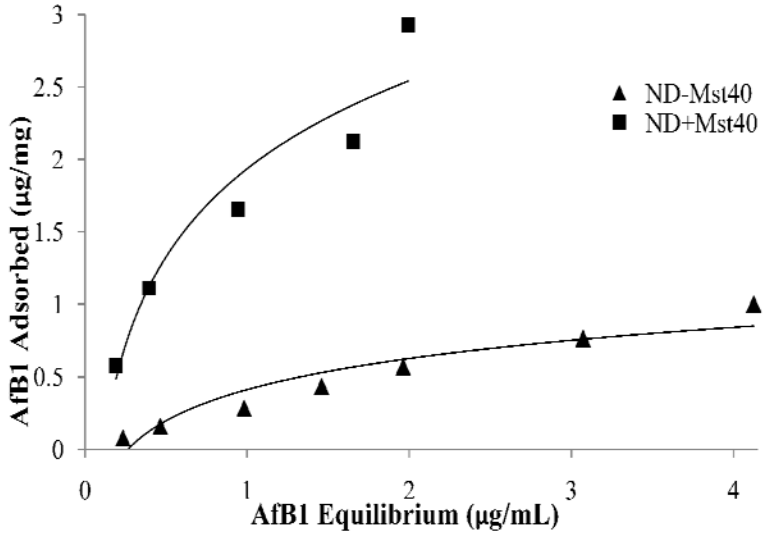

Figure 6.5. Langmuir isotherm for AfB1 on ND^{+}Mst40 and ND^{-}Mst40.

Table 6.4. Transform calculations used to calculate maximum capacity, Q_{max}, and binding strengths, K_d, on ND^-Mst and ND^+Mst40.

	ND^-Mst40		ND^+Mst40	
Transforms	Q_{max} (μg/mg)	K_d (mg/μg)	Q_{max} (μg/mg)	K_d (mg/μg)
Eadie-Hofstee	2.435	0.1470	4.288	0.8361
Lineweaver-Burk	2.895	0.1203	4.308	0.8207
Reciprocal Line	2.807	0.1243	4.960	0.6597
Scratchard	2.851	0.1222	3.392	0.7050
Average	***2.747***	***0.1285***	***4.237***	***0.7554***

6.4 Conclusions

Adsorption to NDs is strongly dependent on the type of ND substrate. PI adsorbed exclusively to negatively charged NDs, but, in addition, ND^-MOz's oxygen-rich surface makes it optimal for high loading capacities. Bound PI was shown to remain electrochemically unaltered. NDs were also shown to bind AfB1 within 5 minutes after introduction, consistent with observations in [10], and the addition of salt does not hinder adsorption. Electrostatic attraction plays a minor role in AfB1 adsorption and size reduction can be used to increase AfB1 adsorption capacities on the ND, but the optimum ND surface chemistry still must be identified for greater adsorption.

Acknowledgements

The authors would like to recognize the National Science Foundation's Materials World Network (Grant No. DMR-0602906) for its financial support and M. Ray for plasma treatments.

References

1. Schrand, A.M., H.J., Huang, C. Carlson, J. Schlager, E. Osawa, S. Hussain. L. Dai, *Are diamond nanoparticles cytotoxic?* Journal of Physical Chemistry , 2007. **111**(1): p. 2-7.

2. Schrand, A.M., S.A. Ciftan Hens, O.A. Shenderova, *Nanodiamond Particles: Properties and Perspectives for Bioapplications.* Critical Reviews in Solid State and Materials Sciences, 2009. **34**: p. 18-74.

3. Foglieni, C., C. Meoni, and A.M. Davalli, *Fluorescent dyes for cell viability: an application on prefixed conditions.* Histochemistry and Cell Biology, 2001. **115**(3): p. 223-229.

4. Schmid, I. W.J. Krall, C.H. Uittenbogaart, J. Braun, V. Giorgi, *Dead cell discrimination with 7-amino-actinomcin D in combination with dual color immunofluorescence in single laser flow cytometry.* Cytometry Part A, 1992. **13**(2): p. 204-208.

5. Yu, S.J., M.W. Kang, H.C. Chang, K.M. Chen, Y.C. Yu, *Bright fluorescent nanodiamonds: No photobleaching and low cytotoxicity***.** Journal of the American Chemical Society, 2005. **127**(50): p. 17604-17605.

6. Phillips, T.D., S.L. Lemke, and P.G. Grant, *Characterization of clay-based enterosorbents for the prevention of aflatoxicosis.* . Advances in Experimental Medicine and Biology, 2002. **504**: p. 157-71.

7. Gibson, N., O. Shenderova, T.J.M. Luo, S. Moseenkov, V. Bondar, A. Puzyr, K. Purtov, Z. Fitzgerald, D.W. Brenner, *Colloidal stability of modified nanodiamond particles.* Diamond and Related Materials, 2009. **18**(4): p. 620-262.

8. Ray, M.A., O. Shenderova, W. Hook, *Cold plasma functionalization of nanodiamond particles.* Diamond and Related Materials, 2006. **15**(11-12): p. 1809-1912.

9. Gibson, N., O. Shenderova, A. Puzyr, K. Purtov, V.Grichko, T.J.M. Luo, Z. Fitzgerald, V. Bondar, D. Brenner, *Nanodiamonds for detoxification.* NSTI Nanotechnology Conference and Trade Show - NSTI Nanotech 2007, Technical Proceedings**,** 2007. **2**: p. 713-716.

10. Puzyr, A.P., K.V. Purtov, O.A. Shenderova, M.Luo, D.W. Brenner, V.S. Bondar, *The adsorption of aflatoxin B1 by detonation-synthesis nanodiamonds***.** Doklady Biochemistry and Biophysics, 2007. **417**(1): p. 299-301.

11. Gibson, N.M., T.J.M Mark Luo, O. Shenderova, Z. Fitzgerald, D.W. Brenner. *Propidium Iodide Adsorption and Binding by Nanodiamond and Nanocarbon Particles*. Chapter 5.

12. Gibson, N.M., T.J.M. Luo, O. Shenderova, Y.J. Choi, Z. Fitzgerald, D.W. Brenner, *Fluorescent dye adsorption on nanocarbon substrates through electrostatic interactions.* Diamond and Related Materials, 2009. **19**(2-3): p. 234-237.

Chapter 7

Aflatoxin B1 and Ochratoxin A Adsorption by Modified Nanodiamonds

Aflatoxin B1 and Ochratoxin A Adsorption by Modified Nanodiamonds

N.M. Gibson[1], T.J.M. Luo[1] O. Shenderova[1, 2], and D.W. Brenner[1]

[1]Department of Materials Science and Engineering, North Carolina State University, 911 Partners Way, Raleigh, NC 27695

[2]International Technology Center, P.O. Box 13740, Research Triangle Park, NC 27709

Abstract

The effectiveness of several modified nanodiamonds (NDs) for the adsorption of mycotoxins, aflatoxin B1 (AfB1) and ochratoxin A (OTA), are investigated in this paper as potential enterosorbents. NDs, which are biocompatible and nontoxic, hold advantages over other mycotoxins enterosorbents due to their high dispersivity over a wide range of pH, important for interacting in the gastrointestinal tract. A thorough study of binding and release mechanisms was completed using an assortment of NDs modified by size reduction techniques and surface treatments, including carboxylation, hydrogenation and hydroxylation. Results indicate that AfB1 adsorption on NDs is directly related to aggregate size, whereas OTA adsorption is primarily based upon electrostatic interactions followed by surface functional groups. Complexities in the Langmuir isotherm and related transform equations were also identified based on preparation procedures, including sorbent concentrations and mycotoxins-ND ratios. Findings show that our modified NDs perform better than yeast cells walls and other NDs but comparable to activated charcoal in AfB1 studies, and outperform clay minerals in OTA studies. Furthermore, adsorption capacities can be preserved in a wide range of pH.

7.1 Introduction

Each year approximately 25 % of the world's cereals are contaminated by mycotoxins, secondary metabolites produced by fungi [1, 2]. These toxins enter the food chain through direct ingestion of contaminated crops or consumption of tainted animal products, including meat and milk [2, 3, 4, 5]. Ingestion of mycotoxins has been linked to toxicosis, cancer [6, 7], and even, death [8]. Two well-known and detrimental mycotoxins are aflatoxin B1 (AfB1) and ochratoxin A (OTA).

AfB1 has been identified as one the most carcinogenic naturally occurring compounds [9] and is typically found in warm (30 to 35 degrees C), humid settings (water activity of 0.90 to 0.99). AfB1 is a known to contaminate of many crops; those which are frequently infected by the producing fungi include cereals, tree nuts, oilseeds and spices [10, 11]. Once ingested, enzymes breakdown AfB1 into epoxilated derivatives that form adducts with DNA [12-14], leading to heritable changes that lead to malignant cell formation, especially in hepatic cells [15]. Because of this, AfB1 is classified as a group 1 carcinogen.

OTA, while less potent than AfB1, receives much attention due to the ability of the producing fungi to proliferate in low temperatures (0 to 31 degrees C, 20 degrees C is optimum) and humidities, and in a wide range of pH (pH 2 to pH 10, pH 6 to 7 is optimum) [16]. Consequently, OTA is found in crops world-wide, but more common in Northern Africa, North America and Europe [17, 18]. In fact, studies conducted in the early and mid-1990's show OTA has been found to be widespread in Europeans' blood and breast milk [19, 20], with exposure primarily gained though ingestion of grains (58 % of the intake), wine (21

%), grape juice (7 %), coffee (5 %), and pork (3 %) [21]. Unlike Af, OTA accumulates in tissue and has been associated with mutagenic, nephrotoxic, nephrocarcinogenic, teratogenic [22], immunosuppressive properties that may lead to the development of certain disease, such as Balkan Endemic Nephropathy (BEN), the development of urinary tract tumors, and possibly connected with testicular cancers [23].

While these mycotoxins have long been identified there has been no economical, easy and practical resolution for removing these toxins from contaminated crops and feedstuff. Methods to remove or decompose mycotoxins in crops have included physical, chemical, and biological means; however, the procedures vary in their effectiveness [24,25] and may discolor and/or decay nutritional contents of the foodstuff [26, 27]. The most recent treatment is the use of non-nutritive binding agents, termed enterosorbents, which adsorb and remove the mycotoxins within the gastrointestinal (GI) tract before absorption into the body. For the enterosorbents to be effective it must meet several requirements, including:

1) having high adsorption affinity for AfB1, as to form a strong bond with the molecule and prevent desorption in latter parts of the GI tract;
2) having a high capacity for AfB1 to prevent saturation of the substrate and/or allowing less of the substrate to be administered;
3) being harmless or nontoxic to the body;
4) selectively binding the aflatoxin molecule, as to not adsorb essential vitamins and minerals [3, 28].

Several enterosorbents have been considered for mycotoxins adsorption. However, due to their inability to bind a wide variety of toxins [2, 4] or concerns in vitamin and mineral uptake [2, 3], alternative enterosorbent materials are being explored. Nanodiamonds (NDs), produced through detonation synthesis, have an advantage over other materials due to their high dispersivity, which allows for easy administration and quantifiable dosing through water substitutions. In addition, their colloidal stability and sorption capacities are preserved over a wide pH range, important for interacting in the GI tract [29, 30]. Furthermore, NDs have been shown to be biocompatible and nontoxic in a variety of *in vitro* and *in vivo* studies [31, 32, 33]. Lastly, because NDs can be tailored with different functional groups during manufacturing and modification treatments, NDs may be able to selectively adsorb AfB1 and OTA while excluding critical nutrients. This paper reports results from assessing AfB1 and OTA adsorption on NDs modified under variety of treatments, including surface termination by hydrogen, carboxyls and hydroxyl groups, as well as determining possible mechanisms of interaction.

7.2 Experimental Details

7.2.1 Nanodiamonds

NDs used in this work were synthesized by the detonation of a mixture of trinitrotoluene (TNT) and 1,3,5-trinitro-1,3,5-*s*-triazine (RDX), followed by treatment in liquid or gas-phase oxidizers, at the manufacturers site, to reduce non-diamond content.

The list of NDs used in our experiments is summarized in Table 7.1. Complete details of manufacturing and hydrosol preparations for Ch-st, I6, RUDDM, RDDM and ozonated NDs (OZ-ND) have previously been reported [29, 30, 34, 35], here only brief processing methods will be discussed.

Ch-st ND (New Technologies, Chelyabinsk, Russia) was purified using a solution of chromic anhydride in sulfuric acid. I6-140 samples were produced from Ch-st through ion-exchange, annealing in air and fractionating. RUDDM1 (Real-Dzerzinsk, LTD, Russia), was produced by purifying detonation soot singlet atomic oxygen in the base environment, followed by treatment in nitric acid, NaCl and fractionation. Centrifugation by fractionation also obtained I6-220 and I6-40, where the number corresponds to the aggregate size. RUDDM1, which has been used previously for adsorption experiments, was also fractionated to a 40 nm particle size. RDDM (Real-Dzerzinsk) was produced by detonation of graphite precursors mixed with RDX and fractionated by centrifugation. Ozonated ND (OZ-ND, New Technologies) was created by treating detonation soot with ozone at 200 ˚C. OZ-Bl, obtained through centrifugation, represents the smaller fractions of the OZ-ND sample. Porous NDs, selected to determine the influence of pores on toxin adsorption, were produced by Alit, Ukraine. Finally, surface termination was conducted on I6-140, to form I6-H, I6-OH and I6-COOH. Hydroxylated ND (I6-OH) manufacturing methods were previously been published [36], showing use of nitrogen atmosphere at room temperature over night followed by drop-wise addition of HCl, centrifugation and drying. ND-COOH was produced by air treatment at 430 ˚C for 1 hrs, followed with treatment in HCl for 1 hrs and washing. ND-H was created

through treatment in H_2 flow for 3 days at 450 C. Surface groups were previously confirmed using FTIR and XPS techniques [36].

It is most important to note that these NDs, all produced under different manufacturing procedures, acquire different zeta potentials (ZPs) and vary in their aggregate sizes. ZP and size measurements were completed with colloid concentrations of 0.1 wt. % in deionized (DI) water [29] on the Malvern Zetasizer.

Table 7.1. NDs used in adsorption experiments with related diameter size measurements (nm) and zeta potentials (ZP, mV).

ND Type	Size, nm	ZP, mV
Ch-st	298.8	19.0
I6-220	219.1	44.6
I6-140	140.2	47.7
I6-40	40.0	50.1
I6-H	128.3	68.1
I6-OH	128.1	52.6
I6-COOH	145.5	-59.4
Porous	177.4	-38.1
RDDM	175.9	-46.1
OZ-ND	175.0	-44.6
OZ-Bl	80.8	-51.2
RUDDM1	79.8	-49.2
RUDDM-40	40.1	-53.3

7.2.2 Aflatoxin B1 Studies

AfB1 (purchased from Sigma Aldrich) was prepared for adsorption studies by first dissolving AfB1 in acetonitrile, followed by deionized (DI) water substitution. The final concentration of the stock solution was 10 μg/mL. NDs (0.1 or 0.5 wt. %) were combined

with AfB1 at a 3:7 ratio and incubated on an orbital shaker. Though adsorption was observed to occur within 5 minutes or less, as confirmed by [30] and [35], 15 minute incubation times were selected with current experiments. Longer incubations times do not lead to increased adsorption. Before centrifugation (14,000 rpm, 25 min) 0.162 μL of NaCl solution (0.3 g/mL) was added to the ND-AfB1 suspension to help sediment the NDs. This was imperative for 40 nm NDs due to their exceptional colloidal stability. It was previously established that the introduction of the NaCl solutions does not interfere with adsorption of AfB1 [35], this is also true for the salt concentrations used in this paper. Following centrifugation, the amount of unbound AfB1 was detected through UV-Vis spectroscopy. By varying the concentration of the AfB1 solution, from 0.5 to 10 μg/mL, Langmuir isotherms were constructed. Separate linear regression transform calculations (i.e., Eadie-Hofstee, Lineweaver-Burk, Reciprocal Line, and Scratchard) were employed to give rise to additional information such as the maximum capacity (Q_{max}) of the sorbent and its binding constants (K_d).

Additional research was completed by varying the ratios of ND (0.5 wt. %) to AfB1 (10 μg/mL). These studies compared the original 3:7 ratio to 1:1 and 3:1 ratios; all other preparation methods remained unchanged. Experiments also observed influences of pH on adsorption. ND suspensions were made to pH 2 and pH 11.5 through the addition of HCl or NaOH, after which, AfB1 was added and experiments proceeded as normal. Final experiments observed toxin desorption by redispersing AfB1 bound ND pellets in 1 mL of DI water with 15 seconds of sonication, before centrifugation and UV-Vis detection.

Redispersion procedures were repeated two more times for each sample in 1 mL of 5 mg/mL NaCl solution or 5 mg/mL $CaCl_2$ solution to observe the role of ionic influences.

7.2.3 Ochratoxin A Studies

OTA (Sigma Aldrich) was dissolved in methanol followed by dilution in DI water to obtain a final concentration of 10 μg/mL. NDs suspensions (0.1 wt. %) were combined with OTA at a 3:7 (ND:OTA) ratio followed by 15 minute incubation times. NaCl additions to sediment NDs were excluded, as salt in the presence of OTA alone resulted in a secondary peak at 383 nm and a slight reduction in the primary peak at 363 nm (Figure 7.1a). However, when NDs were added to the OTA and salt system, further reduction in the primary peak was seen, indicating adsorption is still occurring (Figure 7.1b). Due to the omission of salt, only larger ND aggregates, which were capable of forming a pellet during centrifugation, could be used. Langmuir isotherms were created varying the concentration of OTA from 2 to 10 μg/mL. Maximum capacities and binding constants were found using the linear regression transforms listed above. pH experiments were also conducted to observe their resulting influence on OTA adsorption. Similar to AfB1 studies, ND suspensions were prepared to pH 2 and pH 10 before introducing OTA. All other steps remained unchanged. OTA desorption experiments were conducted using water and NaCl or $CaCl_2$ solutions (3 redispersion cycles for each sample) in a manner identical to AfB1 studies.

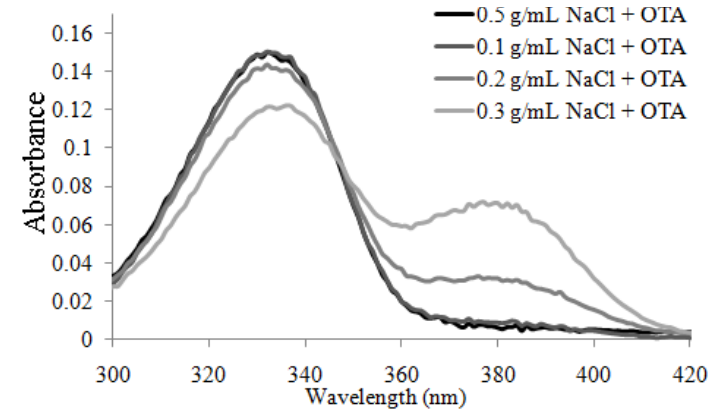

(a)

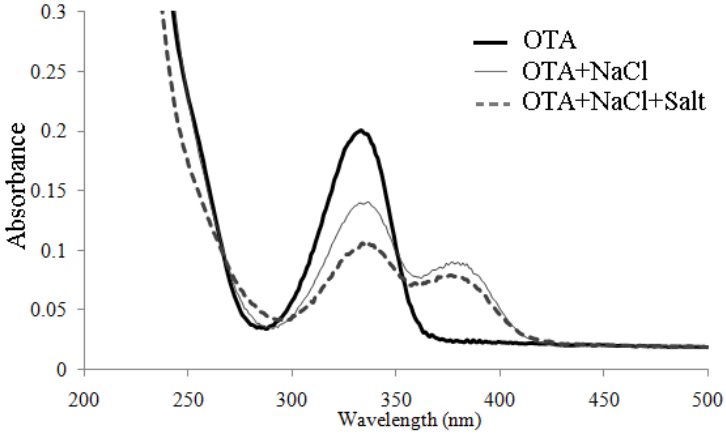

(b)

Figure 7.1. Salt additions to OTA solutions reduce primary peak and create secondary peak (a) salt addition to OTA in the presence of NDs, with all other factors remaining the same, still show adsorption of the toxin (b).

7.3 Results and Discussion

7.3.1 Aflatoxin B1 Studies

The initial evaluation of AfB1 adsorption by various ND substrates can be seen in Figure 7.2. Results indicate that manufacturing and modification treatments drastically influence ND's ability to adsorb AfB1. The largest adsorption influence is attributed to the aggregate sizes of the ND. As seen, smaller aggregate sizes have increased adsorption

capacities due to their larger specific surface areas (SSAs) and increased number of binding sites. This is seen particularly well with I6-140 and I6-40 NDs, where the surface chemistries are identical but size reduction doubles the amount of AfB1 adsorbed. This trend is also identified in the RUDDM series.

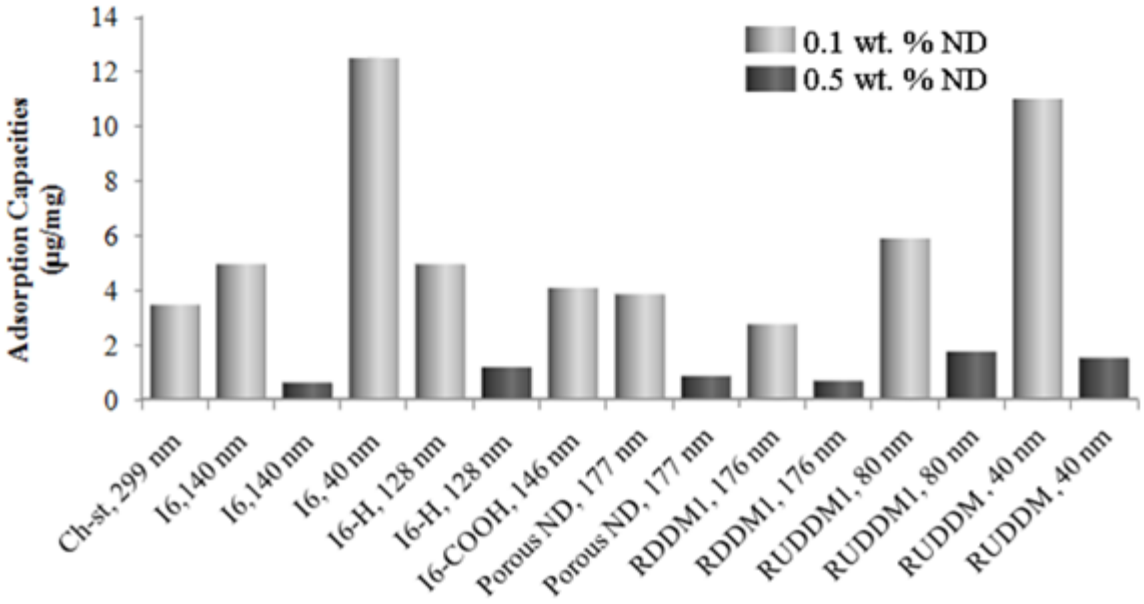

Figure 7.2. Results of AfB1 adsorption on various ND substrates showing different adsorption capacitates based on treatments and aggregate sizes (nm).

The role of electrostatics is seen to be inconsequential for the adsorption of AfB1, as both NDs that hold positive and negative ZPs bind the molecule. Though AfB1 is considered to be a rather neutral molecule, its dicarbonyl system (Figure 7.3) forms a partial positive charge that has been shown to be attracted to hydrated sodium aluminosilicate (HSCAS) enterosorbents [37]. In this case, by comparing two NDs of equal size and opposite polarity (RUDDM-40 and I6-40), it is seen that the ND with the positive ZP binds slightly higher

amounts of AfB1. Consequently, it is believed that AfB1's partial negative charge, associated with the C-4 carbon atom [38], could have greater attraction to NDs with positively charged sites. With the exception of the terminal furan ring, AfB1 is a planar molecule; therefore, special orientation is shown to play a role in how AfB1 is adsorbed. It is possible that the negative portion of the AfB1 molecule orients itself in such a way that the packing density is greatest on positively charged NDs.

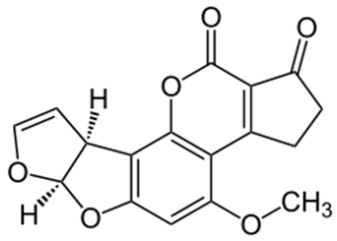

Figure 7.3. Chemical Structure of aflatoxin B1 (AfB1).

Furthermore, surface groups related to these two NDs drastically differ. Surface characterization has previously shown the RUDDM ND is rich in oxygen containing groups, specifically carboxyls, whereas I6 ND has shown to have greater surface diversity and a large presence of carbonyls and hydrocarbon residues [39]. Such difference could also lead to variations in adsorption capacities. For this reason, NDs modified with specific surface groups were examined. Adsorption results show little difference between AfB1's attractions to one surface group over another. Even so, I6-COOH also shows a slight decrease in AfB1 capacity over other surface terminated NDs, as also seen with the COOH-rich RUDDM,

thereby, implicating that carboxyl groups are not the preferred adsorption site for AfB1 molecules. Because major factors for adsorption are based almost exclusively on aggregate size, future research requires evaluation of completely de-aggregated NDs of 4-5 nm.

In efforts to investigate porosity on AfB1 adsorption, porous NDs were utilized. Porous NDs, showed some improvement over RDDM ND, which had comparable aggregate sizes. However, despite the larger presence of pores, this increase was not extraordinary. In attempts to create porous aggregates, NDs with positive and negative ZPs (using 40 nm NDs, RUDDM1 and I6) were mixed at equal proportions, before proceeding as normal with the toxin experiment. Aggregation of the NDs immediately took place, however, no increase in adsorption over the individualized results was observed, despite the ability for AfB1 to electrostatically interact with both positive and negative ND surfaces.

Interestingly, when ND suspensions were prepared to pH 2.5, adsorption capacities were able to be preserved. This is important for enterosorbents where much of the toxin-ND interaction occurs in the stomach. However, in basic environments degradation of the AfB1 molecule was observed. In fact, AfB1 in the presence of NaOH alone showed destruction of approximately 53 % of the sample within 30 minutes, with no greater degradation over the next 21 hours. It is known that in basic environments, the lactone ring in AfB1 is damaged, thereby degrading the AfB1 molecule [30]. However, due to the spectral changes of AfB1 with and without NDs, it appears that NDs are still adsorbing the toxin even in the alkaline environment.

Also effecting adsorption were the concentrations of ND suspension used. Significant differences were seen in adsorption when using ND suspensions of 0.1 or 0.5 wt. %. To further analyze these differences, AfB1-ND ratios were altered. In both cases, concentration increase and ratio adjustment, the number of ND particles in the total system was manipulated and resulted in drastic adsorption differences. By increasing the amount of NDs the removal efficiency, or adsorption percentage, is improved, due an increased number of adsorption sites. However, this increase also corresponds to a drop in uptake capacity, as there are an insufficient number of AfB1 molecules to cover all sites on the ND surface (Figure 7.4). Other published work is consistent with our results [40] and suggests that a substrate concentration be chosen to show a balance between high adsorption percentages and respectable capacities. As a result, all future studies rely only on results from 0.1 wt. % ND suspensions at a 3:7 ratio. However, these studies indicate the complexities in the Langmuir isotherm and how selected sorbent concentrations and adsorbent to adsorbate ratios can alter calculated maximum capacities and binding constants. Such is seen with the construction of the Langmuir isotherm for RUDDM series ND (Figure 7.5).

Select NDs were chosen for the construction of the Langmuir isotherm. The plateauing effect of these isotherms, indicate that the NDs have reached saturation due to binding sites being filled. Maximum capacities, Q_{max}, and binding constants, K_d, were extracted from the isotherm through linear regression curve fitting. Four transform equations were used as each shows different error sensitivities and have biases towards fitting data at

low or high concentration ranges. The results of these transform equations is seen in Table 7.2.

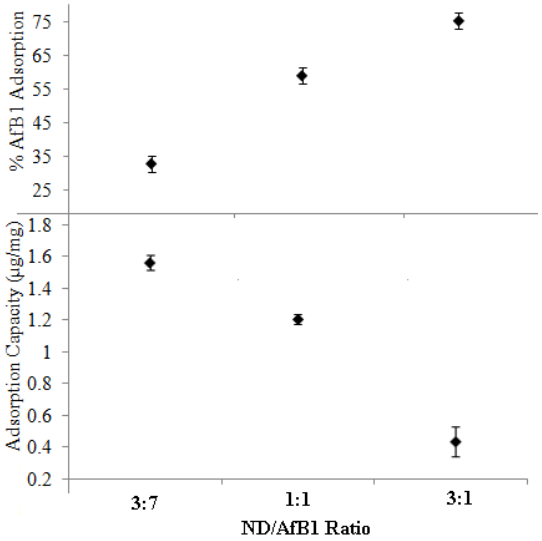

Figure 7.4. Effect of ND:AfB1 ratios on adsorption percentage and capacity. ND concentration (0.5 wt. %) and AfB1 concentration (10 µg/mL) remained consistent.

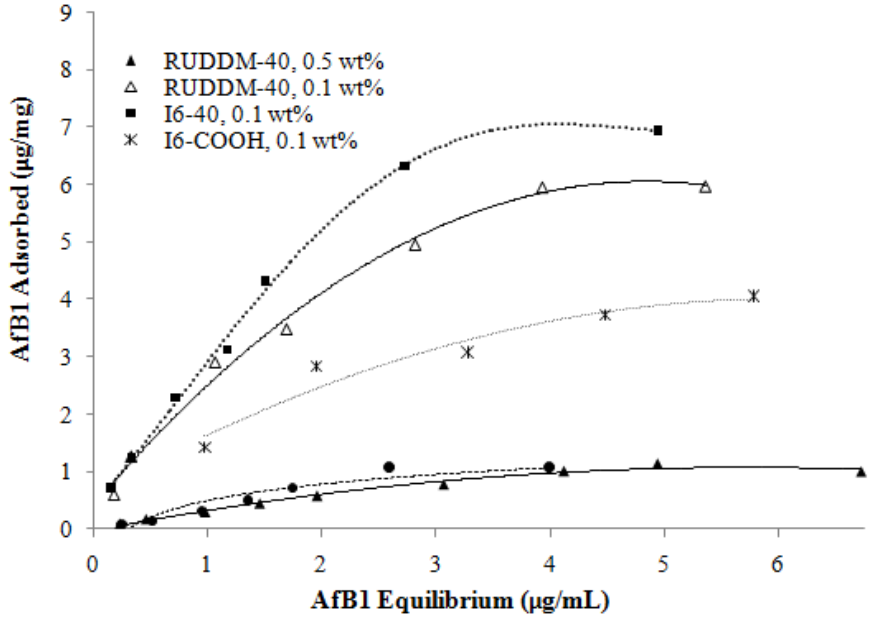

Figure 7.5. Langmuir isotherm for AfB1 on various ND substrates and at different ND concentrations.

Table 7.2. Maximum capacity and binding constants of AfB1 on various NDs based on four Langmuir transform equations.

	RUDDM-40 0.5 wt. %		RUDDM1-40 0.1 wt. %		I6-40 0.1 wt. %		I6-COOH 0.1 wt. %	
Transforms	Q_{max} (μg/mg)	K_d (mg/μg)	Q_{max} (μg/mg)	K_d (mg/μg)	Q_{max} (μg/mg)	K_d (mg/μg)	Q_{max} (μg/mg)	K_d (mg/μg)
Eadie-Hofstee	2.435	0.1470	9.306	0.4042	12.774	0.3183	6.522	0.2842
Lineweaver-Burk	2.895	0.1203	10.341	0.3729	12.485	0.3106	6.468	0.2883
Reciprocal Line	2.807	0.1243	9.234	0.4227	12.853	0.3265	6.596	0.2779
Scratchard	2.851	0.1222	10.119	0.3846	11.767	0.3724	6.606	0.2999
Average	***2.747***	***0.1290***	***9.750***	***0.3961***	***12.470***	***0.3320***	***6.548***	***0.2880***

The transform calculations confirm that higher concentrations of NDs give rise to lower maximum capacities. By using lower concentrations of ND, the calculated maximum capacities and binding constants, which give insight to binding strength, more than tripled. Comparisons of 40 nm RUDDM and I6 show that while I6 has a greater Q_{max}, its binding strength is lower. The lower binding constant likely correlates to I6's diverse surface groups. Though I6 has an increased number of binding sites for AfB1, not all of these sites may equally bind the molecule, whereas RUDDM's fewer preferential sites may have a great affinity to the toxin. As indicated earlier, COOH groups do not show a high preference for the AfB1 molecule, this is further suggested by the lower maximum capacity and binding calculations. Maximum capacity values found in this research, specifically for 40 nm I6 and RUDDM, outperform other AfB1 adsorbents including other NDs [30] and yeast cell walls [41] and behave similarly to some activated charcoals [42].

Finally, desorption experiments were conducted to observe the binding strength of the toxins to the NDs. Studies found that NDs did not release the toxin in the presence of water,

NaCl or $CaCl_2$. Such results indicate the AfB1 adsorption is not based on ionic mechanisms, but possibly, hydrophobic interactions or hydrogen bonding. These results propose that ND enterosorbents will bind the toxin throughout the GI tract.

7.3.2 Ochratoxin A Studies

OTA binding on NDs required slightly longer incubation times, while AfB1 on NDs showed adsorption in 5 minutes or less, OTA required 15 minutes, though from 5 to 15 minutes adsorption increased by only 6 to 10 %. All NDs, surveyed for OTA adsorption in the 15 minute incubation period are seen in Figure 7.4. Differences between OTA adsorption over AfB1 adsorption on NDs are immediately observed with respect to electrostatic interactions. NDs possessing positive ZPs adsorbed greater amounts of OTA than negatively charged NDs, due to the negative nature of the OTA molecule (Figure 7.6). The negatively charged HSCAS clay mineral, whose binding is based on electrostatics, shows little to no adsorption of OTA [43]. Interestingly, our studies indicate negatively charged NDs were still able to adsorb the toxin, despite charge repulsion. Previous studies using charged dye molecules showed no adsorption on NDs of like charges [34, 39]; thereby insinuating that while electrostatic interactions are the dominating mechanism of adsorption, other mechanisms are also taking place. Adsorption studies on cell walls show that functional groups, including carboxyl, hydroxyl, phosphate and amino groups may be responsible for binding OTA [44], additionally, NDs which are primarily hydrophilic in nature may have hydrophobic patches that aid in binding. In comparisons of negatively charged NDs, the

presence of oxygen containing groups, specifically carboxyls on I6-COOH, OZ-ND, OZ-Bl and RUDDM, exhibit the reason for binding.

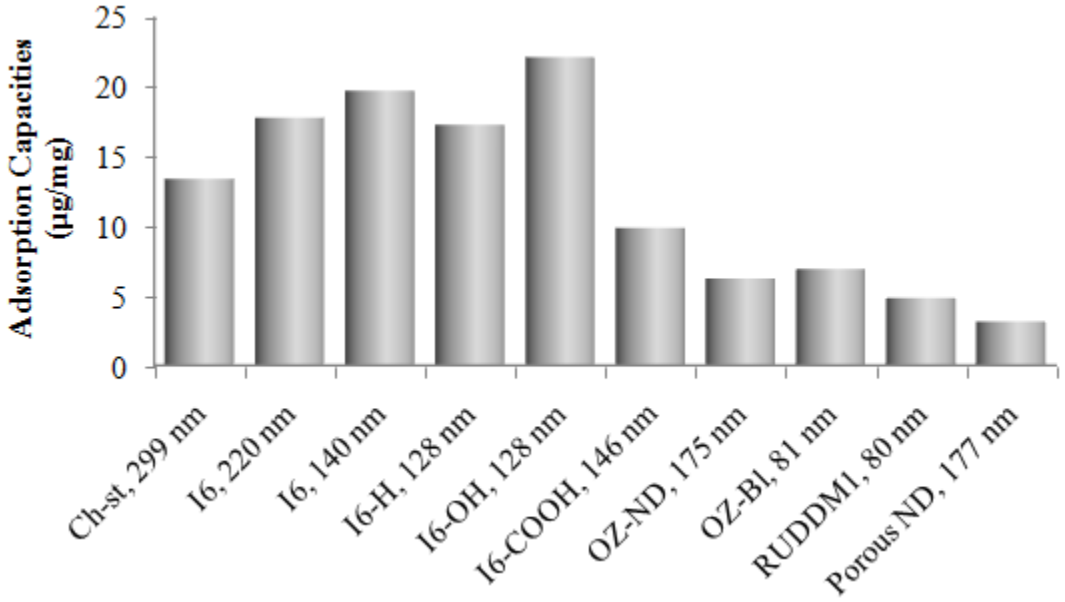

Figure 7.4. Results of OTA adsorption on various ND substrates (0.1 wt. %) showing different adsorption capacitates based on treatments and aggregate sizes (nm).

Unlike AfB1 studies, the degree of adsorption is not based on aggregate size, but instead, surface chemistries. For example, 128 nm hydroxylated NDs perform superior to hydrogenated NDs of the same size, even though I6-H carries a stronger positive ZP (68 mV over 53 mV). However, NDs stemming from the same manufacturing treatments can be altered for greater adsorption by reducing aggregate size and increasing SSA (Ch-st, I6-220 and I6-140 series). The presence of pores in the porous ND sample did not help to elevate adsorption levels.

OTA was studied in acidic and basic environments for their preservation of adsorption capacity. OTA in acidic conditions has a peak shift from 365 to 340 nm.

However, in basic environments the peak shifted to longer wavelengths, 385 nm. Nonetheless, in both cases, the addition of NDs shows adsorption is still occurring even under these harsh environments.

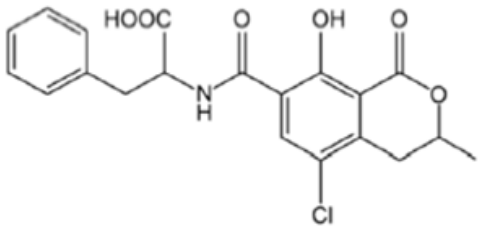

Figure 7.5. Chemical structure of ochratoxin A (OTA).

Select NDs, Ch-st, I6-140 and I6-OH, were chosen for isotherm construction to compare differences of aggregate sizes and surface treatments on maximum capacities. Langmuir isotherms for these three NDs (Figure 7.6), can be categorized as a L1 or L2 shape, based on Giles classification of isotherm shapes, which indicated that the NDs are reaching or has reached a plateau. To determine if a plateau is reached the calculated Q_{max} (Table 7.3) should be compared to the maximum observed quantity. The perceived maximum quantities of OTA on Ch-st, I6-140 and I6-OH are 13.403, 19.731 and 22.173 μg/mg, respectively. This signifies that 83.7, 93.8, and 87.8 % of the sites have been occupied by OTA, a plateau has been reached and the shape is a L2, or completed, isotherm. I6-OH and I6-140 isotherms in this case show a steep curve at the start of the isotherm, unlike Ch-st and NDs used in AfB1 adsorption; this implies a specific type of binding and saturation of that type of site [45]. Binding constants and capacities were highest for I6-OH NDs, making it apparent that

hydroxyl groups have a strong affinity for OTA molecules. However, all other ND binding constants also indicated strong binding. Maximum capacities obtained in this research show greater affinity for OTA over clay mineral enterosorbents, including HSCAS and bentonites and yeast cell walls [43].

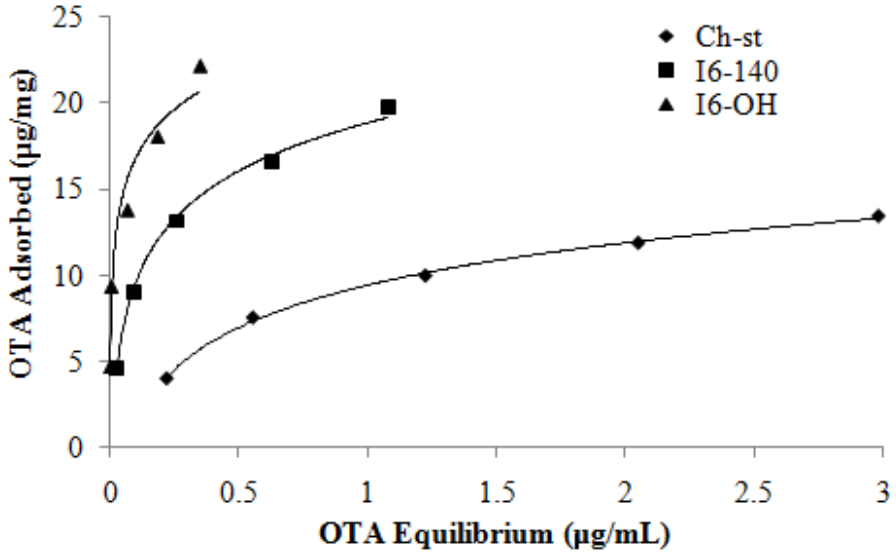

Figure 7.6. Langmuir isotherm for OTA, Ch-st, I6-140 and I6-OH substrates (0.1 wt. %).

Table 7.3. Maximum capacity and binding constants of NDs (0.1 wt. %) based on four Langmuir transform equations.

	I6-OH		I6-140		Ch-st	
Transforms	Q_{max} (µg/mg)	K_d (mg/µg)	Q_{max} (µg/mg)	K_d (mg/µg)	Q_{max} (µg/mg)	K_d (mg/µg)
Eadie-Hofstee	24.821	17.731	20.626	7.974	15.847	1.531
Lineweaver-Burk	24.510	18.545	20.121	8.569	15.949	1.507
Reciprocal Line	26.247	14.111	22.321	5.895	16.287	1.415
Scratchard	25.355	16.447	21.060	7.439	15.958	1.506
Average	***25.233***	***16.708***	***21.032***	***7.469***	***16.010***	***1.489***

Though calculations reveal high binding strengths, in the presence of NaCl and $CaCl_2$ solutions NDs showed considerable desorption of the bound OTA molecule, 25 and 26 %, correspondingly. By repeated redispersion of ND pellets in NaCl or $CaCl_2$ another 6 % or less of the bound OTA molecules were released. This outcome further depicts ionic adsorption mechanisms for OTA's binding on NDs.

7.4 Conclusions

Results of this study show that modification treatments can significantly influence the quantity of the toxin bound. In the case of AfB1, aggregate size shows to be the largest influence of adsorption capacity. Therefore, NDs with the smallest aggregate sizes (40 nm) were shown to adsorb the largest amounts of AfB1. The presence of carboxyl groups on ND surfaces further limited the binding of AfB1; however, the molecules were not released in the presence of salt solutions. In OTA studies electrostatic interactions were shown to dominate. Beyond electrostatic interactions the types of surface functional groups present also influenced OTA adsorption. OTA was shown to have a strong affinity for hydroxylated surfaces, however, in the presence of salt, OTA showed some toxin release due to ionic adsorption mechanisms. In both toxin studies adsorption was preserved under pH changes, even if the toxin molecules themselves underwent chemical changes due to the harsh pH environments. Lastly, it was shown that alterations in preparation procedures, including sorbent concentrations and toxin to ND ratios, provided drastic result differences that could further affect maximum capacity and binding calculations.

Acknowledgements

This study was supported by the Materials World Network under the National Science Foundation (Grant No. DMR-0602906). The authors would like to thank Dr. Suzanne Hens, at the International Technology Center, for her preparation of surface terminated NDs and Tatyana Feygelson, NRL for preparation of hydrogen-terminated ND. Additionally, the authors would like to acknowledge Dr. Gary Payne, Department of Plant Pathology at North Carolina State University for his useful discussions on mycotoxins.

References

1. Devegowda, G., B.I.R. Aravind, and M.G. Morton. *Saccharomyces cerevisiae and mannanoligosaccharides to counteract aflatoxicosis in broilers*. in *Australian Poultry Science Symposium*. 1996.

2. Galvano, F., et al., *Dietary strategies to counteract the effects of mycotoxins: a review* Journal of Food Protection, 2001. **64**(1): p. 120-131.

3. Ramos, A.J. and E. Hernández, *In vitro aflatoxin adsorption by means of a montmorillonite silicate. A study of adsorption isotherms.* Animal Feed Science and Technology, 1996. **62**(2): p. 263-269.

4. Ramos, A.J., J. Fink-Gremmels, and E. Hernandez, *Prevention of toxic effects of mycotoxins by means of nonnutritive adsorbent compounds.* Journal of Food Protection, 1996. **59**(6): p. 631-641.

5. Bryden, W.L., *Mycotoxins in the food chain: human health implications.* Asia Pacific Journal of Clinical Nutrition, 2007. **16**(1): p. 95-101.

6. Gradelet, S., et al., *Dietary carotenoids inhibit aflatoxin B1-induced liver preneoplastic foci and DNA damage in the rat: role of the modulation of aflatoxin B1 metabolism.* Carcinogenesis, 1998. **19**: p. 403-411.

7. Gradelet, S., et al., *Modulation of aflatoxin B1 carcinogenicity, genotoxicity and metabolism in rat liver by dietary carotenoids: evidence for a protective effect of CYP1A inducers.* Cancer Letters, 1997. **114**: p. 221-223.

8. Hussein, H.S. and J.M. Brasel, *Toxicity, metabolism, and impact of mycotoxins on humans and animals.* Toxicology, 2001. **167**(2): p. 101-134.

9. Squire, R.A., *Ranking animal carcinogens: a proposed regulatory approach.* Science, 1981. **214**(4523): p. 877-880.

10. Rensburg, C.V., *The ameliorating effect of oxihumate on aflatoxicosis in broilers*, in *Animal and Wildlife Sciences*. 2005, University of Pretoria: Pretoria.

11. Wood, A.M., *Fungal diseases*, in *Poultry Diseases*, P.M. M. Pattison, J.M. Bradbury, D. Alexander, Editor. 2008, Saunders Elsevier. p. 428.

12. Smela, M.E., et al., *The chemistry and biology of aflatoxin B1: from mutational spectrometry to carcinogenesis.* Carcinogenesis, 2001. **22**(4): p. 535-545.

13. Guengericha, F.P., et al., *Activation and detoxication of aflatoxin B1.* Mutation Research/Fundamental and Molecular Mechanisms of Mutagenesis, 1998. **402**(1-2): p. 121-128.

14. Raney, V.M., T.M. Harris, and M.P. Stone, *DNA conformation mediates aflatoxin B1-DNA binding and the formation of guanine N7 adducts by aflatoxin B1 8, 9-exo-epoxide.* Chemical Research in Toxicology, 1993. **6**(1): p. 64-68.

15. Harris, C.C., *Interindividual variation among humans in carcinogen metabolism,DNA adduct formation and DNA repair* Carcinogenesis, 1989. **10**(9): p. 1563.

16. Pitt, J.I., et al., *Mycotoxins and toxigenic fungi.* Medical Mycology, 2000. **38**(Supplement 1): p. 41-46.

17. Denli, M. and J.F. Perez, *Ochratoxins in feed, a risk for animal and human health: control strategies.* Toxins, 2010. **2**: p. 1065-1077.

18. WHO, *Environmental Health Criteria*. 1990, Geneva. 105.

19. Breitholtz-Emanuelsson, A., et al., *Ochratoxin A in cow's milk and in human milk with corresponding human blood samples* Journal of the Association of Official Analytical Chemists 1993. **76**: p. 842.

20. Miraglia, M., et al., *Ochratoxin A levels in human milk and relted food samples: an exposure assesment.* Natural Toxins, 1995. **3**: p. 436.

21. Murphy, P.A., et al., *Food mycotoxins: an update.* Journal of Food Science and Technology, 2006. **71**(5): p. R51-R65.

22. O'Brien, E. and D.R. Dietrich, *Ochratoxin A: the continuing enigma.* Critical Reviews in Toxicology, 2005. **35**(1): p. 33-60.

23. Soriano, J.M., et al., *Control and decontamination of ochratoxin A in food processing: the key of tracability*, in *New Issues in Food Policy, Control and Research*, A.P. Riley, Editor. 2007, Nova Science: New York, NY.

24. Mishra, H.N. and C. Das, *A review on biological control and metabolism of aflatoxin.* Critical Reviews in Food Science and Nutrition 2003. **43**(3): p. 245-264.

25. Varga, J., et al., *Chemical, physical and biological approaches to prevent ochratoxin induced toxicoses in humans and animals.* Toxins, 2010. **2**: p. 1718-1750.

26. Scott, P.M., *Effects of processing and detoxification treatments on ochratoxin A: introduction.* Food Additives & Contaminants, 1996. **13**(Suppl.): p. 19-21.

27. Peraica, M., A.M. Domijan, Z. Jurjevic, B. Cvjetkovic, *Prevention of exposure to mycotoxins from food and feed.* Arh Hig Rada Toksikol 2002. **53**: p. 229–237.

28. Edrington, T. S., L.F. Kubena, R. B. Harvey, G. E. Rottinghaus, *Influence of a Superactivated Charcoal on the Toxic Effects of Aflatoxin or T-2 Toxin in Growing Broilers1.* Poultry Science, 1997. **76**: p. 1205-1211.

29. Gibson, N., et al., *Colloidal stability of modified nanodiamond particles.* Diamond and Related Materials, 2009. **18**(4): p. 620.

30. Puzyr, A. P., K.V. Purtov, O. A. Shenderova, M. Luo, D. W. Brenner, and V. S. Bondar, *The Adsorption of Aflatoxin B1 by Detonation-Synthesis Nanodiamonds.* Doklady Biochemistry and Biophysics, 2007. **417**(1): p. 299-301.

31. Schrand, A.M., S.A.C. Hens, O.A. Shenderova, *Nanodiamond Particles: Properties and Perspectives for Bioapplications.* Critical Reviews in Solid State and Materials Sciences, 2009. **34**: p. 18-74.

32. Schrand, A.M., et al., *Differential biocompatibility of carbon nanotubes and nanodiamonds.* Diamond and Related Materials, 2007. **16**(2): p. 2118-2123.

33. Puzyr, A.P., V.S. Bondar, and S.E. Al, *Dynamics of the selected physiological responses in laboratory mice under the prolonged oral administration of nanodiamonds suspensions.* Siberian Med. Obozrenie (Siberian Med. Rev.) (in Russian), 2004. **4**: p. 19.

34. Gibson, N.M., T.J.M. Luo, O. Shenderova, Y.J. Choi, Z. Fitzgerald, and D.W. Brenner, *Fluorescent dye adsorption on nanocarbon substrates through electrostatic interactions.* Diamond and Related Materials, 2010. **19**(2-3): p. 234-237.

35. Gibson, N.M., T.J.M. Luo, O. Shenderova, Y.J. Choi, and D.W. Brenner. *Modified Nanodiamonds for Adsorption of Propidium Iodide and Aflatoxin.* MRS Fall 2009 Proceedings, MRS Fall 2009 Proceedings, Available online, Paper # 1236-SS09-05.

36. Hens, S., et al., *Nanodiamond bioconjugate probes and their collection by electrophoresis.* Diamond and Related Materials, 2008. **17**(11): p. 1858-1866.

40. Phillips, T.D., et al., *Reducing human exposure to aflatoxin through the use of clay: a review.* Food Additives & Contaminants: Part A, 2008. **25**(2): p. 134-145.

41. Pachter, R., P.S. Steyn, *Quantum-chemical studies of aflatoxin B1, sterigmatocystin and versicolorin A, and a comparison with their mutagenic activity*. Mutation Research Letters, 1985. **143**(1-2): p. 87-91.

42. Gibson, N.M., T.J.M Mark Luo, O. Shenderova, Z. Fitzgerald, D.W. Brenner. *Propidium Iodide Adsorption and Binding by Nanodiamond and Nanocarbon Particles*. In preparation.

40. Balasubramanian, R., S.V. Perumal, and K. Vijayaraghava. *Equilibrium isotherm studies for the multicomponent adsorption of lead, zinc, and cadmium onto indonesian peat.* Industrial and Engineering Chemistry Research, 2009. **48**(4): p. 2093-2099.

41. Rensburg, C.V., *The ameliorating effect of oxihumate on aflatoxicosis in broilers*, in *Animal and Wildlife Sciences*. 2005, University of Pretoria: Pretoria.

42. Decker, W.J. and D.G. Corby, *Activated charcoal adsorbs aflatoxin B1.* Veterinary and Human Toxicology, 1980. **22**(6): p. 388-389.

43. Huwig, A., et al., *Mycotoxin detoxication of animal feed by different adsorbents.* Toxicological Letters, 2001. **122**(2): p. 178-188.

44. Ringot, D., et al., *In vitro biosorption of ochratoxin A on the yeast industry by-products: comparison of isotherm models.* BioresourceTechnology, 2007. **98**: p. 1812-1821.

45. Grant, P.G., and T.D. Phillips, *Isothermal Adsorption of Aflatoxin B1 on HSCAS Clay.* Journal of Agriculture and Food Chemistry, 1998. **46**(2): p. 599-605.

Chapter 8

Future Directions

To date, mycotoxin adsorption experiments are completed using NDs that have primarily been modified for aggregate sizes and surface chemistries. In efforts to increase mycotoxin adsorption, specifically for AfB1, future research is directed at modifying the surfaces of ND to mimic natural interactions of AfB1 in the body. However, to achieve this objective, in depth knowledge of how the body responds to AfB1 once ingested is required.

The metabolic process of AfB1 *in vivo* has been known for decades. Much of the understanding centers around the metabolic byproducts of the molecule since AfB1 must be metabolized to act harmfully on the body. Once AfB1 is ingested, metabolic breakdown is facilitated by cytochrome P450 enzymes [1, 2]. P450 enzymes are predominantly located on the membrane of the endoplasmic reticulum in cells [3] and while these enzymes are located throughout the body, they occur at the highest levels within the liver [4]. For this reason, AfB1 is associated with hepatocellular carcinoma (HCC).

The byproducts created by P450 largely determine the degree of toxicity *in vivo* [2]. While some metabolites generated are generally less harmful in nature, like the hydroxylated forms which make up AfM1, AfP1 and AfQ1, other forms become much more potent, such is the case with AfB1-*exo*-8,9-epoxide. In this case, oxidation of AfB1 to form the epoxilated derivative has been shown to be the foundation for mutagenic damage to liver cells [5, 6]. The amount of this metabolized product primarily decides the extent of harm to the species, as it has the ability to intercalate into base pairs of the DNA and covalently react with the guanine N7 atom to form various DNA-adducts (Figure 8.1) [5-7]. These DNA adducts, where DNA is bound to a cancer causing substance, causing heritable genetic changes that

lead to malignant cell formation [8]. Figure 8.2 illustrates the AfB1 conversion process along with the principal DNA-adduct formed with AfB1 epoxide, *trans*-8,9-dihydro-8-(N^7-guanyl)-9-hydroxyaflatoxin B1 [6, 7]. The imidazole ring ($C_3H_4N_2$) on the adduct carries a positive charge, which may cause depurination leading to an apurinic (AP) size on the DNA. AP sites located on DNA lack both a purine and pyrimidine and are indicative of DNA damage [5].

Like many other cancers, in the case of AfB1 induced HCC, the reaction affects alters the tumor suppressing gene, p53 [2, 5]. p53 proteins act as an anticancer mechanism to activate DNA repair or apoptosis of damaged cells. If, however, the gene is damaged, the tumor suppressing capabilities are greatly reduced, thereby allowing the damaged cell to proliferate [9]. In the case of AfB1, AfB1-8,9-epoxide binding to the DNA causes a guanine-cytosine to thymine-adenine (GC→TA) transversion at the third base in 249 codon in the p53 protein. This transversion is reported as the mutagenic change inactivating the tumor suppressing gene, allowing the malignant cell to survive and reproduce, and gives rise to AfB1's carcinogenicity [5]. Although the highest mutability occurs at the 249 codon, studies also conclude that neighboring codons also show high levels of mutation [10].

Though the primary focus is on AfB1-DNA binding, research also shows considerable binding of AfB1 to proteins, like serum albumin [11, 12], and intestinal bacterial cells, such as lactic acid bacteria (LAB) [13, 14]. As in the case of DNA, AfB1 requires epoxidation of molecule before binding to albumin. Though AfB1 forms covalent albumin-adducts with the lysine components on the blood protein, the majority of AfB1 is non-covalently attached to albumin for transportation to the liver [15]. However, before

transportation to the liver, poultry studies show a competitive effort between albumin and LAB in the small intestines to bind AfB1 [14].

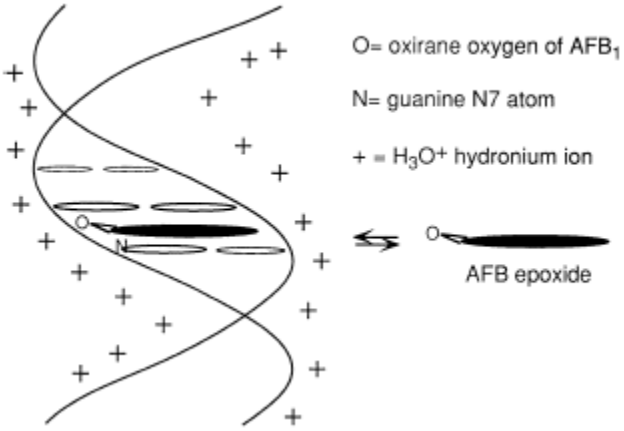

Figure 8.1. Interaction of AfB1 *exo*-8,9-epoxide with DNA [6].

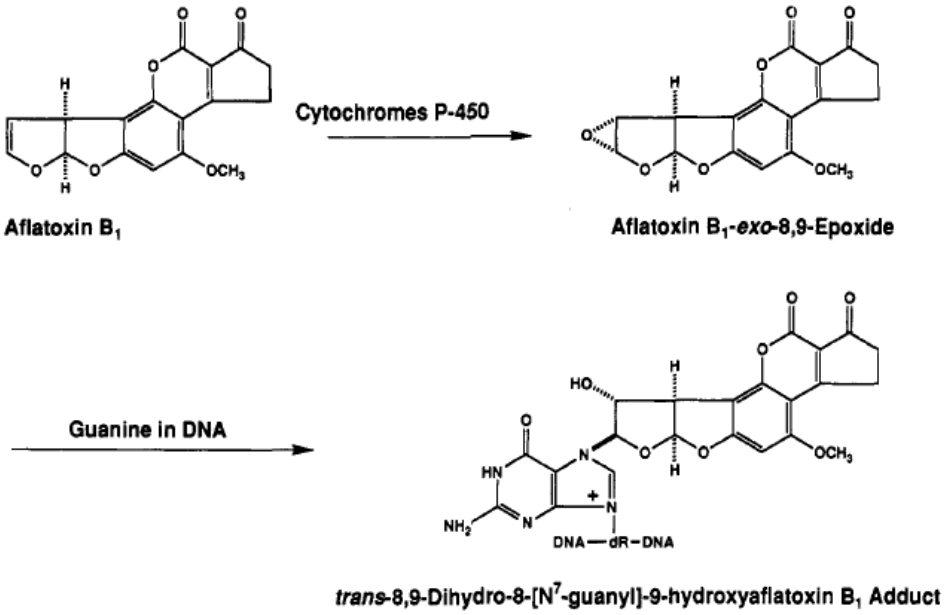

Figure 8.2. Metabolic activation of aflatoxin B1 to AfB1 *exo*-8,9-epoxide is carried out by cytochrome P450. The epoxide reacts region-and stereoselectively with N^7 of guanine to form the primary adduct *trans*-8,9-dihydro-8-(N^7-guanyl)-9-hydroxyaflatoxin B1 [7].

With knowledge of how AfB1 reacts once ingested, we can work to create ND substrates to interact with the pre and post-metabolized AfB1. In doing so, NDs will have the ability to react with the toxins during the entire length of the GI tract. To achieve this, future research will focus on attaching guanine rich nucleic acid strands onto the ND substrates. DNA attachment has been previously demonstrated with ND models [16, 17].

Additionally, prospective experiments may involve altering NDs through the attachment of albumin or select LAB select proteins (listed in [18]). The attachment of these proteins to ND surfaces would assist in AfB1 attachment by mimicking natural interactions in the body. In addition, by imitating adsorption mechanisms of LAB, which include hydrophobic as well as electrostatic interactions, it might be beneficial to attach lipoteichoic acid-like polymers to the ND substrate. The polymer additions, naturally present on LAB, would create a hydrophobic ND surface with a strong negative charge. In short-term experiments, it would be valuable to experiment with NDs that have hydrophobic patches. While this may affect the colloidal stability of the NDs, there may be greater benefit from increased aflatoxin adsorption.

Lastly, future experiments should explore adsorption of other mycotoxins to ND surfaces. Our extensive collection of ND substrates has shown varying success of toxin adsorption. The substitution of AfB1 for OTA demonstrates NDs' specific affinities for different molecules, with these affinities largely based on electrostatic interactions of the mycotoxins to the NDs. Therefore, it is advisable to test other mycotoxins with different molecular structures and charges. One plausible candidate is the highly negatively charged

fumonisin B1 [19], which may show increased adsorption capacities and binding strength on positively charged NDs.

References

1. Mishra, H.N. and C. Das, *A review on biological control and metabolism of aflatoxin.* Critical Reviews in Food Science and Nutrition 2003. **43**(3): p. 245-264.

2. Eaton, D.L. and E.P. Gallagher, *Mechanism of aflatoxin carcinogenesis.* Annual Review of Pharmacology and Toxicology, 1994. **34**: p. 135-172.

3. E.Szczesna-Skorupa, C.D.C., S. Rogers, and B. Kemper, *Mobility of cytochrome P450 in the endoplasmic reticulum membrane* Proceedings of the National Academy of Sciences, 1998. **95**: p. 14793–14798.

4. Guengerich, F.P., et al., *Involvement of cytochrome P450, glutathione S-transferase, and epoxide hydrolase in the metabolism of aflatoxin B1 and relevance to risk of human liver cancer.* Environmental Health, 1996. **104**(3): p. 557-562.

5. Smela, M.E., et al., *The chemistry and biology of aflatoxin B1: from mutational spectrometry to carcinogenesis.* Carcinogenesis, 2001. **22**(4): p. 535-545.

6. Guengericha, F.P., et al., *Activation and detoxication of aflatoxin B1.* Mutation Research/Fundamental and Molecular Mechanisms of Mutagenesis, 1998. **402**(1-2): p. 121-128.

7. Raney, V.M., T.M. Harris, and M.P. Stone, *DNA conformation mediates aflatoxin B1-DNA binding and the formation of guanine N7 adducts by aflatoxin B1 8, 9-exo-epoxide.* Chemical Research in Toxicology, 1993. **6**(1): p. 64-68.

8. Harris, C.C., *Interindividual variation among humans in carcinogen metabolism, DNA adduct formation and DNA repair* Carcinogenesis, 1989. **10**(9): p. 1563.

9. Asker, C., K.G. Wiman, and G. Selivanova, *p53-induced apoptosis as a safeguard against cancer.* Biochemical and Biophysical Research Communications 1999. **265**(1): p. 1-6.

10. Mace, K., et al., *Aflatoxin B1-induced DNA adduct formation and p53 mutations in CYP450-expressing human liver cell lines.* Carcinogenesis, 1997. **18**(7): p. 1291-1297.

11. Sabbioni, G., et al., *Isolation and characterization of the major serum albumin adduct formed by aflatoxin B1 in vivo in rats.* Carcinogenesis, 1987. **8**(6): p. 819-824.

12. Gan, L.S., et al., *Serum albumin adducts in the molecular epidemiology of aflatoxin carcinogenesis: correlation with aflatoxin Bi intake and urinary excretion of aflatoxin M1.* Carcinogenesis, 1988. **9**(7): p. 1323-1325.

13. Haskard, C.A., et al., *Surface binding of aflatoxin B1 by lactic acid bacteria.* Applied and Environmental Microbiology, 2001. **67**(7): p. 3086-3091.

14. Haskard, C., C. Binnion, and J. Ahokas, *Factors affecting the sequestration of aflatoxin by lactobacillus rhamnosus strain GG.* Chemico-Biological Interactions, 2000. **128**(1): p. 39-49.

15. Ewaskiewicz, J.I., T.M. Devlin, and J.J. Ch'ih, *The in vivo disposition of aflatoxin B1 in rat liver.* Biochemical and Biophysical Research Communications, 1991. **179**: p. 1095-1100.

16. Grichko, V., V. Grishko, and O. Shenderova, *Nanodiamond bullets and their biological targets.* NanoBioTechnology, 2006. **2**(1-2): p. 1551-1294.

17. K.V. Purtov , L.P. Burakova, A.P. Puzyr and V.S. Bondar *The interaction of linear and ring forms of DNA molecules with nanodiamonds synthesized by detonation.* Nanotechnology, 2008. **19**(32): p. 325101-325102.

18. Sáncheza, B., P. Bressollier, S. Chaignepainb, J.M. Schmitterb and M.C. Urdacia, *Identification of surface-associated proteins in the probiotic bacteriumLactobacillus rhamnosus GG.* International Dairy Journal, 2009. **19**(2): p. 85-88.

19. Stockmann-Juvala, H., and K. Savolainen, *A review of the toxic effects and mechanisms of action of fumonisin B1.*Human and Experimental Toxicology, 2008. **27**: p. 799-809.

Supplementary Material

Nanodiamond Modification and Evaluation of Colloid Stability

Published in Nanodiamond 2008 Conference Proceedings (2008)

Nanodiamond Modification and Evaluation of Colloid Stability

N.M. Gibson [1], O. Shenderova [1,2], T.J.M. Luo [1], Z. Fitzgerald [1], D.W. Brenner [1]

[1]Dept of Material Sciences and Engineering, North Carolina State University, Raleigh, NC 27695-7907, USA

[2]International Technology Center, Research Triangle Parke, NC 27617-7300, USA

Abstract

Nanodiamonds (ND) are capable of exhibiting exceptional physiochemical properties, including relatively high surface areas, abundant surface chemistries and have the ability to maintain highly charged surfaces when placed in aqueous solutions. However, raw, unmodified ND particles, like those typically received from vendors, possess inhomogeneous sizes and surface characteristics causing the ND to have low surface charges and, thus, low colloidal stability. Methods of modifying these NDs to acquire the desired properties are simple. Through experimentation processes, NDs of different surface chemistries were modified using plasma treatments, size fractionalization, and silane surface coatings. Evaluation of the suspension's stability took place via zeta potential measurements at neutral pH and with titration over a wide pH. Results showed that many ND types are able to maintain high stability over a wide range of pH, which expands the possibility of ND use into biomedical enterosorbent applications.

***Keywords*:** nanodiamond, colloidal stability, enterosorbent, zeta potential, surface modification.

Nanodiamond (ND) research has been expanding exponentially in the past several years largely due to ND's appealing physiochemical properties. While ND particles have reasonably large surface areas (300-400 m^2/g), their key distinctiveness stems from the particle's ability to possess dense surface chemistries as well as a large variety of surface groups. Surface chemistries of the diamond nanoparticles can be managed to acquire specific properties that fit the functional requirements of the final ND application [1]. In manipulating these chemistries, surface charges may also be altered with the possibility to achieve both highly positive and negative ND particles. Alteration of NDs is, in most cases, a requirement. NDs purchased from vendors typically exhibit highly inconsistent properties, which are largely attributed to the methods used to produce the nanoparticle [1,2,3]. NDs are formed by a detonation process of carbon containing explosives, i.e., trinitrotoluene (TNT) and 1,3,5-trrinitro-1,3,5-s-triazine (RDX). After detonation NDs require purification from the soot and removal of metallic impurities, all of which are competed at an industrial level [2, 4, 5]. Each vendors recipe to produce and purify the ND naturally leads to varying surface properties, charges, and aggregate sizes. Depending on the end use application of the ND, these varying properties could drastically affect the results of one's research.

ND modification methods can be completed by either chemical or physical means [2, 3]. Techniques used in our studies include size fractionalization through centrifugation [2, 5], plasma treatments using oxygen and nitrogen plasma, and silane surface coatings using tetramethylorthosilicate (TMOS) and N,N'-bis[(3-trimethoxysilyl)propyl]ethylenediamine (enTMOS). Two types of silane were selected since each carries an opposing charge when

they are hydrolyzed in water, with TMOS being positively charges and enTMOS being negatively charged. Such approaches to ND modification were conducted as to evaluate how each method affects various ND types.

Of the several different types of NDs selected, the first group held positive surface charges. The positive ND group was made up of Ch-st and modified Ch-st referred to as I6. Each of these was purchased from vendors. Vendor's methods to produce and modify these samples are discussed in previous work [4, 5]. Three size fractions of Ch-st (Table SM1) modified by methodology [2] were obtained from the Institute of Biophysics, Krasnoyarsk, Russia. Details on this modification will be published elsewhere [6]. Additional modifications took place at the International Technology Center (ITC), North Carolina, using I6 ND. Effects of plasma treatment were tested with I6 using oxygen plasma for 3, 5, 15, or 30 minutes or nitrogen plasma for 5, 15, or 30 minutes. I6 was also used in testing silane coatings of ND surfaces. Varying concentrations of TMOS and enTMOS were mixed with a fixed ND concentration (20 μL, 50 μL or 100 μL to 5 mL 0.1 wt. % I6 in DI).

The second group tested consisted of negatively charged NDs and included Kr-Black (Kr-B), and Kr-Gray (Kr-Gr) and RUDDM 1, derived from RUDDM, which has agglomerate size of 0-250 nm. These materials, also received from vendors, exhibit adequate as-received stability characteristics. Thus, this class of NDs has not yet been experimentally altered through our additional modification methods. Production details of these NDs can be found in literature, as reported by Gibson *et al*. [4].

Table SM1. Nanodiamond samples prepared at 0.1 wt. % in DI water and sonicated for 4 minutes left to cool to room temperature and measured for zeta potential (mV) and size (nm).

ND, 0.1 wt. %	ZP, mV	Size, nm
Ch-st	17.4 ±0.4	300
Ch-st 1	44.7 ±0.5	101
Ch-st 2	37.0 ±0.4	225
Ch-st 3	33.2 ±0.2	1380
I6	46.8 ±0.9	185
I6-O_2 plasma	44.6 ±1.8	157
I6-N_2 plasma	52.2 ±0.3	157
I6-TMOS coated	52.8 ±1.1	132
I6-enTMOS coated	38.3 ±0.2	148
Kr-Black	-42.9 ±2.1	80
Kr-Gray	-45.5 ±0.6	397
RUDDM 1	-49.3 ±1.9	75

ND suspensions were evaluated using zeta potential (ZP) measurements, which can directly predict the stability of the NDs in suspension by measuring their electrostatic repulsion when the sample is places in solution [2, 4]. ZP values greater than 30 mV or lower than -30 mV are considered stable. As the magnitude of the 30 mV increases suspension's stability becomes greater and can be preserved over longer periods. Previous research showed ZP values were influences by colloid temperature and concentration [4]. Therefore, all NDs were prepared at a 0.1 wt. % concentration in DI water, sonicated and cooled to room temperature. Sonication used a 3 mm titanium horn tip on a Cole-Parmer 750 W Ultrasonic Homogenizer. With an output power of 10 W and output intensity of ~100 W/cm. NDs were sonicated accordingly from 1.5 to 4 minutes depending on the volume of the

suspension prepared, with smaller volumes, in general, requiring shorter sonication times. Earlier studies show ZP was not heavily influenced by sonication times, yet particle size can be greatly affected [4]. ZP measurements for all NDs were conducted before and after modification. The results of these experiments are shown in Table 1.

Results show that not all of the modification methods appear highly effective. Fractionalization of Ch-st samples affect ZP greatly, where smallest monodispersed suspensions show significantly increased stabilities. Of plasma treated samples only the best treatments are shown (5 minute treatment in oxygen and 15 minute treatment in nitrogen). Generally, shorter treatment times have smaller particles than longer treatments. This could be a result of condensation reactions and, thus, agglomeration of initially smaller nanoparticles. ZP measurements with respect to treatment times demonstrated that longer treatment times decreased ZP. Overall, nitrogen plasma treatment for 15 minutes notable increased ZPs of the control I6 ND.

Silane coated NDs also had profound effect on ZP and particle size. I6 treated with positively charged TMOS and negatively charged enTMOS showed different results of ND stability. Though the increase was not drastic, negatively charged silane had increased stability over the originally positive particles. Experimentation showed higher concentrations of enTMOS increased ZP and decreased size. However, positively charged TMOS showed little noticeable changes of ZP and size until the highest concentration, 100 μL TMOS to 5 mL 0.1 wt. % ND, was used. At this mixture, complete agglomeration of ND occurred. This data stayed consistent over 3 weeks, however, due to the reactive nature of the silane,

samples were kept refrigerated. Our experiments revealed that enTMOS coatings at highest silane concentrations preformed better than the untreated I6. Despite this, more detailed experimentation must be conducted before solid conclusions are reached.

Though much of the research was conducted on a more general basis, results were being more closely examined for ND's behavior in potential enterosorbent applications, in other words, as a way to absorb toxins in the gastrointestinal (GI) tract [4, 7]. Developing NDs for enterosorbent use, specifically for aflatoxin B1 (AfB1), will be the focus of future studies. AfB1 is a carcinogenic offshoot of mold growth, which is found in many sources of grains and crops. Ingestion of the toxin has caused widespread infection of animals and humans; primary sufferers comprise those in third world countries [2]. Development of an effective enterosorbent requires a material with relatively high surface areas, chemical inertness, biocompatibility, and non-toxicity, all of which were proved through prior research [8, 9]. Adsorption efficiencies may also be affected by the charge-charge interactions of the toxin molecule and the enterosorbent, dispersivity and agglomerate constructions. For this reason, exploration of ND types and charges are studied.

Due to the enterosorbents' function inside the body, the material will be subjected to various pH conditions within the GI tract. To examine how charge behavior, thus stability, of the ND suspension will behave pH titration was conducted. The pH ranges chosen were wide enough to simulate conditions that would occur within the body. Select ND samples at 0.1 wt. % were chosen for this experiment. All samples chosen were processed and modified by vendors only. It was found that ZP behavior varied depending of the direction of titration.

Consequently, four experiments were conducted for each sample, running suspensions from a neutral pH to 12, neutral pH to 1, pH 1 to pH 12, and pH 12 to pH 1 (Notre: neutral pH values ranged from 5-6). Values of pH were obtained by introducing HCl of NaOH into the systems. Results of this experiment are shown below.

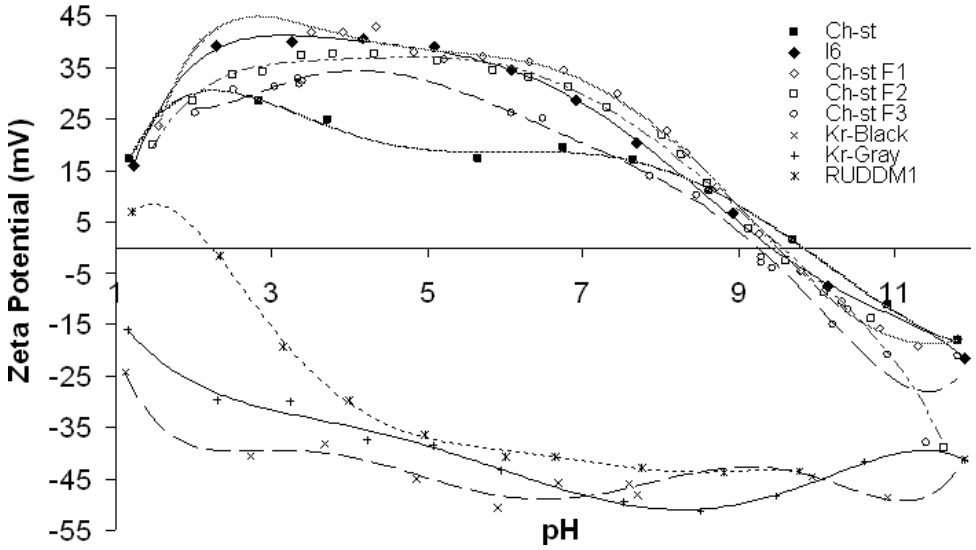

Figure SM1. Titration curves of positive and negative nanodiamonds illustrating the influence of manufacturing treatments on ND behavior under various pH environments. (Titration was completed from the natural pH to 12 and natural pH to 1).

Experiments verified that relatively high ZPs can be preserved over a wide range of pH. Stability preservation occurred more prominently with negatively charged NDs. Specifically, Kr-B and Kr-Gr performed most superior since these samples did not reach an isoelectric point, or point of no charge. Next steps will include titration of modified plasma and silane treated samples, since these samples hold best case scenarios in the positively charged ND group.

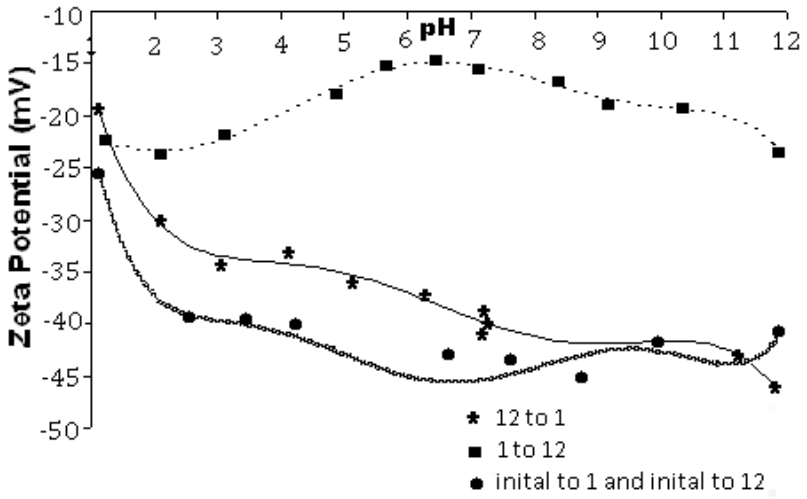

Figure SM2. Titration curves of Kr-Bl ND demonstrating the importance of titration directions.

Preliminary ND enterosorbents experiments have been performed using AfB1 and propidium iodide, chosen as an aflatoxin model. Experiments indicate that ND type and modification method influence the adsorption capacity of the ND [4]. Further research will focus on how to control the surface chemistry and stability of the ND to increase its adsorption efficiency for AfB1 molecules.

Acknowledgements

Acknowledgments would like to be made to the Materials Work Network program of the National Science Foundation (Grant DMR-0602906). For their financial support and V. Bondar, A. Puzyr, L. Purtov, Institute of Biophysics, Siberian Division, and the Russian Academy of Sciences, Krasnoyarsk, Russia for collaboration on modified nanodiamond and aflatoxin adsorption studies.

References

1. Grishko, V.P., O. Shenderova, *Nanodiamond: Designing the Bio-Platform* in *Ultrananocrystalline Diamond: History, Properties and Applications*, O. Shenderova and D. Gruen, Editor. 2006, William-Andrew: Norwich, UK.

2. Bondar, V.S. and A.P. Puzyr, *Nanodiamonds for biological investigations.* Physics of the Solid State, 2004. **46**(4): p. 716.

3. Shenderova, O., G. McGuire, I. Petrov, B. Spitsyn, A. Puzyr, V. Kuznetsov, *Application-Specific Detonation Nanodiamond Particulate*. NSTI Nanotechnology Conference and Trade Show - NSTI Nanotech 2006, Technical Proceedings**,** 2007. **1**: p. 154-157.

4. Gibson, N., O. Shenderova, A. Puzyr, K. Purtov, V.Grichko, T.J.M. Luo, Z. Fitzgerald, V. Bondar, D. Brenner, *Nanodiamonds for detoxification.* NSTI Nanotechnology Conference and Trade Show - NSTI Nanotech 2007, Technical Proceedings**,** 2007. **2**: p. 713-716.

5. Shenderova, O. I. Petrov, J. Walsh, V. Grichko, V. Grishko, T. Tyler, and G. Cunningham, *Modification of detonation nanodiamonds by heat treatment in air.* Diamond and Related Materials, 2006. **15**(11-12): p. 1799-1803.

6. Gibson, N., et al., *Colloidal stability of modified nanodiamond particles.* Diamond and Related Materials, 2009. **18**(4): p. 620-626.

7. Grant, P.G., T.D. Phillips, *Isothermal adsorption of aflatoxin B1 on HSCAS clay.* Journal of Agricultural and Food Chemistry, 1998. **46**(2): p. 599-605.

8. Puzyr, A., V.S. Bondar, Z.Y. Selimhanova, A.G. Tyan, E.V. Bortnikov, E.V. Injevatkin, *Results of studies of possible applications of detonation nanodiamonds as enterosorbents.* Siberian Med. Obozrenie (Siberian Medical Review), 2004. **2-3**: p. 25-28.

9. Puzyr, A.P., V.S. Bondar, and S.E. Al, *Dynamics of the selected physiological responses in laboratory mice under the prolonged oral administration of nanodiamonds suspensions.* Siberian Med. Obozrenie (Siberian Med. Rev.) (in Russian), 2004. **4**: p. 19.

Supplementary Data

Chapter 5:
Propidium Iodide Adsorption and Binding by Nanodiamond and Nanocarbon Particles

Propidium Iodide Adsorption and Binding by Nanodiamond and Nanocarbon Particles

N.M. Gibson[1]*, T.J.M. Luo [1], O. Shenderova [1,2], A.P. Koscheev [3] and D.W. Brenner [1]

[1] Department of Materials Science and Engineering, North Carolina State University, 911 Partners Way, Raleigh, NC, USA 27695

[2] International Technology Center, P.O. Box 13740 Research Triangle Park, NC, USA 27617

[3] State Scientific Center of Russian Federation, Karpov Institute of Physical Chemistry, ul. Vorontzovo Pole, 10, Moscow, Russia 105064

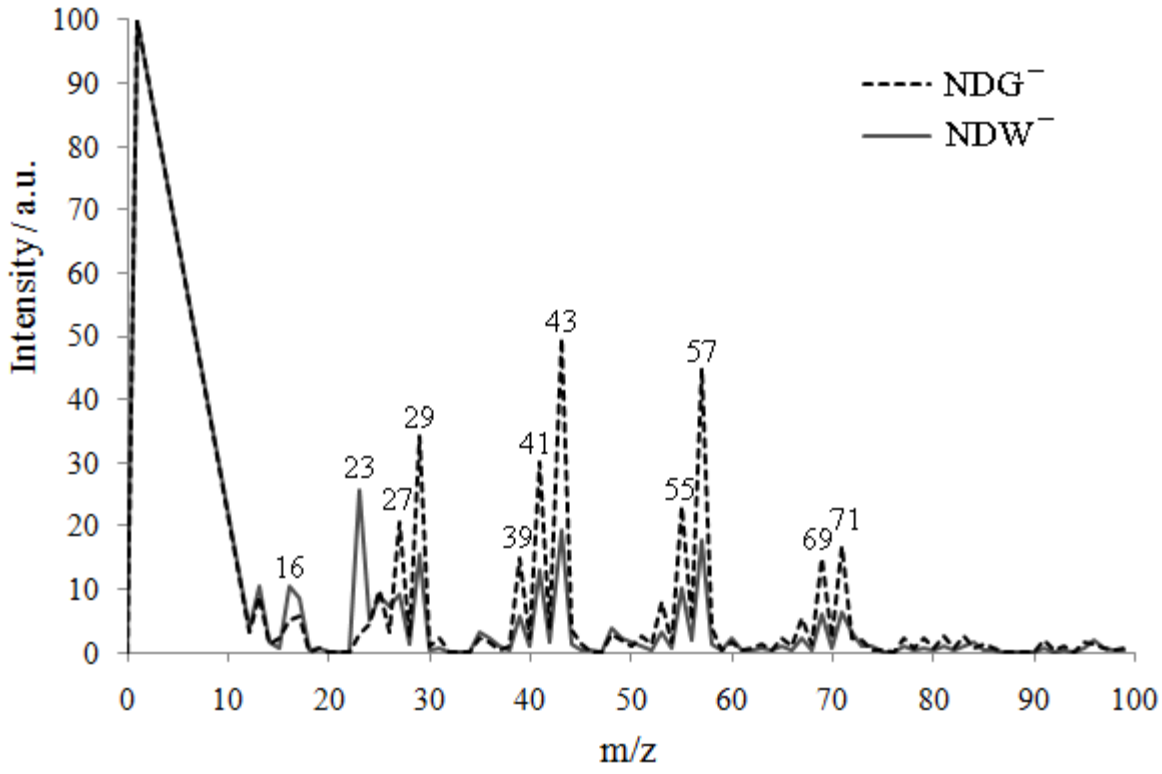

Figure SD1. TOF-SIMS spectra of NDG^- and NDW^- NDs.

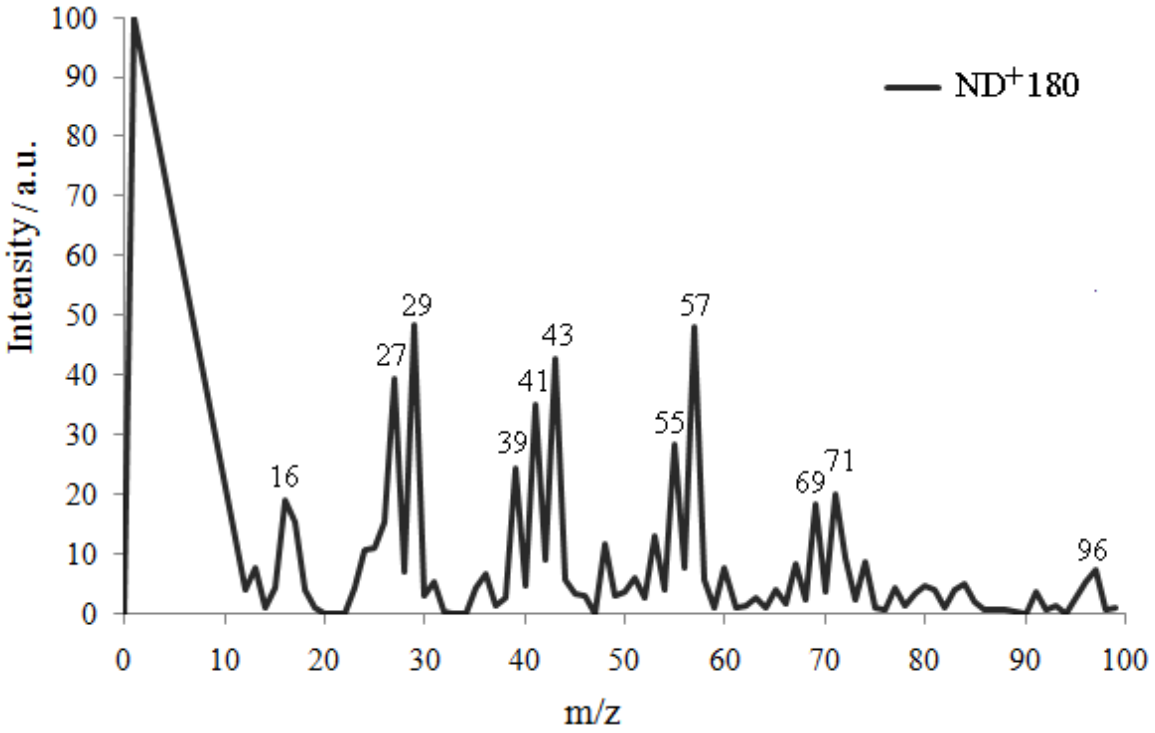

Figure SD2. TOF-SIMS spectra of $ND^{+}180$ ND.